SCUOLA DI DOTTORATO
UNIVERSITÀ DEGLI STUDI DI MILANO-BICOCCA

Department of Biotechnology and Biosciences

PhD program in Converging Technologies for Biomolecular Systems (TeCSBi)
Cycle XXXIV

Resection of DNA double-strand breaks: novel regulatory mechanisms by checkpoint proteins and chromatin remodelers

Casari Erika
780157

Tutor: Prof. Longhese Maria Pia

Supervisor: Prof. Clerici Michela

Coordinator: Prof. Branduardi Paola

ACADEMIC YEAR 2020/2021

INDEX

ABSTRACT

Genome instability is one of the hallmarks of cancer cells and can be due to DNA repair defects. Among different types of DNA damage, DNA double-strand breaks (DSBs) are highly cytotoxic lesions that must be repaired correctly to ensure genome stability maintenance and avoid cell death. Eukaryotic cells deal with DSBs by activating the DNA damage response (DDR), that comprises pathways devoted to repair DNA breaks. DSBs can be repaired by Non-Homologous End Joining (NHEJ), which directly ligates the broken DNA ends, or by Homologous Recombination (HR), which uses sister chromatids or homologous chromosomes as a template to repair the DNA break.

HR is initiated by nucleolytic degradation (resection) of the 5'-terminated strands at both DSB ends. DSB resection is a two-step process, in which an initial short-range step is catalyzed by Mre11-Rad50-Xrs2/NBS1 (MRX/MRN) complex that, together with Sae2 (CtIP in mammals), catalyzes an endonucleolytic cleavage of the 5'-strands. Then, a long-range resection step is carried out by the nucleases Exo1 and Dna2, the latter acting in association with the helicase Sgs1, to generate long 3'-ended single-stranded DNA (ssDNA) tails.

The DDR comprises also surveillance mechanisms, called DNA damage checkpoint (DDC), that couple DSB repair with cell cycle progression. Major checkpoint players include the apical protein kinases Mec1/ATR and Tel1/ATM. Tel1 recognizes unprocessed DSBs, while Mec1 is activated by RPA-coated ssDNA that is generated during the resection process. Once activated, these protein kinases activate by phosphorylation the effector kinases Rad53/CHK2 and Chk1/CHK1. This activation requires the conserved adaptor protein Rad9/53BP1, whose association to chromatin involves multiple

pathways: (i) Rad9 interacts with histone H3 in its K79-methylated form (H3-K79me) and this methylation is introduced by the methyltransferase Dot1; (ii) Rad9 binds histone H2A phosphorylated at Ser129 residue (γH2A) (variant H2AX phosphorylated at Ser139 in mammals) by Mec1/ATR and Tel1/ATM kinases; (iii) Phosphorylation of Rad9 by cyclin-dependent kinase leads to Rad9 interaction with Dpb11/TopBP1, which is recruited to DSBs by the evolutionarily conserved ring-shaped heterotrimer Ddc1-Mec3-Rad17 (Rad9-Hus1-Rad1 in mammals) complex, commonly called 9-1-1.

DSB end resection and DNA damage checkpoint are strongly interconnected to ensure a fine coordination between DNA repair and cell cycle progression. Furthermore, both these mechanisms need to be strictly regulated to avoid excessive ssDNA generation and to achieve efficient DNA damage repair. How short-range resection is regulated and contributes to checkpoint activation remains to be determined.

In this thesis, I contributed to show that abrogation of long-range resection induces a checkpoint response that depends on the 9-1-1 complex, which recruits Dpb11 and Rad9 at damaged DNA. Furthermore, the 9-1-1 complex, independently of Dpb11 and Rad9, restricts short-range resection by negatively regulating Mre11 nuclease. We propose that 9-1-1, which is loaded at the leading edge of resection, plays a key function in regulating Mre11 nuclease and checkpoint activation once DSB resection is initiated.

Repair of DSBs occurs in a chromatin context. In fact, eukaryotic genomes are compacted into chromatin, which restricts the access to DNA of the enzymes devoted to repair DSBs and raises the question as to how DNA end resection occurs in the context of chromatin. To facilitate the access of DNA repair proteins, chromatin near DSBs undergoes extensive modifications by a series of

conserved chromatin remodelers that are recruited to DSBs. These modifications include nucleosome sliding, nucleosomes or histones removal and histones post-translational modifications. Thus, given the importance of chromatin remodeling in DSB repair, in the second part of this thesis, I investigated the role of the chromatin remodeling protein Dpb4 in DSB repair. Budding yeast Dpb4 (POLE3/CHRAC17 in mammals) is a highly conserved histone fold protein that is shared by two protein complexes: the chromatin remodeler ISW2/hCHRAC and the DNA polymerase ε (Pol ε) holoenzyme. In *Saccharomyces cerevisiae*, Dpb4 forms histone-like dimers with Dls1 in the ISW2 complex and with Dpb3 in the Pol ε complex. I showed that Dpb4 plays two functions in sensing and processing DSBs. Dpb4 promotes histone removal and DSB resection by interacting with Dls1 to facilitate the association of the Isw2 ATPase to DSBs. Furthermore, it promotes checkpoint activation by interacting with Dpb3 to facilitate the association of the checkpoint protein Rad9 to DSBs. Persistence of both Isw2 and Rad9 at DSBs is enhanced by the A62S mutation that is located in the Dpb4 histone fold domain and increases Dpb4 association at DSBs. Thus, Dpb4 exerts two distinct functions at DSBs depending on its interactors.

In the last part of my thesis, to better understand the link between chromatin remodeling and DNA end resection, I contributed to examine the role in DSB repair of the *Saccharomyces cerevisiae* ATP-dependent chromatin remodeling protein Chd1, whose human counterpart is frequently mutated in prostate cancer. We showed that Chd1 participates in both short- and long- range resection by promoting the association of MRX and Exo1 to the DSB ends. Furthermore, Chd1 reduces histone occupancy near the DSB ends and promotes DSB repair by HR. All these functions require Chd1 ATPase activity,

supporting a role for Chd1 in the opening of chromatin at the DSB site to facilitate MRX and Exo1 processing activities.

All the findings reported in this thesis contributed to elucidate the molecular mechanisms modulating DNA repair and maintaining genome stability in response to DSBs.

RIASSUNTO

L'instabilità genomica è una delle caratteristiche delle cellule tumorali e può essere dovuta a difetti nella riparazione dei danni al DNA. Tra le differenti tipologie di danno al DNA, le rotture della doppia elica di DNA (DNA *double-strand breaks, DSBs*) sono lesioni altamente citotossiche che devono essere correttamente riparate per garantire il mantenimento della stabilità genomica ed evitare la morte cellulare. Le cellule eucariotiche affrontano questi danneggiamenti attivando una risposta al danno del DNA, che presenta differenti vie molecolari dedite alla riparazione delle rotture del DNA. I DSBs possono essere riparati mediante NHEJ (*Non-Homologous End Joining*), che lega direttamente le estremità rotte del DNA, o mediante ricombinazione omologa (*Homologous Recombination, HR*), che utilizza il cromatidio fratello o il cromosoma omologo come templato per riparare la rottura del DNA.

La ricombinazione omologa è avviata dalla degradazione nucleolitica (DNA *end resection*) delle estremità 5' del DSB. La *resection* è un processo a due fasi, in cui la prima fase, definita *short-range*, è catalizzata dal complesso Mre11-Rad50-Xrs2/NBS1 (MRX/MRN) che, insieme a Sae2 (CtIP nei mammiferi), catalizza un taglio endonucleolitico alle estremità 5’ del DNA rotto. Dopo di che, la seconda fase, denominata *long-range*, prevede l’intervento delle due nucleasi Exo1 e Dna2, quest'ultima in associazione con l'elicasi Sgs1. Queste proteine sono necessarie per generare lunghe code di DNA a singolo filamento con estremità sporgente in 3’.

Una volta che si verifica una rottura della doppia elica di DNA, le cellule attivano anche un’altra via molecolare altamente conservata, chiamata checkpoint da danno al DNA, che coordina la riparazione del DSB con la progressione del ciclo cellulare. Tra i principali attori del checkpoint ci sono le protein-chinasi Mec1/ATR e Tel1/ATM. Tel1 riconosce le rotture del doppio

filamento di DNA non processate, mentre Mec1 è attivato dal DNA a singolo filamento, prodotto dal processo di *resection*, rivestito dal complesso RPA. Una volta stimolate, queste due chinasi apicali attivano per fosforilazione le chinasi effettrici Rad53/CHK2 e Chk1/CHK1. Questa attivazione richiede anche la proteina conservata Rad9/53BP1 la cui associazione alla cromatina coinvolge molteplici vie: (i) Rad9 interagisce con l'istone H3 nella sua forma metilata sulla K79 (H3-K79me) e tale modificazione è introdotta dalla metiltransferasi Dot1; (ii) Rad9 può anche legarsi all'istone H2A fosforilato sul residuo Ser129 (γH2A) (variante H2AX fosforilata sul residuo Ser139 nei mammiferi); (iii) la fosforilazione di Rad9 da parte delle chinasi ciclina-dipendenti porta all'interazione di Rad9 con Dpb11/TopBP1, che a sua volta viene reclutato al DSB dal complesso eterotrimerico conservato a forma di anello Ddc1-Mec3-Rad17 (Rad9-Hus1-Rad1 nei mammiferi), comunemente chiamato 9-1-1.

Resection e checkpoint da danno al DNA sono fortemente interconnessi tra loro per garantire un buon coordinamento tra la riparazione del DNA e la progressione del ciclo cellulare. Inoltre, devono essere rigorosamente regolati per evitare un'eccessiva generazione di DNA a singolo filamento e per ottenere un'efficiente riparazione del danno al DNA. Resta da determinare come la *short-range resection* sia regolata e contribuisca all'attivazione del checkpoint.

In questa tesi, ho contribuito a dimostrare che l'inibizione della *long-range resection* induce una risposta di checkpoint che dipende dal complesso 9-1-1, che recluta Dpb11 e Rad9 al DNA danneggiato. Inoltre, il complesso 9-1-1, indipendentemente da Dpb11 e Rad9, limita la *short-range resection* regolando negativamente la nucleasi Mre11. Il nostro modello propone che il complesso 9-1-1, che viene caricato all'inizio della *resection*, svolga una funzione chiave

nella regolazione della nucleasi Mre11 e nell'attivazione del checkpoint, una volta avviata la *resection* al danno al DNA.

La riparazione dei danni della doppia elica di DNA coinvolge anche la cromatina. Infatti, i genomi eucariotici sono compattati in una struttura cromatinica che limita l'accesso al DNA agli enzimi dedicati alla riparazione dei danni e solleva la questione di come avvenga la *resection* in tale contesto. È noto che la cromatina che affianca una rottura della doppia elica di DNA subisce ampie modificazioni da parte di una serie di rimodellatori della cromatina, evolutivamente conservati, che vengono reclutati al DSB. Queste modificazioni includono principalmente lo scorrimento dei nucleosomi, la rimozione dei nucleosomi o degli istoni e le modifiche post-traduzionali istoniche.

Pertanto, data l'importanza del rimodellamento della cromatina nella riparazione delle rotture della doppia elica di DNA, nella seconda parte di questa tesi, ho studiato il ruolo della proteina di rimodellamento della cromatina Dpb4 nella riparazione dei DSBs. Nel lievito gemmante, la proteina conservata evolutivamente Dpb4 (POLE3/CHRAC17 nei mammiferi) presenta un dominio istonico ed è condivisa da due complessi proteici: il rimodellatore della cromatina ISW2/hCHRAC e l'oloenzima DNA polimerasi ε (Pol ε). In *Saccharomyces cerevisiae*, Dpb4 interagisce con Dls1 nel complesso ISW2 e con Dpb3 nel complesso Pol ε. In questa tesi ho dimostrato che Dpb4 svolge due funzioni nel rilevamento e nel processamento delle rotture del doppio filamento del DNA. Dpb4 promuove la rimozione degli istoni e la *resection* interagendo con Dls1 per facilitare l'associazione dell'ATPasi Isw2 al DNA danneggiato. Inoltre, promuove l'attivazione del checkpoint interagendo con Dpb3 per facilitare l'associazione della proteina di checkpoint Rad9 ai DSBs.

La persistenza di Isw2 e Rad9 sul DNA è potenziata dalla presenza della mutazione A62S, che si trova nel dominio istonico della proteina Dpb4, la quale aumenta l'associazione di Dpb4 al DNA danneggiato. Pertanto, Dpb4 esercita due funzioni distinte sui danni della doppia elica di DNA a seconda dei suoi interattori.

Nell'ultima parte della tesi, per comprendere meglio il legame tra il rimodellamento della cromatina e la *resection*, ho contribuito a studiare il ruolo nella riparazione dei DSBs della proteina di rimodellamento della cromatina Chd1, frequentemente mutata nel cancro della prostata. Abbiamo dimostrato che tale proteina partecipa sia nella *short-* che nella *long- range resection*, promuovendo l'associazione di MRX ed Exo1 alle estremità di una rottura del DNA. Inoltre, Chd1 consente la rimozione degli istoni vicino alle estremità del DNA danneggiato e promuove la riparazione del DSB attraverso il meccanismo di ricombinazione omologa. Tutte queste funzioni richiedono l'attività ATPasica di Chd1, supportando un ruolo di Chd1 nell'apertura della cromatina nelle regioni rotte di DNA che facilita le attività di processamento di MRX ed Exo1.

In generale, i risultati riportati in questa tesi hanno contribuito ad identificare nuovi meccanismi molecolari alla base della riparazione del DNA danneggiato e del mantenimento dell’integrità genomica.

PUBLICATIONS

List of publications (Nov 2018 – Oct 2021)

- **Casari E**, Gobbini E, Gnugnoli M, Mangiagalli M, Clerici M, Longhese MP (2021) Dpb4 promotes resection of DNA double-strand breaks and checkpoint activation by acting in two different protein complexes. *Nat Commun* **12,** 4750.

- Gnugnoli M, **Casari E**, Longhese MP (2021) The chromatin remodeler Chd1 supports MRX and Exo1 functions in resection of DNA double-strand breaks. *PLOS Genet* **17**, e1009807.

- **Casari E**, Gobbini E, Clerici M, Longhese MP (2021) Resection of a DNA Double-Strand Break by Alkaline Gel Electrophoresis and Southern Blotting. *Methods Mol Biol* **2153**, 33-45.

- Gobbini E, **Casari E**, Colombo CV, Bonetti D, Longhese MP (2020) The 9-1-1 Complex Controls Mre11 Nuclease and Checkpoint Activation during Short-Range Resection of DNA Double-Strand Breaks. *Cell Rep* **33**, 108287.

- **Casari E***, Rinaldi C*, Marsella A, Gnugnoli M, Colombo CV, Bonetti D, Longhese MP (2019) Processing of DNA Double-Strand Breaks by the MRX Complex in a Chromatin Context. *Front Mol Biosci* **6**, 43.

  *These authors contributed equally to the work.

- Marsella A, Cassani C, **Casari E**, Tisi R, Longhese MP (2019) Structure-function relationships of the Mre11 protein in the control of DNA end bridging and processing. *Curr Genet* **65**, 11-16.

INTRODUCTION

Genome instability and cancer: the role of the DNA damage response

Cancer is one of the leading causes of death worldwide and, for this reason, biological, clinical, and medical scientists have focused on tumors to better understand the features related to cancers cells. Different hallmarks typical of cancer cells have been identified (Figure 1).

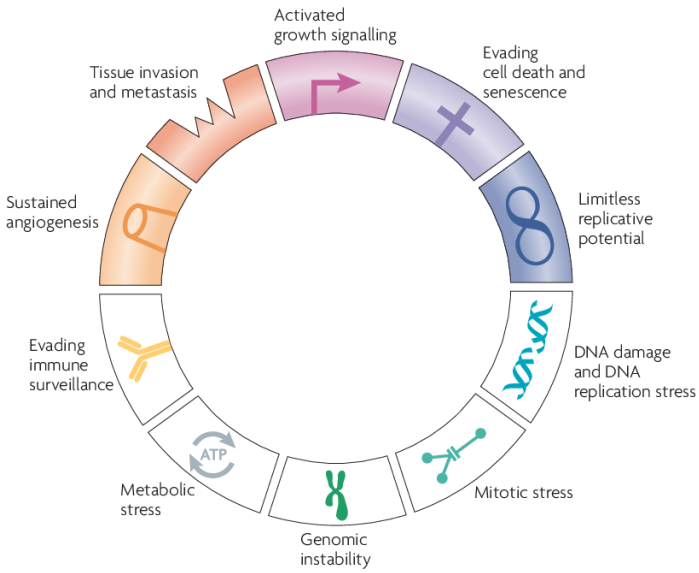

Figure 1. Schematic depiction of the hallmarks of cancer cells [adapted from Negrini *et al*., 2010].

As shown, genomic instability is one of the characteristics of many cancer cells and can result from point mutations or chromosome rearrangements. Futhermore, it is clear the importance of maintaining genome integrity for all

the living organisms not only for cells functionality but also to ensure faithful transmission of genetic heritage to progeny.

DNA damage can result from different physical or chemicals agents and from cellular or extracellular environment [Roos *et al*., 2016]. Spontaneous DNA alterations can result from defective meiosis, DNA replication errors, uncontrolled recombination, off-target mutation, inaccurate V(D)J, bases deamination, DNA depurination or depyrimidination, collisions of replication/transcription, telomere shortening, and production of Reactive Oxygen Species (ROS) that can oxidize DNA bases and generate DNA breaks. DNA damage can be also induced by exogenous causes as viral infections or environmental agents such as ultraviolet light (UV), ionizing radiation (IR) and different kind of genotoxic chemicals like intercalating agents and substances that modify DNA bases (base analogues, alkylating agents, hydroxylating agents) [Friedberg *et al*., 2005]. DNA damaging agents can induce different kind of DNA lesions such as Single-Strand Breaks (SSBs), Double-Strand Breaks (DSBs), DNA crosslinks, base modifications or depletions, stalled replication forks or mismatches (Figure 2).

In the presence of DNA lesions, cells activate a complex network, called the DNA damage response (DDR), that includes mechanisms devoted to repair DNA lesions. For example, mispaired bases are excised as single nucleotides by the MisMatch Repair (MMR), whereas damaged bases are excised as single free base by the Base Excision Repair (BER) or as an oligonucleotide fragment by the Nucleotide Excision Repair (NER). Furthermore, DSBs can be repaired by either the Non-Homologous End Joining (NHEJ) or the Homologous Recombination (HR) pathway (Figure 2).

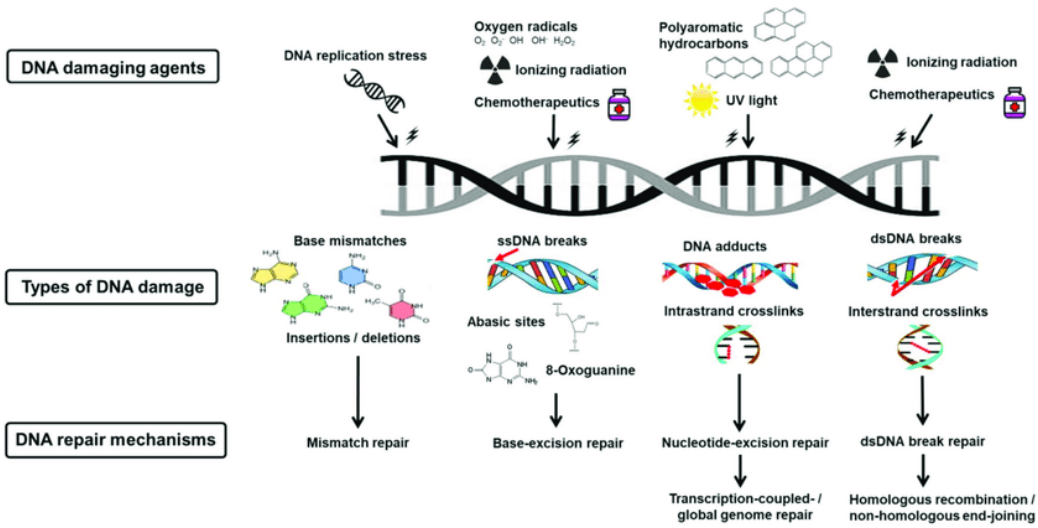

Figure 2. DNA Damage Repair: endogenous and exogenous DNA lesions and repair mechanisms [Adapted from Helena *et al.*, 2018].
Various DNA damaging agents cause a wide range of DNA lesions. Each lesion is corrected by a specific DNA repair mechanism.

Besides triggering the most appropriate DNA repair mechanisms, the activation of the DDR induces also other cellular processes such as DNA damage checkpoints, damage tolerance mechanisms, and senescence or apoptosis if the damage is not repairable (Figure 3). The DDR is essential for human health: transmissible defects in DDR pathways can lead to different kind of diseases, such as neurological degeneration, immune deficiency, premature aging, and severe cancer susceptibility [Hoeijmakers, 2009]. Thus, a detailed understanding of the mechanisms and proteins controlling the DDR is key to unmask new vulnerabilities for targeted therapeutics. As most of the proteins involved in the DDR are remarkably conserved during evolution [Aylon & Kupiec, 2004], the model organism *Saccharomyces cerevisiae*, which combines precise genetic manipulability with a high level of conservation with humans of

the DDR [O'Neil *et al.*, 2017], can be used to better understand the molecular mechanisms underlying genome integrity pathways.

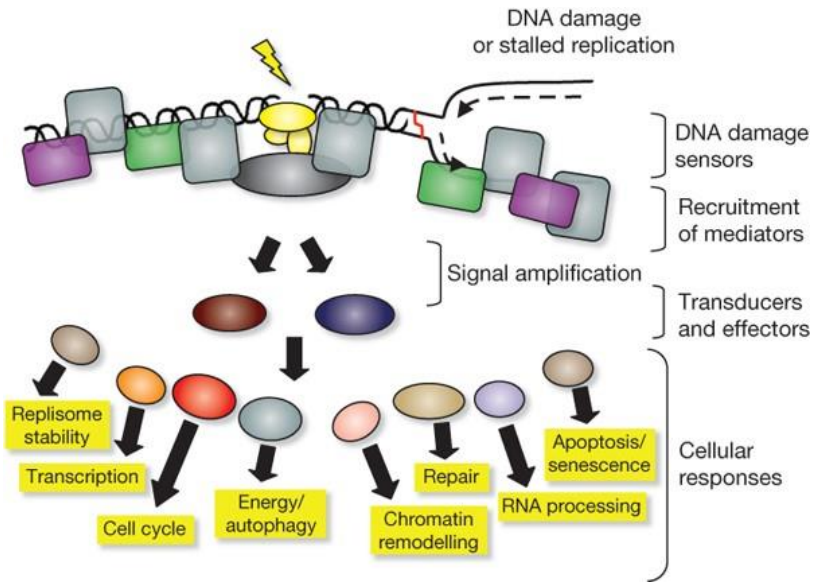

Figure 3. Model for the DNA Damage Response [Adapted from Jackson & Bartek, 2009].
The presence of a lesion on DNA is recognized by various sensor proteins. These sensors initiate signalling pathways that have an impact on a wide variety of cellular processes and responses.

DNA Double-Strand Breaks

Among the many types of DNA lesions, the DNA double-strand break (DSB) is one of the most severe ones, because it can cause mutations and chromosomal rearrangements [Gobbini *et al.,* 2015]. DSBs are generated when the sugar phosphate backbones on both DNA strands are broken in or near the same location to allow the physical dissociation of the DNA double helix into two molecules [Aparicio *et al.,* 2014].

DSBs can occur either accidentally during normal cell metabolism or can be induced by exposure to exogenous agents, such as certain kinds of chemotherapeutic drugs or ionizing radiation (IR) [Sturzenegger *et al.,* 2014]. Substances that can induce DSBs include: base alkylating agents, such as methyl methanesulfonate (MMS), that stall replication forks and inhibit transcription; cross-linking agents, such as cisplatin and psoralens, that covalently crosslink bases belonging to the same strand (intrastrand) or to complementary strands (interstrand); radiomimetic agents, such as phleomycin (phleo) or bleomycin (bleo), that introduce DSBs around the genome by mimicking the action of IR; ribonucleotide reductase inhibitors, such as hydroxyurea (HU), that depletes the deoxyribonucleotides pool; DNA topoisomerase inhibitors, like camptothecin (CPT) and their derivatives (irinotecan and topotecan), that introduce DSBs by blocking topoisomerase-DNA intermediates (cleavable complexes) [Deng *et al.,* 2005].

DSBs are also generated during cell metabolism, most of the times by Reactive Oxygen Species. Moreover, DSBs are intermediates during physiological processes of the cell, such as immunoglobulin class switching [Bassing *et al.,* 2004] or T-cell receptor loci during lymphoid cell development.

Additionally, the neuronal activity stimulation triggers DSB formation during DNA transcription [Madabhushi *et al*., 2015].

In addition, meiotic recombination requires formation of programmed Spo11-dependent DSBs on every chromosome [Manfrini *et al.*, 2010]. These DSBs are not randomly induced, but they are generated in specific chromosomal regions. Repair of these DSBs leads to exchange of genetic material between homologous chromosomes, guaranteeing genetic variability. As well, this helps chromosomes to segregate correctly during the first meiotic division [Longhese *et al.*, 2009].

Furthermore, the DNA replication process itself is thought to be the major source of DSBs in proliferating cells since DNA intermediates at replication forks are fragile and susceptible to breakage [Aparicio *et al.*, 2014].

Finally, collision between transcription and replication or the presence of DNA:RNA hybrids can generate DSBs by causing the arrest of replication forks [Rinaldi *et al.*, 2021].

Defects in the cellular response to DSBs can lead to the development of different inheritable human diseases including cancer, neurological defects, immunodeficiencies, and genetic syndromes such as Ataxia Telangiectasia, Ataxia Telangiectasia-Like Disorder [McKinnon, 2012], Nijmegen Breakage syndrome, Severe Combined ImmunoDeficiency (SCID), LIG4-syndrome, ATR-Seckel syndrome, and Fanconi Anaemia [O'Driscoll *et al.*, 2006].

Non-Homologous End Joining (NHEJ)

DSBs can be repaired by Non-Homologous End Joining (NHEJ), which directly re-ligates the DNA broken ends with little or no DNA-end processing [Chang *et al.*, 2017]. NHEJ is conserved from prokaryotes to humans and is the main pathway to repair DSBs in mammals. The NHEJ mechanism can be summarized in three steps: binding of specific proteins to DSBs, processing of the broken DNA strands and re-ligation.

In both yeast and mammals, the first step in NHEJ is the recognition of the DSB by the highly conserved Ku heterodimer (Figure 4), which is composed of the Ku70 and Ku80 subunits [Chang *et al*., 2017; Hefferin *et al*., 2005; Dudášová *et al*., 2004]. By forming a ring around DNA, Ku can achieve high-affinity binding without recourse to sequence-specific bonding interactions. Moreover, this feature supports the ability of Ku to slide on DNA and to allow recruitment of mammalian DNA-PK kinase, a member of the Phosphatidylinositol 3-kinase-related kinase (PIKK) family, which interacts with the Ku complex with its C-terminal domain and phosphorylates different substrates involved in NHEJ [Williams *et al*., 2014]. Once Ku is bound to the DSB ends, it directly or indirectly recruits other NHEJ factors, including the DNA Ligase IV (Dnl4/Lig4 in *S. cerevisiae* and DNL4 in mammals). In yeast, the DNA Ligase IV enzyme, in association with its cofactor Lif1 (XRCC4 in humans), is recruited to the DSB through a direct interaction with the Xrs2 subunit of the highly conserved MRX/MRN complex (Mre11, Rad50 and Xrs2 in budding yeast; MRE11, RAD50 and NBS1 in mammals) (Figure 4). In *S. cerevisiae*, recruitment of Lig4-Lif1 also requires Ku70, whereas Lif1 association to DSBs requires the presence of Nej1 (XLF in human) [Hefferin *et al*., 2005; Daley *et*

al., 2005] (Figure 4). In addition, a specific group of DNA polymerases is recruited to DNA by direct interaction with the Ku heterodimer, to fill possible DNA gaps. In mammalian, the DNA polymerase μ (POLμ) and the DNA polymerase λ (POLλ) can fill gaps created during NHEJ repair [Chang *et al*., 2017]. In yeast, Pol4 plays this role [Dudášová *et al*., 2004].

The NHEJ machinery is active only on blunt or DNA ends not extensively processed and NHEJ is an error prone repair mechanism. Despite it is highly efficient, it can lead to mutations, inversions, or translocations at the joining sites [Lieber, 2010]. Since most DSBs possess no compatible ends, several factors are required to process the DNA broken ends to allow the re-ligation. For example, the mammalian exo- and endo- nuclease ARTEMIS is recruited at DSBs and activated by DNA-PKcs. Other proteins, like CtIP, the WRN helicase, the FEN1 endonuclease and the EXO1 exonuclease have been involved in DSB processing for NHEJ (Figure 4). In yeast, the most studied NHEJ endonuclease is Rad27, ortholog of FEN1.

In humans, NHEJ dysfunction can lead to different genetic diseases such as the Lig4-syndrome, a rare disorder caused by mutations in the Lig4 gene and characterized by immune deficiency, microcephaly, and delay in development [Davis & Chen, 2013]. Moreover, a reduced NHEJ efficiency could cause genomic instability and subsequent tumoral transformation [Hefferin *et al*., 2005; Lieber, 2010]. Yeast cells without Ku70 and/or Ku80 are totally defective in NHEJ even if they are not sensitive to any kind of genotoxic agent. On the contrary, these cells cannot grow at high temperature, indicating a role for the Ku complex in other essential physiological processes [Hefferin *et al*., 2005].

NHEJ is inhibited by the nucleolytic degradation of the 5'-strands (DNA end resection) that leads to homologous recombination and is particularly efficient in the G1 phase of cell cycle, when resection is not induced [Clerici *et al*.,

2008]. In addition, the Ku complex prevents end resection in G1 and, within MRX, mediates recruitment of the others NHEJ factors [Lee *et al.*, 1998; Palmbos *et al.*, 2008].

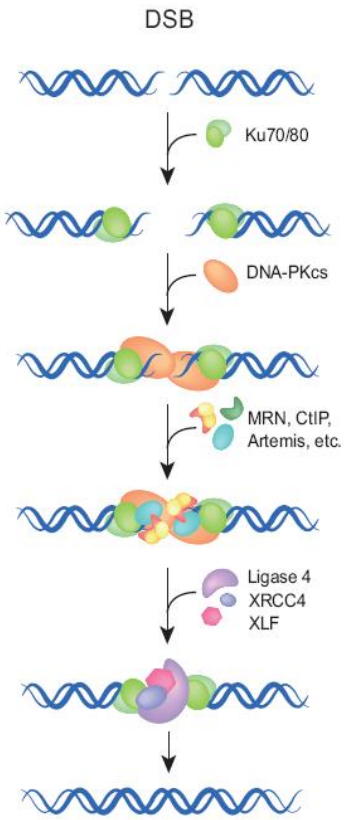

Figure 4. Mechanism of NHEJ repair in higher eukaryotes [Adapted from Dueva *et al.*, 2013].
Once the DSB is generated, cells recruit the heterodimer Ku at the DNA broken ends. At this point, all the proteins necessary for the repair, such as DNA-PKcs, MRN, XRCC4 are recruited. Finally, the tethered ends are ligated by the DNA ligase IV. The damage is repaired, although the NHEJ mechanism could lead to mutations at joined site.

Homologous Recombination (HR)

Homologous recombination (HR) is a highly conserved DSB repair pathway that is defined as the exchange of genetic information between a donor DNA and a damaged recipient DNA that present similar or identical sequences. In general, HR is an error-free process for the repair of DSBs because it copies the information from an homologous donor [San Filippo *et al.*, 2008]. However, if the repair uses misaligned repetitive sequences, it can create deletions or duplications events. Furthermore, the use of homologous chromosome can induce loss of heterozygosity (LHO) events. Finally, if HR takes place between sites with very low homology, this can induce deletions, translocations, inversions, or duplications. All these events can trigger genetic diseases and oncogenesis.

Availability of a homologous sequence for recombinational repair is defined by ploidy and the cell cycle phase, with the latter being regulated by cyclin-CDKs (Cyclin-Dependent Kinases) [Mehta & Haber, 2014; Huertas, 2010; Ferretti *et al*., 2013]. However, additional factors, like the proximity between donor DNA and recipient DNA, chromatin structure, and nuclear compartmentalization concur to the disposability of a donor sequence for HR [Mathiasen & Lisby, 2014]. In fact, HR in mitosis involves sister chromatids that are linked together by cohesin complex to promote the recombination event, rather than homologous chromosomes that can be distant in the cell nucleus [Litwin *et al.*, 2018]. Recombination in meiosis shares similarities with mitotic recombination, but also exhibits many unique features. During meiosis, homologous chromosomes, which cohesion is mediated by synaptonemal complex, undergo dynamic structural changes and line up in pairs for recombination, which is

initiated by the formation of programmed DSBs catalyzed by Spo11 [Lee *et al*., 2021].

Finally, HR occurs only in nucleoplasm, because it is hampered in the nucleolus and in the nuclear periphery [Mathiasen & Lisby, 2014].

While NHEJ is the main pathway for DSB repair in G1, HR is the mechanism that is used during the S/G2 phase. In fact, processing of the 5'-DSB DNA ends when cells are in the S or G2 cell cycle phase of the cell cycle, and generates 3'-ended ssDNA tails that inhibit NHEJ and commit DSB repair to HR.

Several information on the molecular mechanisms of HR derives from the yeast *S. cerevisiae* experimental model [Haber, 2016]. Three different HR models are described: the canonical Double-Strand Break Repair model (DSBR), the Synthesis-Dependent Strand Annealing (SDSA) and the Break Induced Replication (BIR) (Figure 5) [Sebesta & Krejci, 2016]. These models share some crucial steps:

a) Nucleolytic processing (DNA end resection) of the DSB ends to obtain ssDNA.

b) Formation of recombinogenic single-stranded DNA filament.

c) Strand invasion and Holliday junction(s) (HJ) formation.

d) DNA synthesis.

e) Resolution of the Holliday junction(s).

Regarding the first step, HR requires that the 5'-terminated strands at both DNA ends are nucleolytically degraded (resected) in a process defined DNA end resection [see paragraph 'A key step in Homologous Recombination: DNA end resection']. This degradation leads to the formation of 3'-ended single-stranded DNA (ssDNA) ends that can invade and anneal with an undamaged homologous DNA template [Symington & Gautier, 2011; Mehta & Haber, 2014; Tisi *et al*., 2020]. Because ssDNA can be extremely unstable and exposed

to degradation, it is covered by Replication Protein A (RPA), a heterotrimeric complex formed by RPA70, RPA32 and RPA14 subunits in humans and Rfa1, Rfa2 and Rfa3 in *S. cerevisiae* [Symington & Gautier, 2011; San Filippo *et al.*, 2008]. Next, RPA is replaced by Rad51 and Dmc1 recombinases, necessary to invade the donor DNA. These recombinases facilitate the pairing and the shuffling of DNA sequences during HR in a process called homologous DNA pairing and strand exchange. Rad51 is essential for mitotic and meiotic HR, while Dmc1 is involved only during meiosis.

Rad51 is a recombinase highly conserved in eukaryotes that shows a strong conservation with the bacterial RecA recombinase [San Filippo *et al.*, 2008]. The importance of Rad51 in DNA repair is underlined by the high sensitivity of *rad51* yeast mutant cells to genotoxic agents. Additionally, RAD51 is an essential gene in mammalian cells [Symington & Gautier, 2011]. Rad51 functions in three stages: pre-synaptic, synaptic, and post-synaptic [Sung *et al.*, 2003]. In the pre-synaptic phase, Rad51 is loaded onto ssDNA. The resulting Rad51-ssDNA filament, or pre-synaptic filament, is right-handed and consist of six Rad51 molecules and 18 nucleotides per helical turn. The stretching of this presynaptic filament is crucial for an efficient homology research. During synapsis, Rad51 facilitates the connection between the invading DNA and the homologous duplex DNA template, leading to the generation of a heteroduplex DNA, known as D-loop (Figure 5). Finally, during post-synapsis step, DNA is re-synthesized using the invading 3'-end as a primer and Rad51 dissociates from dsDNA to expose the 3'-OH needed for DNA synthesis [Krejci *et al.*, 2012]. This Rad51 dissociation is performed by the translocase Mph1 (FANCM in humans).

Due to the fact that Rad51 is not able to displace RPA from ssDNA because of its high affinity for ssDNA and the high concentration of the RPA complex

respect to that of Rad51, replacement of RPA by Rad51 requires other recombination mediators [Symington *et al*., 2014]. In yeast, these include the Rad52 and the Rad51 paralogues Rad55 and Rad57. Genetic and biochemical analyses shown that Rad52 directly interacts with Rad51 and can also bind RPA [Seong *et al*., 2008]. The mediator function of Rad52 resides into its C-terminus domain, where both the Rad51- and the DNA-interacting domains are situated [San Filippo *et al*., 2008]. In humans, the principal RAD51 mediator is the BRCA2 protein. Although BRCA2 has very poor homology with yeast Rad52, BRCA2 is considered its functional equivalent. BRCA2 is known as cancer suppressor and several BRCA2 mutations can predispose to the development of breast and ovarian cancer [Roy *et al*., 2012]. BRCA2 binds RAD51 by two different domains: the BRC repeats and the C-terminal domain CTRB. Moreover, BRCA2 binds DNA with three OB fold domains and interacts with RPA with an N-terminal region [San Filippo *et al.,* 2008]. Like Rad51, the Rad55-Rad57 heterodimer displays ATPase activity and binds ssDNA; but differently from Rad51, the heterodimer cannot catalyze the strand-exchange reaction. The Rad55-Rad57 heterodimer can also form co-filaments with Rad51 to protect the nucleofilament from the Srs2 anti-recombinase [Krejci *et al*., 2012], which is a helicase implicated in the disruption of Rad51 presynaptic filament in an ATP-dependent manner. Although no Srs2 homologues have been identified in mammalian by now, different helicases (as RTEL, hFBH1 and PAR1) can perform similar functions [Wilkinson *et al*., 2020].

Studies in *E. coli* cells suggest that the homology searching activity depends on random collisions between the Rad51 filament and the donor sequence. When this interaction is established, there is the formation of the synaptic complex. The invasion induces the displacement of the strand, inducing the D-loop structure, that is crucial for DNA synthesis [San Filippo *et al.,* 2008]. In *S.*

cerevisiae, all the steps of pairing, homology searching, and D-loop formations are positively regulated by the chromatin remodeler Rad54 [Symington *et al*., 2014]. Rad54 physically interacts with Rad51 and is required for several HR steps: in the early stages to promote search for DNA homology, chromatin remodeling and D-loop formation, and in the post-synaptic stage to catalyze the removal of Rad51 from dsDNA. The capability of Rad54 to take off Rad51 from dsDNA is assumed to be necessary to avoid non-specific association of Rad51 with chromatin and to provide access to DNA polymerases to the 3'-OH termini of the D-loop to initiate the DNA synthesis [Sung *et al*., 2003]. Later, the invading strand primes DNA synthesis in a process that requires DNA polymerases, such as Polδ and DNA replication proteins PCNA, RFC and Dpb11 [Symington *et al*., 2014].

Different mechanisms exist to conclude HR (Figure 5). One is the canonical Double-Strand Break Repair model (DSBR), in which, after the formation of the D-loop, the other DSB end, which is resected to generate a ssDNA 3' protruding filament, anneals with the complementary DNA strand of the D-loop. This process is called second end capture and triggers new DNA synthesis starting from the 3'-OH of the second DNA end [Krejci *et al.,* 2012]. This event leads to secondary structures with cross intermediates, called Holliday Junctions (HJs) [San Filippo *et al.,* 2008]. The enzymes devoted to the resolution of HJs are a class of nucleases called resolvases. They perform nucleolytic cleavage on the HJs that result in CrossOver (CO) or Non-CrossOver (NCO) structures. In yeast, the resolvases are the Mus81-Mms4 complex and Yen1, while, in mammals, resolution of HJs is made by the orthologs MUS81-EME1 and GEN1.

The resolution of HJs is also possible with the use of helicase-topoisomerase complexes. The yeast STR complex, formed by Sgs1, Top3 and Rmi1 and their

human orthologs BLM, TOP3α and RMI1/2, resolves the HJs, generating only NCO products [Lilley, 2017; Bizard & Hickson, 2014].

Another model of HR is the Synthesis Dependent Strand Annealing (SDSA), in which the 3'-OH terminated strand invades the homologous DNA donor generating a D-loop that, after DNA synthesis, is displaced. If this synthesis elongates sufficiently the invading strand allowing the re-annealing with the damaged molecule, the repair process can conclude with fill-in synthesis and DNA ligation. Subsequently, only NCO products are generated. The SDSA mechanism is the preferred HR mechanism during mitosis, whereas resolution of dHJs via the DSBR mechanism occurs predominantly in meiosis.

The last HR model is the Break Induced Replication (BIR), which is a recombination-dependent replication that results in non-reciprocal transfer of DNA from the donor sequence to the recipient chromosome, where the D-loop structure can assemble into a replication fork that can copy the entire chromosome arm in a single-ended invasion process. Throughout BIR, only a ssDNA of one DSB end invades the homologous duplex and initiates replication stimulating the migration of the D-loop. BIR can arise by different cycles of strand invasion, DNA synthesis, dissociation and this can lead to chromosome rearrangements when dissociation and/or reinvasion occur in repetitive sequences [Symington *et al*., 2014]. All the mentioned mechanisms involve Rad51, except for some sub-types of BIR.

DSBs can be repaired by other recombination pathways that do not involve strand invasion and therefore do not require Rad51. One of them is the Single-Strand Annealing (SSA). SSA occurs when the DSB is flanked by two direct repeats that, once resected, can anneal to each other. This repair mechanism leads to the deletion of the DNA between the direct repeats and one of the repeats [Krejci *et al*., 2012].

Furthemore, DSBs can be sealed by Microhomology-Mediated End Joining (MMEJ), in which micro homologous regions anneal to each other. The MMEJ model involves five steps: resection of the DSB ends, annealing of microhomologous region, removal of heterologous flaps, fill-in synthesis and ligation by DNA ligase Lig3/Lig1 (DNA ligase III/I in humans) [Wang & Xu, 2017; McVey *et al*., 2008; Seol *et al*., 2018]. MMEJ and HR may share the initial end resection step in DSB repair [Truong *et al*., 2013]. However, while HR requires extensive end resection to recruit Rad51 recombinase, limited end resection is sufficient for exposing of micro homologous region and promoting MMEJ.

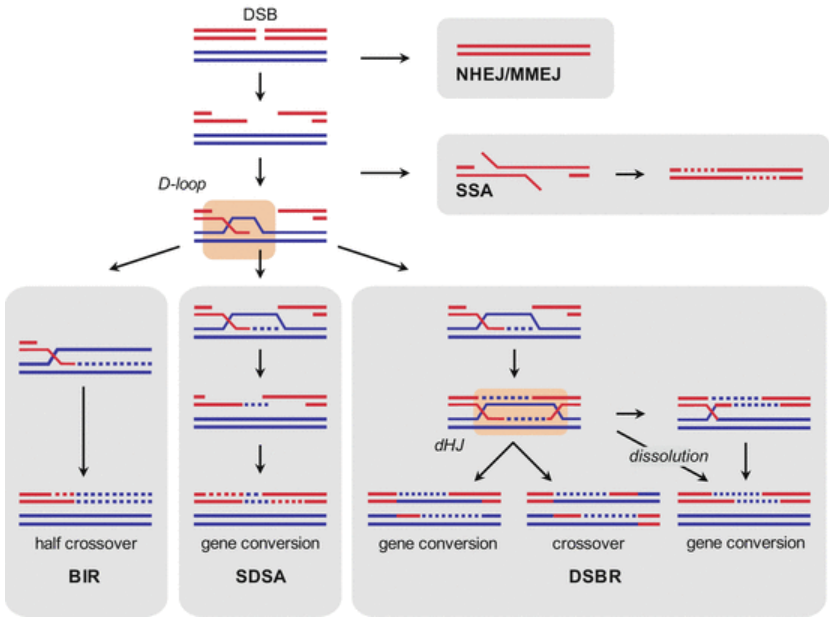

Figure 5. Main pathways for DSB repair [Adapted from Sebesta & Krejci, 2016]. When DSB arises on the DNA, repair can proceed by several pathways. DNA filaments are resected to generate 3'-protruding ends (ssDNA) followed by formation of Rad51-covered filaments able to invade the homologous donor template and to generate D-loop structures. After beginning of DNA synthesis, three pathways can be implicated. In the DSBR pathway, the second DNA end is captured and dHJ intermediates are formed. Resolution of dHJs can generate crossover (CO) or non-crossover (NCO) products. Alternatively, dHJs can be resolved by the action of Sgs1-Top1-Rmi1 to generate only NCO products. In the SDSA pathway, the newly synthetized DNA strand is displaced, followed by pairing with the other 3'-ssDNA tail and DNA synthesis. Another pathway is known as BIR and it starts when the second end is absent, allowing the D-loop turning into a replication fork able of both strand synthesis. Three Rad51-independent recombinational repair pathways are also indicated. In SSA, extensive resection can reveal complementary sequences at two repeats, allowing DNA annealing. The 3'-ssDNA ends are removed, and the created nicks are ligated. To conclude, DSB can be directly repaired with NHEJ or with MMEJ that requires little DNA-end processing. Dotted lines represent newly synthesized DNA.

A key step in Homologous Recombination: DNA end resection

HR initiates with the nucleolytic degradation of the 5'-terminated strands at both DNA ends, leading to the formation of 3'-tailed ssDNA that acts as substrate for RPA and the strand exchange protein Rad51. The mechanism of resection and most of the proteins involved are highly conserved from yeast to humans and similar pathways have been found in prokaryotes too [Cejka, 2015]. Initiation of resection is critical for the repair pathway choice: when resection starts, Ku heterodimer is not able to bind ssDNA and cells are committed to HR [Symington & Gautier, 2011]. In addition, resection is regulated during cell cycle because it occurs primarily in the S/G2 phases of the cell cycle when Cdk1 activity is high and a sister chromatid is present as donor template [Symington & Gautier, 2011].

It has been demonstrated that DSB resection takes place in two steps: firstly, in a step called short-range resection, a short DNA tract is removed from the 5'-strand to generate a short 3'-ssDNA at the DSB ends. Next, in the long-range resection step, the short single-strand DNA intermediate is processed further to produce long ssDNA tracts at the DSB ends.

Short-range resection

During short-range resection, the MRX/N (Mre11, Rad50, Xrs2/NBS1) complex is recruited to the DSB ends [Lisby *et al*., 2004] to catalyse an endonucleolytic cleavage of the 5'terminated DNA strands. This cleavage, which requires the Sae2/CtIP protein [Sartori *et al.,* 2007; Clerici *et al*., 2005] is essential to resect DSBs that possess proteins, such as the Ku complex, associated at their ends, or DNA adducts that can be generated after genotoxic treatments, like DNA-protein adducts that arise following camptothecin action. On the contrary, resection of "clean" DSB ends, as the ones generated by endonucleases, can occur also in the absence of MRX-Sae2 [Gobbini *et al.*, 2013].

It has been demonstrated that Sae2 promotes the endonuclease activity of the Mre11 nuclease [Cannavo & Cejka, 2014]. This is supported by the sensitivity to DNA damaging agents and by the delay in DSB resection of yeast cells deleted for *SAE2* [Clerici *et al.,* 2015]. MRX-Sae2 remove oligonucleotides from the 5'-termini of the break, generating short 3'-ended ssDNA tails of about 50-300 nucleotides that are subjected to extensive processing [Mimitou *et al.,* 2008; Zhu *et al.,* 2008].

The function of Sae2 in resection requires its phosphorylation on Ser267 by CDKs [Huertas *et al.,* 2008] both *in vivo* and *in vitro* [Huertas *et al.,* 2008; Cejka, 2015]. In fact, *sae2-S267A* cells display defective generation of 3'-ssDNA and reduced HR-mediated DSB repair. Therefore, the CDK-dependent regulation of Sae2 is a crucial step ensuring that resection takes place only in the S/G2 phase of the cell cycle when a homologous template is present. It is important to note that DSB resection is more severily affected in *mre11*Δ cells

than in *sae2*Δ cells and this is due to the role of MRX in promoting recruitment of other proteins involved in resection (Sgs1, Dna2 and Exo1) [Gobbini *et al.*, 2013]. Deletion of *SAE2* results in a resection defect that is stronger than that of *mre11-nd* (nuclease-dead, defective in nuclease activity) mutants. The explanation of this observation comes from different studies that demonstrate additional roles of Sae2 in end-tethering, Ku and MRX removal after DSB formation and in checkpoint activation [Clerici *et al.*, 2006; 2015; Puddu *et al.*, 2015; Chen *et al.*, 2015].

Short-range resection: focus on the MRX/N complex

MRX/N acts as a dimer [Hopfner *et al.,* 2002; Hohl *et al.,* 2011] with high affinity for DNA ends, as shown *in vitro* assays [Trujillo *et al.*, 2003].

Mre11 exhibits 3'-5' exonuclease activity on dsDNA and 3'-5' endonuclease activity on ssDNA [Paull & Gellert, 1998; Trujillo *et al*., 1998]. Furthermore, we have shown that Mre11 possesses a C-linker domain that divides the protein into two distinct domains that mediate different functions of the MRX complex at DSBs [Marsella *et al.,* 2019]. While MRX recruitment at DSBs and its ability to promote resection are under the control of the N-terminal domain, the C-terminus influences the tethering activity of MRX by mediating the interaction between Mre11 and Rad50.

Rad50 possesses an ATPase domain that regulates conformation changes of the complex, controlling MRX functions in DSB resection, end-tethering, and DNA damage signalling [Deshpande *et al.*, 2014]. Rad50 presents two domains that interact to each other and are essential to bind ATP: the N-terminal Walker A domain and the C-terminal Walker B domain [DE Jager *et al.,* 2001]. The crystal structure of Mre11-Rad50 revealed that the Walker domains of two Rad50 molecules interact with two Mre11 molecules, forming a domain for DNA binding and for the nuclease activity of MRX. The central domain of Rad50, that divides the two Walker motifs, is characterized by two symmetrical coiled-coil domains that constitute the branches of the MRX complex [Lammens *et al.,* 2011; Deshpande *et al.,* 2014; Symington & Gautier, 2011]. These coiled-coil domains are separated by a Cys-X-X-Cys motif foundamental for the coordination of a Zinc atom. The coordination of this Zinc atom,

promoted by the two Rad50 subunits, bridges together two MRX complexes and, consequently, the two broken DNA ends [Hopfner *et al.*, 2002].

There are two different parts where Rad50 and Mre11 interact to form this complex: one is on the coiled-coil domain of Rad50 that interacts with the C-terminal of Mre11, the other is in the Rad50 ATPase domain that interacts with the Mre11 capping domain [Lammens *et al.*, 2011].

The ATPase domain of Rad50 is responsible for changes in MRX conformation. In fact, upon ATP binding, Rad50 closes into a rigid conformation, in which the head domains interact with each other and dimerize to form a central groove that can accommodate dsDNA. This conformation is responsible for high affinity binding to DNA. This Rad50 closed state (ATP-bound state) renders dsDNA inaccessible to the Mre11 nuclease active site and stimulates both DNA binding and tethering activities of the complex [Paull *et al.*, 2014]. When MRX is in this conformation, the resection process is inhibited. Consequently, the closed conformation promotes NHEJ and checkpoint activation. By contrast, ATP hydrolysis induces conformational changes that induces the split of Rad50 dimer (ADP-bound state) and DNA melting, allowing Mre11 access to DNA and initiation of DSB resection [Deshpande *et al.*, 2014; Symington *et al.*, 2014; Paull *et al.*, 2014] (Figure 6).

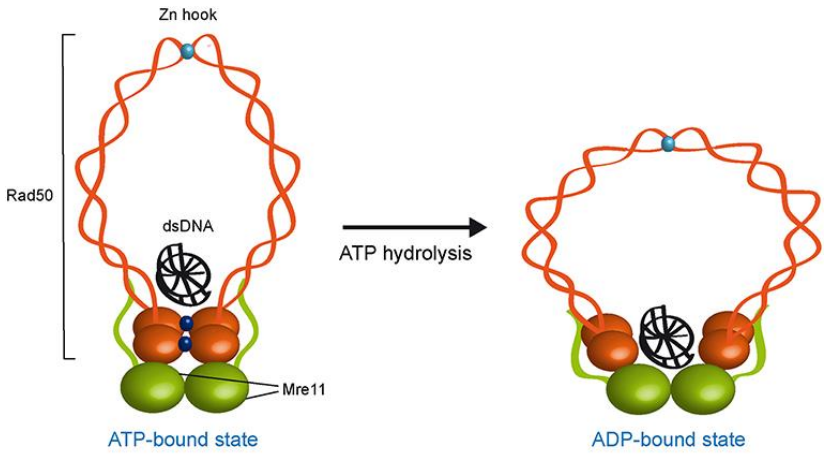

Figure 6. ATP- and ADP-bound state of the MRX complex [Casari *et al.*, 2019]. The Mre11 dimer (green) is bound to Rad50 dimer (orange) with a double-stranded DNA molecule located on the top surface of Rad50. The ATP-bound state of Rad50 supports DNA binding, end-tethering, and checkpoint signalling whereas it renders the dsDNA inaccessible to the Mre11 nuclease active sites and therefore negatively regulates Mre11 nuclease activity. ATP hydrolysis by Rad50 opens the complex to allow the Mre11 active sites to access DNA. Whether the ADP-bound state maintains an interlinked assembly is unknown. ATP molecules are indicated as blue dots. Zn^{2+} atoms are indicated as light blue dots. Xrs2 is not represented.

The last subunit of MRX is Xrs2/NBS1, which is the less conserved. Both Xrs2 and NBS1 are responsible for nuclear localization of Mre11, for the interaction with the checkpoint protein Tel1/ATM [see paragraph 'The DNA damage checkpoint response'] and for NHEJ function [Oh *et al.*, 2016], but seems to be dispensable for resection. Both Xrs2 and NBS1 contain BRCT and FHA domains separated from the motif that binds Mre11 and Tel1/ATM. Both domains can also bind the regulatory protein Sae2/CtIP [Symington & Gautier, 2011].

Long-range resection

Extensive resection of DSBs is promoted by the 5'-3' exonuclease Exo1 and by the endonuclease Dna2, with the latter acting with the 3'-5' helicase Sgs1/BLM. Exo1 and Dna2 control two partly redundant pathways [Mimitou & Symington, 2008; Zhu *et al.,* 2008]. Major defects in resection can be shown when both pathways are inactivated simultaneously, as in *exo1*Δ *sgs1*Δ double mutant [Zhu *et al.,* 2008; Mimitou & Symington, 2008].

Exo1 is a member of the XPG family of nucleases. Two *in vitro* studies showed that Exo1 is stimulated by both RPA and MRX [Nicolette *et al,* 2010; Cannavo *et al,* 2013]. RPA stimulates Exo1 by avoiding non-productive Exo1-ssDNA bindings, whereas MRX promotes DNA binding of Exo1 [Cannavo *et al,* 2013, Myler *et al.,* 2017]. Exo1 activity is stimulated by both RPA and MRX also i*n vivo,* even in the absence of the nuclease activity of Mre11 [Nicolette *et al,* 2010]. The increased Exo1 resection activity leads to a decreased association of the Ku complex to DSBs and to an enhanced DSB resection in the G1 phase, indicating that Exo1 has a direct function in preventing Ku association at DSBs. Molecular dynamics simulations show that rotation of the Mre11 capping domains can induce unwinding of dsDNA, indicating that MRX creates a specific DNA end structure that promotes Exo1 resection activity by facilitating the persistence of this nuclease on the DSB ends [Gobbini *et al.,* 2018]. Since Exo1 exerts its nuclease activity starting from dsDNA, no helicase activity has been required [Tran *et al.,* 2002].

Sgs1 is a DNA helicase of the RecQ family [Cejka & Kowalczykowski, 2010]. It translocates on one DNA strand and unwinds DNA in 3'-5' direction in an ATP-dependent manner. Sgs1 interacts with the topoisomerase Top3 and the

oligonucleotide/oligosaccharide-binding (OB)-fold protein Rmi1 to form the STR complex [Cejka *et al.*, 2010; Niu *et al.*, 2010]. However, in *S. cerevisiae*, only Sgs1 has been involved in the long-range resection, whereas Top3-Rmi1 plays only a structural and not a catalytic role [Zhu *et al.*, 2008]. In detail, the STR complex participates in the dissolution of dHJs to promote NCO products, preventing sister chromatid exchanges and chromosome instability.

The ssDNA formed by Sgs1 unwinding is degraded by the endonuclease Dna2 [Chen *et al.*, 2011]. Dna2 is a bifunctional helicase-nuclease, having both 3'-5' and 5'-3' nuclease activities and a DNA helicase activity with a 5'-3' polarity. Dna2 loads on a free ssDNA end and then degrades DNA endonucleolytically, generating products of 5-10 nucleotides [Zhu *et al.*, 2008; Niu *et al.*, 2010; Cejka *et al.*, 2010]. As Sgs1, also Dna2 has other functions unrelated to DNA end resection. It is responsible for removing DNA flaps that can be generated after strand displacement synthesis of DNA polymerase δ in lagging strand DNA synthesis. The Okazaki fragment processing function of Dna2 is essential, although the viability of *dna2*Δ mutants can be rescued by different mechanisms [Cejka, 2015].

Resection in humans is regulated by two pathways, like in *S. cerevisiae*. In one of them, BLM, the ortholog of Sgs1, and DNA2 physically interact and collaborate to resect the DSB ends, while MRN promotes resection by recruiting BLM to DNA ends [Nimonkar *et al.*, 2008]. In addition, DNA2 interacts with another RecQ family helicase, Werner (WRN). In the second pathway, MRN, RPA and BLM stimulate resection by promoting the action of EXO1, with BLM enhancing EXO1 affinity for DSB ends and MRN increasing EXO1 processivity [Nimonkar *et al.*, 2011]. Mutations in BLM are responsible for a recessive disease called Bloom syndrome [Bernstein *et al.*, 2010].

DNA resection: negative regulators

Negative regulators of DNA end resection prevent that nucleolytic degradation occurs in the wrong cell cycle phase and avoid excessive generation of ssDNA. As previously mentioned, Ku70/80 inhibits DSB resection in *S. cerevisiae* G1 cells. In addition, G1 cells lacking Ku show an enhanced Mre11 recruitment at the DSB ends [Gobbini *et al.*, 2013]. This imply that Ku and MRX compete for DSBs binding and that Ku restricts the formation of ssDNA by impairing the association and/or the activity of the resection factors.

Long-range resection is inhibited by the checkpoint protein Rad9 [see paragraph 'The DNA damage checkpoint response'], which behaves as a barrier for the long-range resection nucleases Exo1 and Sgs1/Dna2 [Lazzaro *et al.*, 2008; Lee *et al.*, 1998]. The ATP-dependent chromatin remodeler Fun30 can bypass the Rad9 barrier promoting both Exo1 and Sgs1/Dna2 resection activity [Chen *et al.*, 2012; Eapen *et al.*, 2012]. Extension of DSB resection is influenced also by histone H2A modifications. In fact, one way to recruit Rad9 at the sites of damage depends on Rad9 interaction with histone H2A phosphorylated on Ser129 (γH2A) [Shroff *et al.*, 2004; Javaheri *et al.*, 2006; Toh *et al.*, 2006; Hammet *at al.*, 2007]. In addition, the protein complex Slx4-Rtt107 can reduce Rad9 binding to chromatin by competing with Rad9 for the binding to γH2A [Symington, 2016]. Consequently, deletion of SLX4 and/or RTT107 decreases the efficiency of resection [Dibitetto *et al.*, 2016]. The actual model for DSBs end resection in yeast *S. cerevisiae* is summarized in Figure 7.

Similarly, the mammalian Rad9 ortholog, 53BP1, was found to inhibit DNA end resection. 53BP1 inhibits BRCA1-CtIP mediated resection during the G1 phase of the cell cycle by recruiting at DSB sites RIF1, a promoter of NHEJ [Di

Virgilio *et al.*, 2013; Zimmermann *et al.*, 2013]. Instead, during the S/G2 phase, BRCA1-CtIP, activated through CDK1-dependent phosphorylation, lead to the removal of 53BP1-RIF1 from the DNA ends, allowing the resection to start [Krishnaprasad *et al.*, 2014].

Recently, other two 53BP1 partners have been identified and involved in resection inhibition: PTIP and REV7/MAD2L2 [Symington, 2016; Boersma *et al.*, 2015]. Another mammalian negative regulator of resection is the HELB protein, which is recruited to ssDNA by RPA and inhibits both EXO1 and BLM-DNA2 [Tkáč *et al.*, 2016].

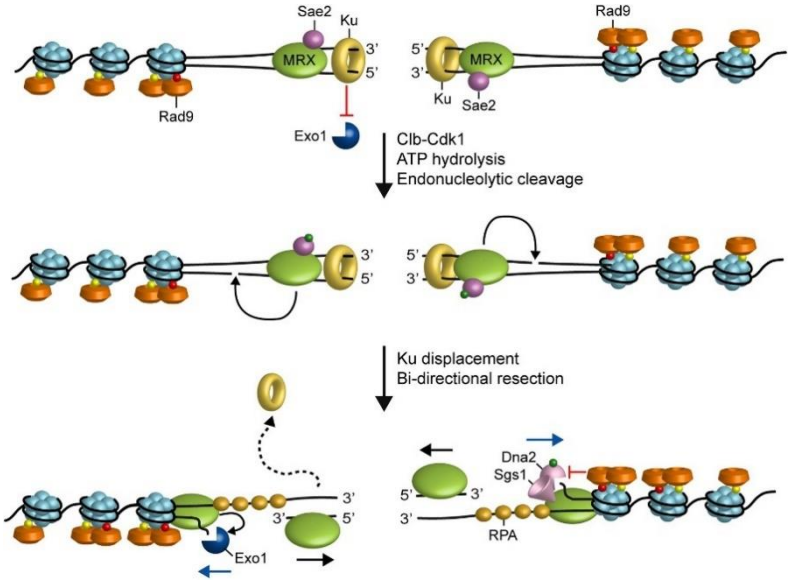

Figure 7. Model for resection of DNA double-strand breaks [Adapted from Bonetti *et al.*, 2018].

The first proteins recruited to the DSB are MRX, Sae2 and Ku. Ku inhibits Exo1 access to DNA ends, while Rad50, in its ATP-bound state, blocks the Mre11 nuclease activity. After ATP hydrolysis by Rad50, Mre11 catalyses the endonucleolytic cleavage of the 5'-strands of the DSB. Mre11-dependent processing is promoted by Sae2, after phosphorylation by Cdk1. The first incision by MRX-Sae2 creates an entry site for Exo1 and Sgs1-Dna2, that process DNA in the 5'-3' direction from the nick (blue arrows), while MRX degrades in the 3'-5' direction toward the DSB ends (black arrows). The MRX complex also promotes Exo1 and Sgs1-Dna2 association at the DSB ends, where Rad9 inhibits their resection activity.

The DNA damage checkpoint response

The DDR comprises also surveillance mechanisms called DNA damage checkpoints that, when activated by DNA damage, can induce transient cell cycle arrest until the DNA damage is repaired. In addition, activation of the DNA damage checkpoint induces activation of transcription and promotes DNA repair or, if the damage is unrepairable, cellular senescence or programmed cell death (apoptosis) [Ciccia & Elledge, 2010].

In *S. cerevisiae*, there are three different DNA damage checkpoints during the cell cycle: a) the G1/S checkpoint slows down the G1/S transition [Fitz Gerald *et al.*, 2002] by delaying bud emergence, spindle pole body duplication and S-phase entry, thus giving time to repair lesions before initiation of DNA replication [Fitz Gerald *et al.*, 2002]; b) the intra-S phase checkpoint controls origin firing and stabilizes the replisome on damaged DNA to ensure an efficient recovery of DNA replication once the lesions are repaired; c) the G2/M checkpoint slows down the metaphase to anaphase transition, avoiding cells to separate damaged sister chromatids. These three DNA damage checkpoints are conserved from yeasts to humans and share many components: (i) sensors that detect the presence of DNA lesions and initiate the transduction cascade; (ii) transducers, typically protein kinases, that transmit and amplify the damage signal by phosphorylating other kinases and/or downstream target proteins; (iii) effectors that include downstream targets of the transducer protein kinases [Nyberg *et al.*, 2002].

Key players in the checkpoint response are the yeast Tel1 and Mec1, orthologs of ATM (Ataxia-Telangiectasia-Mutated) and ATR (ATM and Rad3-related) respectively, in mammals. Both Tel1 and Mec1 are activated by DNA damage,

but if Tel1 senses unprocessed DSBs, Mec1 recognizes a broad spectrum of DNA lesions that induces the generation of ssDNA [Ciccia & Elledge, 2010]. In cooperation with accessory proteins, these kinases respond to DNA damage by phosphorylating downstream effectors [Ciccia & Elledge, 2010].

Mec1/ATR and Tel1/ATM are members of the PIKK family, whose consensus motif for phosphorylation is hydrophobic-X-hydrophobic-[S/T]-Q. The PIKK enzymes are large proteins (270-450 kDa) characterized by N-terminal HEAT repeat domains followed by kinase domains [Lempiäinen & Halazonetis, 2009]. The kinase domain is in the C-terminus and is flanked by two regions called FAT (FRAP, ATM, TRRAP) and FATC (FAT C-terminus), which can interact and contribute to the regulation of the kinase activity [Bosotti *et al.*, 2000]. The remaining part of each protein consists of multiple α-helical HEAT repeats [Perry & Kleckner, 2003], which mediate protein-DNA interactions.

Tel1/ATM activation requires the MRX/N complex. In fact, cells defective in any MRX/N component show defects in Tel1/ATM activation, even if only the interaction with the C-terminal domain of Xrs2/NBS1 is required to recruit Tel1/ATM at DSBs [Nakada *et al.*, 2003; Lee *et al.*, 2005].

ATM has an important function in human, as ATM deficiency results in Ataxia-Telangiectasia [Savitsky *et al.*, 1995], a rare, autosomal recessive disorder characterized by progressive cerebellar ataxia, neurodegeneration, radiosensitivity, checkpoint defects, genome instability and cancer predisposition. However, *TEL1* defective yeast cells do not show hypersensitivity to DNA damaging agents or impaired checkpoint activation in response to a single DSB [Mantiero *et al.*, 2007]. This can be explained by the ability of yeast cells to rapidly resect the DSB ends to generate ssDNA that stimulate Mec1 kinase activity. Full activation of human ATM is also dependent on autophosphorylation on Ser1981, resulting in dissociation of the

two ATM dimer into active monomers [Bakkenist *et al.,* 2003]. Besides Ser1981, also autophosphorylation of Ser367, Ser1893 and Ser2996 play a role in ATM activation.

In both yeast and mammals, Mec1/ATR is the main checkpoint kinase activated in response to a broad spectrum of DNA lesions. Mec1/ATR recruitment at the DSB sites requires the presence of RPA-coated ssDNA 3'-overhangs. Recognition of ssDNA by Mec1/ATR depends on an Mec1/ATR interacting protein, called Ddc2 in *S. cerevisiae* and ATRIP in mammals. Loss of Ddc2/ATRIP causes the same phenotypes as loss of Mec1/ATR, indicating that Ddc2/ATRIP is required for full Mec1/ATR activity [Gobbini *et al.,* 2013]. Also the co-localization of Mec1-Ddc2 with the 9-1-1 complex at damage sites directly stimulates Mec1 kinase activity [Navadgi-Patil & Burgers, 2009; Finn *et al.,* 2012]. 9-1-1 is an heterotrimeric ring-shaped complex (Ddc1-Rad17-Mec3 in *S. cerevisiae*; RAD9-RAD1-HUS1 in humans) that is loaded at the junctions between ssDNA and dsDNA by the RFC-like clamp loader (Rad24-Rfc2-5 in *S. cerevisiae* and RAD17- RFC2-5 in mammals).

In humans, mutations in ATR are associated with Seckel syndrome, a disorder characterized by growth retardation and severe microcephaly [O'Driscoll *et al.,* 2003].

As previously mentioned, Tel1/ATM recognizes unprocessed DSBs, while Mec/ATR activation requires the presence of RPA-coated ssDNA, produced by DSB resection. For these reasons, the resection process is crucial for the choice between Tel1/ATM and Mec1/ATR activation. In *S. cerevisiae,* when a DSB occurs, the MRX complex recruits Tel1 and activates a Tel1-dependent DNA damage checkpoint. Tel1 helps the activity of the MRX complex by structurally stabilizing it on DNA. The ssDNA created by Exo1 and Sgs1-Dna2 is covered by RPA and recruits Mec1. Mec1 can also regulate the generation of ssDNA

inducing Mec1-dependent phosphorylation of Sae2 [Clerici *et al.,* 2006]. Thus, as resection process takes place, there is a switch from Tel1 to Mec1 signalling (Figure 8).

Mec1/ATR and/or Tel1/ATM promote the activation of the effector kinases Rad53 and Chk1 (CHK2 and CHK1 in vertebrate). In *S. cerevisiae*, Mec1 and Tel1 activate both Rad53 and Chk1, while in humans ATM and ATR stimulate CHK2 and CHK1, respectively. Rad53 is essential for the response to DNA damage in all cell cycle phases and to replication blocks, while Chk1 is required only for the DNA damage G2/M checkpoint. On the contrary, CHK1, phosphorylated on Ser317/Ser345, is the primary effector of both the DNA damage and replication checkpoints in vertebrates, whereas CHK2 plays a minor role [Finn *et al.*, 2012]. When activated, Rad53 and Chk1 phosphorylate numerous downstream targets that are involved in cell cycle progression and transcriptional regulation. Rad53 belongs to a subfamily of protein kinases characterized by at least one phospho-Threonine recognition domain called ForkHead Associated (FHA). Rad53 contains two FHA domains, FHA1 and FHA2 [Durocher *et al.*, 1999]. Rad53 also contains two Serine-Glutamine/Threonine-Glutamine (SQ/TQ) cluster domains (SCD), potential targets of phosphorylation. Mammalian CHK2 is similar to Rad53 but it contains only one SCD and one FHA domain at the N-terminus. Mutations in the FHA2 domain reduces Rad53 phosphorylation, whereas mutations in FHA1 sensitizes cells to hydroxyurea and impairs the S-phase checkpoint [Sun *et al.*, 1998; Schwartz *et al.*, 2003]. Once activated, Rad53 can also inhibit Exo1 activity [Morin *et al.*, 2008] and restrict the access to the DSB of Sgs1-Dna2 (Figure 8).

Activation of the effector kinases Rad53 and Chk1 requires mediator proteins such as the BRCT-domain-containing proteins Rad9 (53BP1 in mammals) and

Mrc1 (Claspin in humans). Rad9 promotes Rad53 activation in response to DNA damage, whereas Mrc1 is specific for the response to replication stress. Recruitment of Rad9/53BP1 to chromatin includes different pathways. In absence of DNA damage, Rad9 is already present on DNA with an interaction between its Tudor domain and histone H3 methylated at residue Lys79 by Dot1 [Giannattasio *et al.*, 2005; Javaheri *et al.*, 2006; Hammet *et al.*, 2007; Granata *et al.*, 2010]. However, Rad9 binding to H3-K79me increases after damage formation. Rad9 binding is also stimulated by the interaction between its BRCT domain and phosphorylated Ser129 residue of histone H2A (γH2A) by Mec1/ATR [Javaheri *et al.*, 2006; Toh *et al.*, 2006; Hammet *et al.*, 2007]. This recruitment spreads to many kilobases around the DNA break [Shroff *et al.*, 2004]. It is important to underline that Mec1 phosphorylation on histone H2A induces Rad9 recruitment that inhibits Exo1 [Eapen *et al.*, 2012] (Figure 8). Finally, Rad9 is recruited to chromatin through an interaction with Dpb11 (TopBP1 in mammals) [Granata *et al.*, 2010], which is recruited at the break site by the 9-1-1 complex. Dpb11-Rad9 interaction requires cyclin-dependent kinase (Cdk1)-mediated Rad9 phosphorylation on the S462 and T474 residues, which bind directly to the N-terminal domain of Dpb11 [Pfander & Diffley, 2011]. Rad9 contribute to Chk1 activation with a mechanism involving its N-terminal portion, not required for Rad53 activation [Harrison & Haber, 2006]. Rad9 phosphorylation also generates a binding site for Rad53, which then undergoes in-trans activation. Rad53 is then released from the phosphorylated Rad9 in an ATP-dependent manner [Gilbert *et al.*, 2001].

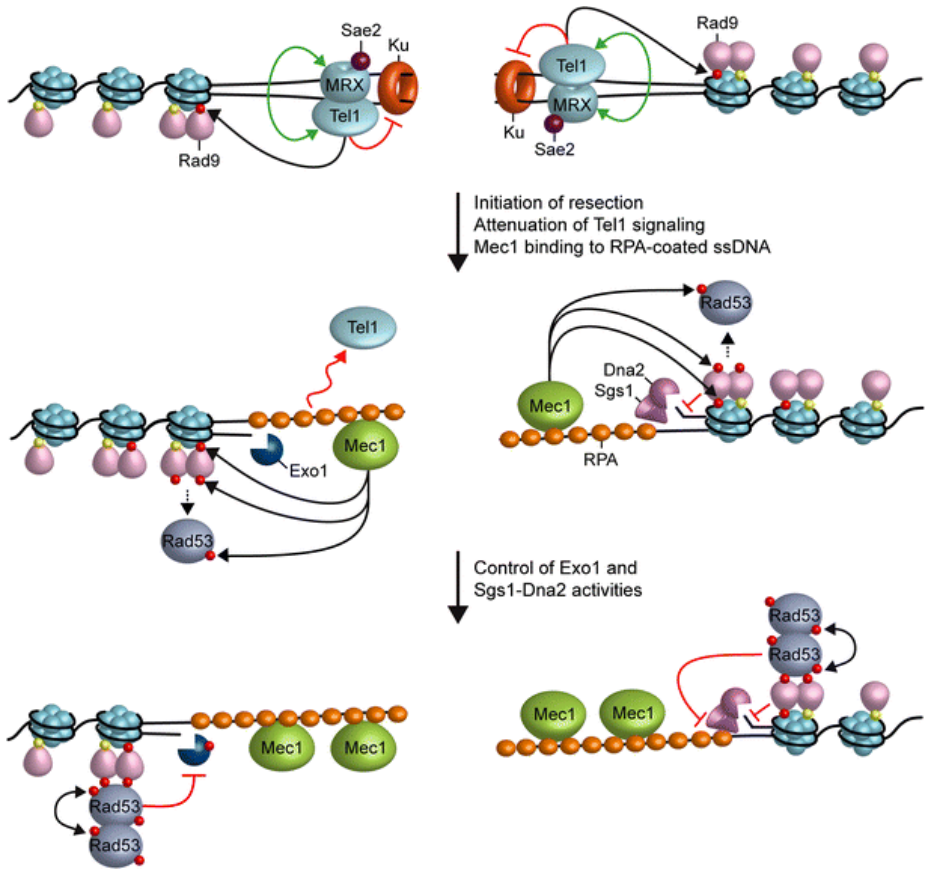

Figure 8. Interplays between end resection and checkpoint [Adapted from Villa *et al.*, 2016].
Rad9 is bound to methylated histone H3 (yellow dots) even in the absence of DSBs. When a DSB occurs, MRX/Sae2 localize to the DSB ends. MRX is required for the recruitment at DSBs of Tel1, which stabilizes MRX retention at DSBs in a positive feedback loop (double green arrows). Tel1 promotes the removal of Ku from the DSB and the initiation of resection and it contributes to the recruitment of Rad9 to the DSB ends through γH2A generation (red dots). When DSB resection starts, the resulting 3′-ssDNA attenuates Tel1 signalling activity and, once coated by RPA, allows activation of Mec1. Activated Mec1 contributes to γH2A generation that leads to a further enrichment of Rad9 at DSBs, which provides a barrier to the resection activity of Sgs1-Dna2. Mec1 also phosphorylates Rad9 creating binding sites for Rad53, which undergoes in-trans autophosphorylation and activation (double black arrows). Mec1-dependent phosphorylation of Rad53 allows further autoactivation. Once activated, Rad53 counteracts DSB resection by phosphorylating and inhibiting Exo1 and by restricting the access to the DSB of Sgs1-Dna2 possibly by reducing Sgs1 binding to RPA-coated DNA. Phosphorylation events are indicated by black arrows and red dots.

Chromatin dynamics in DNA damage repair

The negatively charged DNA wraps with 147 bp around a protein core made of eight proteins defined as a histone octamer. This packaged DNA structure forms a higher order structure called chromatin. Each nucleosome is composed of two H2A, two H2B, two H3 and two H4 histones. They are formed by a conserved hydrophobic region, called histone fold domain. There is also another protein, histone H1, which stabilizes the nucleosome.

This chromatin structure raises the question as to how DNA end resection occurs in the context of chromatin [Casari *et al.,* 2019]. Chromatin surrounding DSBs undergoes extensive modification and several highly conserved nucleosome remodelers are recruited to DSBs. While some of them deposit covalent modifications on histone tails to facilitate DNA damage signaling and recruitment of repair components, others alter chromatin structure either by exchanging canonical histones with histone variants or by sliding or evicting nucleosomes [Hauer & Gasser, 2017]. These functions are carried out by proteins that use the energy of ATP hydrolysis to translocate on dsDNA and to disrupt histone-DNA contacts [Osley *et al.,* 2007; Narlikar *et al.,* 2013; Clapier *et al.,* 2017]. Chromatin remodelers not only act in the presence of DNA lesions, but also in physiological processes such as transcription or replication. Chromatin immunoprecipitation experiments support nucleosome disassembly near DSBs in both yeast and human cells [Li & Tyler, 2016; Tsabar *et al.,* 2016], suggesting that nucleosome eviction occurs during resection and that nucleosomes represent barriers to exonucleases activity. A key question is whether nucleosomes are evicted prior to the onset of resection or whether

chromatin remodelers help the resection machinery to navigate through chromatin, with nucleosome loss occurring because of nucleolytic degradation.
A genome-wide analysis of resection endpoints around Spo11-induced DSBs during yeast meiosis suggest that MRX-Sae2 catalyzes the endonucleolytic cleavage preferentially on an internucleosomal DNA region at +1 and +2 nucleosomes proximal to meiotic DSB ends [Mimitou *et al.*, 2017], suggesting that MRX preferably binds at nucleosome-free chromatin regions. Furthermore, MRX-Sae2 endonucleolytically cleaves the 5′ DNA strand bordering a nucleosome [Wang *et al.*, 2017], thus explaining the 100-nucleotide incremental cleavages detected at endonuclease-induced DSBs in *sgs1*Δ *exo1*Δ cells [Zhu *et al.*, 2008]. Thus, if nucleosomes are evicted near a DSB, their removal might occur after Mre11-dependent incision of the 5′-terminated strands. Consistent with a coexistence of both nucleosomes and MRX bound at DSB ends, single-molecule imaging studies have shown that MRX can diffuse along dsDNA even in the presence of nucleosomes [Myler *et al.*, 2017]. Interestingly, by using an *in vitro*-reconstituted chromatin assay, it has been shown that the presence of nucleosomes impedes resection by both Exo1 and Sgs1-Dna2, with Exo1-dependent resection much more strongly affected [Adkins *et al.*, 2013]. This finding suggests that nucleosome destabilization or removal occurs before nucleolytic processing by Exo1 (Figure 9), with a constraint on resection length based on how many nucleosomes are removed [Mimitou *et al.*, 2017].

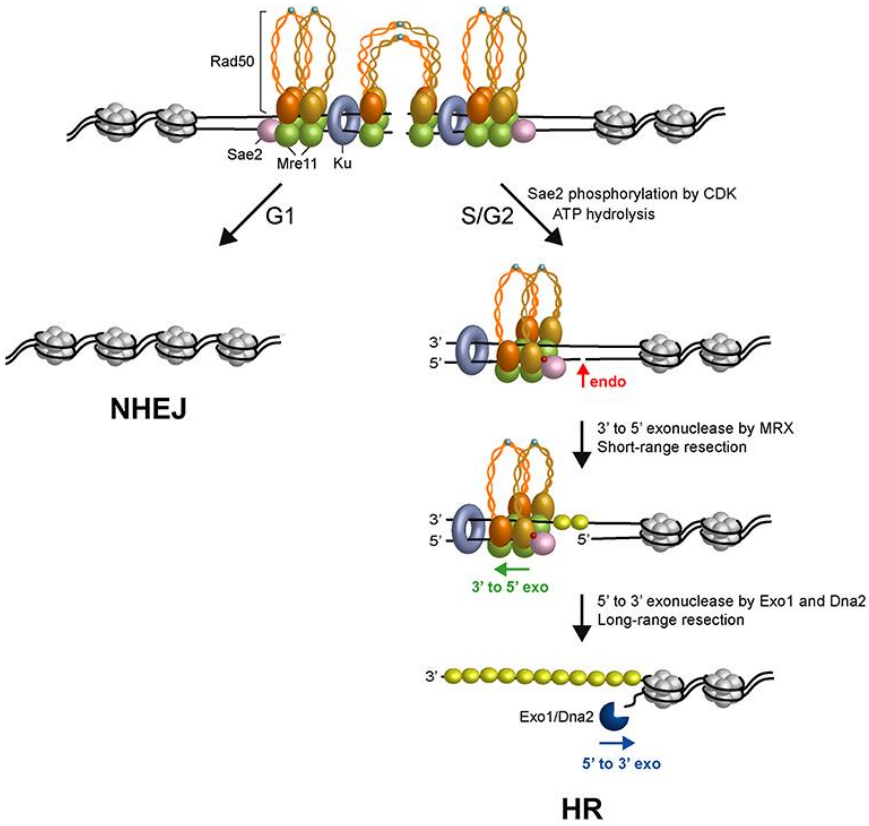

Figure 9. Model for DSB resection in a chromatin context [Casari *et al.*, 2019]. Two ATP-bound MRX complexes are loaded onto the DSB, with Ku and Sae2 proteins. Two Rad50 interact through the Zn-hook to form intra-linked complexes. The Zn-hook and coiled-coil domains may switch to form interlinked complexes that maintain the DSB ends tethered to each other. In the interlinked assembly, Mre11-Rad50 molecules are pictured separated from each other to visualize the DNA interruption. In G1, the DSB is repaired mainly by NHEJ because Sae2 is not phosphorylated, Rad50 is an ATP-bound state that blocks the Mre11 nuclease and Ku inhibits Exo1. In the S and G2 phases of the cell cycle, upon Sae2 phosphorylation by CDK and ATP hydrolysis by Rad50, Rad50 dimerization interface opens, and dsDNA becomes accessible to the Mre11 nuclease active sites. Phosphorylated Sae2 then stimulates the Mre11 endonuclease to incise the 5′-terminated strands (red arrows) at Ku-bound DNA ends or adjacent to nucleosomes. MRX proceeds back toward the DSB end using the Mre11 3′-5′ exonuclease activity. Exo1 or Sgs1-Dna2 nucleases then can degrade DNA in the 5′-3′ direction. ssDNA generated by resection is coated by RPA to initiate HR. Phosphorylation is indicated as red dots. $Zn2^{+}$ atoms are indicated as light blue dots. The Rad50 subunits belonging to a dimeric assembly are indicated with the same colour (orange or gold). Xrs2 is not represented.

Chromatin Remodelers and their mechanisms of action

Eukaryotes have four subfamilies of chromatin remodeling factors, namely SWI/SNF, INO80/SWR, ISW1, and CHD1.

The ATPase domain of SWI/SNF remodelers contains two RecA-type lobes and an N-terminal HSA (Helicase/SANT-Associated) domain. Furthermore, the ATPase subunit has two AT-hooks domains and a Bromine domain in the C-terminal, which respectively recognize AT regions of DNA and acetylated lysine residues on histones. Organisms usually have two subtypes of SWI/SNF remodelers. *S. cerevisiae* contains two closely related chromatin-remodeling complexes of this family, ySWI/SNF (SWItching defective and Sucrose NonFermenting) and RSC (Remodel the Structure of Chromatin) [Martens & Winston, 2002]. Both the RSC and the SWI/SNF complexes appear to promote MRX association with DSBs and subsequent DSB processing by catalyzing eviction or mobilization of nucleosomes adjacent to a DSB [Chai *et al.*, 2005; Shim *et al.*, 2007; Wiest *et al.*, 2017].

In yeast, the INO80/SWR subfamily includes two ATPases: Ino80 and Swr1. These proteins contain a variable insertion between the two RecA-type lobes and different binding domains acting as scaffolds for different interactors. INO80 complex is recruited to DSBs and participates in removal of nucleosomes to facilitate Rad51 nucleoprotein filament formation [Morrison *et al.*, 2004; van Attikum *et al.*, 2004, 2007; Tsukuda *et al.*, 2009]. Furthermore, two other remodelers have been shown to facilitate long-range resection: SWR-C complex by replacing the H2A/H2B dimers with H2A.Z/H2B in an ATP-dependent manner [Mizuguchi *et al.*, 2004] and Fun30/SMARCAD1 by

alleviating a Rad9-dependent chromatin barrier that inhibits Exo1 resection activity [Morillo-Huesca *et al.,* 2010; Chen *et al.,* 2012; Costelloe *et al.,* 2012; Eapen *et al.,* 2012; Adkins *et al.,* 2013]. In fact, the resection defect of *fun30*Δ cells is suppressed by elimination of Rad9.

Another subfamily of chromatin remodelers is ISWI. The remodelers of this family can contain from 2 to 4 subunits and the complexes consist of one or two different catalytic subunits, associated with specific proteins [Clapier & Cairns, 2009]. The translocation ATPase domain contains two RecA-type lobes and a C-terminal HAND-SANT-SLIDE domain, which recognizes unmodified histone H3 tail and the DNA linker that flanks the nucleosome.

In *S. cerevisiae*, there are two ATPases of the ISWI family, Isw1 and Isw2, that assembly in different complexes. The Isw1a complex is composed of Isw1 and Ioc3, while the Isw1b complex consists of Isw1, Ioc2, and Ioc4 [Mueller & Bryk, 2007]. The third complex, in the budding yeast, is ISW2 (hCHRAC in human [Poot *et al.,* 2000; Corona *et al.,* 2000]), in which the Isw2 ATPase assembles with the subunits Dpb4, Dls1 (Dpb3-like subunit 1) and Itc1 [Clapier & Cairns, 2009] (Figure 10).

ISW2 principally catalyzes nucleosome sliding. The Itc1 subunit can bind the DNA linker and the nucleosomal DNA. Its role is to determine the direction of nucleosomes displacement, orienting the ISW2 complex correctly on the DNA [Dang *et al.,* 2007]. The Dpb4 and Dls1 subunits are two histone fold like proteins that form a Dpb4-Dls1 heterodimer able to influence the activity of the ISW2 complex in nucleosome spacing, in the ability to identify the presence of an adjacent nucleosome and in regulation of remodeling. Furthermore, the Dpb4 subunit acts as an anchor for Isw2 and Itc1 binding to DNA [Dang *et al.,* 2007]. In the mammalian ISW2 complex, the catalytic hSNF2H subunit has been implicated in repair of DSBs by stimulating BRCA1 association with them

[Smeenk *et al.*, 2013], while the noncatalytic ACF1 subunit directly interacts with the NHEJ protein complex KU70/80 and promotes its accumulation to DSBs [Sánchez-Molina *et al.*, 2011; Lan *et al.*, 2010]. It is important to underling that Dpb4 is also part of the DNA polymerase ε (Pol ε) holoenzyme, which is largely responsible for leading-strand synthesis during DNA replication. Pol ε complex, which directly interacts also with Dpb11, consists of Pol2, Dpb2, Dpb4 (POLE3/CHRAC17 in mammals) and Dpb3 (POLE4 in mammals) [Muramatsu *et al.*, 2010; Goswami *et al.*, 2018; Yuan *et al.*, 2020], that is considered a Dls1 paralog [McConnell *et al.*, 2004] (Figure 10).

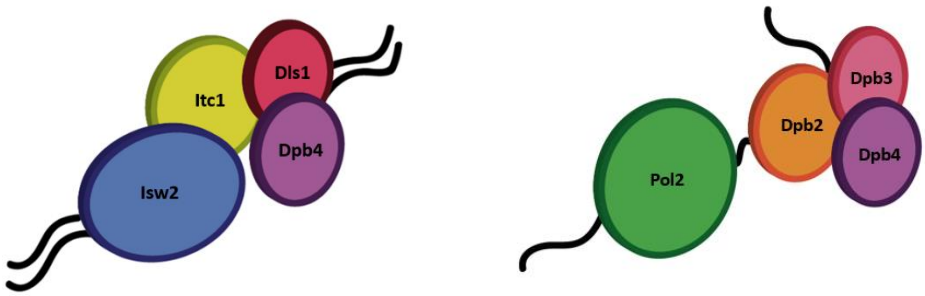

Figure 10. Schematic structure of the ISW2 complex and of the DNA Polymerase ε complex of *S. cerevisiae.*
The ISW2 complex with the Isw2, Itc1, Dls1 and Dpb4 subunits is shown on the left. On the right, the DNA Pol ε complex is shown, with the Pol2, Dpb2, Dpb3 and Dpb4 subunits.

Dpb3 and Dpb4 each contain a histone fold domain, through which they interact to form a H2A-H2B-like complex, that is not essential for cell viability in budding yeast [Araki *et al.*, 1991; Ohya *et al.*, 2000]. In both yeast and mammals, the Dpb3-Dpb4 complex binds H3-H4 tetramers and facilitates their

transfer onto the leading strand during DNA replication through an intrinsic chaperone activity [Bellelli *et al.*, 2018; Yu *et al.*, 2018].

In the replicative context, the two ancillary subunits Dpb3 and Dpb4, which interact to each other to form a heterodimer, stabilize the interaction between DNA Pol ε and DNA, indirectly influencing the replicative fidelity of the enzyme. Interestingly, genetic studies reveal a role for Dpb4 and Dpb3 in the maintenance of the chromatin silenced state [Iida & Araki, 2004; Tsubota *et al.*, 2006; He *et al.*, 2017], suggesting that a defect in parental H3-H4 transfer in *dpb3*Δ and *dpb4*Δ cells could compromise epigenetic inheritance. The maintenance of heterochromatin silencing also requires Pol2, the catalytic subunit of Pol ε [Iida & Araki, 2004; Tsubota *et al.*, 2006] and this function seems to be dependent upon Dpb3 and Dpb4, both able to bind double-stranded DNA and to increase Pol ε association to it [Tsubota *et al.*, 2003].

The last subfamily of chromatin remodelers is the evolutionary conserved chromodomain-helicase-DNA-binding protein 1 (Chd1), which is an ATP-dependent chromatin remodeling factor containing two N-terminal chromodomains, a split ATPase motor domain and the DNA binding SANT and SLIDE domains [Farnung *et al.*, 2017] (Figure 11).

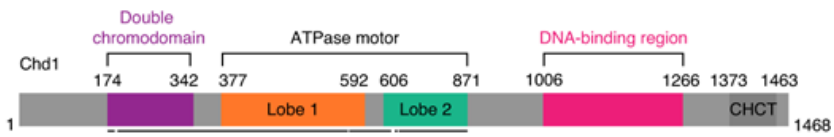

Figure 11. Chd1 domain architecture [Adapted from Farnung *et al.*, 2021].
Chd1 protein presents a double chromodomain in N-terminal followed by the ATPase motor constituted by two different lobes. The C-terminal region contains the DNA-binding region formed by SANT and SLIDE domains and the CHCT (CHD1 helical C-terminal domain) that can bind DNA and nucleosomes.

In contrast to most chromatin remodelers, Chd1 is active as a monomer and does not assemble as a multisubunit complex. Only one CHD protein is expressed in yeast (Chd1), although nine CHD proteins are found in vertebrates. CHD1, CHD2, CHD3, CHD4, CHD6 and CHD7 have been implicated in the cellular response to DNA damage. In particular, CHD2, CHD3, CHD4 and CHD7 accumulate at DNA regions flanking a DSB and stimulate the recruitment of proteins involved in NHEJ [Rother & van Attikum, 2017], whereas CHD6 is crucial in the signaling and transcriptional response to ROS [Moore *et al., 2019*].

Chd1 can assemble histones along DNA and induce a regular nucleosome spacing [Simic *et al.,* 2003; Lusser *et al.,* 2005; Gkikopoulos *et al.,* 2011; Lieleg *et al.,* 2015]. In yeast, Chd1 was shown to associate with RNA polymerase II elongation factors on actively transcribed genes. Chd1 is also important for the recycling of histones over coding regions during transcription [Radman-Livaja *et al.,* 2012; Smolle *et al.,* 2012; Lee *et al.,* 2017]. Experiments in yeasts have demonstrated that Chd1 is essential for generating spaced nucleosomes at the 5'-end of most genes [Gkikopoulos *et al.,* 2011; Hennig *et al.,* 2012; Pointner *et al.,* 2012; Shim *et al.,* 2012]. In addition to its role in transcription, Chd1 is also involved in other cellular processes.

In humans, CHD1 is one of the most frequently inactivated genes in prostate cancer [Burkhardt *et al.,* 2013; Grasso *et al.,* 2012; Huang *et al.,* 2012] and its loss sensitizes prostate cancer cells to chemotherapeutic DNA-damaging agents, suggesting a role in DSB repair [Shenoy *et al.,* 2017]. Consistent with this hypothesis, CHD1 is recruited to UV-damaged nucleosomes depending on the DNA binding protein XPC [Rüthemann *et al.,* 2017]. Furthermore, it promotes the repair of UV-damaged DNA by stimulating the handover between XPC protein and the TFIIH complex at DNA damaged sites [Rüthemann *et al.,*

2017]. CHD1 is recruited to chromatin in response to DSBs in an MRE11-dependent manner, where it promotes the loading of CtIP [Kari *et al.,* 2016; Zhou *et al.,* 2018]. Additionally, loss of CHD1 affects HR and decreases the assembly of RPA and RAD51 foci at DNA breaks and stalled replication forks [Kari *et al.,* 2016; Delamarre *et al.,* 2019], indicating a role in DSB resection.

Finally, in *S. cerevisiae*, Chd1 interacts with Exo1 and is implied in the generation of meiotic crossovers by allowing the processing of joint molecules by both Exo1 and the mismatch repair complex Mlh1-Mlh3 (MutLγ) [Wild *et al.,* 2019]. However, precisely how CHD1 activity remodels chromatin at DSBs remains to be determined.

RESULTS

Cell Reports

2020 Oct 20; 33(3):108287

doi: 10.1016/j.celrep.2020.108287

The 9-1-1 complex controls Mre11 nuclease and checkpoint activation during short-range resection of DNA double-strand breaks

Elisa Gobbini[1], **Erika Casari**[1], Chiara Vittoria Colombo[1],

Diego Bonetti[1], Maria Pia Longhese[1*]

[*] Corresponding Author

[1] Dipartimento di Biotecnologie e Bioscienze, Università degli Studi di Milano-Bicocca, Milano, 20126, Italy

DNA double-strand breaks (DSBs) can be repaired by homologous recombination (HR), which uses intact homologous duplex DNA as a template to restore the genetic information lost at the break site [Kowalczykowski, 2015; Mehta & Haber, 2014]. The first step of HR is the degradation of the 5′-terminated DNA strands on either side of the DSB to generate 3'-ended single-stranded DNA (ssDNA) tails through a process termed DNA end resection [Bonetti *et al.,* 2018].

In both yeast and mammals, DNA end resection can be a two-step process that involves sequential engagement of short-range and long-range nucleases [Bonetti *et al.,* 2018]. In short-range resection, the endonuclease activity of the Mre11-Rad50-Xrs2/NBS1 (MRX/N) complex, aided by the Sae2 protein (CtIP in mammals), cleaves the 5'-terminated DNA strand of the DSB end [Cannavo & Cejka, 2014], followed by the Mre11 3'-5' exonuclease that proceeds back towards the DSB end [Mimitou & Symington, 2008; Zhu *et al.,* 2008; Garcia *et al.,* 2011; Shibata *et al.,* 2014; Reginato *et al.,* 2017; Wang *et al.,* 2017]. Although this resection is limited to the vicinity of the DNA end, it has the capacity to process DNA ends with secondary DNA structures and bound protein blocks. The second phase is a long-range resection, which resects nucleotides in the 5'-3' direction away from the DSB ends and is carried out by either Exo1 or Dna2 in conjunction with the helicase Sgs1 (WRN or BLM in mammals) [Mimitou & Symington, 2008; *Zhu et al.,* 2008; Cejka *et al.,* 2010; Nicolette *et al.,* 2010; Niu *et al.,* 2010; *Nimonkar et al.,* 2011; Cannavo *et al.,* 2013; Reginato *et al.,* 2017; Wang *et al.,* 2017].

The resection activity of Sgs1-Dna2 is inhibited by the *S. cerevisiae* Rad9 protein (53BP1 in mammals) [Lazzaro *et al.,* 2008; Clerici *et al.,* 2014; Bonetti *et al.,* 2015; Ferrari *et al.,* 2015], whose association to chromatin involves multiple pathways. Rad9 interacts with histone H3 in its K79-methylated form

(H3-K79me) [Wysocki *et al.,* 2005; Grenon *et al.,* 2007], a chromatin modification that is introduced by the methyltransferase Dot1 [Giannattasio *et al.,* 2005; Toh *et al.,* 2006]. Rad9 can also bind to histone H2A that has been phosphorylated at Ser 129 (γH2A) by the checkpoint kinases Mec1 (ATR in mammals) and Tel1 (ATM in mammals) [Downs *et al.,* 2000; Shroff *et al.,* 2004; Toh *et al.,* 2006; Hammet *et al.,* 2007]. Finally, phosphorylation of Ser 462 and Thr 474 residues of Rad9 by cyclin-dependent kinase (Cdk1) leads to Rad9 interaction with the multi-BRCT domain protein Dpb11 (TopBP1 in mammals) [Granata *et al.,* 2010; Pfander & Diffley, 2011; Cussiol *et al.,* 2015]. Dpb11 in turn is recruited to DSBs by the evolutionarily conserved Ddc1-Mec3-Rad17 (Rad9-Hus1-Rad1 in mammals) complex (hereafter referred to as 9-1-1), which is a ring-shaped heterotrimer that is loaded at ssDNA-double-stranded DNA (dsDNA) junctions by the clamp loader Rad24 (RAD17 in mammals)-replication factor C subunits 2-5 (Rfc2-5) [Majka *et al.,* 2006; Navadgi-Patil & Burgers, 2009]. In budding yeast, the interaction between Dpb11 and 9-1-1 requires phosphorylation of Ddc1 Thr 602 and this phospho-dependent Dpb11-Ddc1 binding is conserved in mammals [Delacroix *et al.,* 2007; Puddu *et al.,* 2008; Navadgi-Patil & Burgers, 2009]. By promoting the association of Rad9 at DSBs, the 9-1-1 complex counteracts the resection activity of the long-range resection nucleases Exo1 and Dna2 [Ngo & Lydall, 2015]. Furthermore, Rad9, Dpb11 and 9-1-1 are required to activate the checkpoint kinase Mec1 (ATR in humans) [Mordes *et al.,* 2008; Navadgi-Patil & Burgers, 2008, 2009], which senses the presence of ssDNA via interaction with replication protein A (RPA) [Zou & Elledge, 2003] and activates the downstream effector kinases Rad53 (CHK2 in mammals) and Chk1 [Villa *et al.,* 2016].

Although much progress has been made in understanding the structural and functional activities of the MRX complex, how its nuclease activity is controlled remains to be determined. Furthermore, the physiological relevance of the long-range resection is not obvious, because although *exo1*Δ *sgs1*Δ budding yeast cells suffer sensitivity to DNA damaging agents, the 100-300 nucleotides of ssDNA generated by MRX-Sae2 cleavage events are sufficient for meiotic recombination and result only in a moderate decrease of ectopic recombination in vegetative growing *exo1*Δ *sgs1*Δ cells [Gravel *et al.,* 2008; Zhu e*t al., 2*008; Chung *et al.,* 2010; Zakharyevich *et al.,* 2010; Keelagher *et al.,* 2011; Westmoreland & Resnick, 2016; Guo *et al.,* 2017].

Here we show that failure of 9-1-1 to recruit Dpb11 and Rad9 at damaged sites partially restores DNA damage resistance of *exo1*Δ *sgs1*Δ cells by decreasing Rad53 activation. Furthermore, the lack of 9-1-1 extends DSB resection in *exo1*Δ *sgs1*Δ cells in a manner that depends on Mre11 nuclease activity, but not on 9-1-1 function in recruiting Dpb11 and Rad9 to DSBs. Altogether, these data lead to a model whereby 9-1-1 plays a dual function during short-range resection, promoting checkpoint activation by recruiting Rad9 at damaged sites and negatively regulating MRX nuclease.

Screen for suppressors of the DNA damage sensitivity of *exo1*Δ *sgs1*Δ cells

Budding yeast cells lacking both Exo1 and Sgs1 can generate only short 3'-ended ssDNA tails resulting from MRX-Sae2-dependent cleavage events [Zhu *et al.,* 2008; Mimitou & Symington, 2008; Guo *et al.,* 2017]. These cells show decreased viability even in the absence of DNA lesions. Moreover, they are hypersensitive both to the topoisomerase poison camptothecin (CPT), which leads to DSBs by stabilizing DNA topoisomerase I cleavage complexes, and to the ionizing radiation-mimetic compound phleomycin (phleo). To identify mechanisms responsible for the DNA damage hypersensitivity of *exo1*Δ *sgs1*Δ cells, we searched for extragenic mutations that suppress their CPT and/or phleomycin sensitivity. CPT- and/or phleomycin-resistant *exo1*Δ *sgs1*Δ clones were crossed to each other and to the wild-type strain to identify, by tetrad analysis, 20 single-gene suppressor mutants that fell into 8 distinct allelism groups. Genome sequencing of two non-allelic suppressor clones identified a *RAD24* single base-pair substitution, which introduces a STOP codon in place of Asp 334 (*rad24-E334**), and a *DPB11* single base-pair substitution, causing the replacement of Leu 410 residue with Phe (*dpb11-L410F*) (Figure 12A). The identity of the genes that are mutated in the remaining suppressor clones remains to be determined. As shown in Figure 12A, both *rad24-E334** and *dpb11-L410F* alleles partially suppressed the hypersensitivity to CPT and phleomycin of *exo1*Δ *sgs1*Δ cells. Suppression by the *rad24-E334** allele is likely due to loss of Rad24 function, as *RAD24* deletion suppressed the DNA damage sensitivity of *exo1*Δ *sgs1*Δ cells (Figure 12A). This test could not be performed for Dpb11 that is essential for cell viability.

The lack of 9-1-1-mediated recruitment of Dpb11 suppresses the DNA damage sensitivity of *exo1*Δ *sgs1*Δ cells

Rad24 is part of the Rad24-RFC clamp loader, which loads the 9-1-1 complex to the ssDNA-dsDNA junctions at DNA lesions [Majka *et al.*, 2006; Navadgi-Patil & Burgers, 2009]. Once loaded onto the DNA, the 9-1-1 clamp recruits Dpb11 to sites of DNA damage via interaction with Ddc1 [Wang & Elledge, 2002; Puddu *et al.*, 2008; Pfander & Diffley, 2011] (Figure 12B). The interaction between Dpb11 and 9-1-1 requires phosphorylation by Mec1 of Thr 602 of Ddc1, which is then recognized by the BRCT3 and 4 domains of Dpb11 (aa 276-600) [Puddu *et al.*, 2008]. As the *dpb11-L410P* mutation is located in the BRCT domain that mediates the interaction between Dpb11 and 9-1-1 [Pfander & Diffley, 2011], we asked whether 9-1-1 failure to recruit Dpb11 to damage sites was responsible for the suppression of *exo1*Δ *sgs1*Δ cells. The *ddc1-T602A* allele, which specifically abrogates 9-1-1 binding to Dpb11, partially suppressed the DNA damage sensitivity of *exo1*Δ *sgs1*Δ cells to an extent similar to that of *DDC1* deletion (Figure 12C). Thus, 9-1-1 failure to recruit Dpb11 to the damaged sites is sufficient to restore DNA damage resistance in *exo1*Δ *sgs1*Δ cells.

The lack of Dpb11-mediated recruitment of Rad9 suppresses the DNA damage sensitivity of *exo1*Δ *sgs1*Δ cells

The 9-1-1 complex can recruit Dpb11 to sites of DNA lesions, which in turn interacts with Rad9 (referred to as the 9-1-1 axis) [Puddu *et al.,* 2008; Pfander & Diffley, 2011] (Figure 12B). Dpb11-Rad9 interaction requires Cdk1-mediated phosphorylation of Rad9 Ser 462 and Thr 474 residues, which bind directly to the N-terminal BRCT repeats 1 and 2 of Dpb11 [Pfander & Diffley, 2011] (Figure 12B). To evaluate whether *exo1*Δ *sgs1*Δ suppression depends on the lack of Dpb11-Rad9 interaction, we used a *dpb11* allele lacking the BRCT 1 and 2 domains (*dpb11-*Δ*N*) and the *rad9-S462A, T474A* allele (*rad9-STAA*), encoding a Rad9 mutant variant that fails to interact with Dpb11 [Pfander & Diffley, 2011]. Both *dpb11-*Δ*N* and *rad9-STAA* alleles were able to suppress the DNA damage hypersensitivity of *exo1*Δ *sgs1*Δ cells to extents similar to those of *dpb11-L410F* and *rad24*Δ alleles (Figure 12D), indicating that the lack of Dpb11-Rad9 interaction is responsible for the suppression.

Rad9 recruitment to sites of DNA damage relies also on Rad9 interaction with histone γH2A [Downs *et al.,* 2000; Toh *et al.,* 2006; Hammet *et al.,* 2007] and with histone H3 methylated at Lys79 by the methyltransferase Dot1 [Wysocki *et al.,* 2005; Grenon *et al.,* 2007; Giannattasio *et al.,* 2005]. We investigated the contribution of these two pathways in the DNA damage sensitivity of *exo1*Δ *sgs1*Δ cells by analyzing the effect of abrogating Rad9 binding to H3-K79me or γH2A. The lack of *DOT1* (Figure 13A) or the expression of *hta1-S129A* (Figure 13B), which abolishes H3-K79me and γH2A generation, respectively, did not suppress the DNA damage sensitivity of *exo1*Δ

*sgs1*Δ cells. Rather, *hta1-S129A exo1*Δ *sgs1*Δ cells were more sensitive to DNA damaging agents compared to *exo1*Δ *sgs1*Δ cells (Figure 13B). Altogether, these data indicate that Rad9 recruitment to damaged sites by Dpb11 is particularly detrimental in *exo1*Δ *sgs1*Δ cells.

The lack of Fun30 exacerbates the DNA damage sensitivity of *exo1*Δ *sgs1*Δ cells in a Rad9-dependent manner

The Swr1-like family remodeler Fun30 (SMARCAD1 in mammals) interferes with Rad9 function at DSBs [Costelloe *et al.,* 2012; Eapen *et al.,* 2012; Bantele *et al.,* 2017]. In particular, the lack of Fun30 increases the association of Rad9 to DSBs [Chen *et al.,* 2012; Dibitetto *et al.,* 2016]. The finding that Fun30 and Rad9 share the same interaction site on Dpb11 [Pfander & Diffley, 2011] suggests that Fun30 might interfere with Rad9 function by competition. We then investigated the effect of *FUN30* deletion in *exo1*Δ *sgs1*Δ cells. *FUN30* deletion exacerbated the DNA damage sensitivity of *exo1*Δ *sgs1*Δ cells (Figure 12E). The increased DNA damage sensitivity of *fun30*Δ *exo1*Δ *sgs1*Δ triple mutant cells requires Rad9-Dpb11 interaction. In fact, *fun30*Δ *exo1*Δ *sgs1*Δ cells expressing the *rad9-STAA* allele, which abrogates Rad9-Dpb11 interaction and suppresses the DNA damage hypersensitivity of *exo1*Δ *sgs1*Δ cells, were as resistant to DNA damaging agents as *rad9-STAA exo1*Δ *sgs1*Δ cells (Figure 12F). These findings further support the hypothesis that the Dpb11 function in recruiting Rad9 at sites of DNA lesions is detrimental when long-range resection is defective.

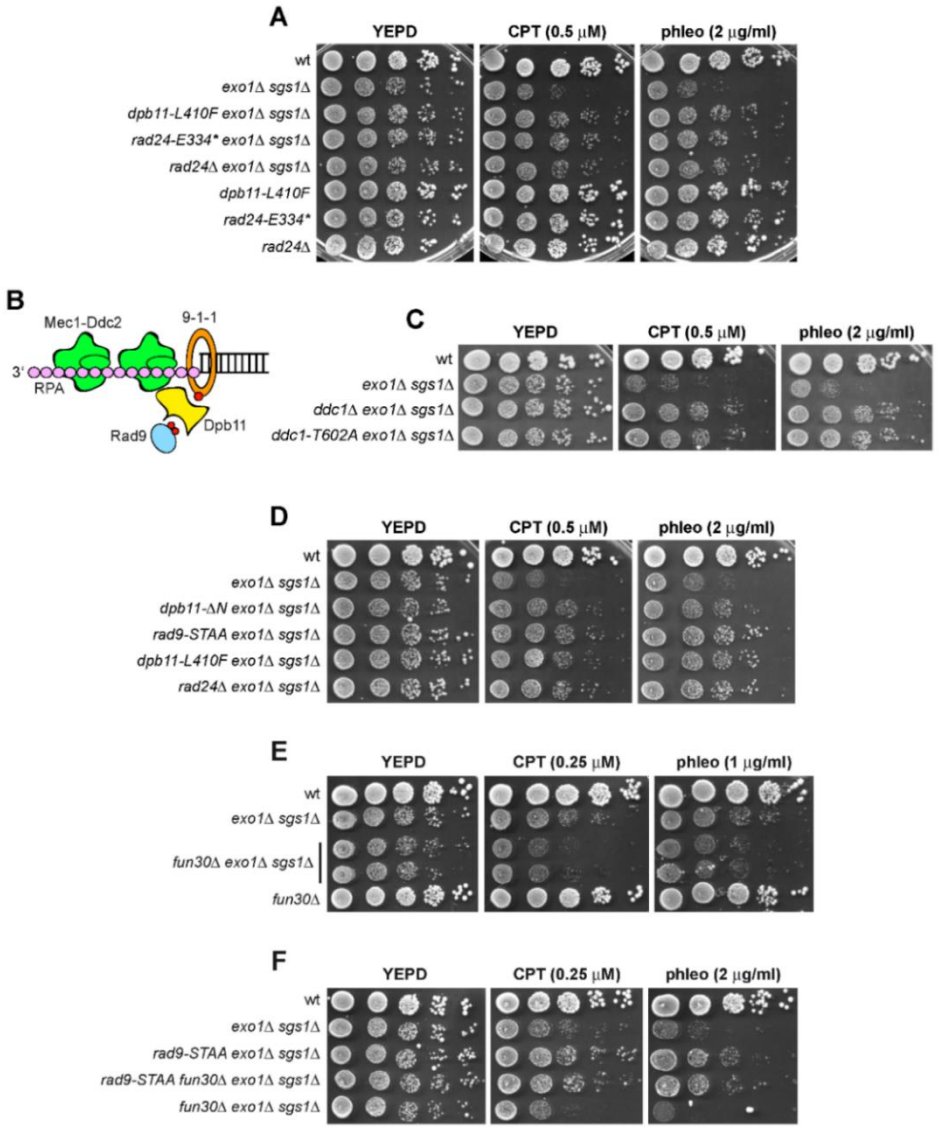

Figure 12. Failure of 9-1-1 to recruit Dpb11 and Rad9 partially suppresses the DNA damage sensitivity of *exo1*Δ *sgs1*Δ cells.
(A) Exponentially growing cultures were serially diluted (1:10) and each dilution was spotted out onto YEPD plates with or without CPT or phleomycin. (B) The 9-1-1 axis. The 9-1-1 complex recruits Dpb11 to the 5'-recessed end of a DSB, which in turn contributes to the association of Rad9 to DSBs. Red dots indicate phosphorylation events. (C-F) Exponentially growing cultures were serially diluted (1:10) and each dilution was spotted out onto YEPD plates with or without camptothecin (CPT) or phleomycin (phleo).

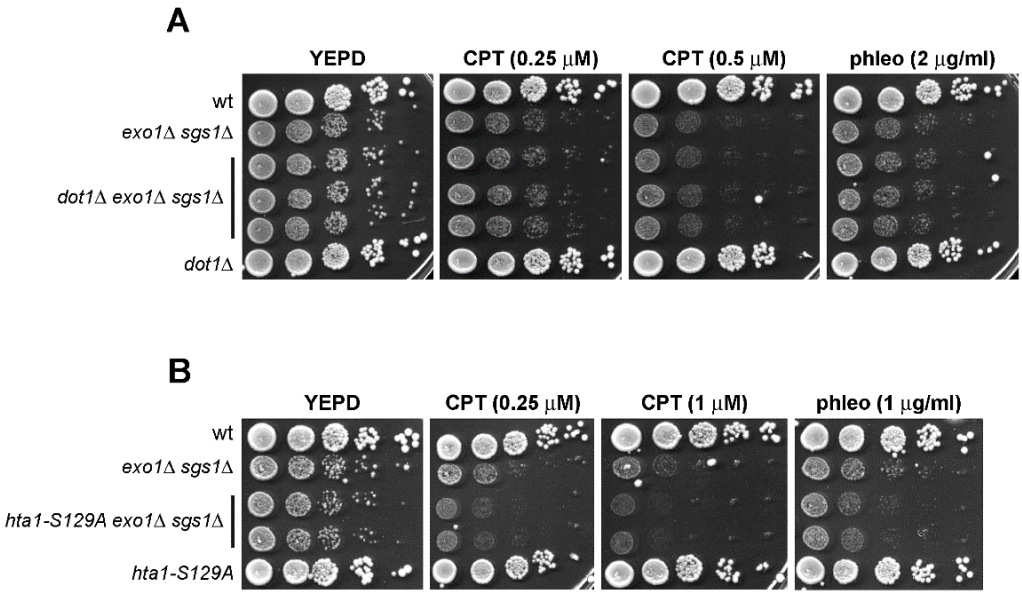

Figure 13. Abrogation of H3-K79 methylation or γH2A did not suppress the DNA damage sensitivity of *exo1*Δ *sgs1*Δ cells.
(A,B) Exponentially growing cells were serially diluted (1:10) and each dilution was spotted onto YEPD plates with or without CPT or phleomycin at the indicated concentrations.

The lack of both Exo1 and Sgs1 hyperactivates the checkpoint in response to DNA damaging agents

DSB formation leads to the activation of a checkpoint response that depends primarily on Mec1, which binds RPA-coated ssDNA and promotes Rad53 activation [Zou & Elledge, 2003]. Rad9 links the signal transduction from Mec1 to Rad53 by acting as a scaffold to allow Rad53 intermolecular autophosphorylation and activation [Gilbert *et al.,* 2001; Sweeney *et al.,* 2005; Schwartz *et al.,* 2002]. The lack of both Exo1 and Sgs1 has been reported to impair Rad53 activation in response to a single site-specific DSB [Zhu *et al.,* 2008; Gravel *et al.,* 2008; Bantele *et al.,* 2019]. Thus, we evaluated the ability of *exo1*Δ *sgs1*Δ cells to phosphorylate Rad53 not only after generation of a single DSB but also after genotoxic treatments. To induce a single unrepaired DSB, we used JKM139 derivative strains that express the site-specific HO (homothallic switching) endonuclease gene from a galactose-inducible promoter. Galactose addition leads to HO induction that catalyzes a single DSB at the *MAT* locus. The HO cut cannot be repaired by HR because the homologous donor sequences *HML* and *HMR* are deleted. Consistent with previous data [Zhu *et al.,* 2008; Gravel *et al.,* 2008; Bantele *et al.,* 2019], Rad53 phosphorylation, which is required for checkpoint activation and is detectable as a decrease of Rad53 electrophoretic mobility, was lower in *exo1*Δ *sgs1*Δ cells than in wild-type cells after HO induction (Figure 14A). By contrast, when methyl methanesulphonate (MMS) or phleomycin was added to exponentially growing cells, Rad53 phosphorylation was higher in *exo1*Δ *sgs1*Δ cells than in wild-type cells (Figure 14B,C). A certain level of Rad53 phosphorylation was

detectable in *exo1*Δ *sgs1*Δ cells even in the absence of DNA damage, possibly due to DNA replication defects (Figure 14B,C).

Interestingly, replication of damaged DNA template is not responsible for checkpoint activation in phleomycin-treated *exo1*Δ *sgs1*Δ cells. In fact, significant changes in Rad53 electrophoretic mobility could be detected after phleomycin treatment of G2-arrested *exo1*Δ *sgs1*Δ cells that were kept in G2 after phleomycin addition (Figure 14D). This Rad53 phosphorylation depends mainly on Mec1, as Rad53 phosphorylation was dramatically reduced when phleomycin was added to G2-arrested *mec1*Δ *exo1*Δ *sgs1*Δ cells (kept viable by *SML1* deletion) (Figure 14D). Since Mec1 is known to activate Rad53 in a manner that strongly depends on the ssDNA length [Pellicioli *et al.,* 2001; Bantele *et al.,* 2019], this finding suggests that nucleases other than Exo1 and Dna2 are responsible for ssDNA generation to induce Mec1 activation in *exo1*Δ *sgs1*Δ cells. DSB resection in *exo1*Δ *sgs1*Δ cells depends on Mre11 nuclease activity [Zhu *et al.,* 2008; Mimitou & Symington, 2008)] and phleomycin addition failed to induce Rad53 phosphorylation in G2-arrested *exo1*Δ *sgs1*Δ cells expressing the *mre11-H125N* nuclease-dead allele (*mre11-nd*) (Figure 14D). This finding indicates that the Mre11 processing activity is responsible for ssDNA generation and checkpoint activation in *exo1*Δ *sgs1*Δ cells. Since resection in *exo1*Δ *sgs1*Δ cells by Mre11 nuclease is limited to the vicinity of the DSB ends [Zhu *et al.,* 2008; Mimitou & Symington, 2008], the amount of ssDNA generated at the ends of a single DSB could not reach the threshold level for Mec1 activation, thus explaining the inability of *exo1*Δ *sgs1*Δ cells to activate the checkpoint in response to a single DSB. By contrast, processing by Mre11 nuclease of the multiple DNA lesions caused by exposure to DNA

damaging agents should generate higher total amount of ssDNA that can be enough to activate Mec1.

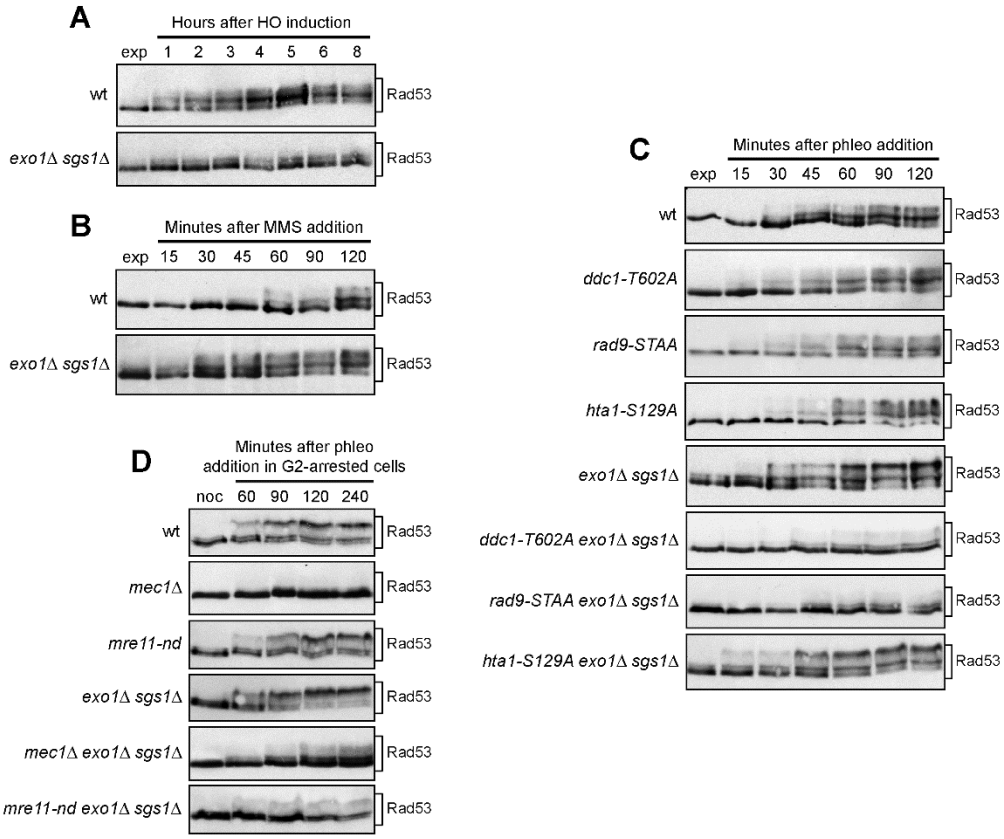

Figure 14. Checkpoint activation in *exo1Δ sgs1Δ* cells depends primarily on 9-1-1 function in recruiting Dpb11 and Rad9 at damaged DNA.
(A) HO expression was induced after galactose addition and protein extracts were analyzed by western blot using anti-Rad53 antibodies. (B-C) MMS (0.015%) (B) or phleomycin (10 µg/ml) (C) was added to exponentially growing cells and protein extracts were analyzed by western blot using anti-Rad53 antibodies. (D) Phleomycin (10 µg/ml) and nocodazole (15 µg/ml) were added to nocodazole-arrested cell cultures. Protein extracts were analyzed by western blot using anti-Rad53 antibodies.

The lack of 9-1-1 axis suppresses the DNA damage sensitivity of *exo1*Δ *sgs1*Δ cells by dampening Rad53 activation

Rad9 is recruited to chromatin by binding to H3-K79me, γH2A and Dpb11 [Puddu *et al.*, 2008; Mordes *et al.*, 2008; Navadgi-Patil & Burgers, 2008; Pfander & Diffley, 2011]. Previous studies have shown that Dpb11 acts redundantly with Dot1 in promoting Rad53 activation in response to genotoxic treatments [Puddu *et al.*, 2008; Pfander & Diffley, 2011]. Consistent with this finding, Rad53 phosphorylation in phleomycin-treated *ddc1-T602A* and *rad9-STAA* cells was similar to that observed in wild-type cells (Figure 14C). Surprisingly, the presence of either the *rad9-STAA* or the *ddc1-T602A* allele dramatically decreased Rad53 phosphorylation in phleomycin-treated *exo1*Δ *sgs1*Δ cells compared not only to *exo1*Δ *sgs1*Δ but also to wild-type cells (Figure 14C). By contrast, the *hta1-S129A* allele did not decrease Rad53 phosphorylation in response to phleomycin addition either in the presence or in the absence of Exo1 and Sgs1 (Figure 14C). Altogether, these findings indicate that *exo1*Δ *sgs1*Δ cells activate a checkpoint in response to genotoxic treatments that is stronger than wild-type cells and that depends primarily on the 9-1-1 axis.

The importance of the 9-1-1 axis in Rad53 activation in *exo1*Δ *sgs1*Δ cells prompted us to investigate whether the *ddc1-T602A* and *exo1*Δ *sgs1*Δ *rad9-STAA* alleles restore DNA damage resistance of *exo1*Δ *sgs1*Δ cells by dampening the checkpoint response. If this were the case, inactivation of Rad53 kinase activity should restore DNA damage resistance of *exo1*Δ *sgs1*Δ cells. Furthermore, enforcing Rad53 recruitment to damaged DNA independently of

both Rad9 and 9-1-1 by fusing Rad53 with the Mec1 regulatory subunit Ddc2 [Lee *et al.*, 2004], should re-sensitize *exo1*Δ *sgs1*Δ *rad24*Δ and *exo1*Δ *sgs1*Δ *rad9-STAA* mutants to DNA damaging agents. Indeed, we found that expression of the *rad53-K227A* (*rad53-kd*) allele, which specifically impairs Rad53 kinase activity, suppressed the sensitivity of *exo1*Δ *sgs1*Δ cells to CPT and phleomycin treatments (Figure 15A). Furthermore, *exo1*Δ *sgs1*Δ *rad9-STAA* and *exo1*Δ *sgs1*Δ *rad24*Δ mutants, transformed with a plasmid carrying a DDC2-RAD53 in-frame fusion, were more sensitive to DNA damaging agents compared to *exo1*Δ *sgs1*Δ *rad9-STAA* and *exo1*Δ *sgs1*Δ *rad24*Δ transformed with an empty vector (Figure 15B). These findings indicate that checkpoint hyperactivation can account for the increased DNA damage sensitivity of *exo1*Δ *sgs1*Δ cells and that the lack of 9-1-1 ability to recruit Dpb11 and Rad9 at damaged sites can restore DNA damage resistance of *exo1*Δ *sgs1*Δ cells by inhibiting checkpoint activation.

Interestingly, neither *RAD9* nor *MEC1* deletion suppressed the DNA damage hypersensitivity of *exo1*Δ *sgs1*Δ cells (Figure 15C,D). Rather, both *rad9*Δ *exo1*Δ *sgs1*Δ and *mec1*Δ *exo1*Δ *sgs1*Δ triple mutants (kept viable by *SML1* deletion) were more sensitive to phleomycin and MMS than *exo1*Δ *sgs1*Δ cells (Figure 15C,D), suggesting that Rad9 and Mec1 have additional Rad53-independent functions in supporting DNA damage resistance of *exo1*Δ *sgs1*Δ cells.

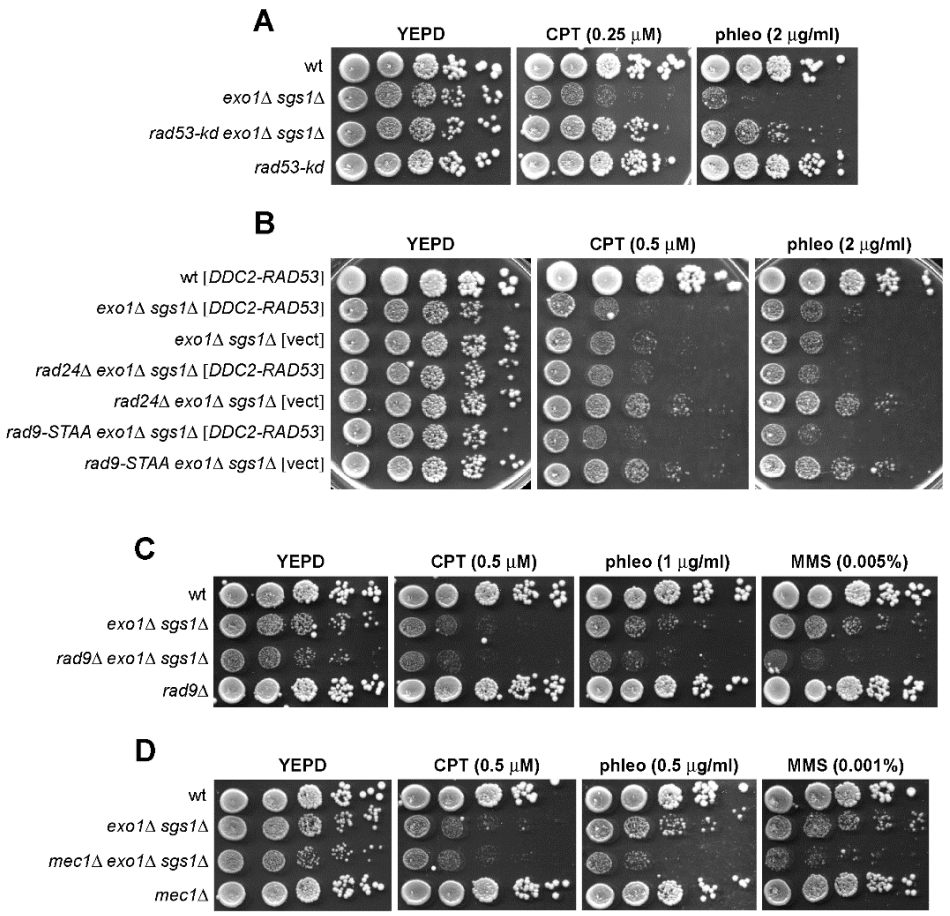

Figure 15. Dampening Rad53 activation supresses the DNA damage sensitivity of *exo1*Δ *sgs1*Δ cells.

(A-D) Exponentially growing cultures were serially diluted (1:10) and each dilution was spotted out onto YEPD plates with or without CPT, phleomycin or MMS.

The 9-1-1 complex inhibits short-range resection by restricting Mre11 nuclease

Resection in *exo1*Δ *sgs1*Δ cells is limited to the vicinity of the DSB end and depends on Mre11 nuclease activity [Zhu *et al.,* 2008; Mimitou & Symington, 2008]. To exclude possible effects of either 9-1-1, Rad9 or Rad53 on DSB resection in *exo1*Δ *sgs1*Δ cells, we used JKM139 derivative strains, where a single irreparable DSB at the *MAT* locus can be generated by expressing the HO endonuclease gene [Lee *et al.,* 1998]. Resection of DNA regions flanking the HO-induced DNA break renders the DNA sequence resistant to cleavage by restriction enzymes, resulting in the appearance of resection intermediates (r1 to r6) that can be detected by Southern blot analysis with a probe that anneals to the 3′ end at one side of the break (Figure 16A).

Consistent with previous data showing that only 30% of *exo1*Δ *sgs1*Δ cells process DSB ends beyond 100 or 200 nucleotides 4 hr after HO induction [Zhu *et al.,* 2008], only the r1 resection product was barely detectable in *exo1*Δ *sgs1*Δ cells and did not accumulate throughout the experiment (Figure 17A-C), indicating that resection in most cells failed to proceed beyond the *Ssp*I site located 0.9 kb from the HO cut site. By contrast, the r1 resection product accumulated much more abundantly in both *ddc1*Δ *exo1*Δ *sgs1*Δ (Figure 17A,C) and *rad24*Δ *exo1*Δ *sgs1*Δ cells (Figure 17B,C) compared to *exo1*Δ *sgs1*Δ cells, indicating that most cells were capable of resecting the HO-induced DSB beyond 0.9 kb from the HO cutting site. Furthermore, both *ddc1*Δ *exo1*Δ *sgs1*Δ and *exo1*Δ *rad24*Δ *sgs1*Δ cells showed appearance of the r2 resection product (Figure 17A-C), indicating that resection in some cells proceeded beyond the *Ssp*I site located 1.7 kb from the HO cleavage site.

Consistent with a more extensive resection in *ddc1*Δ *exo1*Δ *sgs1*Δ and *exo1*Δ *rad24*Δ *sgs1*Δ cells compared to *exo1*Δ *sgs1*Δ, Rad50 chromatin immunoprecipitation (ChIP) signals were greatly enriched in sequences within a few hundred nucleotides from the DSB in *exo1*Δ *sgs1*Δ and decreased rapidly with increasing distance from the break site (Figure 17D). By contrast, although it has to be considered that resolution of the ChIP signals depends on the DNA fragment sizes (200–1,000 bp) obtained after sonication, Rad50 signals close to the break site were lower in both *ddc1Δ exo1Δ sgs1Δ* and *rad24Δ exo1Δ sgs1Δ* than in *exo1Δ sgs1Δ* cells. Furthermore, they were present at higher levels in DNA sequences 1.8 and 5.4 kb from the DSB (Figure 17D).

Interestingly, inhibition of DSB resection by the 9-1-1 complex appears to occur independently of Rad53 activation and 9-1-1 function in recruiting Dpb11 and Rad9. In fact, although our assay did not allow to detect differences in ssDNA generation within 0.9 kb from the HO cutting site, the *rad9-STAA*, *ddc1-T602A* and *rad53-kd* alleles did not appear to extend resection in *exo1*Δ *sgs1*Δ cells (Figure 16B).

Resection in *exo1*Δ *sgs1*Δ cells depends on Mre11 nuclease activity [Zhu *et al.*, 2008; Mimitou & Symington, 2008]. Expression of the *mre11-H125N* nuclease-dead allele (*mre11-nd*) reduced resection of the HO-induced DSB to undetectable level not only in *exo1*Δ *sgs1*Δ cells but also in *ddc1*Δ *exo1*Δ *sgs1*Δ cells (Figure 18A,B), indicating that the enhanced resection in *ddc1*Δ *exo1*Δ *sgs1*Δ cells is due to Mre11 nuclease activity. The 3'-ssDNA tails generated by resection are converted to Rad51-coated nucleoprotein filaments that invade a duplex repair template to generate a region of heteroduplex DNA (hetDNA), where the invading strand is paired with the complementary strand [Guo *et al.*, 2017]. Interestingly, the lack of both Exo1 and Sgs1 was shown to cause a ~ 10 fold reduction of ectopic recombination by decreasing hetDNA length [Guo *et*

al., 2017]. To test the effect of *DDC1* and *RAD24* deletion on ectopic recombination, we used a *LYS2*-based assay, where the recipient allele was constructed by inserting an I-*Sce*I cleavage site into the endogenous *LYS2* locus, the insertion of which creates a frameshift mutation [Guo *et al.,* 2017]. As repair donor, a 3'-truncated *lys2* allele (*lys*2Δ3'), which contains a non-cleavable I-*Sce*I site due to a 4-bp duplication, was integrated at the *CAN1* locus. During repair, the 4-bp duplication in the donor allele is copied into the recipient allele, producing Lys^+ recombinant clones. Consistent with previous findings [Mimitou & Symington, 2008; Chung *et al.,* 2010; Guo *et al.,* 2017], *exo1*Δ *sgs1*Δ cells showed an ~10 fold decrease in the frequency of Lys^+ clones compared to wild-type (Figure 18C). In agreement with a role of 9-1-1 in inhibiting DSB resection in *exo1*Δ *sgs1*Δ cells independently of Rad9 and Rad53, Lys^+ recombination frequency increased in both *rad24*Δ *exo1*Δ *sgs1*Δ and *ddc1*Δ *exo1*Δ *sgs1*Δ triple mutants compared to *exo1*Δ *sgs1*Δ cells (Figure 18C). By contrast, the *rad9-STAA* and *rad53-kd* alleles, which did not appear to extend resection in *exo1*Δ *sgs1*Δ cells, did not increase *exo1*Δ *sgs1*Δ Lys^+ recombination frequency (Figure 18C).

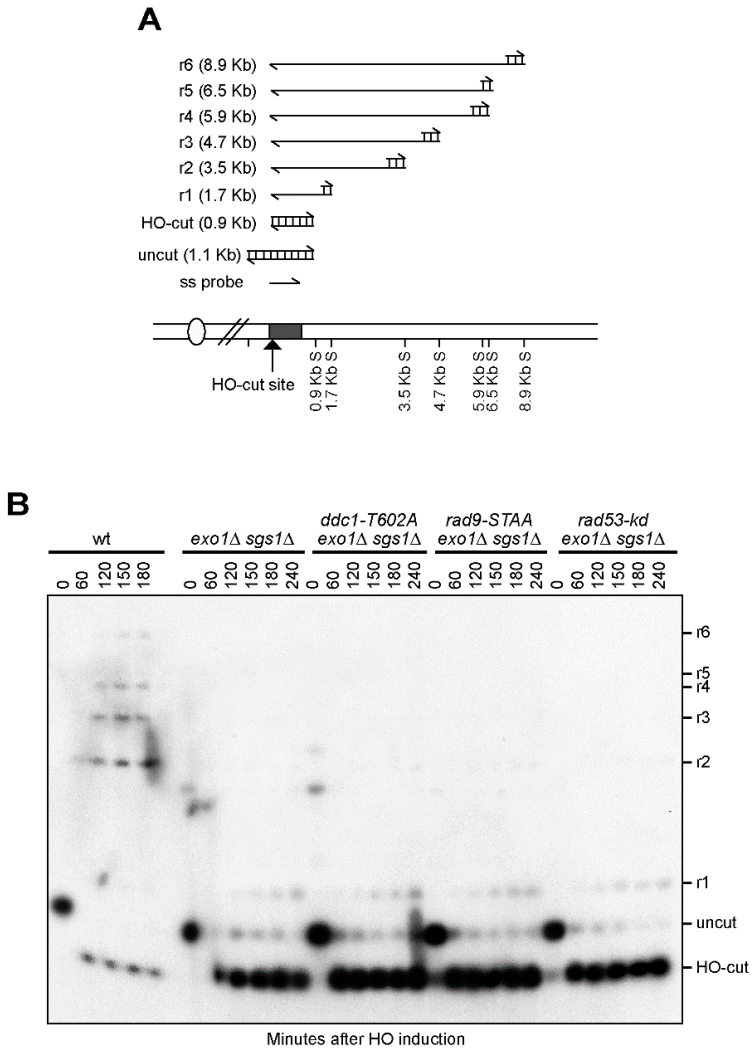

Figure 16. The *ddc1-T602A*, *rad9-STAA* and *rad53-kd* alleles did not extend resection in *exo1*Δ *sgs1*Δ cells.

(A) Map of the JKM139 chromosome III region. 5'-3' resection progressively eliminates *Ssp*I sites, producing longer *Ssp*I fragments (r1 through r6). The distance of the *Ssp*I sites from the HO cleavage site is indicated. (B) YEPR exponentially growing cell cultures were transferred to YEPRG at time zero to induce HO expression. *Ssp*I-digested genomic DNA separated on alkaline agarose gel was hybridized with a single-stranded *MAT* probe that anneals with the unresected strand. 5'-3' resection progressively produces longer *Ssp*I fragments (r1 through r6) detected by the probe.

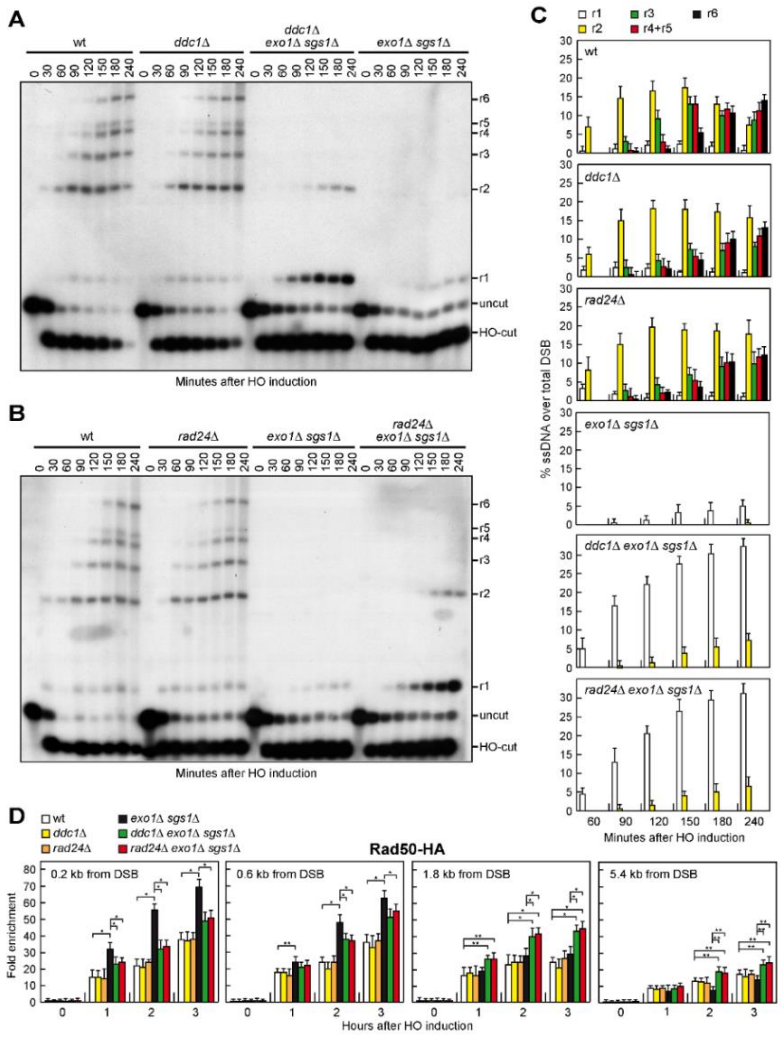

Figure 17. The lack of Ddc1 or Rad24 extends DSB resection in *exo1*Δ *sgs1*Δ cells. (A,B) YEPR exponentially growing cell cultures were transferred to YEPRG at time zero to induce HO expression. *Ssp*I-digested genomic DNA separated on alkaline agarose gel was hybridized with a single-stranded *MAT* probe that anneals with the unresected strand. 5'-3' resection progressively eliminates *Ssp*I sites, producing longer *Ssp*I fragments (r1 through r6) detected by the probe. (C) Densitometric analysis. The experiment (as in A and B) was independently repeated and the mean values are represented with error bars denoting s.d. (n=3). (D) ChIP and qPCR. Exponentially growing YEPR cell cultures were transferred to YEPRG, followed by ChIP analysis of the recruitment of Rad50-HA at the indicated distance from the HO-cut. In all diagrams, ChIP signals were normalized for each time point to the corresponding input signal. The mean values are represented with error bars denoting (n=3). $^{*}p < 0.005$; $^{**}p < 0.05$ (Student's t test).

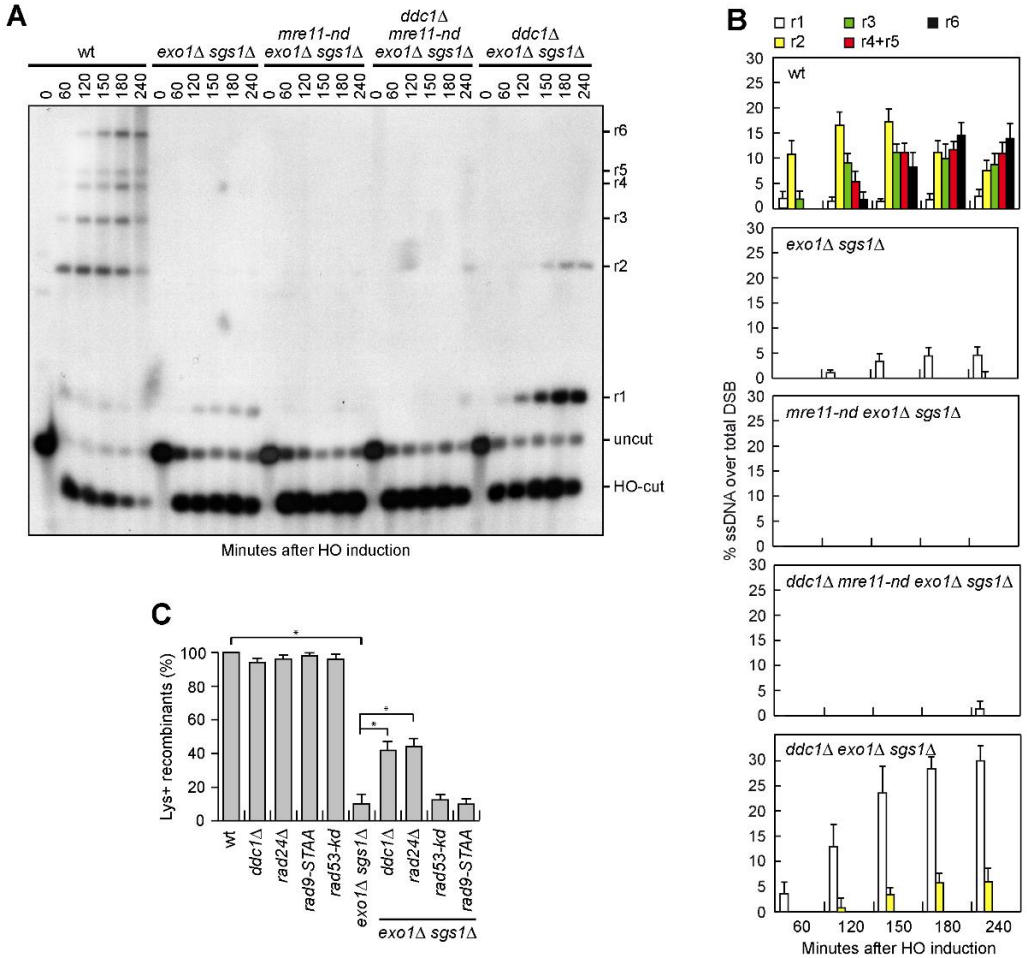

Figure 18. DSB resection in *ddc1*Δ *exo1*Δ *sgs1*Δ cells depends on Mre11 nuclease. (A) YEPR exponentially growing cell cultures were transferred to YEPRG at time zero to induce HO expression. *Ssp*I-digested genomic DNA separated on alkaline agarose gel was hybridized as described in Figure 16B. (B) Densitometric analysis. The experiment as in (A) was independently repeated and the mean values are represented with error bars denoting s.d. (n=3). (C) Recombination frequency. I-*Sce*I expression was induced by galactose addition. Cells were plated on YEPD and SC-Lys (Synthetic Complete without lysine) media, and repair frequencies were calculated as the ratio of Lys^+ to total colonies in at least three independent experiments, with 15 independent cultures per experiment. Data are expressed as percentage of Lys^+ colonies relative to wild-type that was set up at 100% with error bars denoting s.d. *p<0.005 (Student's t-test).

Nature Communications

2021 Aug 06; 12:4750

doi: 10.1038/s41467-021-25090-9

Dpb4 promotes resection of DNA double-strand breaks and checkpoint activation by acting in two different protein complexes

Erika Casari[1], Elisa Gobbini[1], Marco Gnugnoli[1],

Marco Mangiagalli[1], Michela Clerici[1], Maria Pia Longhese[1*]

[*] Corresponding Author

[1] Dipartimento di Biotecnologie e Bioscienze, Università degli Studi di Milano-Bicocca, Milano, 20126, Italy

DNA double-strand breaks (DSBs) are harmful genomic lesions that threaten genome stability and cell survival. Eukaryotic cells use two main pathways for the repair of DSBs: non-homologous end-joining (NHEJ) and homologous recombination (HR) [Lieber, 2010; Mehta & Haber, 2014]. HR requires that the 5'-strands at both DSB ends undergo nucleolytic degradation (resection), generating 3'-ended single-stranded DNA (ssDNA) tails that can invade the undamaged homologous DNA template [Bonetti *et al.*, 2018]. DSB resection is initiated by the binding to the DSB ends of the evolutionarily conserved Mre11-Rad50-Xrs2/NBS1 (MRX/N) complex [Syed & Tainer, 2018]. The Sae2 protein (CtIP in mammals) activates a latent endonuclease activity of Mre11, which cleaves the 5'-terminated strands at both DNA ends [Cannavo & Cejka, 2014]. The resulting nick generates an entry site for both Mre11, which degrades back toward the DSB end in a 3'-5' direction, and the long-range resection Exo1 and Dna2 nucleases, which catalyze extended resection in a 5'-3' direction away from the DSB [Mimitou & Symington, 2008; Zhu *et al.*, 2008; Cejka *et al.*, 2010; Niu *et al.*, 2010; Garcia *et al.*, 2011; Shibata *et al.*, 2014; Reginato *et al.*, 2017; Wang *et al.*, 2017]. The MRX complex is also necessary to recruit Exo1 and Dna2 to DSBs [Bonetti *et al.*, 2018].

Repair of DSBs occurs within chromatin, raising the question of how DSBs can be detected, signaled, and repaired within this context. Different subfamilies of chromatin remodeling enzymes catalyze a broad range of chromatin modifications, which include sliding histone octamer across the DNA, changing the conformation of nucleosomal DNA or the composition of the histone octamer [Zhou *et al.*, 2016]. Eukaryotes have four subfamilies of chromatin remodeling factors, namely SWI/SNF, ISWI, CHD, and INO80/SWR. In yeast, the RSC and the SWI/SNF complexes, two members of the SWI/SNF chromatin remodeler family, promote MRX recruitment to DSBs and DSB

resection by catalyzing eviction of nucleosomes adjacent to a DSB [Chai *et al.*, 2005; Shim *et al.*, 2007; Wiest *et al.*, 2017]. ssDNA generation at the DSB ends requires also the Ino80 complex that participates in eviction of nucleosomes on either side of a DSB [Morrison *et al.*, 2004; van Attikum *et al.*, 2004, 2007; Tsukuda *et al.*, 2009].

Generation of DSBs elicits a cellular response, termed DNA damage checkpoint, that senses DNA damage and transduces this information to regulate several cellular processes, including cell cycle progression, DNA repair, and DNA replication [Ciccia & Elledge, 2010]. Key players of the checkpoint cascade include the *Saccharomyces cerevisiae* protein kinases Mec1 and Tel1, as well as their mammalian orthologs ATR and ATM [Villa *et al.*, 2016]. Upon DNA damage recognition, these apical kinases activate the downstream effector kinases Rad53 (CHK2 in mammals) and Chk1. Rad53 and Chk1 activation requires Rad9, which acts both as an adaptor between Mec1 and Rad53 and as a scaffold to promote Rad53 autophosphorylation and activation [Gilbert *et al.*, 2001; Schwartz *et al.*, 2002; Sweeney *et al.*, 2005].

In *S. cerevisiae*, Mec1 activation requires additional factors including the highly conserved Ddc1-Mec3-Rad17 (hereafter called 9-1-1) complex and the replication factor Dpb11 (TopBP1 in mammals) [Mordes *et al.*, 2008; Navagi-Patil & Burgers, 2008, 2009]. The 9-1-1 complex, structurally related to the replication sliding clamp PCNA, recruits to DNA damaged sites Dpb11, which in turn interacts with the checkpoint protein Rad9 [Wang & Elledge, 2002; Puddu *et al.*, 2008; Pfander & Diffley, 2011]. Dpb11-Rad9 interaction requires cyclin-dependent kinase (Cdk1)-mediated Rad9 phosphorylation on the S462 and T474 residues, which bind directly to the N-terminal domain of Dpb11 [Pfander & Diffley, 2011].

Dpb11 is also part of the DNA polymerase ε (Pol ε) holoenzyme, which is largely responsible for leading-strand synthesis during DNA replication. Pol ε consists of Pol2, Dpb2, Dpb3 (POLE4 in mammals) and Dpb4 (POLE3/CHRAC17 in mammals) subunits [Muramatsu *et al.,* 2010; Goswami *et al.,* 2018¸Yuan *et al.,* 2020]. Both Dpb3 and Dpb4 contain a histone fold domain, through which they interact to form a H2A-H2B-like complex that is not essential for cell viability in budding yeast [Araki *et al.,* 1991; Ohya *et al.,* 2000]. In both yeast and mammals, the Dpb3-Dpb4 complex binds H3-H4 tetramers and facilitates their transfer onto the leading strand during DNA replication through an intrinsic chaperone activity [Bellelli *et al.,* 2018; Yu *et al.,* 2018]. Interestingly, genetic studies reveal a role for Dpb3 and Dpb4 in maintaining the silenced state of chromatin [Iida & Araki, 2004; Tsubota *et al.,* 2006; He *et al.,* 2017], suggesting that a defect in parental H3-H4 transfer in *dpb3*Δ and *dpb4*Δ cells might compromise epigenetic inheritance. The maintenance of heterochromatin silencing also involves the catalytic subunit of Pol ε [Iida & Araki, 2004; Tsubota *et al.,* 2006] and this function appears to be dependent upon Dpb3 and Dpb4, which bind double-stranded DNA (dsDNA) and increase Pol ε association to it [Tsubota *et al.,* 2003].

Of note, in yeast, *Drosophila melanogaster*, and humans, Dpb4/POLE3/CHRAC17 is also a component of the ISW2/hCHRAC chromatin remodeling complex [Iida & Araki, 2004; Corona *et al.,* 2000; Poot *et al.,* 2000], which catalyzes nucleosome sliding through the ATPase motor protein Isw2/hSNF2H [Clapier *et al.,* 2017]. In the budding yeast ISW2 complex, Dpb4 interacts with the histone fold protein Dls1 that is considered a Dpb3 paralog [McConnell *et al.,* 2004]. In the mammalian ISW2 complex, the catalytic hSNF2H subunit has been implicated in repair of DSBs by stimulating the

association to them of the recombination protein BRCA1 [Smeenk *et al.,* 2013], while the noncatalytic ACF1 subunit directly interacts with the NHEJ protein complex KU70-80 and promotes its accumulation to DSBs [Sánchez-Molina *et al.,* 2011; Lan *et al.*, 2010].

Here we show that the lack of *S. cerevisiae* Dpb4 reduces both histone removal from the DSB ends and MRX accumulation at DSBs. The poor MRX retention in *dpb4*Δ cells leads to a defective DSB resection. Furthermore, the lack of Dpb4 impairs activation of the checkpoint response by reducing Rad9 association to DSBs. Dpb4 promotes DSB resection and checkpoint activation by acting in two different protein complexes. In fact, Dpb4 interacts with Dls1 to promote Isw2 association to DSBs, histone removal, and DSB resection, while it interacts with Dpb3 to promote Rad9 association to DSBs and checkpoint activation.

The *dpb4-A62S* allele exacerbates the sensitivity to camptothecin of *tel1*Δ and *sae2*Δ cells more severely than *DPB4* deletion

Cells lacking Tel1 are specifically sensitive to camptothecin (CPT) [Menin *et al.*, 2018], which stabilizes DNA topoisomerase I cleavage complexes, yielding to replication-dependent DSBs [Deng *et al.*, 2005]. We have previously searched for extragenic mutations that exacerbated the CPT hypersensitivity of *tel1*Δ cells [Cassani *et al.*, 2016]. Genome sequencing and genetic analysis revealed that one of the mutations responsible for the increased CPT sensitivity of *tel1*Δ cells was a single nucleotide change in the *DPB4* gene that caused replacement of Ala62 with Ser. The synthetic cytotoxicity caused by the *dpb4-A62S* allele turned out to be not specific for *tel1*Δ cells (Figure 19A), as the same mutation also exacerbated the sensitivity to CPT of *sae2*Δ cells (Figure 19B).

To understand whether the *dpb4-A62S* mutation exacerbates the DNA damage sensitivity of *tel1*Δ and *sae2*Δ cells by disrupting Dpb4 function, we analyzed the effect of *DPB4* deletion. *dpb4*Δ *tel1*Δ and *dpb4*Δ *sae2*Δ cells were less sensitive to CPT than *dpb4-A62S tel1*Δ and *dpb4-A62S sae2*Δ cells, respectively (Figure 19A,B), suggesting that the synthetic effect caused by the *dpb4-A62S* allele is not due to loss of Dpb4 function. Although the *DPB4* deletion increased less severely the DNA damage sensitivity of *tel1*Δ and *sae2*Δ cells compared to *dpb4-A62S*, *dpb4*Δ cells were more sensitive than *dpb4-A62S* cells not only to a high CPT dose, but also to phleomycin and methyl methanesulfonate (MMS) (Figure 19C). Altogether, these data suggest that the

dpb4-A62S allele increases the DNA damage sensitivity of *tel1*Δ and *sae2*Δ cells by altering specific Dpb4 function(s).

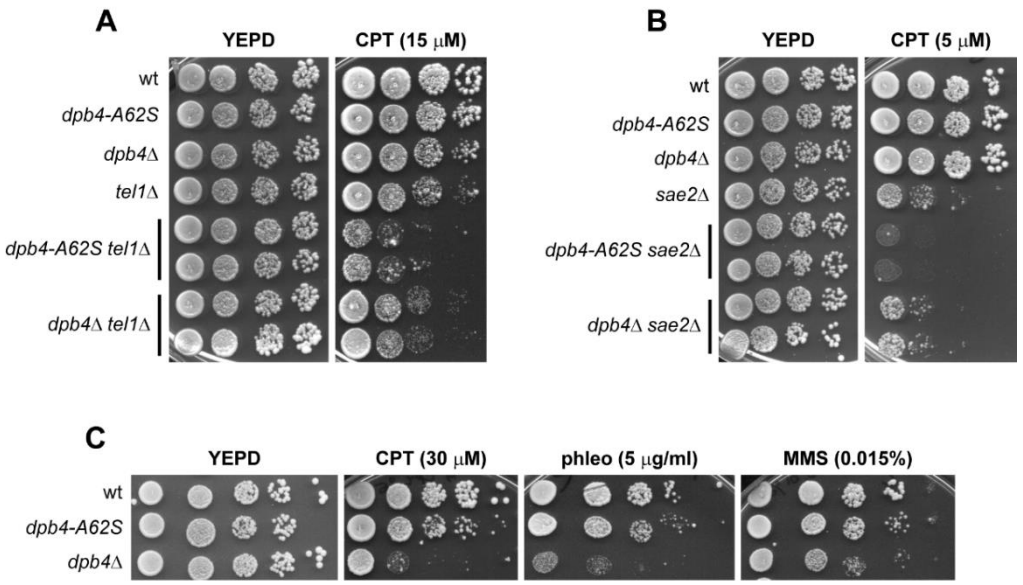

Figure 19. The *dpb4-A62S* mutation exacerbates the CPT sensitivity of *tel1*Δ and *sae2*Δ cells.
(A-C) Exponentially growing cell cultures with the indicated genotypes were serially diluted (1:10) and each dilution was spotted out onto YEPD plates with or without camptothecin (CPT), phleomycin (phleo), or methyl methanesulfonate (MMS) at the indicated concentrations.

Dpb4 promotes DSB resection and MRX association at DSBs

To assess the possible role of Dpb4 in DSB repair, we directly monitored ssDNA generation at the DSB ends by deleting *DPB4* or introducing the *dpb4-A62S* allele in a haploid strain carrying the *HO* gene under the control of a galactose-inducible promoter. In this strain, production of the HO endonuclease by galactose addition leads to the generation at the *MAT* locus of a single DSB that cannot be repaired by HR due to the lack of the homologous donor loci *HML* and *HMR* [Lee *et al.,* 1998]. Cells exponentially growing in raffinose were transferred to galactose to induce HO expression and genomic DNA was analyzed at different time points after HO induction. Because ssDNA is resistant to cleavage by restriction enzymes, progressively longer restriction fragments terminating at the broken end are generated as 5'-3' nucleolytic degradation uncovers one after another *Ssp*I site (Figure 20A). The progression of resection can be monitored by following the kinetics of appearance of these longer restriction fragments after denaturing gel electrophoresis and Southern blot analysis with a ssRNA probe that anneals to the unresected strand at one side of the DSB. The intensity of each resection band to the total amount of DSB products is used to measure the kinetics of resection. As previously observed [Lee *et al.,* 1998; Shroff *et al.,* 2004], the resection products persisted throughout the experiment, suggesting that resection initiates asynchronously after HO-catalyzed DSB formation. The appearance of the ssDNA intermediates at the HO-induced DSB was less efficient in both *dpb4*Δ and *dpb4-A62S* cells compared to wild-type cells, with *dpb4*Δ cells showing the strongest resection defect (Figure 20B,C).

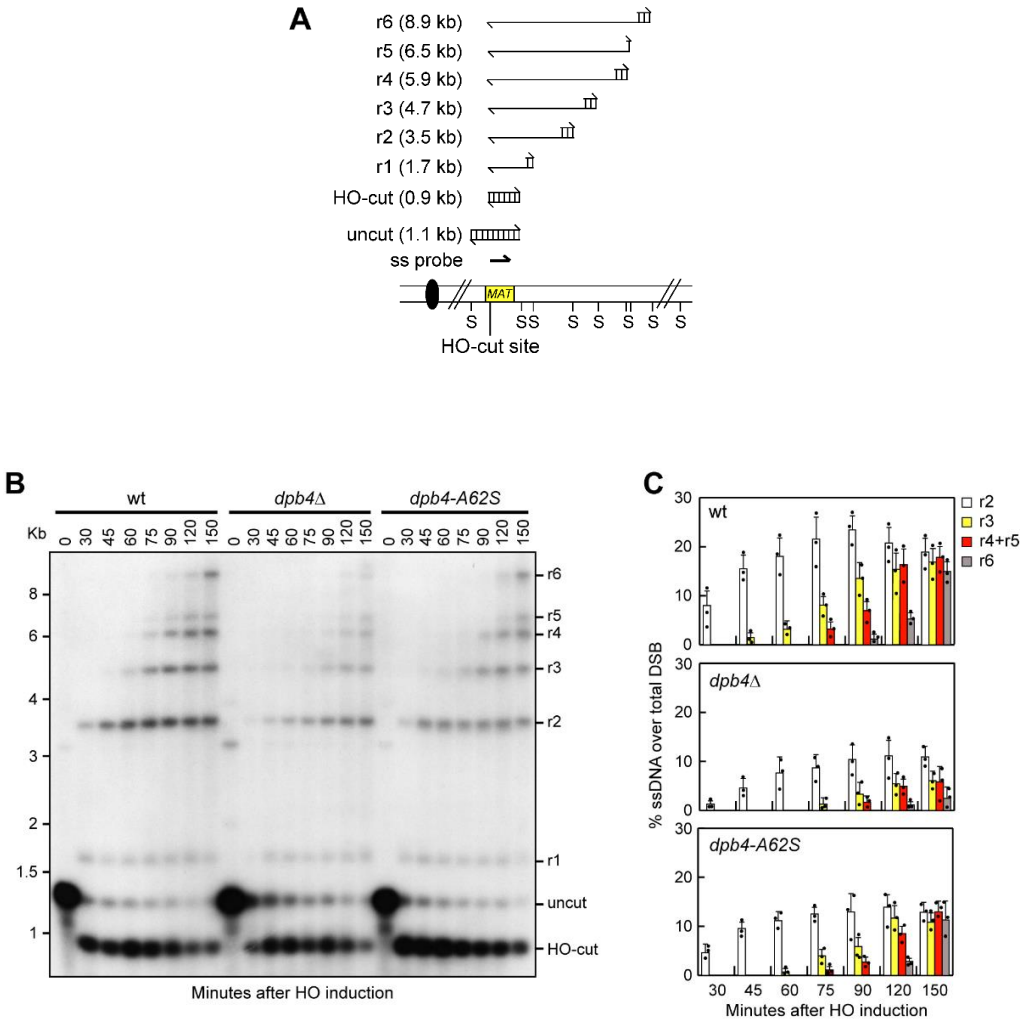

Figure 20. *dpb4*Δ and *dpb4-A62S* alleles reduce DSB resection.
(A) Resection of the DSB end progressively eliminates *Ssp*I sites (S), producing longer *Ssp*I fragments (r1 through r6) that can be separated on an alkaline agarose gel and visualized after hybridization with a single-stranded RNA probe that anneals to the unresected strand st one site of the DSB. (B) DSB resection. YEPR exponentially growing cell cultures of JKM139 derivative strains, carrying the HO cut site at the *MAT* locus, were transferred to YEPRG at time zero. *Ssp*I-digested genomic DNA was hybridized with a single-stranded *MAT* probe that anneals with the unresected strand. 5'-3'resection produces *Ssp*I fragments (r1 through r6) detected by the probe. (C) Densitometric analysis of the resection products. The mean values of three independent experiments as in (B) are represented with error bars denoting standard deviation (s.d.).

The MRX complex binds rapidly to DSBs, where it initiates DSB resection [Villa *et al.*, 2016]. Thus, we used chromatin immunoprecipitation (ChIP) and quantitative real-time PCR (qPCR) to monitor Mre11 recruitment near the HO-induced DSB in wild-type, *dpb4*Δ and *dpb4-A62S* cells expressing fully functional Myc-tagged Mre11 (Figure 21D). As resection of the DSB ends has the potential to cause a 50% decrease of input DNA, the ChIP signals were normalized not only to the efficiency of DSB induction, but also to the corresponding input for each time point. Mre11 association to the HO-induced DSB was lower in *dpb4*Δ and *dpb4-A62S* cells than in wild-type cells (Figure 21A), with *dpb4*Δ cells again showing the strongest reduction. This decreased Mre11 recruitment was not due to lower Mre11 protein levels, as similar Mre11 amounts could be detected in protein extracts from wild-type, *dpb4*Δ and *dpb4-A62S* cells (Figure 21B). The reduction of Mre11 association at DSBs correlates with the severity of the DSB resection defect displayed by *dpb4*Δ and *dpb4-A62S* cells, suggesting that the decreased Mre11 persistence at DSBs can account for the resection defect displayed by these mutants.

Dpb4 promotes histone removal near DSBs

DSB repair occurs within a chromatin context, in which DNA is packaged into nucleosomes. The density of nucleosome packaging has the potential to influence DSB repair and is regulated by ATP-dependent chromatin remodelers, which use the energy derived from ATP hydrolysis to evict, assemble, reposition or exchange histones throughout the genome [Clapier *et al.,* 2017]. Chromatin immunoprecipitation experiments indicate that nucleosomes are removed around a DSB in both yeast and mammalian cells, supporting the hypothesis that nucleosomes represent barriers to nuclease activity [Chai *et al.,* 2005; Shim *et al.,* 2007; Wiest *et al.,* 2017 Morrison *et al.,* 2004; van Attikum *et al.,* 2004; 2007; Tsukuda *et al.,* 2009, 2005; Adkins *et al.,* 2013].

Dpb4 is part of the chromatin remodeling ISW2/hCHRAC complex [Iida & Araki, 2004; Corona *et al.,* 2000; Poot *et al.,* 2000], which catalyzes nucleosome sliding [Kukimoto *et al.,* 2004; Hartlepp *et al.,* 2005; Gangaraju *et al.,* 2009]. Thus, we asked whether the poor Mre11 association and the resection defect displayed by *dpb4*Δ and *dpb4-A62S* cells are due to nucleosome retention at the DSB ends. We used ChIP analysis and qPCR to evaluate histone H2A and H3 occupancy centromere-proximal to the irreparable HO-induced DSB at the *MAT* locus. To exclude possible effects of DNA replication on histone association to DNA, HO expression was induced by galactose addition to G2-arrested cells that were kept arrested in G2 with nocodazole. As expected, H2A and H3 signals near the HO-induced DSB decreased in wild-type cells, while they remained high in both *dpb4*Δ and *dpb4-A62S* cells, with *dpb4*Δ cells showing the strongest removal defect (Figure

21C). Taken together, these findings indicate that Dpb4 is required for nucleosome removal at DSBs, suggesting that the lack of this function can account for both the poor MRX association at DSBs and the delay of DSB resection of *dpb4*Δ and *dpb4-A62S* cells.

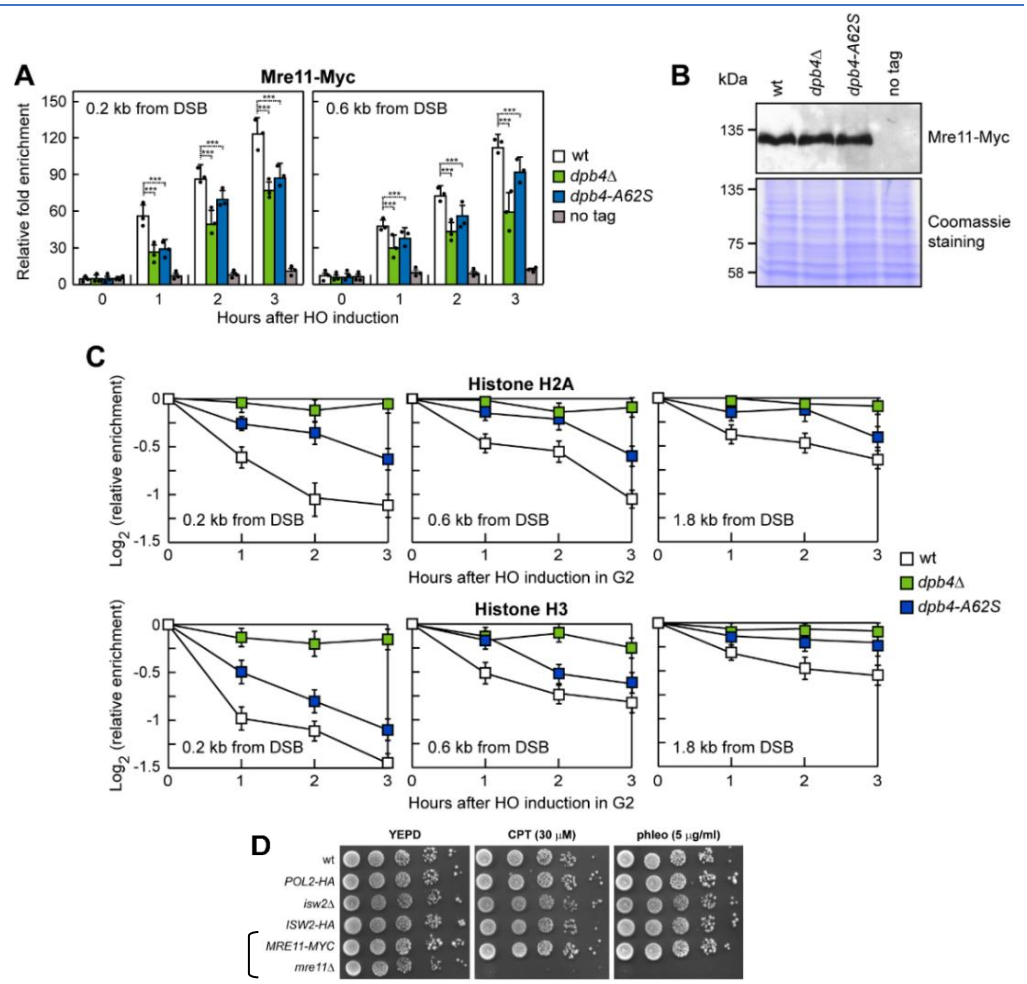

Figure 21. *dpb4Δ* and *dpb4-A62S* alleles reduce MRX association at DSBs and histone removal from the DSB ends.

(A) Exponentially growing YEPR cell cultures of JKM139 derivative strains were transferred to YEPRG to induce HO. Relative fold enrichment of Mre11-Myc at the HO-induced DSB was evaluated after ChIP with anti-Myc antibody and qPCR. The mean values of three independent experiments are represented with error bars denoting s.d. ***p<0.005 (unpaired two-tailed Student's t-test). (B) Western blot with anti-Myc antibodies of protein extracts from exponentially growing cells. This experiment was performed independently three times with similar results. (C) HO expression was induced at time zero by galactose addition to G2-arrested cells that were kept arrested in G2 by nocodazole throughout the experiment. Relative fold enrichment of H2A or H3 at the HO-induced DSB was evaluated after ChIP with anti-H2A or anti-H3 antibody and qPCR analysis. The mean values of three independent experiments are represented with error bars denoting s.d. (D) Exponentially growing cell cultures with the indicated genotypes were serially diluted (1:10) and each dilution was spotted out onto YEPD plates with or without camptothecin (CPT) or phleomycin (phleo) at the indicated concentrations.

Dpb4 promotes checkpoint activation in response to DSBs

The lack of Dpb4 impairs DSB resection, Mre11 association at DSBs, and histone removal more severely than the presence of the Dpb4-A62S mutant variant (Figures 20,21). However, Dpb4-A62S exacerbates the DNA damage sensitivity of both *tel1*Δ and *sae2*Δ cells more severely than *DPB4* deletion (Figure 19A,B), suggesting that the synthetic effects caused by Dpb4-A62S are due to changes of Dpb4 function in cellular processes other than DSB resection.
DSB formation leads to the activation of a checkpoint response that depends primarily on Mec1, which promotes activation of the Rad53 effector kinase [Zou *et al.,* 2003]. Rad9 links the signal transduction from Mec1 to Rad53 by acting as a scaffold to allow Rad53 intermolecular autophosphorylation and activation [Gilbert *et al.,* 2001; Schwartz *et al.,* 2002; Sweeney *et al.,* 2005]. We measured checkpoint activation in *dpb4*Δ and *dpb4-A62S* cells after HO-induced DSB formation or phleomycin treatment, by following Rad53 phosphorylation that is required for activation of Rad53 as a kinase and is detectable as a decrease of its electrophoretic mobility. When HO was induced by galactose addition to exponentially growing cells, the amount of slowly migrating phosphorylated Rad53 was much lower in *dpb4*Δ cells than in wild-type (Figure 22A). Similar results were obtained also when exponentially growing cells were treated with the radiomimetic drug phleomycin (Figure 22B), indicating that Dpb4 is required to activate a checkpoint in response to DSBs. By contrast, the amount of the slowest migrating Rad53 form was slightly higher in *dpb4-A62S* cells than in wild-type cells and further increased in *dpb4-A62S tel1*Δ and *dpb4-A62S sae2*Δ cells compared to *dpb4-A62S*, *tel1*Δ

and *sae2*Δ cells both after HO induction (Figure 22A) and phleomycin addition (Figure 22B).

Thus, the lack of Dpb4 reduces Rad53 activation in response to DSBs, whereas the Dpb4-A62S mutant variant enhances it.

As Dpb4 was shown to facilitate the association of the checkpoint protein Rad9 with telomeres by an unknown mechanism [Deshpande *et al.*, 2011], we analyzed Rad9 association at the HO-induced DSB by ChIP analysis and qPCR in cells expressing fully functional HA-tagged Rad9 (Figure 22E). Rad9 association to the HO-induced DSB was decreased in *dpb4*Δ cells compared to wild-type, while it was increased in *dpb4-A62S* cells (Figure 22C), although similar Rad9 amounts could be detected in protein extracts prepared from wild-type, *dpb4*Δ and *dpb4-A62S* cells (Figure 22D). These findings indicate that Dpb4 promotes Rad9 association at DSBs and checkpoint activation, and that this Dpb4 checkpoint function is enhanced by the *dpb4-A62S* mutation that leads to an increased Rad9 persistence at DSBs.

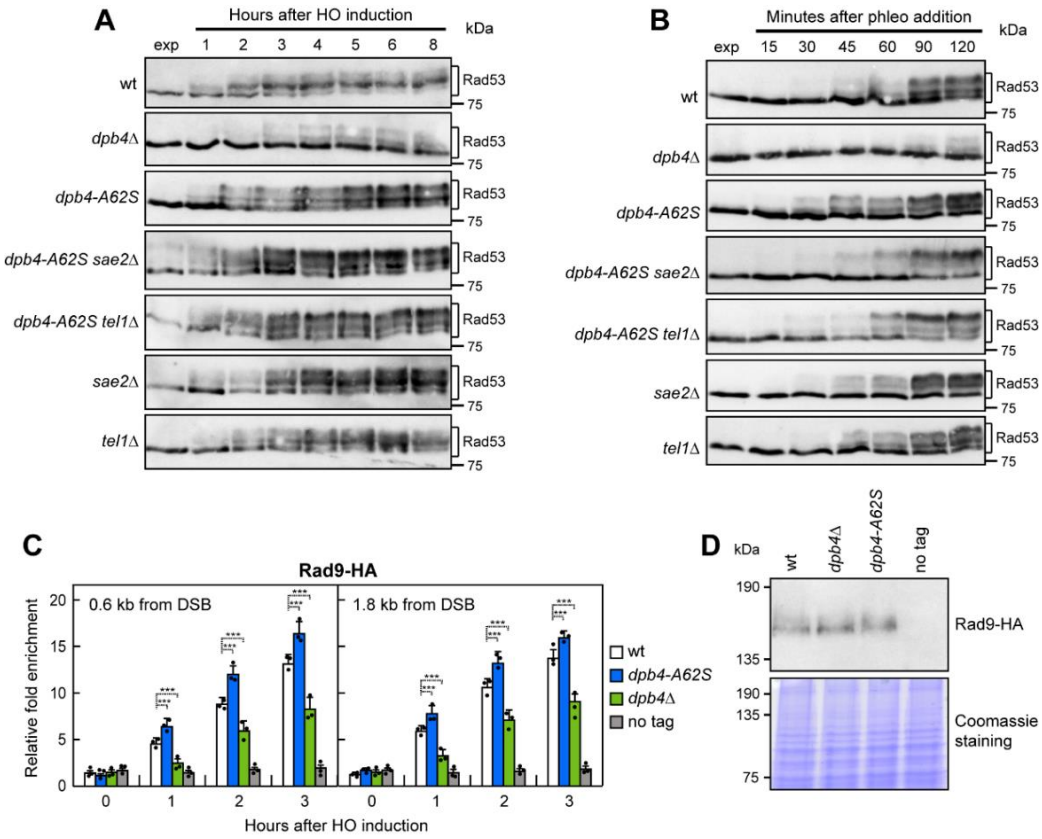
A
Hours after HO induction
kDa
exp 1 2 3 4 5 6 8
wt
dpb4Δ
dpb4-A62S
dpb4-A62S sae2Δ
dpb4-A62S tel1Δ
sae2Δ
tel1Δ
Rad53
75
B
Minutes after phleo addition
kDa
exp 15 30 45 60 90 120
C
Rad9-HA
0.6 kb from DSB
1.8 kb from DSB
Relative fold enrichment
Hours after HO induction
wt
dpb4-A62S
dpb4Δ
no tag
D
kDa
wt
dpb4Δ
dpb4-A62S
no tag
190
135
75
Rad9-HA
Coomassie staining

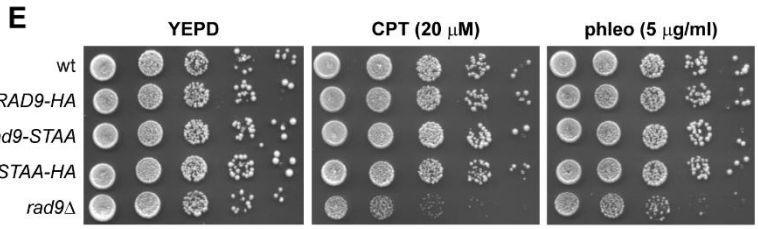
E
YEPD
CPT (20 μM)
phleo (5 μg/ml)
wt
RAD9-HA
rad9-STAA
rad9-STAA-HA
rad9Δ

Figure 22. Opposite effect of *dpb4Δ* and *dpb4-A62S* on checkpoint activation and Rad9 association at DSBs.
(A) YEPR exponentially growing cell cultures of JKM139 derivative strains were transferred to YEPRG at time zero. Western blot analysis with anti-Rad53 antibodies of protein extracts from samples taken at the indicated times after HO induction. The experiment was performed independently two times with similar results. (B) Phleomycin (10 μg/ml) was added to exponentially growing cells followed by western blot analysis with anti-Rad53 antibodies. The experiment was performed independently four times with similar results. (C) Exponentially growing YEPR cell cultures of JKM139 derivative strains were transferred to YEPRG to induce HO expression. Relative fold enrichment of Rad9-HA at the HO-induced DSB was evaluated after ChIP with anti-HA antibody and qPCR. The mean values of three independent experiments are represented with error bars denoting s.d. ***$p<0.005$ (unpaired two-tailed Student's t-test). (D) Western blot with anti-HA antibodies of protein extracts from exponentially growing cells. The experiment was performed independently three times with similar results. (E) Exponentially growing cell cultures with the indicated genotypes were serially diluted (1:10) and each dilution was spotted out onto YEPD plates with or without camptothecin (CPT) or phleomycin (phleo) at the indicated concentrations.

The finding that the *dpb4-A62S* allele increases Rad53 activation raises the possibility that the severe DNA damage hypersensitivity of *dpb4-A62S tel1*Δ and *dpb4-A62S sae2*Δ cells compared to *tel1*Δ and *sae2*Δ cells might be due to the hyperactivation of the checkpoint response. If this were the case, either *RAD9* deletion or expression of the kinase defective *rad53-K227A* (*rad53-kd*) allele should decrease the DNA damage hypersensitivity of *dpb4-A62S tel1*Δ and *dpb4-A62S sae2*Δ cells. Indeed, *RAD9* deletion suppressed the CPT hypersensitivity of *dpb4-A62S tel1*Δ cells, as *dpb4-A62S tel1*Δ *rad9*Δ cells were as sensitive to CPT as *tel1*Δ *rad9*Δ cells (Figure 23A). Furthermore, *RAD9* deletion was epistatic to *dpb4-A62S* with respect to the CPT sensitivity of *sae2*Δ cells. In fact, *dpb4-A62S sae2*Δ *rad9*Δ cells, which were less sensitive to DNA damaging agents than *dpb4-A62S sae2*Δ cells, were as sensitive as *sae2*Δ *rad9*Δ cells (Figure 23B).

Unfortunately, due to the poor viability of *rad53-kd tel1*Δ double mutant even in the absence of DNA damaging agents, we could not evaluate the effect of the *rad53-kd* allele on *dpb4-A62S tel1*Δ cells. In any case, expression of *rad53-kd*, which partially suppressed the DNA damage sensitivity of *sae2*Δ cells [Gobbini *et al.*, 2015], was epistatic to *dpb4-A62S* with respect to the CPT sensitivity of *dpb4-A62S sae2*Δ cells, as *dpb4-A62S sae2*Δ *rad53-kd* cells were as sensitive to CPT as *sae2*Δ *rad53-kd* cells (Figure 23C). Thus, Rad9 and Rad53 kinase activity are required for Dpb4-A62S to increase the DNA damage sensitivity of *tel1*Δ and *sae2*Δ cells, suggesting that the enhanced checkpoint activation by Dpb4-A62S leads to DNA damage-induced lethality in the presence of unrepaired DNA lesions.

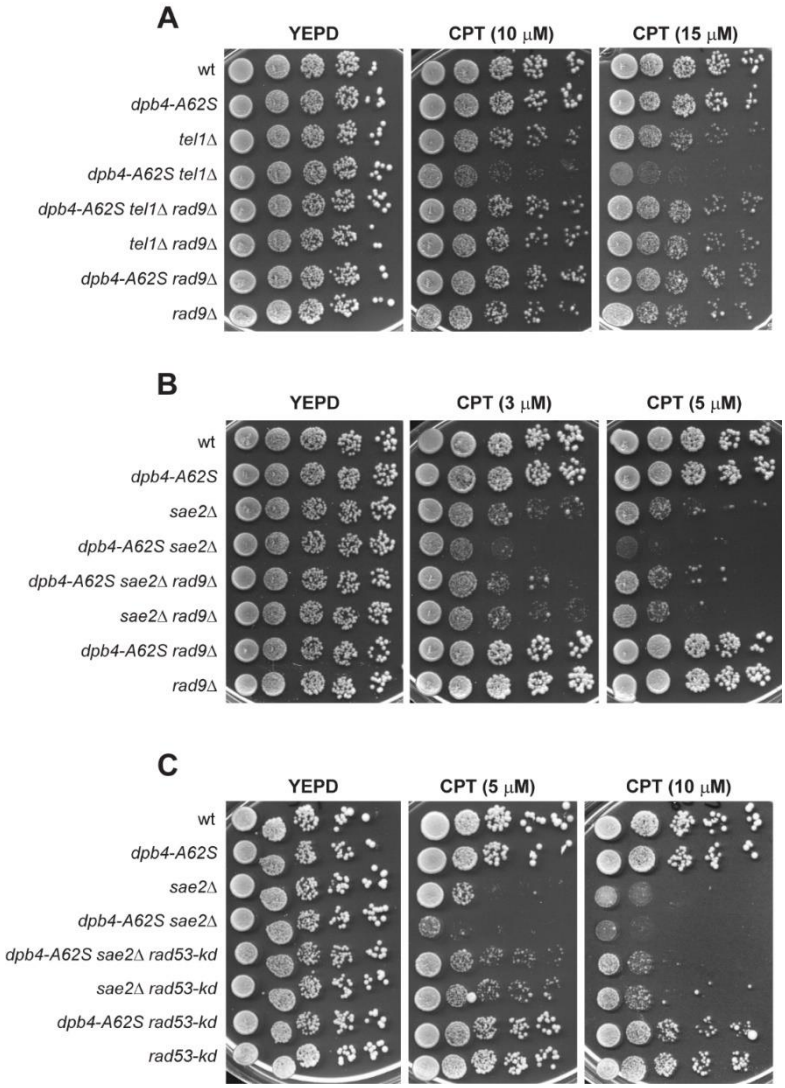

Figure 23. Dpb4-A62S increases the DNA damage sensitivity of *tel1*Δ and *sae2*Δ cells in a Rad9- and Rad53- dependent manner.
(A-C) Exponentially growing cultures with the indicated genotypes were serially diluted (1:10) and each dilution was spotted out onto YEPD plates with or without CPT.

Dpb4 and Dot1 promote Rad9 association to DSBs by acting in the same pathway and independently of Dpb11 and γH2A

In both yeast and mammals, Rad9 association to chromatin involves at least three pathways. First, Rad9 is constitutively bound to chromatin even in the absence of DNA damage through an interaction with histone H3 methylated at Lys79 (H3-K79me), a modification that is catalyzed by the methyltransferase Dot [Giannattasio *et al.,* 2005; Wysocki *et al.,* 2005; Grenon *et al.,* 2007; Huyen *et al.,* 2004; Feng *et al.,* 2002; van Leeuwen *et al.,* 2002]. Furthermore, phosphorylation of Ser 462 and Thr 474 Rad9 residues by Cdk1 leads to Rad9 interaction with Dpb11 [Pfander & Diffley, 2011; Granata *et al.,* 2010], which is recruited to DSBs by the 9-1-1 complex [Navadgi-Patil & Burgers, 2009; Majka *et al.,* 2006]. Finally, DNA damage induces Rad9 binding to histone H2A that has been phosphorylated at Ser129 (γH2A) by the checkpoint kinases Mec1/ATR and Tel1/ATM [Shroff *et al.,* 2004; Downs *et al.,* 2000; Toh *et al.,* 2006; Hammet *et al.,* 2007].

To investigate whether Dpb4 promotes Rad9 association to DSBs by acting in one of the above pathways, we analyzed the contribution of Dpb4 in supporting Rad9 association to DSBs in cells that were defective in Rad9 binding to either H3-K79me, γH2A, or Dpb11. As expected, the lack of Dot1, which abolishes H3-K79me generation [Giannattasio *et al.,* 2005; Wysocki *et al.,* 2005; Grenon *et al.,* 2007], decreased Rad9 association to the HO-induced DSB (Figure 24A). A similar decrease of Rad9 persistence at DSBs could be detected upon expression of either the *rad9-S462A, T474A* (*rad9-STAA*) (Figure 24B) or the

hta1-S129A allele (Figure 24C), which abolish Rad9-Dpb11 interaction and γH2A generation, respectively.

Interestingly, *DPB4* deletion did not further decrease the amount of Rad9 bound to DSBs in *dot1*Δ cells (Figure 24A), indicating that Dpb4 and Dot1 promote Rad9 association at DSBs by controlling the same pathway. By contrast, Rad9 association at DSBs was dramatically decreased in both *rad9-STAA dpb4*Δ (Figure 24B) and *hta1-S129A dpb4*Δ (Figure 24C) double mutants compared to each single mutant, indicating that Dpb4 function in promoting Rad9 association at DSBs occurs independently of Rad9-γH2A and Dpb11-Rad9 interactions. Consistent with this conclusion, when HO was induced in exponentially growing cells expressing fully functional Dpb4-HA tagged protein (Figure 24E), Dpb4 recruitment to the HO-induced DSB requires neither the 9-1-1 complex nor the interaction between 9-1-1 and Dpb11. In fact, the lack of Ddc1 or the presence of the *ddc1-T602A* allele, which specifically abrogates 9-1-1 binding to Dpb11 [Puddu *et al.*, 2008], did not decrease Dpb4 association to the HO-induced DSB (Figure 24D).

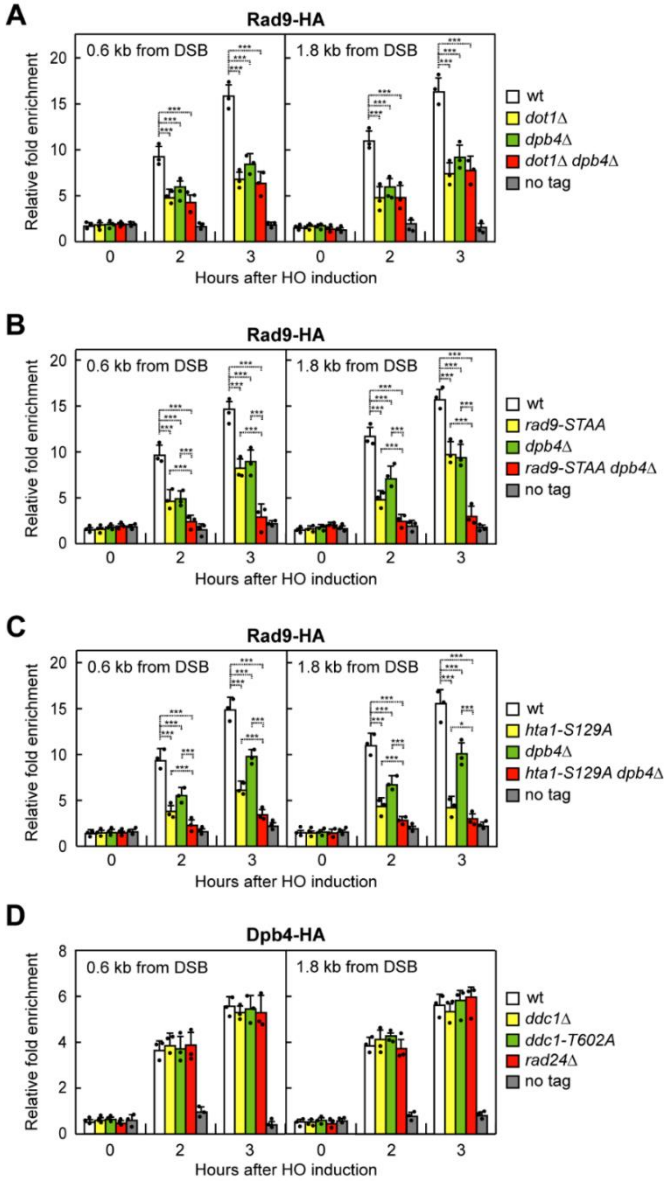
A
Rad9-HA
0.6 kb from DSB
1.8 kb from DSB
Relative fold enrichment
Hours after HO induction
wt
dot1Δ
dpb4Δ
dot1Δ dpb4Δ
no tag
B
Rad9-HA
rad9-STAA
rad9-STAA dpb4Δ
C
Rad9-HA
hta1-S129A
hta1-S129A dpb4Δ
D
Dpb4-HA
ddc1Δ
ddc1-T602A
rad24Δ

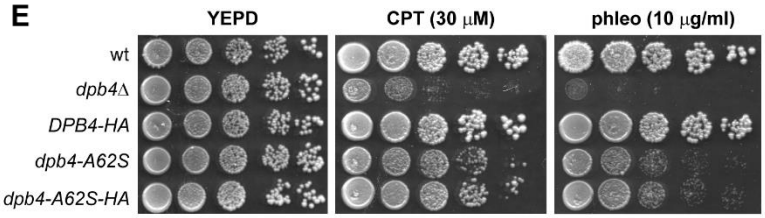
E
YEPD
CPT (30 μM)
phleo (10 μg/ml)
wt
dpb4Δ
DPB4-HA
dpb4-A62S
dpb4-A62S-HA

Figure 24. Dpb4 promotes Rad9 association at DSBs independently of γH2A and Dpb11-Rad9 interaction and by acting in the same pathway of Dot1.
(A-D) Exponentially growing YEPR cell cultures of JKM139 derivative strains were transferred to YEPRG to induce HO expression. Relative fold enrichment of Rad9-HA (A-C) and Dpb4-HA (D) at the HO-induced DSB at the *MAT* locus was evaluated after ChIP with anti-HA antibody and qPCR. Strains carrying the *hta1-S129A* allele also contain the deletion of the *HTA2* gene. The mean values of three independent experiments are represented with error bars denoting s.d. ***$p<0.005$; *$p<0.05$ (unpaired two-tailed Student's t-test). (E) Exponentially growing cell cultures with the indicated genotypes were serially diluted (1:10) and each dilution was spotted out onto YEPD plates with or without camptothecin (CPT) or phleomycin (phleo) at the indicated concentrations.

Different interactors support Dpb4 functions in DSB resection and checkpoint activation

The Dpb4 protein is shared by two highly conserved protein complexes: the chromatin remodeling ISW2 [Iida & Araki, 2004; Corona *et al.*, 2000; Poot *et al.*, 2000] and the Pol ε complexes [Muramatsu *et al.*, 2010; Goswami *et al.*, 2018; Yuan *et al.*, 2020]. In both complexes, Dpb4 forms a dimer that resembles H2A-H2B by interacting with two different histone fold proteins: Dls1 in the ISW2 complex and Dpb3 in the Pol ε complex [Yuan *et al.*, 2020; Iida & Araki, 2004; Poot *et al.*, 2000].

Both Pol2 and Dpb2 subunits of the Pol ε complex are essential for cell viability. We, therefore, investigated the effects of deleting *DPB3*, *DLS1*, and the ATPase encoding gene *ISW2* in order to assess the contribution of Pol ε and ISW2 complexes in supporting Dpb4 functions in DSB resection and checkpoint activation. Deletion of *ISW2* and *DLS1*, but not of *DPB3*, severely reduced removal of H2A and H3 histones (Figure 25A) from the HO-induced DSB. Furthermore, *isw2*Δ and *dls1*Δ cells showed decreased Mre11 association to the HO-induced DSB, whereas *dpb3*Δ cells did not (Figure 25B). Consistent with the finding that Isw2 is the catalytic subunit, whereas both Dpb4 and Dls1 help nucleosome sliding by ISW2 [Hartlepp *et al.*, 2005], *isw2*Δ cells showed a more severe impairment of Mre11 association to the HO-induced DSB compared to both *dpb4*Δ and *dls1*Δ cells (Figure 25B). *DPB4* deletion did not further decrease the amount of Mre11 bound at DSB in *isw2*Δ cells (Figure 25B), indicating that Dpb4 and Isw2 promote MRX association by acting in the same pathway. Finally, both *isw2*Δ and *dls1*Δ cells were defective in resection of the HO-induced DSB compared to wild-type cells (Figure 25C,D).

Altogether, these findings indicate that Dpb4 promotes histone removal, MRX association to DSBs, and DSB resection by acting in the ISW2 complex.

It has been proposed that Dpb4 acts as an anchor point on DNA for Isw2 [Dang *et al.*, 2007], prompting us to test whether the defect in histone removal in *dpb4*Δ cells is due to a decreased association of the Isw2 catalytic subunit to DSBs. The amount of Isw2 bound at the HO-induced DSB was markedly reduced in *dpb4*Δ cells (Figure 25E), although similar Isw2 levels were present in both wild-type and *dpb4*Δ cell extracts (Figure 25F), indicating that Dpb4 promotes Isw2 association to DSBs. By contrast, *dpb4-A62S* cells, which showed defective nucleosome eviction from DSBs (Figure 21C) exhibited increased Isw2 persistence at the HO-induced DSB (Figure 25E), suggesting that not only a decreased but also an increased Isw2 association at DSBs might impair histone removal. Consistent with this hypothesis, deletion of the negatively charged C-terminus of the *D. melanogaster* Dpb4 ortholog enhances DNA binding but inhibits nucleosome sliding [Hartlepp *et al.*, 2005].

In agreement with the conclusion that Dpb3 did not support Dpb4 function in removing histones and in promoting Mre11 association to DSBs (Figure 25A,B), *dpb3*Δ cells were not defective in DSB resection (Figure 26A,B). Instead, Dpb3, but not the ISW2 complex, supports Dpb4 function in checkpoint activation. In fact, *dpb3*Δ cells, but not *isw2*Δ cells, showed decreased Rad53 phosphorylation after HO induction (Figure 27A) or phleomycin treatment (Figure 27B). Similarly, *dpb3*Δ cells, but not *isw2*Δ cells, showed reduced Rad9 association at the HO-induced DSB compared to wild-type cells (Figure 27C). The lack of Dpb4 did not further decrease the amount of Rad9 bound at DSB in *dpb3*Δ cells, indicating that Dpb3 and Dpb4 act in the same pathway to promote Rad9 association to DSBs (Figure 27C). Consistent

with the finding that the ISW2 complex is not involved in checkpoint activation, Isw2 and Dls1 proteins are not required to increase the DNA damage sensitivity of *dpb4-A62S tel1*Δ cells, as *dpb4-A62S dls1*Δ *tel1*Δ and *dpb4-A62S isw2*Δ *tel1*Δ cells were as sensitive to CPT as *dpb4-A62S tel1*Δ cells (Figure 27D,E). Altogether, these findings indicate that Dpb4 acts in the ISW2 complex to promote MRX association at DSBs and DSB resection, whereas it acts with Dpb3 to promote checkpoint activation.

The Dpb3-Dpb4 heterodimer is part of the Pol ε holoenzyme [Yuan *et al.*, 2020], which was previously shown to promote checkpoint activation in response to DNA replication stress [Araki *et al.*, 1995; Navas *et al.*, 1995; Wang & Elledge, 1999; Puddu *et al.*, 2011]. The Dpb3-Dpb4 complex was shown to enhance both the processivity of Pol ε [He *et al.*, 2017; Tsubota *et al.*, 2003; Aksenova *et al.*, 2010] and the DNA binding activity of Pol2 [Tsubota *et al.*, 2006]. The Pol ε checkpoint function relies on the C-terminal domain of Pol2, which is essential for cell viability, making it difficult to assess whether Dpb3-Dpb4 promotes Rad9 association to DSBs and checkpoint activation by acting within the Pol ε complex. As the enhanced checkpoint activation caused by Dpb4^{A62S} is likely due to the increased Rad9 association to DSBs, if the Dpb4 checkpoint function involves the Pol ε holoenzyme, Dpb4^{A62S} should cause an increased Pol2 persistence to DSBs. To exclude possible effects of DNA replication, HO expression was induced by galactose addition to G2-arrested cells that were kept arrested in G2 with nocodazole. Following HO induction, Pol2 was recruited to the HO-induced DSB (Figure 27F). Furthermore, although wild-type, *dpb4*Δ and *dpb4-A62S* cells contained similar amount of Pol2 (Figure 27G), the A62S mutation increased Pol2 occupancy at the HO-induced DSB, whereas the lack of Dpb4 decreased it (Figure 27F),

suggesting that Dpb4 might act through Pol ε to promote checkpoint activation in response to DSBs.

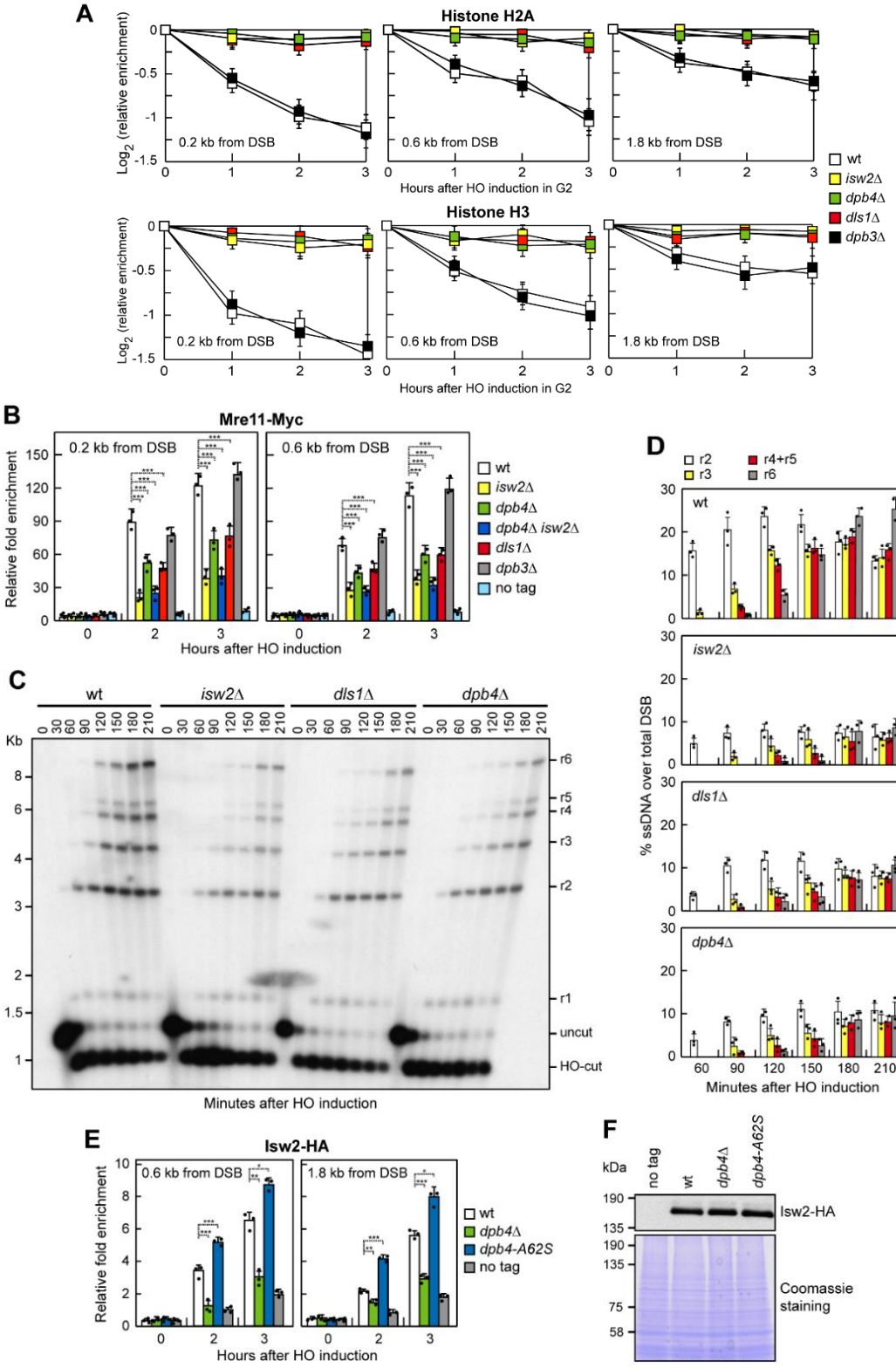
A
Histone H2A
Histone H3
Log2 (relative enrichment)
0.2 kb from DSB
0.6 kb from DSB
1.8 kb from DSB
Hours after HO induction in G2
wt
isw2Δ
dpb4Δ
dls1Δ
dpb3Δ
B
Mre11-Myc
Relative fold enrichment
Hours after HO induction
dpb4Δ isw2Δ
no tag
C
wt
isw2Δ
dls1Δ
dpb4Δ
Kb
r6
r5
r4
r3
r2
r1
uncut
HO-cut
Minutes after HO induction
D
r2
r3
r4+r5
r6
% ssDNA over total DSB
Minutes after HO induction
E
Isw2-HA
dpb4-A62S
F
kDa
no tag
Isw2-HA
Coomassie staining

Figure 25. The lack of Dls1 and Isw2, but not of Dpb3, impairs histone removal and MRX association to DSBs.
(A) HO expression was induced at time zero by galactose addition to G2-arrested cells that were kept arrested in G2 by nocodazole. Relative fold enrichment of H2A and H3 at the HO-induced DSB was evaluated after ChIP with anti-H2A and anti-H3 antibody and qPCR. The mean values of three independent experiments are represented with error bars denoting s.d. (B) Exponentially growing YEPR cell cultures were transferred to YEPRG to induce HO expression. Relative fold enrichment of Mre11-Myc at the HO-induced DSB was evaluated after ChIP with anti-Myc antibody and qPCR. The mean values of three independent experiments are represented with error bars denoting s.d. ***$p<0.005$ (unpaired two-tailed Student's t-test). (C) DSB resection. YEPR exponentially growing cell cultures were transferred to YEPRG at time zero to induce HO production. *Ssp*I-digested genomic DNA was analyzed as in Figure 20B. (D) Densitometric analysis of the resection products. The mean values of three independent experiments as in (C) are represented with error bars denoting s.d. (unpaired two-tailed Student's t-test). (E) Exponentially growing YEPR cell cultures of JKM139 derivative strains were transferred to YEPRG to induce HO expression. Relative fold enrichment of Isw2-HA at the HO-induced DSB was evaluated after ChIP with anti-HA antibody and qPCR. The mean values of three independent experiments are represented with error bars denoting s.d. ***$p<0.005$; **$p<0.01$; *$p<0.05$ (unpaired two-tailed Student's t-test). (F) Western blot with anti-HA antibodies of protein extracts from exponentially growing cells. The experiment was performed independently three times with similar results.

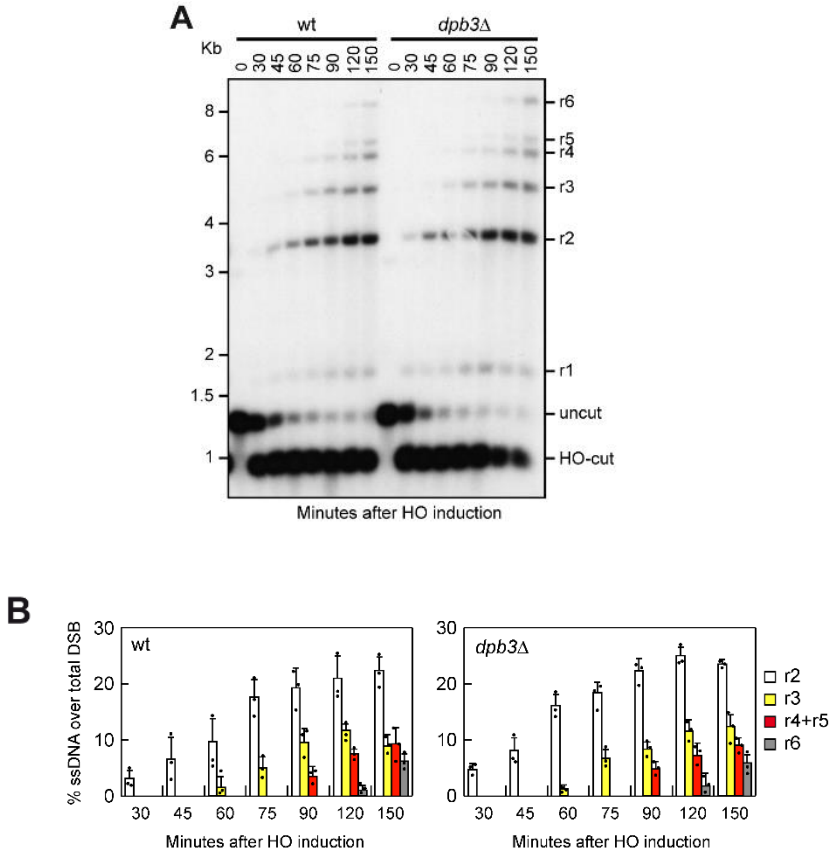

Figure 26. The lack of of Dpb3 does not impair DSB resection.
(A) DSB resection. YEPR exponentially growing cell cultures were transferred to YEPRG at time zero to induce HO production. *Ssp*I-digested genomic DNA was analyzed as in Figure 20B. The experiment was performed independently three times with similar results (B) Densitometric analysis of the resection products. The mean values of three independent experiments as in (A) are represented with error bars denoting s.d. (unpaired two-tailed Student's t-test).

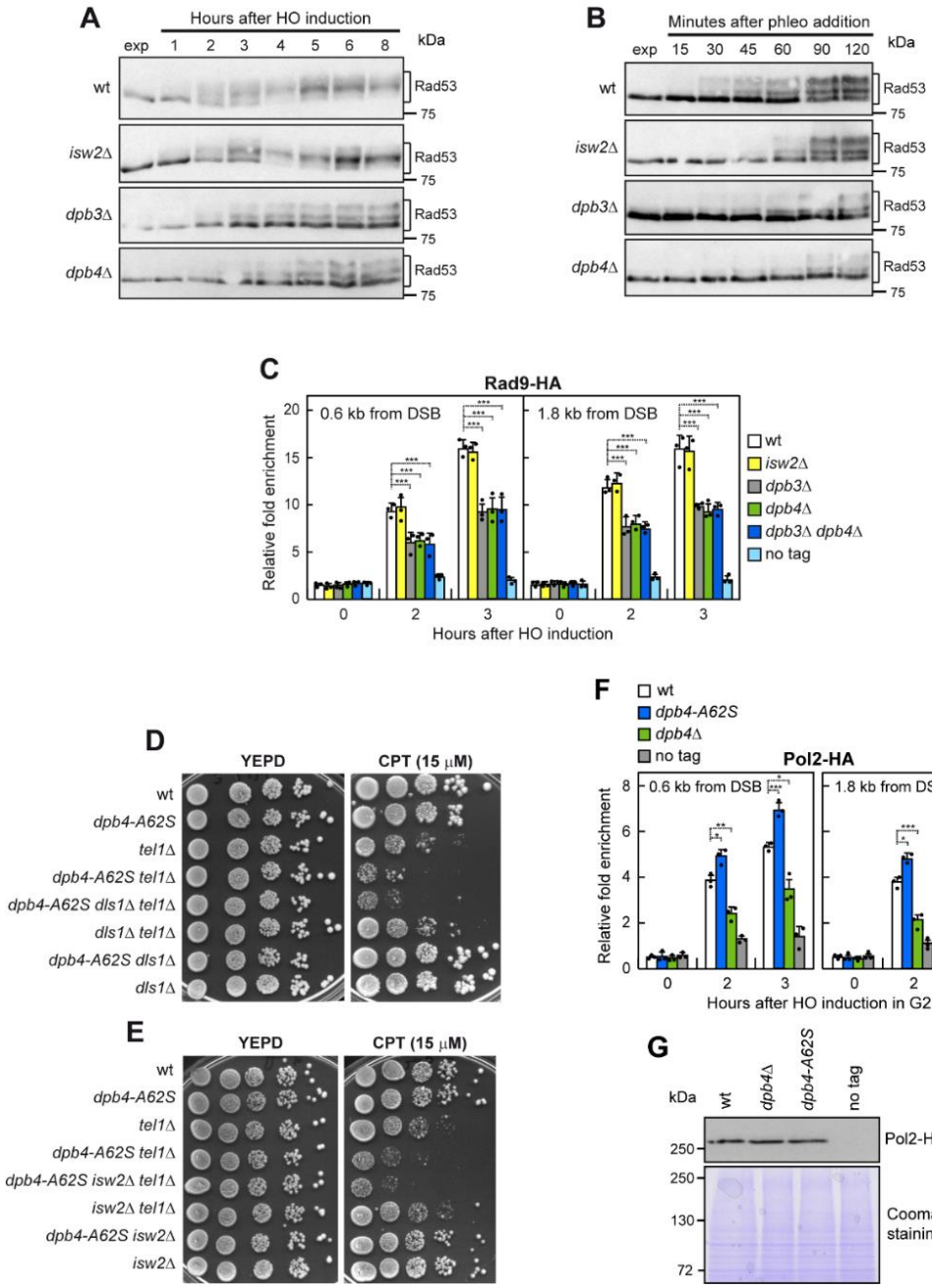
A
Hours after HO induction
exp 1 2 3 4 5 6 8
kDa
wt
isw2Δ
dpb3Δ
dpb4Δ
Rad53
75
B
Minutes after phleo addition
exp 15 30 45 60 90 120
kDa
C
Rad9-HA
0.6 kb from DSB
1.8 kb from DSB
Relative fold enrichment
Hours after HO induction
wt
isw2Δ
dpb3Δ
dpb4Δ
dpb3Δ dpb4Δ
no tag
D
YEPD
CPT (15 μM)
dpb4-A62S
tel1Δ
dpb4-A62S tel1Δ
dpb4-A62S dls1Δ tel1Δ
dls1Δ tel1Δ
dpb4-A62S dls1Δ
dls1Δ
E
dpb4-A62S isw2Δ tel1Δ
isw2Δ tel1Δ
dpb4-A62S isw2Δ
isw2Δ
F
Pol2-HA
Hours after HO induction in G2
G
Pol2-HA
Coomassie staining
250
130
72

Figure 27. The lack of Dpb3, but not of Isw2, impairs Rad9 association to DSB and checkpoint activation.
(A) YEPR exponentially growing cell cultures of JKM139 derivative strains were transferred to YEPRG at time zero to induce HO. Protein extracts were subjected to western blot analysis with anti-Rad53 antibodies. (B) Phleomycin (10 μg/ml) was added to exponentially growing cells followed by western blot analysis with anti-Rad53 antibodies. The experiments in (A) and (B) were performed independently two times with similar results. (C) Exponentially growing YEPR cell cultures of JKM139 derivative strains were transferred to YEPRG to induce HO expression. Relative fold enrichment of Rad9-HA at the HO-induced DSB was evaluated after ChIP with anti-HA antibody and qPCR. The mean values of three independent experiments are represented with error bars denoting s.d. ***$p<0.005$ (unpaired two-tailed Student's t-test). (D,E) Serial dilutions of exponentially growing cultures onto YEPD plates with or without CPT. (F) HO expression was induced at time zero by galactose addition to G2-arrested cells that were kept arrested in G2 by nocodazole. Relative fold enrichment of Pol2-HA at the HO-induced DSB was evaluated after ChIP with anti-HA antibody and qPCR. The mean values of three independent experiments are represented with error bars denoting s.d. ***$p<0.005$; **$p<0.01$; *$p<0.05$ (unpaired two-tailed Student's t-test). (G) Western blot with anti-HA antibodies of protein extracts from G2-arrested cells. The experiment was performed independently three times with similar results.

The A62S mutation favors formation of high order Dpb4-Dpb3 and Dpb4-Dls1 complexes on DNA

Dpb4, Dpb3 and Dls1 contain a histone fold (helix–turn–helix–turn–helix) domain (Figure 28A), through which they interact to form H2A-H2B-like Dpb3-Dpb4 and Dls1-Dpb4 heterodimers [Iida & Araki, 2004; Corona *et al.*, 2000; Poot *et al.*, 2000; Gnesutta *et al.*, 2013]. Sequence and structural analyses indicate that the A62 residue is localized on the α2 helix within the histone fold domain and interacts with I74 and I87 residues that are localized on the α3 helix of the histone fold domain of Dpb3 and Dls1, respectively (Figure 28B).

The A62S mutation did not impair Dpb3-Dpb4 and Dls1-Dpb4 complex formation *in vivo*. In fact, when Dpb4-HA or Dpb4^{A62S}-HA was immunoprecipitated with anti-HA antibodies, a similar amount of Dpb3-Myc could be detected in the immunoprecipitates (Figure 29A). Similarly, when Dls1-HA was immunoprecipitated with anti-HA antibodies, similar amounts of Dpb4-Myc and Dpb4^{A62S}-Myc could be detected in the immunoprecipitates (Figure 29B).

The lack of Dpb4 impairs the association to DSBs of both Isw2 and Pol2, whereas the A62S mutation increases it, prompting us to test whether the functions of Dpb4 in both histone eviction and checkpoint activation rely on its DNA binding activity that can be enhanced by the A62S mutation. When HO was induced by galactose addition to G2-arrested cells that were kept arrested in G2 with nocodazole to exclude possible effect of DNA replication, Dpb4 was efficiently recruited close to the HO cut site (Figure 30A). Although the A62S substitution did not affect Dpb4 protein level within cells (Figure 30B) and the

addition of the HA tag at the Dpb4^{A62S} C-terminus did not alter the DNA damage sensitivity of *dpb4-A62S* cells (Figure 24E), the amount of Dpb4^{A62S} bound at the HO-induced DSB was higher than that of wild-type Dpb4 (Figure 30A). This finding suggests that the A62S mutation increases Dpb4 association to dsDNA.

To investigate whether the A62S mutation enhances Dpb4 occupancy at DSBs by increasing the DNA binding affinity of Dpb3-Dpb4 and/or Dls1-Dpb4 complexes, we expressed and purified Dpb3-Dpb4, Dpb3-Dpb4^{A62S}, Dls1-Dpb4 and Dls1-Dpb4^{A62S} heterodimers as soluble protein complexes from *Escherichia coli* cells (Figure 31A,B). Circular dichroism (CD) spectra of Dpb3-Dpb4 and Dls1-Dpb4 present two minima at 208 nm and 222 nm, which are typical of α-helix structures (Figure 31C,D). The CD spectra of Dpb3-Dpb4^{A62S} and Dls1-Dpb4^{A62S} are similar to those of the wild-type complexes, indicating that the A62S substitution does not affect the protein secondary structure (Figure 31C,D). The thermal stability of the chimeric heterodimers was investigated by CD spectroscopy at fixed wavelength (208 nm) in the 25-90°C temperature range. The unfolding transition midpoint temperatures (T_m) of Dpb3-Dpb4 and Dls1-Dpb4 are 61.57 ± 0.39 and 57.05 ± 0.31 °C, respectively, whereas the A62S mutation decreases the T_m of Dpb3-Dpb4 and Dls1-Dpb4 complexes of ~ 3°C and 2°C, respectively (Figure 31E,F), suggesting that the A62S mutation induces slight conformational changes in both complexes. To test the DNA binding properties of these protein complexes, increasing concentrations of purified Dpb3–Dpb4, Dpb3–Dpb4^{A62S}, Dls1–Dpb4, and Dls1–Dpb4^{A62S} protein complexes were incubated with a fixed amount of a 61-mer dsDNA substrate to test their ability to bind DNA in a gel electrophoretic mobility shift assay (EMSA). As previously reported [Tsubota *et al.*, 2006], the addition of wild-type Dpb3-Dpb4 or Dls1-Dpb4 complexes was capable of

shifting the dsDNA oligomer into a distinct slower migrating band (Figure 32A,B), indicating that both complexes can bind dsDNA. Notably, both Dpb3-Dpb4^{A62S} and Dls1-Dpb4^{A62S} were capable of generating a similar slower migrating band although less efficiently compared to the corresponding wild-type complexes (Figure 32A,B).

However, they both showed the appearance of a second slower migrating band (Figure 32A,B), suggesting that the A62S amino acid substitution favors transition to higher order Dpb3-Dpb4-DNA and Dls1-Dpb4-DNA complexes that can explain the increased amount of Dpb4 bound to DSBs detected by ChIP.

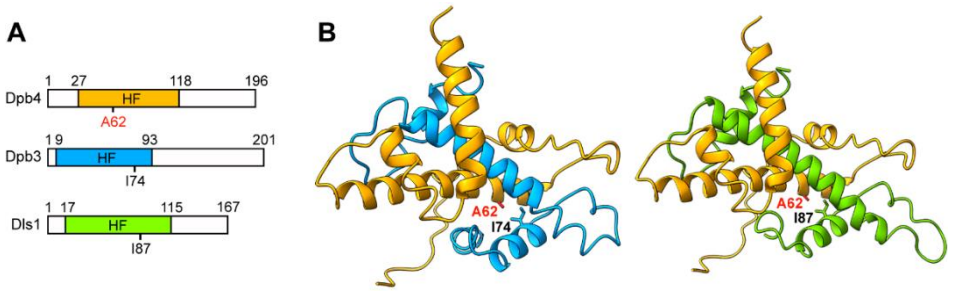

Figure 28. Architecture and 3D structure of Dpb3-Dpb4 and Dls1-Dpb4 heterodimers.

(A) Representation of Dpb4, Dpb3 and Dls1 proteins. The histone fold domain (HF) is shown. (B) 3D structure of Dpb4-Dpb3 and Dpb4-Dls1 heterodimers. The histone fold domain of Dpb4 is in orange, while that of Dpb3 and Dls1 is in light blue and green, respectively. A62 is shown as a red stick. The 3D structure of Dpb4-Dpb3 was extracted from PDB 6WJV, while the 3D model of Dls1 was built using I-TASSER.

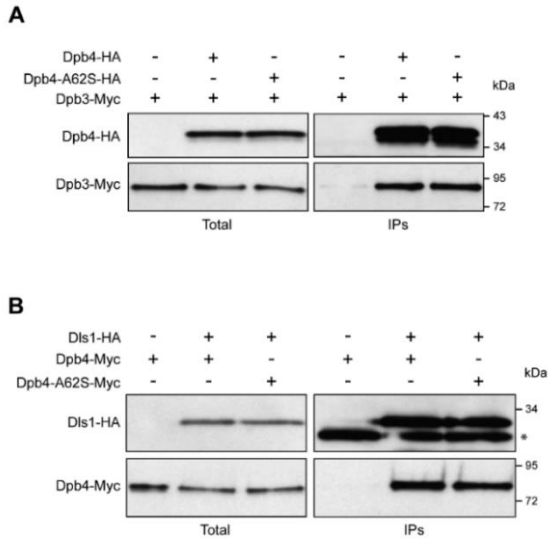

Figure 29. The A62S mutation does not affect Dpb3-Dpb4 and Dls1-Dpb4 complex formation.

(A,B) Protein extracts from exponentially growing cells treated with phleomycin (15 μg/ml) were analyzed by western blotting with anti-HA or anti-Myc antibodies either directly (total) or after immunoprecipitation (IP) with anti-A antibody. The asterisk indicates the immunoglobulins present in the immunoprecipitates. The experiments in (A) and (B) were performed independently two times with similar results.

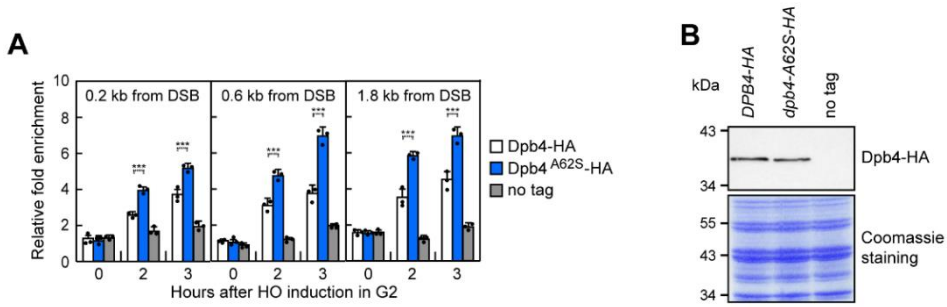

Figure 30. *In vivo* effect of the A62S mutation on the DNA binding properties of Dpb4 protein.

(A) HO expression was induced at time zero by galactose addition to G2-arrested cells that were kept arrested in G2 by nocodazole. Relative fold enrichment of Dpb4-HA and Dpb4-A62S-HA compared to untagged Dpb4 (no tag) was evaluated after ChIP with anti-HA antibodies and qPCR analysis. The mean values of three independent experiments are represented with error bars denoting s.d. ***$p<0.005$ (unpaired two-tailed Student's t-test). (B) Western blot with anti-HA antibodies of protein extracts from G2-arrested cells. The experiment was performed independently three times with similar results

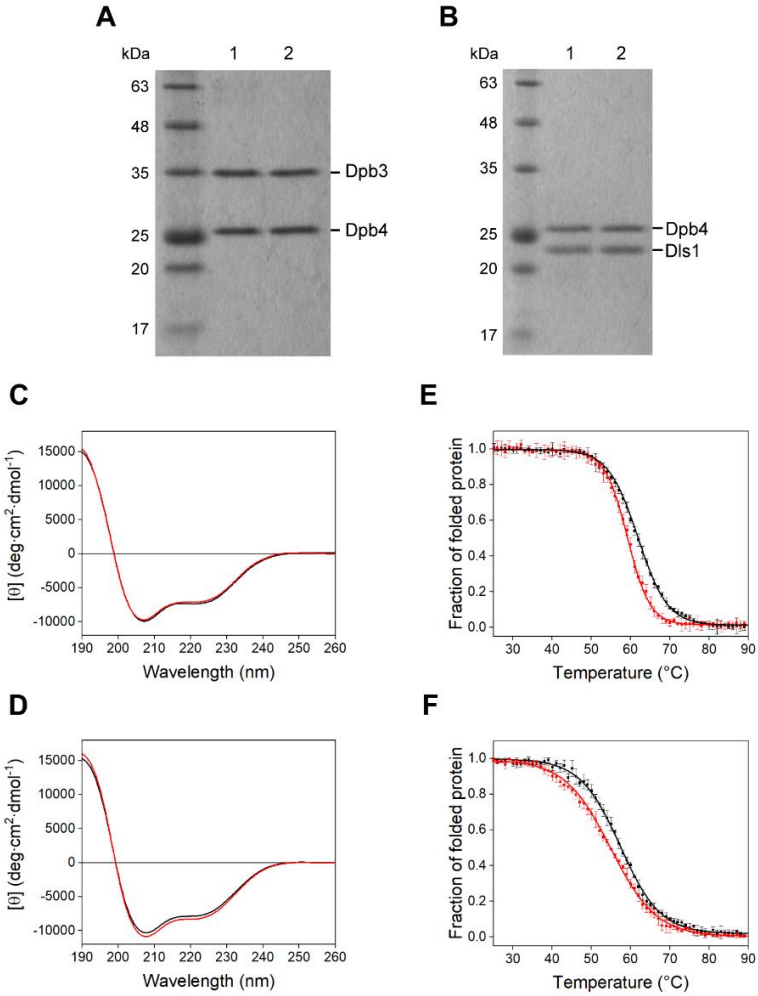

Figure 31. Purification of Dpb3-Dpb4 and Dls1-Dpb4 heterodimers.
(A) SDS-PAGE analysis of purified Dpb3-Dpb4 (lane 1) and Dpb3-Dpb4^{A62S} (lane 2) complexes. (B) SDS-PAGE analysis of purified Dls1-Dpb4 (lane 1) and Dls1-Dpb4^{A62S} (lane 2) complexes. The experiments in (A) and (B) were performed independently two times with similar results. (C) Far-UV CD spectra of Dpb3-Dpb4 (black line) and Dpb3-Dpb4^{A62S} (red line). (D) Far-UV CD spectra of Dls1-Dpb4 (black line) and Dls1-Dpb4^{A62S} (red line). For (C) and (D) one of three independent measurements was shown. (E) Thermal stability of Dpb3-Dpb4 (black line) and Dpb3-Dpb4^{A62S} (red line). The mean values of three independent measurements are represented with error bars indicating s.d. (F) Thermal stability of Dls1-Dpb4 (black line) and Dls1-Dpb4^{A62S} (red line). The mean values of three independent measurements are represented with error bars indicating s.d.

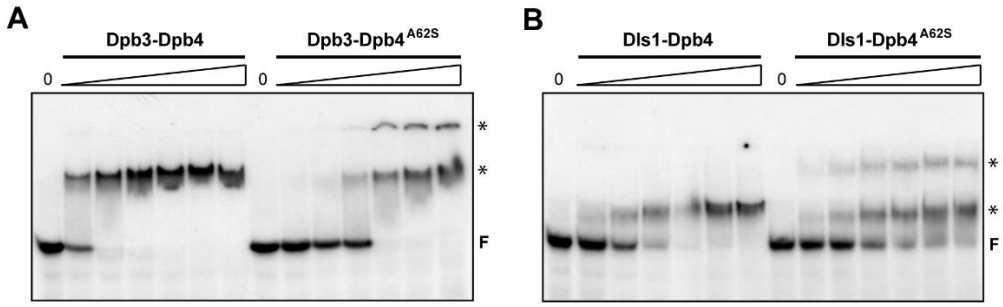

Figure 32. Effect of the A62S mutation on the DNA binding properties of Dpb3-Dpb4 and Dls1-Dpb4 heterodimers.
(A,B) EMSA with a 61 bp dsDNA and increasing concentrations of Dpb3-Dpb4 and Dpb3-Dpb4^{A62S} (A), and Dls1-Dpb4 and Dls1-Dpb4^{A62S} (B) complexes. Bands corresponding to free DNA (F), and protein-DNA complexes with higher stoichiometry (asterisk) are denoted. The experiments were performed independently two times with similar results.

PLOS Genetics

2021 Sept 14; 17(9): e1009807

doi: 10.1371/journal.pgen.1009807

The chromatin remodeler Chd1 supports MRX and Exo1 functions in resection of DNA double-strand breaks

Marco Gnugnoli[1], **Erika Casari**[1], Maria Pia Longhese[1*]

[*] Corresponding Author

[1] Dipartimento di Biotecnologie e Bioscienze, Università degli Studi di Milano-Bicocca, Milano, 20126, Italy

DNA double-strand breaks (DSBs) are the most common cause of genomic instability because their inaccurate repair can generate chromosomal rearrangements. DSBs can be repaired by either homologous recombination (HR), which uses homologous DNA from sister chromatids or homologous chromosomes as a template for repair, or non-homologous end joining (NHEJ), which directly re-ligates the broken DSB ends [Kowalczykowski, 2015].

HR is initiated by nucleolytic degradation of the 5'-terminated strand at the DSB end to generate 3'-ended single-stranded DNA (ssDNA), in a process called resection [Casari *et al.*, 2019]. In both yeast and mammals, DSB resection is initiated by the Mre11-Rad50-Xrs2/NBS1 (MRX/N) complex that, aided by the Sae2 protein (CtIP in mammals), cleaves the 5'-terminated DNA strand on either side of a DSB [Cannavo & Cejka, 2014]. This step is followed by 3'-5' nucleolytic degradation by Mre11, which proceeds back towards the DNA end and by the Exo1 or Dna2 nuclease, which degrades double-stranded DNA (dsDNA) in the 5'-3' direction [Mimitou & Symington, 2008; Zhu *et al.*, 2008; Cejka *et al.*, 2010; Niu *et al.*, 2010; Garcia *et al.*, 2011; Shibata *et al.*, 2014; Reginato *et al.*, 2017; Wang *et al.*, 2017]. The resulting 3'-ended ssDNA is first coated by the Replication Protein A (RPA) complex, which is replaced by the Rad51 recombinase, creating a nucleoprotein filament that searches and anneals to a homologous DNA sequence [Kowalczykowski, 2015]. Repair can then take place via Synthesis-Dependent Strand Annealing (SDSA) or the canonical recombination pathway that involves formation of a double Holliday junction [Mehta & Haber, 2014].

The repair of DSBs is challenged by the packaging of genomic DNA through histone and non-histone proteins into a high-order structure called chromatin, raising the question as to how the DNA repair machineries overcome this barrier to gain access to the damaged DNA. The presence of nucleosomes

inhibits DSB resection *in vitro* [Adkins *et al.,* 2013]. Furthermore, a genome-wide analysis of resection endpoints around Spo11-induced DSBs during meiosis showed that resection frequently terminates at nucleosomes, suggesting that nucleosomes represent barriers to nucleases processivity *in vivo* [Mimitou *et al.,* 2017]. Chromatin immunoprecipitation experiments support nucleosome eviction around DSBs [Tsukuda *et al.,* 2005]. Furthermore, recent data clearly indicate that histones exclusively associate with dsDNA and the rate of histone loss correlates with DSB resection [Peritore *et al.,* 2021], suggesting that nucleosome eviction occurs concomitantly with resection.

Indeed, chromatin structure is tuned by various processes such as nucleosome remodeling by ATP-dependent chromatin remodelers. These protein complexes use the energy derived from ATP hydrolysis to alter histone-DNA interactions, resulting in nucleosome sliding, eviction, and/or histone exchange [Narlikar *et al.,* 2013; Clapier *et al.,* 2017]. Several ATP-dependent nucleosome remodelers have been implicated in HR, particularly with regard to DSB resection [Chambers *et al.,* 2012; Seeber *et al.,* 2013; Poli *et al.,* 2017]. In budding yeast, the RSC, INO80 and SWI/SNF protein complexes are recruited to chromatin regions adjacent to a nuclease-induced DSB [van Attikum *et al.,* 2004; Chai *et al.,* 2005; Shim *et al.,* 2005; Bennett *et al.,* 2015]. Furthermore, their lack strongly reduces not only nucleosome removal/sliding but also DSB resection [van Attikum *et al.,* 2004; Chai *et al.,* 2005; Shim *et al.,* 2007; van Attikum *et al.,* 2007; Tsukuda *et al.,* 2005; Chambers *et al.,* 2012; Wiest *et al.,* 2017], suggesting that nucleosome eviction and resection are intrinsically coupled. These changes in chromatin compaction have been shown to facilitate the access to DSBs of DNA repair proteins, such as MRX, Rad51 and Rad52 [van Attikum *et al.,* 2004; Chai *et al.,* 2005; Shim *et al.,* 2007; Tsukuda *et al.,* 2005].

Another chromatin remodeler implicated in DSB resection is Fun30 (SMARCAD1 in mammals), which has highest sequence homology to INO80-like remodelers but lacks the split ATPase domain [Chen *et al.,* 2012; Costelloe *et al.,* 2012; Eapen *et al.,* 2012]. In contrast to INO80 that promotes DSB resection either by removing histones or by controlling distribution of the histone variant H2A.Z adjacent to a DSB [van Attikum *et al.,* 2004; 2007; Tsukuda *et al.,* 2005; Papamichos-Chronakis *et al.,* 2011; Alatwi *et al.,* 2015], Fun30 promotes DSB resection by antagonizing the association with DSBs of Rad9 that inhibits the processing activity of Exo1 [Chen *et al.,* 2012; Costelloe *et al.,* 2012; Eapen *et al.,* 2012].

The evolutionary conserved chromodomain-helicase-DNA-binding protein 1 (Chd1) is an ATP-dependent chromatin remodeler that contains a N-terminal tandemly arranged chromodomain and a central ATPase-helicase domain that confers nucleosome spacing, removal or exchange activity [Farnung *et al.,* 2017; Smolle *et al.,* 2018]. In contrast to most chromatin remodelers, Chd1 is active as a monomer and does not assemble as a multi-subunit complex. Chd1 has the ability to assemble histones along dsDNA and to induce a regular nucleosome spacing [Simic *et al.,* 2003; Lusser *et al.,* 2005; Gkikopoulos *et al.,* 2011; Lieleg *et al.,* 2015]. In yeast, Chd1 was shown to associate with RNA polymerase II elongation factors on actively transcribed genes and to be important for recycling histones over coding regions during transcription [Radman-Livaja *et al.,* 2012; Smolle *et al.,* 2012; Lee *et al.,* 2017]. Experiments in yeasts have shown that Chd1 is also important for generating spaced nucleosomes at the 5'-end of several genes [Gkikopoulos *et al.,* 2011; Hennig *et al.,* 2012; Pointner *et al.,* 2012; Shim *et al.,* 2012]. Only one CHD protein is present in yeast (Chd1), whereas at least nine CHD proteins are expressed in vertebrates. Among them, CHD1, CHD2, CHD3, CHD4, CHD6 and CHD7

have been implicated in the cellular response to DNA damage. In particular, CHD2, CHD3, CHD4 and CHD7 accumulate at DNA regions flanking a DSB and promote the recruitment of proteins involved in NHEJ [Rother *et al.,* 2017], whereas CHD6 is a key component of the signaling and transcriptional response to reactive oxygen species [Moore *et al.,* 2019].

In humans, CHD1 is one of the most frequently inactivated genes in prostate cancer [Burkhardt *et al.,* 2013; Grasso *et al.,* 2012; Huang *et al.,* 2012]. Furthermore, its loss sensitizes prostate cancer cells to chemotherapeutic DNA-damaging agents, suggesting a role in the DNA damage response [Shenoy *et al.,* 2017]. Consistent with this hypothesis, CHD1 is recruited to UV-damaged nucleosomes in a manner dependent on the DNA binding protein XPC [Rüthemann *et al.,* 2017]. Furthermore, it promotes the repair of UV-damaged DNA by stimulating the handover between XPC protein and the TFIIH complex at DNA damaged sites [Rüthemann *et al.,* 2017]. CHD1 is also recruited to chromatin in response to DSBs, where it promotes the loading of CtIP [Kari *et al.,* 2016; Zhou *et al.,* 2018]. Furthermore, loss of CHD1 decreases the assembly of RPA and RAD51 foci at DNA breaks and stalled replication forks [Kari *et al.,* 2016; Zhou *et al.,* 2018; Delamarre *et al.,* 2020], suggesting a role in DSB resection. Finally, in *Saccharomyces cerevisiae*, Chd1 interacts with Exo1 and participates in the generation of meiotic crossovers by enabling the processing of joint molecules by both Exo1 and the mismatch repair complex Mlh1-Mlh3 (MutLγ) [Wild *et al.,* 2019].

In this study, we found that *Saccharomyces cerevisiae* Chd1 improves the efficiency of nucleosome eviction from the DSB ends. Furthermore, it promotes DSB resection by enhancing the association of the MRX complex and Exo1 with the DSB ends. The lack of its ATPase activity impairs all these functions,

suggesting that Chd1 promotes MRX and Exo1 resection activities by increasing their accessibility to DSBs.

Chd1 is recruited to a DSB and its lack reduces histone removal

To investigate whether Chd1 has a direct role in the repair of DSBs, we first evaluated whether Chd1 is physically enriched at a DSB by chromatin immunoprecipitation (ChIP). To this end, we used a strain background carrying a galactose-inducible HO endonuclease, which generates a single DSB at the *MAT* locus in the presence of galactose [Lee *et al.*, 1998]. To minimize the effect of DSB repair, the *MAT* homology regions *HML* and *HMR* were deleted, leading to a DSB that cannot be repaired by HR [Lee *et al.*, 1998]. Following HO induction by galactose addition, Chd1-Myc was recruited near the HO-induced DSB and its binding increases over three hours (Figure 33A).

After a DSB is formed, nucleosomes are rapidly evicted at both sides of the DSB and this process is thought to promote DSB repair by facilitating the access of DNA repair proteins [Chambers *et al.*, 2012; Seeber *et al.*, 2013; Poli *et al.*, 2017]. As Chd1 has a nucleosome eviction activity [Farnung *et al.*, 2017], we analyzed occupancy of histone H3 near the HO-induced DSB at both the *LEU2* and the *MAT* loci. To exclude possible effects of DNA replication on histone association to DNA, HO expression was induced by galactose addition to G2-arrested cells that were kept arrested in G2 with nocodazole for the duration of the experiment. Furthermore, to exclude that possible differences in histone occupancy were due to different repair kinetics, repair of the HO-induced DSB at the *LEU2* locus was prevented by deleting *RAD52*, whereas repair of the HO-induced DSB at the *MAT* locus was prevented by deleting the homologous donor loci *HML* and *HMR*. H3 signal bound near the HO-induced DSB at the *LEU2* and the *MAT* loci remained higher in *chd1*Δ than in wild-type

cells, indicating that Chd1 participates in histone removal at DSBs (Figure 33B).

Chd1 carries an ATP-binding domain (AAA domain) that contains conserved Walker A and B motifs [Hanson *et al.*, 2005]. Within the P-loop of Walker A, a conserved lysine residue (K407 in Chd1) in the consensus sequence GXXXXGK[T/S] (where X is any amino acid) directly interacts with the phosphates of ATP. Mutation of this residue eliminates both ATP binding and ATPase activity [Matveeva *et al.*, 1997; Babst *et al.*, 1998; Corona *et al.*, 1999]. The Walker B motif contains aspartate (D513 in Chd1) and glutamate (E514 in Chd1) residues within the hhhhDE sequence (where h represents a hydrophobic amino acid) that are crucial for ATPase activity, with the D residue coordinating Mg^{2+} and the E residue activating water for the hydrolysis reaction [Weibezahn *et al.*, 2003]. Mutation of the E residue was shown to impair nucleotide hydrolysis without affecting ATP binding [Babst *et al.*, 1998; Weibezahn *et al.*, 2003; Dalal *et al.*, 2004]. To test whether the ATPase activity of Chd1 is required for histone eviction around the DSB, we introduced either the K407R or the E514A amino acid substitution into Chd1. Both *chd1-K407R* and *chd1-E514A* mutant cells were as defective in histone removal from the HO-induced DSB as *chd1*Δ cells (Figure 33B).

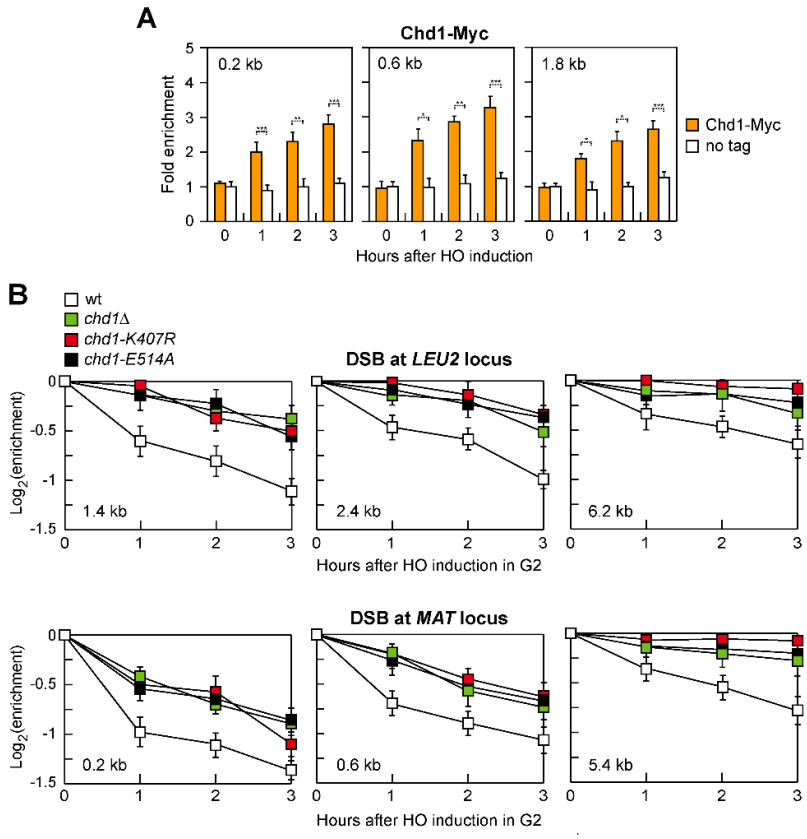

Figure 33. Chd1 recruitment to a DSB and histone removal.

(A) Exponentially growing YEPR cell cultures of JKM139 derivative strains were transferred to YEPRG, followed by Chd1-Myc ChIP at the indicated distances from the HO-cut site compared to untagged Chd1 (no tag). Data are expressed as fold enrichment at the HO-cut site over that at a non-cleavable locus (*ARO1*), after normalization to the corresponding input for each time point. Fold enrichment was then normalized to cut efficiency. Plotted values are the mean values ± s.d. from three independent experiments. ***P<0.005, **P<0.01, *P<0.05, t-test. (B) HO expression was induced by galactose addition to G2-arrested cells carrying the HO system at the *LEU2* or at the *MAT* locus. Cells were kept arrested in G2 by nocodazole throughout the experiment. Histone H3 ChIP with anti-H3 antibody at the indicated distances from the HO cut site. Data are expressed as fold enrichment at the HO-cut site over that at a non-cleavable locus (*ARO1*) after normalization to the corresponding input for each time point. Fold enrichment was then normalized to cut efficiency. Plotted values are the mean values ± s.d. from three independent experiments.

Chd1 promotes DSB resection

Nucleosome eviction from DSBs occurs concomitantly with DSB resection [Peritore *et al.,* 2021], prompting us to monitor directly the generation of ssDNA at the HO-induced DSB in *chd1*Δ, *chd1-K407R* and *chd1-E514A* mutant cells. Because ssDNA cannot be cleaved by most restriction enzymes, generation of ssDNA was assessed by testing resistance to cleavage as resection proceeds beyond restriction sites located at different distances from the HO cut site at the *MAT* locus (Figure 34A). First, we used a Southern blot analysis approach to detect the appearance of slower migrating bands (r1-r6) after denaturing gel electrophoresis of *Ssp*I-digested genomic DNA and hybridization with a probe that anneals to the unresected strand at one side of the DSB (Figure 34B). When HO was induced by galactose addition to exponentially growing cells, the resection products (r2 to r6) appeared less efficiently in galactose-induced *chd1*Δ, *chd1-K407R* and *chd1-E514A* mutant cells compared to wild-type cells (Figure 34B,C). The resection defect of *chd1*Δ cells was similar to that of *sae2*Δ cells, whereas it was less severe than that of *mre11*Δ cells (Figure 34G).

Detection of *Ssp*I-resistant ssDNA by denaturing gel electrophoresis does not allow to monitor the resection events that do not proceed beyond the *Ssp*I site located 0.9 kb from the HO-induced DSB. Furthermore, the signal for the r1 resection product, which can be detected when resection does not proceed beyond the *Ssp*I site located 1.7 kb from the DSB, is very low and difficult to quantify. Thus, we used a quantitative PCR-based method to evaluate generation of restriction enzyme-resistant ssDNA [Zierhut *et al.,* 2008]. *CHD1* deletion caused a reduction in ssDNA generation very close to the cut site (0.15, 0.65, 0.9 kb) (Figure 34D), indicating a defect in initiation of resection.

The same analysis at more distant sites (1.7 and 3.5 kb) (Figure 34D) confirmed the long-range resection defect that was detected by denaturing Southern blotting. We can conclude that Chd1 is involved in both short- and long-range resection.

The 3'-ended ssDNA generated during DSB resection is coated by the RPA complex, which is replaced by Rad51 to generate a nucleoprotein filament that invades and anneals to a homologous DNA sequence [Kowalczykowski, 2015]. Although protein extracts from wild-type, *chd1*Δ, *chd1-K407R* and *chd1-E514A* cells contained similar Rad51 amount (Figure 34E), Rad51 association at different distances from the HO-induced DSB was reduced in *chd1*Δ, *chd1-K407R* and *chd1-E514A* cells compared to wild-type cells (Figure 34F), consistently with a role of Chd1 in both initiation and extension of DSB resection.

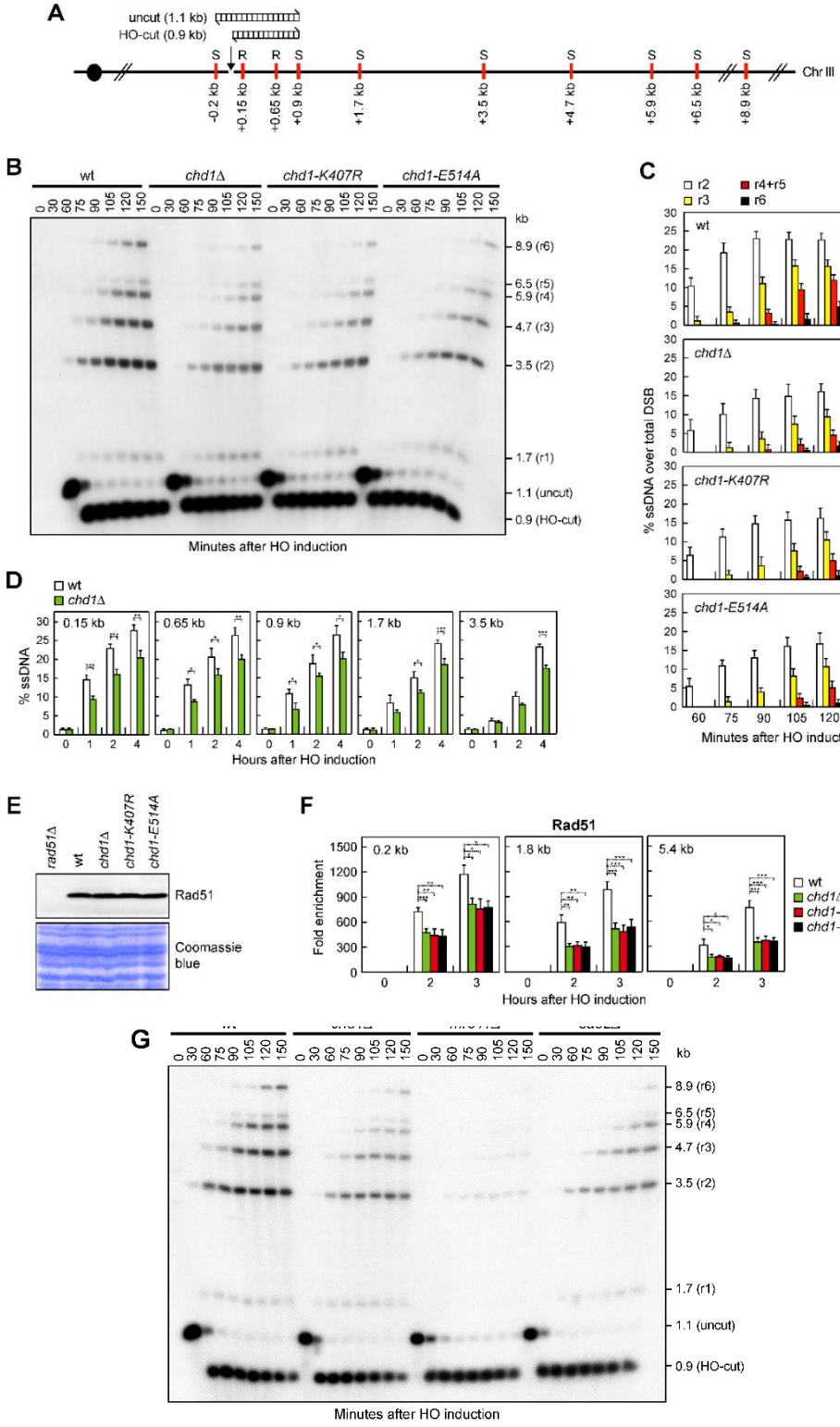
A
uncut (1.1 kb)
HO-cut (0.9 kb)
S R R S S S S S S S
Chr III
-0.2 kb
+0.15 kb
+0.65 kb
+0.9 kb
+1.7 kb
+3.5 kb
+4.7 kb
+5.9 kb
+6.5 kb
+8.9 kb
B
wt
chd1Δ
chd1-K407R
chd1-E514A
kb
8.9 (r6)
6.5 (r5)
5.9 (r4)
4.7 (r3)
3.5 (r2)
1.7 (r1)
1.1 (uncut)
0.9 (HO-cut)
Minutes after HO induction
C
r2
r3
r4+r5
r6
wt
chd1Δ
chd1-K407R
chd1-E514A
% ssDNA over total DSB
Minutes after HO induction
D
wt
chd1Δ
0.15 kb
0.65 kb
0.9 kb
1.7 kb
3.5 kb
% ssDNA
Hours after HO induction
E
rad51Δ
wt
chd1Δ
chd1-K407R
chd1-E514A
Rad51
Coomassie blue
F
Rad51
0.2 kb
1.8 kb
5.4 kb
Fold enrichment
wt
chd1Δ
chd1-K407R
chd1-E514A
Hours after HO induction
G
kb
8.9 (r6)
6.5 (r5)
5.9 (r4)
4.7 (r3)
3.5 (r2)
1.7 (r1)
1.1 (uncut)
0.9 (HO-cut)
Minutes after HO induction

Figure 34. Chd1 dysfunction reduces DSB resection.
(A) Schematic representation of the MAT locus and the distance of *Rsa*I (R) and *Ssp*I (S) restriction sites from the HO cut site. The DNA fragments detected in panel B before (uncut) and after HO cleavage (HO-cut) were also indicated. (B) YEPR exponentially growing cell cultures of JKM139 derivative strains were transferred to YEPRG at time zero. Southern blot analysis of *Ssp*I-digested genomic DNA after alkaline gel electrophoresis with a probe that anneals to the unresected strand. 5'-3' resection progressively eliminates *Ssp*I sites (S), producing *Ssp*I fragments (r1 through r6) detected by the probe. (C) The experiment as in panel B has been independently repeated three times, and the mean values are represented with error bars denoting s.d. (D) Quantification of ssDNA by qPCR at the indicated distances from the HO cut site. Plotted values are the mean values of three independent experiments, with error bars denoting s.d. ***P < 0.005, **P < 0.01, *P < 0.05, t-test. (E) Western blot with anti-Rad51 antibodies of extracts used for the ChIP analysis shown in panel F. The same amount of extracts was separated by SDS-PAGE and stained with Coomassie Blue as loading control. (F) Rad51 ChIP at the indicated distances from the HO-induced DSB. Data are expressed as fold enrichment at the HO-cut site over that at a non-cleavable locus (*ARO1*), after normalization to the corresponding input for each time point. Fold enrichment was then normalized to cut efficiency. Plotted values are the mean values ± s.d. from three independent experiments. ***P<0.005, **P<0.01, *P<0.05, t-test. (G) YEPR exponentially growing cell cultures of JKM139 derivative strains were transferred to YEPRG at time zero. Southern blot analysis of *Ssp*I-digested genomic DNA after alkaline gel electrophoresis with a probe that anneals to the unresected strand. 5'-3' resection progressively eliminates *Ssp*I sites (S), producing *Ssp*I fragments (r1 through r6) detected by the probe.

Chd1 promotes MRX and Exo1 association with DSBs

DSB resection involves sequential action of short- and long-range nucleases. In short-range resection, Mre11 endonuclease, aided by Sae2, cleaves the 5'-terminated DNA strand at ~250-300 nucleotides from the DSB ends, followed by degradation toward the DNA ends by Mre11 exonuclease. Then, Exo1 or Dna2 resects thousands of nucleotides in length in the 5'-3' direction away from the DSB ends [Cannavo & Cejka, 2014; Mimitou & Symington, 2008; Zhu *et al.,* 2008; Cejka *et al.,* 2010; Niu *et al.,* 2010; Garcia *et al.,* 2011; Shibata *et al.,* 2014; Reginato *et al.,* 2017; Wang *et al.,* 2017]. While MRX and Sae2 association with DSBs occurs independently of each other [Lisby *et al.,* 2004], MRX has a structural role in promoting Exo1 and Dna2 association with DSBs [Shim *et al.,* 2010], thus explaining the more severe resection defect caused by the lack of any MRX subunit compared to that caused by the lack of Mre11 nuclease activity.

As Chd1 dysfunction leads to a defect in both short- and long-range resection, we measured MRX, Sae2 and Exo1 association at the HO-induced DSB. The amount of Mre11 (Figure 35A) and Exo1 (Figure 35B) bound at the HO-induced DSB was lower in *chd1*Δ, *chd1-K407R* and *chd1-E514A* cells than in wild-type cells. The decreased Mre11 and Exo1 recruitment was not due to lower protein levels, as protein extracts prepared from wild-type, *chd1*Δ, *chd1-K407R* and *chd1-E514A* cells contained similar amount of Mre11 (Figure 35C) and Exo1 (Figure 35D). By contrast, Sae2 association with the HO-induced DSB was similar in wild-type, *chd1*Δ, *chd1-K407R* and *chd1-E514A* cells (Figure 35E). Thus, we can conclude that Chd1 facilitates MRX and Exo1 association with DSBs.

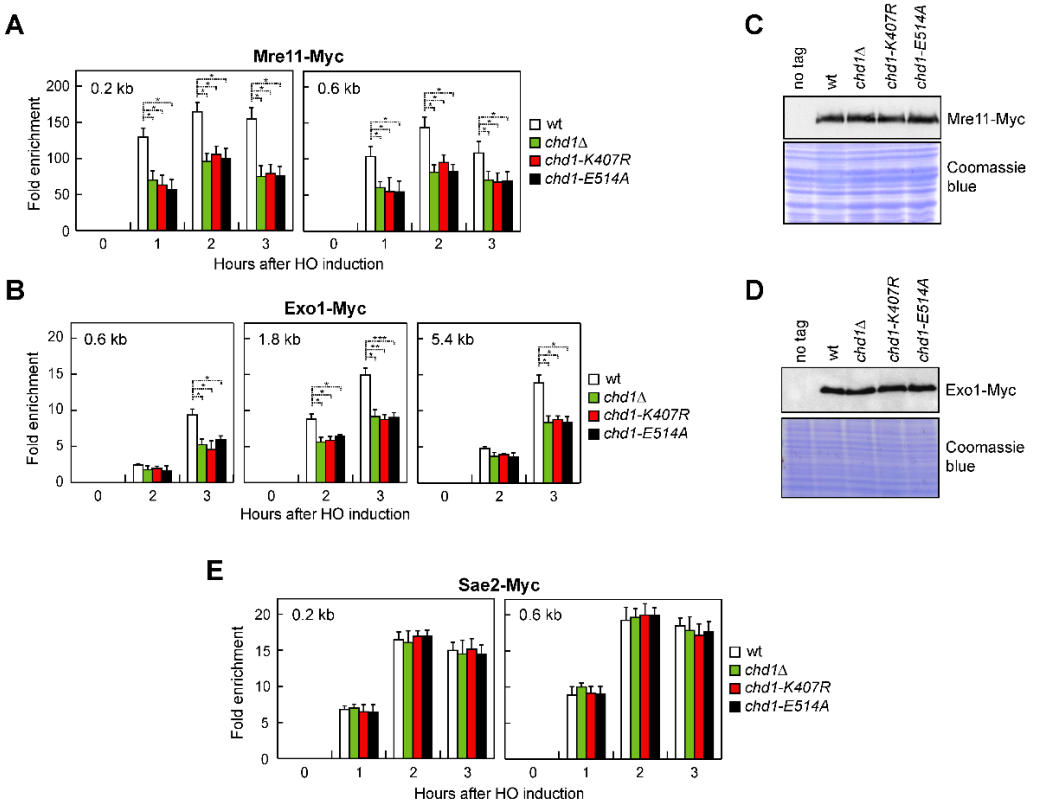

Figure 35. Chd1 dysfunction impairs MRX and Exo1 association with a DSB. (A,B) Mre11-Myc (A) and Exo1-Myc (B) ChIP at the indicated distances from the HO cleavage site. Data are expressed as fold enrichment at the HO-cut site over that at a non-cleavable locus (*ARO1*), after normalization to the corresponding input for each time point. Fold enrichment was then normalized to cut efficiency. Plotted values are the mean values ± s.d. from three independent experiments. ***P<0.005, **P<0.01, *P<0.05, t-test. (C,D) Western blot with anti-Myc antibodies of extracts used for the ChIP analysis shown in panels A and B. (E) Sae2-Myc ChIP at the indicated distances from the HO-cut site.

Chd1 promotes DSB repair by HR

The finding that Chd1 promotes DSB resection led us to investigate whether Chd1 has a role in HR. Among the HR repair pathways, single-strand annealing (SSA) is used to repair a DSB flanked by direct DNA repeats when resection uncovers the complementary DNA sequences that can then anneal to each other [Fishman-Lobell *et al.,* 1992]. To measure the efficiency of SSA, we used YMV45 derivative strains that carry the *GAL-HO* construct and tandem repeats of the *LEU2* gene located 4.6 kb apart on chromosome III, with the HO cutting site adjacent to one of the repeats (Figure 36A) [Vaze *et al.,* 2002]. HO was induced by galactose addition to exponentially growing cells and galactose was maintained in the medium in order to re-cleave the HO sites that can be rejoined by NHEJ. When DSB repair was monitored by Southern blot analysis with a *LEU2* probe, accumulation of the SSA repair product was delayed in *chd1*Δ, *chd1-K407R* and *chd1-E514A* cells compared to wild-type cells (Figure 36B,C), indicating a role for Chd1 in the SSA repair mechanism. Consistent with a defective DSB repair by SSA, *chd1*Δ, *chd1-K407R* and *chd1-E514A* cells showed a decreased viability on galactose-containing plates (HO expression on) compared to wild-type cells (Figure 36D).

Because the SSA repair mechanism does not require strand invasion and therefore does not involve the Rad51 protein [Ivanov *et al.,* 1996], we investigated the role of Chd1 in the generation of Rad51-dependent crossover (CO) and non-crossover (NCO) events by ectopic recombination. In the canonical HR pathway, ssDNA invades the homologous dsDNA to form a D-loop structure consisting of heteroduplex DNA and displaced ssDNA.

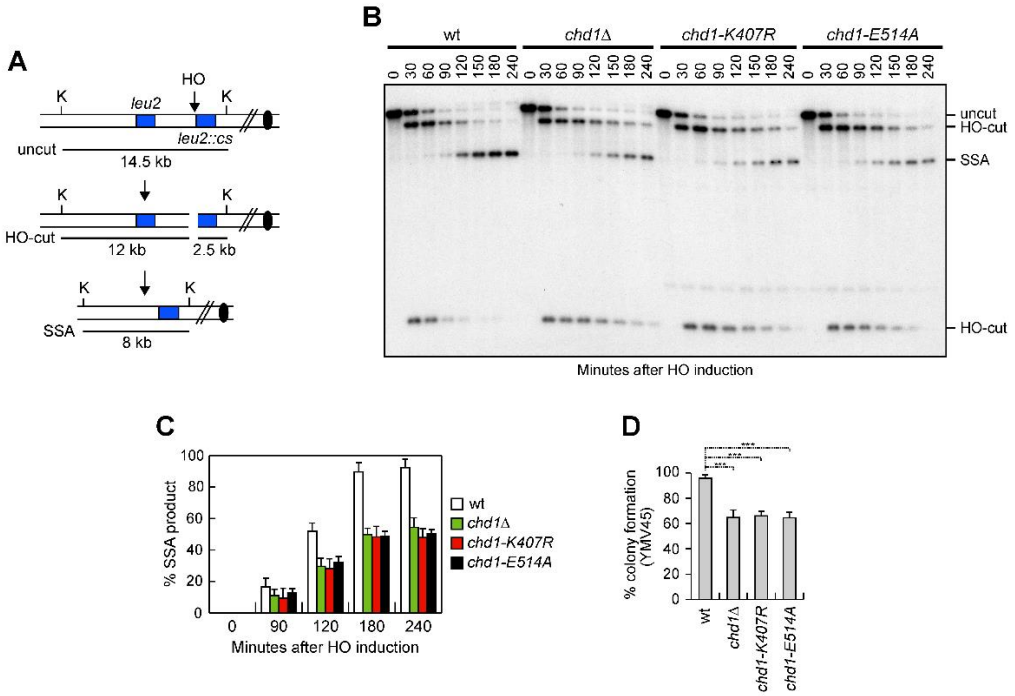

Figure 36. Chd1 dysfunction reduces DSB repair by SSA.
(A) Schematic representation of the YMV45 chromosome III region, where a unique HO-cut site is adjacent to the *leu2::cs* sequence, which is 4.6 kb apart from the homologous *leu2* sequence. HO-induced DSB results in generation of 12 kb and 2.5 kb DNA fragments (HO-cut) that can be detected by Southern blot analysis with a *LEU2* probe of *Kpn*I-digested genomic DNA. DSB repair by SSA generates a product of 8 kb (SSA). K, *Kpn*I. (B) Exponentially growing YEPR cell cultures of YMV45 derivative strains were transferred to YEPRG. Southern blot analysis of *Kpn*I-digested genomic DNA. (C) Densitometric analysis of the SSA product. The normalized intensity of the SSA product band was normalized to cut efficiency by subtracting the value of the uncut band from the total amount of DSB products for each time point. Plotted values are the mean values of three independent experiments as in panel B, with error bars denoting s.d. (D) Percentage of colony formation on YEPRG plates relatives to colony formation on YEPD plates. The reported values are the mean values of three independent experiments, with error bars denoting s.d. ***P<0.005, t-test.

If the displaced ssDNA anneals with the complementary sequence on the other side of the break, extension by DNA synthesis and ligation result in the formation of a double Holliday junction, whose cleavage results in equal number of NCO and CO products. However, if the invading strand extended by DNA synthesis is displaced and anneals with the complementary sequences on the other side of the DSB, this event leads to NCO products by SDSA [Strathern *et al.*, 1982; Ferguson & Holloman, 1996].

To analyze formation of CO and NCO products, we used tGI354 derivative strains that carry two copies of the *MAT*a sequence [Saponaro *et al.*, 2010]. One copy carries the HO cutting site and is located ectopically on chromosome V, whereas the endogenous *MAT* sequence on chromosome III carries a single base pair mutation that prevents cleavage by HO (*MAT*a-*inc*) (Figure 37A). The HO-induced DSB at the *MAT* sequence on chromosome V can be repaired by using the uncleaved *MAT*a-*inc* sequence on chromosome III, resulting in CO and NCO products (Figure 37A) [Saponaro *et al.*, 2010; Prakash *et al.*, 2009]. HO was induced by galactose addition to G2-arrested cells and galactose was maintained in the medium to cleave the HO sites that were eventually reconstituted by NHEJ. Both the 3 kb and the 3.4 kb band resulting from NCO and CO recombination events, respectively, accumulated less efficiently in *chd1*Δ and *chd1-E514A* cells compared to wild-type cells (Figure 37B,C), indicating a role for Chd1 in Rad51-dependent HR.

Consistent with defective DSB repair by ectopic recombination, a lower percentage of *chd1*Δ and *chd1-E514A* cells were able to form colonies on galactose-containing plates compared to wild-type cells (Figure 37D).

The role of Chd1 in supporting DSB repair appears to be restricted to HR-based mechanisms. In fact, when we measured the ability of cells to re-ligate by NHEJ a plasmid that was linearized before being transformed into the cells, the

efficiency of plasmid re-ligation was similar in wild-type, *chd1*Δ and *chd1-E514A* cells (Figure 37E). Furthermore, the amount of Ku70 bound at the HO-induced DSB in both *chd1*Δ and *chd1-E514A* cells was similar to that of wild-type cells (Figure 37F).

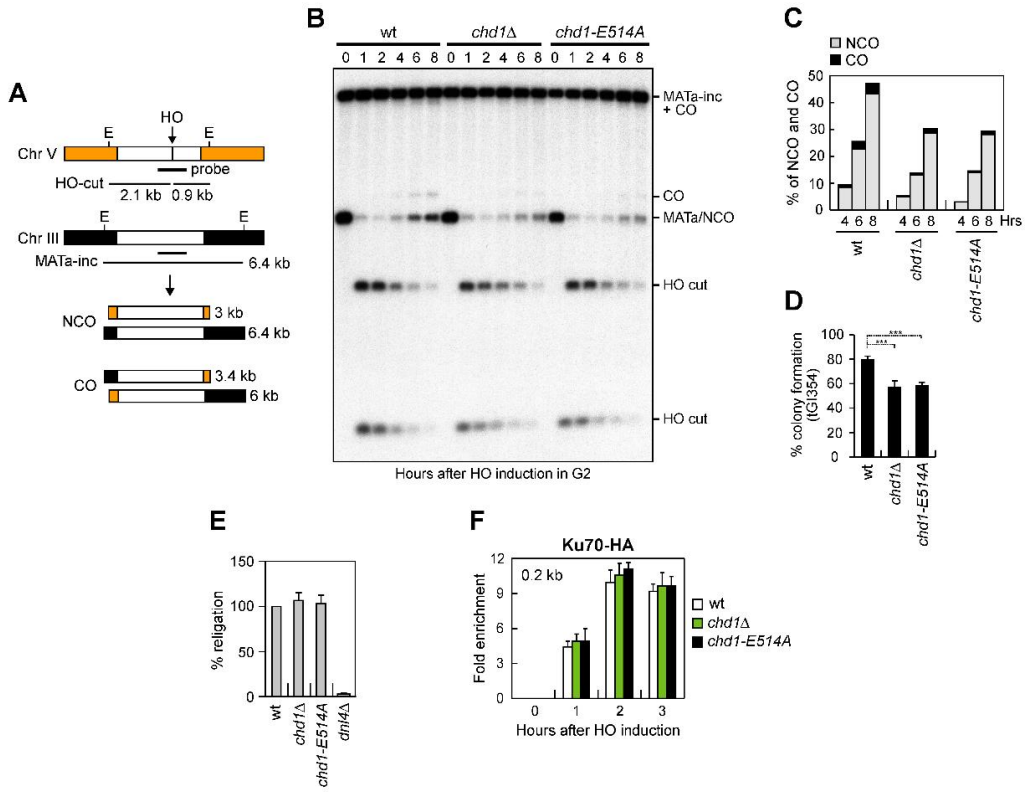

Figure 37. Chd1 dysfunction reduces DSB repair by HR.
(A) System to detect ectopic recombination. HO generates a DSB at a *MATa* DNA sequence inserted on chromosome V, while the homologous *MATa-inc* region on chromosome III cannot be cut by HO and is used as a donor for HR-mediated repair, which can generate both noncrossover (NCO) and crossover (CO) products. E, *Eco*RI. (B) G2-arrested YEPR cell cultures of tGI354 derivative strains were transferred to YEPRG at time zero and were kept arrested in G2 by nocodazole. Southern blot analysis of *Eco*RI-digested genomic DNA with the *MATa* probe depicted in panel A. (C) Densitometric analysis of CO (3.4 kb) versus NCO (3 kb) repair bands at the indicated times after HO induction. (D) Percentage of colony formation on YEPRG plates relatives to colony formation on YEPD plates. Plotted values are the mean values of three independent experiments, with error bars denoting s.d. ***P<0.005, t-test. (E) Plasmid re-ligation assay. Cells were transformed with the same amounts of *Bam*HI-linearized pRS316 plasmid DNA. Data are expressed as percentage of re-ligation relative to wild-type that was set up at 100% after normalization to the corresponding transformation efficiency of the uncut plasmid. (F) Ku70-HA ChIP at the indicated distance from the HO-cut site.

Chd1 supports DNA damage resistance and long-range resection when MRX is not fully functional

The *rad50-V1269M* (*rad50-VM*) mutation leads to a decreased $MR^{VM}X$ association at DSBs [Cassani *et al.,* 2016]. To investigate whether the diminished MRX association with DSBs in *chd1*Δ cells is physiologically important, we analyzed the effect of Chd1 dysfunction in *rad50-VM* cells. *CHD1* deletion and the presence of *chd1-K407R* or *chd1-E514A* allele, which caused by themselves a mild sensitivity to high doses of phleomycin (phleo), camptothecin (CPT) or methyl methanesulfonate (MMS) (Figure 38A), exacerbated the sensitivity to genotoxic agents of *rad50-VM* cells (Figure 38B).
As previously reported [Cassani *et al.,* 2016], *rad50-VM* cells slightly decreased Mre11 association with the HO-induced DSB (Figure 38C). Although similar amount of Mre11 can be detected in protein extracts from wild-type, *chd1*Δ, *rad50-VM* and *chd1*Δ *rad50-VM* cells (Figure 38D), the amount of Mre11 bound at the HO-induced DSB was lower in *chd1*Δ *rad50-VM* cells than in *chd1*Δ and *rad50-VM* cells (Figure 38C), thus explaining the increased DNA damage sensitivity of *chd1*Δ *rad50-VM* double mutant cells.
We also monitored the resection kinetics by following resistance to cleavage by restriction enzymes at different distances from the HO-induced DSB. As previously reported [Cassani *et al.,* 2016], the *rad50-VM* mutation affected DSB resection only very mildly (Figure 38E). ssDNA generation close to the HO cut site (0.15 or 0.65 kb) in *chd1*Δ *rad50-VM* cells was similar to that of *chd1*Δ cells (Figure 38E). By contrast, *chd1*Δ *rad50-VM* cells showed a reduction in ssDNA generation at more distant sites (1.7, 3.5, 6.5 or 8.9 kb) compared to both *chd1*Δ and *rad50-VM* cells (Figure 38E), indicating a more

severe long-range resection defect in the double mutant. Consistent with a role of Chd1 in promoting extended DSB processing, the DNA damage sensitivity of both *chd1*Δ and *chd1*Δ *rad50-VM* cells was partially suppressed by *EXO1* overexpression (Figure 38F), indicating that part of their DNA damage sensitivity was due to defects in DNA processing.

While DSB repair by SSA requires that resection reaches the complementary DNA sequences that can anneal to each other, DSB repair by ectopic recombination does not require extensive processing of the DSB ends [Chung *et al.,* 2010; Westmoreland *et al.,* 2016; Guo *et al.,* 2017]. Consistent with the finding that *chd1*Δ *rad50-VM* cells compromised extended DSB resection more severely than *chd1*Δ cells, percentage of survival of *chd1*Δ *rad50-VM* cells was lower than that of *chd1*Δ cells upon generation of a HO-induced DSB that is repaired by SSA (Figure 38G). By contrast, *chd1*Δ and *chd1*Δ *rad50-VM* cells showed similar percentage of survival upon generation of a HO-induced DSB that is repaired by ectopic recombination (Figure 38H).

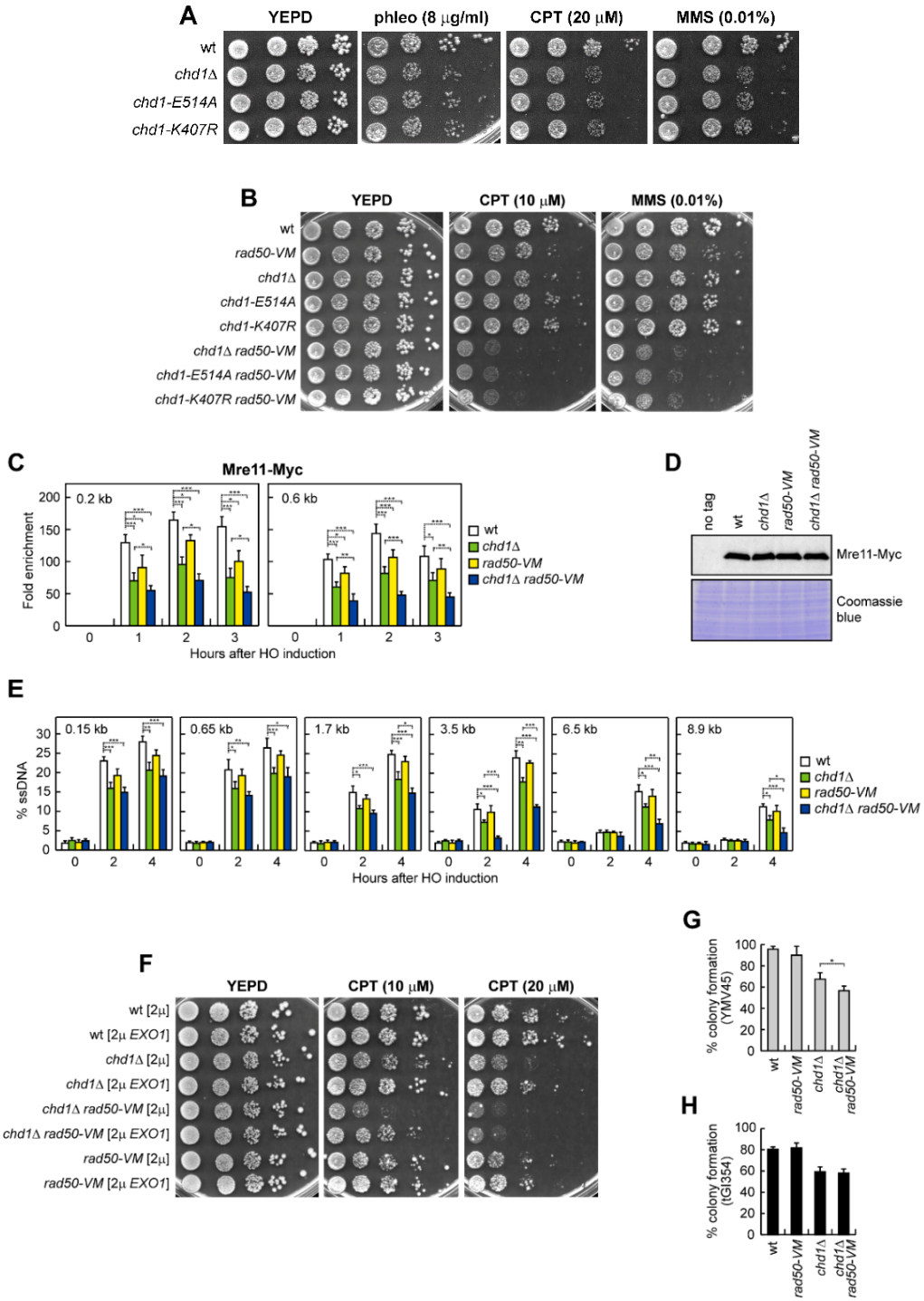
A
YEPD
phleo (8 µg/ml)
CPT (20 µM)
MMS (0.01%)
wt
chd1Δ
chd1-E514A
chd1-K407R
B
YEPD
CPT (10 µM)
MMS (0.01%)
wt
rad50-VM
chd1Δ
chd1-E514A
chd1-K407R
chd1Δ rad50-VM
chd1-E514A rad50-VM
chd1-K407R rad50-VM
C
Mre11-Myc
0.2 kb
0.6 kb
Fold enrichment
Hours after HO induction
wt
chd1Δ
rad50-VM
chd1Δ rad50-VM
D
no tag
wt
chd1Δ
rad50-VM
chd1Δ rad50-VM
Mre11-Myc
Coomassie blue
E
0.15 kb
0.65 kb
1.7 kb
3.5 kb
6.5 kb
8.9 kb
% ssDNA
Hours after HO induction
wt
chd1Δ
rad50-VM
chd1Δ rad50-VM
F
YEPD
CPT (10 µM)
CPT (20 µM)
wt [2µ]
wt [2µ EXO1]
chd1Δ [2µ]
chd1Δ [2µ EXO1]
chd1Δ rad50-VM [2µ]
chd1Δ rad50-VM [2µ EXO1]
rad50-VM [2µ]
rad50-VM [2µ EXO1]
G
% colony formation (YMV45)
wt
rad50-VM
chd1Δ
chd1Δ rad50-VM
H
% colony formation (tGI354)
wt
rad50-VM
chd1Δ
chd1Δ rad50-VM

Figure 38. Chd1 dysfunction exacerbates the DNA damage sensitivity and the long-range resection defect of *rad50-VM* cells.
(A-B) Exponentially growing cultures were serially diluted (1:10) and each dilution was spotted out onto YEPD plates with or without CPT or MMS. (C) Mre11-Myc ChIP at the indicated distances from the HO cleavage site. Data are expressed as fold enrichment at the HO-cut site over that at a non-cleavable locus (*ARO1*), after normalization to the corresponding input for each time point. Fold enrichment was then normalized to cut efficiency. Plotted values are the mean values ± s.d. from three independent experiments. ***P<0.005, **P<0.01, *P<0.05, t-test. (D) Western blot with anti-Myc antibodies of extracts used for the ChIP analysis shown in panel B. (E) Quantification of ssDNA by qPCR at different distance from the HO cut site. Plotted values are the mean values of three independent experiments, with error bars denoting s.d. ***P<0.005, **P<0.01, *P<0.05, t-test. (F) Exponentially growing cultures were serially diluted (1:10) and each dilution was spotted out onto YEPD plates with or without CPT. (F,G) Percentage of colony formation in YMV45 (G) and tGI354 (H) derivative strains on YEPRG plates relative to colony formation on YEPD plates. Plotted values are the mean values of three independent experiments, with error bars denoting s.d. *P<0.05, t-test.

DISCUSSION

DNA double-strand breaks (DSBs) are cytotoxic lesions that must be repaired to ensure genomic stability and avoid carcinogenesis or cell death. Thus, an efficient response to DSBs is important to guarantee the transmission of a correct genetic heritage to the progeny and to avoid cancer transformation. In eukaryotic cells, DSBs can be repaired by two different mechanisms called Non-Homologous End Joining (NHEJ), which directly ligates the broken DNA ends, and Homologous Recombination (HR), which uses sister chromatids or the homologous chromosome as a template for repair [Mehta & Haber, 2014; Kowalczykowski, 2015].

The first step of HR requires the nucleolytic degradation of the 5'-strands of the DSB to generate 3'-single-stranded DNA (ssDNA) in a process called DNA end resection [Bonetti *et al.,* 2018]. Different proteins are involved in the resection process. The MRX/MRN complex, consisting of Mre11, Rad50, Xrs2/NBS1 subunits, binds near the DSB and Sae2/CtIP stimulates the endonuclease activity of Mre11 to generate an endonucleolytic cleavage of the 5'-ends strands [Cannavo & Cejka, 2014]. Then, ssDNA is rapidly processed in 5'-3' direction by the nucleases Exo1 and Dna2, the latter acting in association with the helicase Sgs1, that degrade long tracts of dsDNA [Mimitou & Symington, 2008; Cejka *et al.*, 2010; Niu *et al.*, 2010]. The DNA is also processed in 3'-5' direction by Mre11 exonuclease activity [Shibata *et al.*, 2014; Reginato *et al.*, 2017; Wang *et al.*, 2017]. Subsequently, the ssDNA tails generated during the resection process are first coated by the Replication Protein A (RPA), which is then replaced by the recombinase Rad51 [Kowalczykowski, 2015]. This replacement leads to the formation of a right-handed helical filament that searches for homologous DNA molecules and catalyzes strand invasion [Villa *et al.*, 2016].

DSB occurrence also activates a highly conserved pathway, called DNA damage checkpoint, which combines DSB repair with cell cycle progression [Ciccia & Elledge, 2010]. Major checkpoint players include the protein kinases Mec1/ATR and Tel1/ATM [Ciccia & Elledge, 2010]. Tel1 binds to unprocessed DSBs (dsDNA), while Mec1 is stimulated by RPA-coated ssDNA, produced by resection. Once activated, they induce phosphorylation signals to activate the downstream protein kinases Rad53/CHK2 and Chk1/CHK1. This activation involves the conserved protein Rad9/53BP1 [Villa *et al.*, 2016], whose association to chromatin involves multiple pathways: (i) Rad9 interacts with histone H3 in Lys79-methylated form (H3-K79me) [Wysocki *et al.*, 2005; Grenon *et al.*, 2007], a methylation event that is introduced by the methyltransferase Dot1 [Giannattasio *et al.*, 2005; Toh *et al.*, 2006]; (ii) Rad9 can bind to phosphorylated histone H2A (γH2A) [Toh *et al.*, 2006; Hammet *et al.*, 2007]; (iii) phosphorylation of Rad9 by cyclin-dependent kinase leads to Rad9 interaction with Dpb11/TopBP1 [Granata *et al.*, 2010; Pfander & Diffley, 2011; Cussiol *et al.*, 2015]. In turn, Dpb11 is recruited to DSBs by the evolutionarily conserved Ddc1-Mec3-Rad17 (Rad9-Hus1-Rad1 in mammals) complex, commonly called 9-1-1, which is a ring-shaped heterotrimer.

DSB end resection needs to be strongly regulated to avoid excessive ssDNA generation and to achieve efficient DNA damage repair. Since much of the knowledge about the above mechanisms and their regulation has come from genetic and biochemical studies in the budding yeast *Saccharomyces cerevisiae*, we have used this experimental model to perform our studies.

In the first part of this thesis, I have contributed to elucidate a new level of regulation of DSB resection. In particular, I showed that abrogation of long-range resection induces a checkpoint response that decreases DNA damage resistance.

A previous study showed that the 9-1-1 complex inhibits the activity of the long-range resection nucleases by promoting the association of Rad9 with DSBs [Ngo & Lydall, 2015]. I provided evidence that Rad9 recruitment to damaged DNA by the 9-1-1 complex plays a key role in activating the checkpoint in response to DNA damaging agents when long-range resection is abrogated by the lack of both Exo1 and Sgs1. This checkpoint activation, which requires both Mre11 nuclease activity and Mec1, contributes to increase the DNA damage sensitivity of *exo1*Δ *sgs1*Δ cells. In fact, failure of 9-1-1 to recruit Dpb11 and Rad9 at DSBs, but not abrogation of the association of Rad9 with γH2A and H3-K79me, partially restores DNA damage resistance of *exo1*Δ *sgs1*Δ cells.

It is worth pointing out that while γH2A and H3-K79me spread kilobases around the lesion and throughout euchromatin, respectively [Shroff *et al.*, 2004; Nguyen & Zhang, 2011], the 9-1-1 complex is loaded at the ssDNA-dsDNA junction [Majka & Burgers, 2003; Majka *et al.*, 2006]. Furthermore, the 3'-ssDNA tail stemming from the short-range resection is expected to be bound by RPA, which was shown to promote 9-1-1 foci formation [Lisby *et al.*, 2004]. The finding that the 9-1-1 axis appears to be more specifically located at damaged DNA could explain the specific involvement of 9-1-1 in activating the checkpoint in *exo1*Δ *sgs1*Δ cells. Thus, I propose that MRX and Sae2 start resection in *exo1*Δ *sgs1*Δ cells, generating a recessed 5'-end structure for 9-1-1, Dpb11, and Rad9 loading. This initial resection is suboptimal for DSB repair by HR, causing persistent Rad53-mediated cell cycle arrest that depends primarily on 9-1-1 and decreases survival to genotoxic treatments (Figure 39).

Interestingly, the lack of either Rad9 or Mec1 not only fail to restore DNA damage resistance of *exo1*Δ *sgs1*Δ cells, but it also exacerbates their DNA damage sensitivity, suggesting that Rad9 and Mec1 play a role in DSB repair

independently of their function in checkpoint activation. Consistent with this hypothesis, Rad9 was shown to promote long-tract gene conversion, crossover recombination, and Break Induced Replication by facilitating stable annealing between the recombinogenic filament and the donor template [Ferrari *et al.*, 2020].

In addition of inhibiting Exo1 and Dna2-Sgs1 activity by promoting Rad9 association at DSBs [Ngo & Lydall, 2015], the 9-1-1 complex also negatively regulates MRX-mediated short-range resection. In fact, the lack of either Rad24 or the Ddc1 subunit of 9-1-1 partially suppresses the resection defect and increase recombination frequency of *exo1*Δ *sgs1*Δ cells. DSB resection in *ddc1*Δ *exo1*Δ *sgs1*Δ requires Mre11 nuclease activity, indicating that the 9-1-1 clamp restricts MRX-mediated resection of DSB ends.

Although our assay does not allow to detect differences in ssDNA generation very close to the break site, this control of MRX processing activity does not seem to rely on 9-1-1 recruitment of Dpb11 and Rad9, as the *ddc1-T602A* and *rad9-STAA* alleles are not capable of extending resection in *exo1*Δ *sgs1*Δ cells. Furthermore, *rad9-STAA* does not increase the recombination frequency of *exo1*Δ *sgs1*Δ cells. The extent of suppression of the DNA damage sensitivity of *exo1*Δ *sgs1*Δ by the *rad9-STAA* allele, which downregulates checkpoint activation but does not appear to extend DSB resection in *exo1*Δ *sgs1*Δ cells, is similar to that caused by the lack of Rad24 or Ddc1. This finding suggests that loss of the checkpoint rather than a more extensive resection plays the major role in increasing DNA damage resistance of *ddc1*Δ *exo1*Δ *sgs1*Δ and *rad24*Δ *exo1*Δ *sgs1*Δ cells. Although the short ssDNA tails resulting from MRX-Sae2-dependent cleavage result only in a moderate decrease of ectopic recombination [Mimitou & Symington, 2008; Westmoreland & Resnick, 2016; Zhu *et al.*, 2008], the lack of both Exo1 and Sgs1 might cause the persistence of DNA

lesions that are not lethal by themselves but whose processing can activate a checkpoint that decreases DNA damage resistance by causing a persistent cell-cycle arrest.

The control of MRX nuclease activity in the vicinity of DSB ends is poorly understood. In *exo1*Δ *sgs1*Δ cells, the MRX-dependent resection can reach up to 100-300 nucleotides possibly resulting from multiple MRX-Sae2-dependent cleavage events [Mimitou & Symington, 2008; Zhu *et al.,* 2008; Guo *et al.,* 2017]. Consistent with this hypothesis, a recent reconstitution of the *S. cerevisiae* short-range resection machinery revealed the ability of MRX-Sae2 to resect the 5'-terminated strand at DSBs in a stepwise manner, in which one MRX-Sae2 ensemble stimulates DNA cleavage by another MRX-Sae2 ensemble that is bound at adjacent sites internal to the DSB [Cannavo *et al.,* 2019]. The 3'-5' exonucleolytic activity is then limited to degrading DNA between the endonucleolytic incision sites.

Interestingly, the 9-1-1 complex is known to associate at the ssDNA-dsDNA junctions in a resection-dependent manner [Ellison & Stillman, 2003; Majka & Burgers, 2003; Majka *et al.,* 2006; Bantele *et al.,* 2019]. Furthermore, both 9-1-1 and MRX are capable of sliding along dsDNA [Majka & Burgers, 2003; Myler *et al.,* 2017]. Our finding that the 9-1-1 complex negatively regulates Mre11 nuclease suggests a model whereby the generation of ssDNA by MRX-mediated stepwise incision allows the loading to the resection border of the 9-1-1 complex, which, by sliding on dsDNA, might limit MRX diffusion and therefore additional cleavage events (Figure 39). Consistent with such a function, Rad50 ChIP signals, which accumulated in *exo1*Δ *sgs1*Δ very close to the break site, were broader distributed and persisted longer with increasing distance from the DSB end in both in *ddc1*Δ *exo1*Δ *sgs1*Δ and *rad24*Δ *exo1*Δ *sgs1*Δ than in *exo1*Δ *sgs1*Δ cells. 9-1-1 binding to the DSB ends also recruits

Dpb11, which in turn provides a scaffolding function for Rad9 and Mec1-Ddc2, to form a protein complex that allows Rad53 phosphorylation and activation in proximity to DNA lesions (Figure 39) [Gilbert *et al.*, 2001; Sweeney *et al.*, 2005; Schwartz *et al.*, 2002].

In conclusion, our findings reveal that the 9-1-1 complex, in addition to regulating long-range resection nucleases [Ngo & Lydall, 2015], also inhibits short-range resection by restricting MRX nuclease activity to prevent unscheduled DNA degradation. Furthermore, the 9-1-1 function in recruiting Dpb11 and Rad9 can couple the control of DSB resection with checkpoint activation. Since the 9-1-1 complex is evolutionarily conserved, it will be interesting to investigate whether a similar regulatory mechanism on DSB resection and checkpoint activation also occurs in mammalian cells.

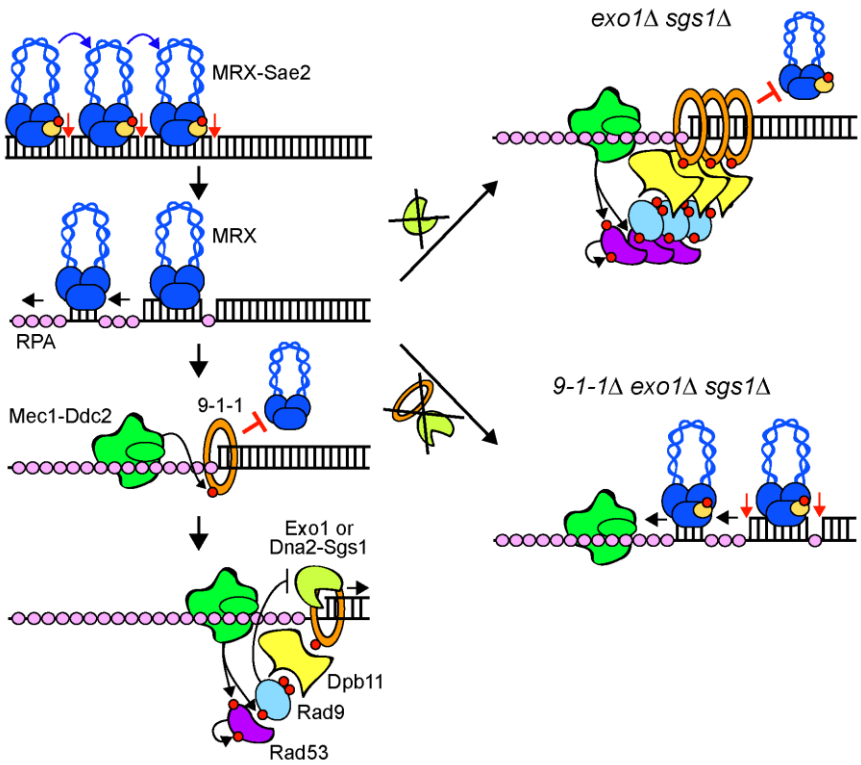

Figure 39. Model for 9-1-1 function during short-range resection.
MRX, aided by phosphorylated Sae2, promotes cleavage (red arrows) of dsDNA by another MRX complex that binds DNA at an adjacent site (blue arrows). The nicks are followed by exonucleolytic degradation of the DNA between the incision sites (black arrows). When a certain amount of ssDNA coated by RPA is generated, the loading of 9-1-1 at the ssDNA-dsDNA junction is allowed and limits MRX diffusion and additional MRX-mediated DNA cleavage events. Exo1 and Dna2-Sgs1 extend the resected tracts. The generation of RPA-coated ssDNA allows the recruitment of Mec1-Ddc2, which creates a docking site on 9-1-1 for Dpb11 binding. Dpb11 in turn engages interactions with Rad9 and Mec1-Ddc2 to allow Rad53 phosphorylation and activation. Rad9 and Rad53, in turn, inhibit the activity of Exo1 and Dna2-Sgs1. In the absence of both Exo1 and Dna2-Sgs1 (*exo1Δ sgs1Δ*), accumulation of short 3′ ssDNA tails generated by Mre11 nuclease leads to an increased association of 9-1-1 with the ss-dsDNA junction, which leads to Dpb11- and Rad9- mediated Rad53 hyperactivation that decreases DNA damage resistance. The absence of 9-1-1 in *exo1Δ sgs1Δ* cells (*exo1Δ sgs1Δ 9-1-1Δ*) prevents checkpoint activation and allows the sliding on dsDNA of MRX, which catalyzes additional cleavage events. Red dots indicate phosphorylation events.

Repair of DSBs also occurs in a chromatin context [Casari *et al.,* 2019]. When engaged in nucleosome structures, DNA tends to be refractory to be processed. To facilitate the access of DNA repair proteins, chromatin structure near DSBs undergoes extensive modifications by a series of chromatin remodelers [Zhou *et al.,* 2016]. These modifications include nucleosome sliding, nucleosomes or histones removal and histones post-translational modifications. Thus, given the role of chromatin remodeling in DSBs repair, in the second part of this thesis, I have contributed to study the importance of chromatin remodeling for DSB resection and checkpoint activation, by exploring the role of the protein Dpb4.

I showed that the conserved histone fold protein Dpb4 is involved in at least two aspects of the cellular response to DSBs: i) it promotes MRX association to DSBs, thus allowing DSB resection; ii) it promotes Rad9 association to DSBs, thus allowing checkpoint activation. I found that Dpb4 is required to remove histones around a DSB. As the presence of nucleosomes inhibits resection both *in vitro* and *in vivo* [Adkins *et al.,* 2013; Mimitou *et al.,* 2017], these data support the view that failure to remove histones from the DSB ends can account for the decreased MRX association to DSBs and the resection defect of *dpb4*Δ cells.

Dpb4 is shared by two highly conserved protein complexes: the chromatin remodeling ISW2/hCHRAC, which is known to slide nucleosomes by disrupting histone-DNA interactions [Clapier *et al.,* 2017; Hada *et al.,* 2019; Sinha *et al.,* 2017], and the Pol ε complex, which is implicated in DNA replication and heterochromatin maintenance [Iida & Araki, 2004; Tsubota *et al.,* 2006]. In both complexes, Dpb4 interacts with a histone fold protein, namely Dls1 in the ISW2 complex and Dpb3 in the Pol ε complex, to form

H2A-H2B-like complexes [Iida & Araki, 2004; Corona *et al.*, 2000; Poot *et al.*, 2000; Gnesutta *et al.*, 2013].

I found that Dpb4 promotes DSB resection by acting with Dls1 and Isw2 subunits of the ISW2 complex, whereas it facilitates Rad9 association to DSBs and checkpoint activation by acting with Dpb3. In fact, similar to *DPB4* deletion, the lack of Dls1 or Isw2, but not of Dpb3, severely reduces histone removal from the DSB ends, MRX association to DSBs and DSB resection. By contrast, the lack of Isw2 does not reduce checkpoint activation and Rad9 association to DSBs. Rather, the Dpb4 checkpoint function relies on Dpb4 interaction with Dpb3, whose lack reduces Rad9 association to DSBs and DSB-induced Rad53 phosphorylation. The lack of Dpb4 does not further reduce Rad9 persistence at DSBs in *dpb3*Δ cells, indicating that Dpb3 and Dpb4 promote Rad9 association to DSBs by acting in the same pathway. The Dpb4-mediated histone removal and Rad9 loading to DSBs occurs independently to each other, as the lack of Isw2 impairs histone removal from DSBs but not Rad9 association to DSBs, whereas the lack of Dpb3 impairs Rad9 association to DSBs but not histone removal from DSBs. Furthermore, the finding that *dpb3*Δ cells, but not *isw2*Δ cells, showed reduced Rad53 activation indicates that the checkpoint defect of *dpb4*Δ cells is caused by the decreased Rad9 association at DSBs, rather than by the reduced amount of ssDNA caused by defective resection.

The function of Dpb4 in promoting Isw2 and Rad9 association to DSBs is enhanced by the A62S mutation that leads to an increased Dpb4 persistence at DSBs, suggesting that the Dpb4 functions in both chromatin remodeling and checkpoint activation rely on its DNA binding property. Interestingly, although the A62S mutation slightly reduces the DNA binding affinity of both Dpb3-

Dpb4 and Dls1-Dpb4 complexes, it favors formation of higher order DNA-Dpb3-Dpb4 and DNA-Dls1-Dpb4 complexes. Although the nature of these complexes requires further investigation, their formation suggests that the increased amount of chromatin-bound Dpb4^{A62S} detected by ChIP is due to a transition to high stoichiometry protein-DNA complexes.

The Dpb4^{A62S} mutant variant enhances Isw2 association to DSBs but reduces histone removal from the DSB ends. Similarly, deletion of the negatively charged C-terminus of the *D. melanogaster* Dpb4 ortholog enhances DNA binding but inhibits nucleosome sliding [Hartlepp *et al.,* 2005], suggesting that not only a poor, but also an increased Isw2 persistence to DSBs impairs Isw2 activity. As nucleosome mobilization by Isw2 involves DNA translocation inside the nucleosome that requires Isw2 ability to break and reform DNA-histone contacts [Zofall *et al.,* 2006], increasing the interaction between Isw2 and the nucleosomal DNA might enhance the energetic barrier to nucleosome repositioning, thus explaining the histone removal defect of *dpb4-A62S* cells.

The Dpb3-Dpb4 complex is flexibly tethered to the core subunits of Pol ε [Yuan *et al.,* 2020], which was previously shown to activate a checkpoint in response to DNA replication stress independently of the 9-1-1 complex [Araki *et al.,* 1995; Navas *et al.,* 1995; Wang & Elledge, 1999; Puddu *et al.,* 2011]. This finding raises the question of whether Dpb3-Dpb4 dimer acts through Pol ε to activate the checkpoint. I found that Pol2 is recruited to DSBs independently of DNA replication and Dpb4^{A62S} leads to an increased Pol2 association at DSBs, suggesting that Dpb4 might act within the Pol ε holoenzyme to enhance Rad9 association to DSBs and checkpoint activation.

One possibility is that Dpb4 promotes Rad9 association to DSBs by directly recruiting Rad9 to the DSB sites. However, I failed to detect any interaction

between Dpb4 and Rad9 by coimmunoprecipitation. Interestingly, Dpb4 promotes Rad9 association to DSBs by acting in the same pathway of Dot1, which is known to drive Rad9 association to DSBs by catalyzing H3-K79 methylation. H3-K79 is constitutively methylated by Dot1 in both mammalian and yeast cells [Feng *et al.,* 2002; van Leewen *et al.,* 2002; Lacoste *et al.,* 2002]. Furthermore, at least in human cells, irradiation does not lead to increased histone H3-K79 methylation [Huyen *et al.,* 2004], raising the question of how DSBs expose methylated H3-K79 to Rad9 recognition. The Dpb3-Dpb4 complex has been shown to bind histones H3 and H4 in the context of chromatin, and to possess intrinsic H3-H4 chaperone and DNA supercoiling activities [Bellelli *et al.,* 2018; Yu *et al.,* 2018]. Thus, it would be tempting to speculate that the Dpb3-Dpb4 complex, possibly as part of the Pol ε holoenzyme, induces re-deposition/exchange of histones H3 and H4 at the DSB ends, where subsequent H3 methylation by Dot1 would lead to exposure of histone H3 to Rad9 recognition (Figure 40).

In conclusion, I propose that the Dls1-Dpb4 dimer binds the DSB ends and facilitates the loading of the ISW2/hCHRAC complex, which in turn promotes MRX association to DSBs and DSB resection by sliding/removing nucleosomes from the DSB ends (Figure 40). The Dpb3-Dpb4 complex in turn promotes Rad9 association to the DSB and checkpoint activation by inducing exposure of histone H3 to Rad9 binding. Because Dpb4 is evolutionarily conserved, it will be interesting to investigate whether, depending on its interactors, it plays similar roles in DSB resection and checkpoint activation also in mammalian cells.

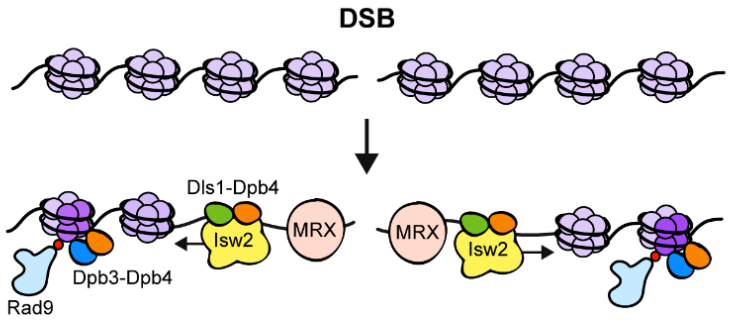

Figure 40. Model for Dpb4 function at DSBs.
After DSB formation, the Dls1-Dpb4 dimer promotes the association of Isw2 to the DSB, which catalyzes nucleosome sliding/removal and facilitates MRX association to them. The Dpb3-Dpb4 dimer, possibly in complex with Pol ε, in turn uses its histone chaperone activity to induce re-deposition/exchange of H3 and H4 histones (dark violet), whose subsequent H3 methylation by Dot1 (red dots) leads to H3 exposure to Rad9 recognition.

In the last part of the thesis, I have contributed to elucidate the role of Chd1, another chromatin remodeling protein, that facilitates both short- and long-range resection by promoting the association of MRX and Exo1 to the DSB ends and DSB repair by homologous recombination.

In mammals, loss of the ATP-dependent chromatin remodeling protein CHD1 impairs DSB repair and decreases the assembly of RPA and RAD51 foci [Kari *et al.*, 2016], suggesting a role for this protein in DSB resection. I showed that the lack of *S. cerevisiae* Chd1 reduces nucleosome eviction from the DSB ends.

Furthermore, its lack impairs both short- and long- range resection by reducing MRX and Exo1 association with DSBs. The Chd1 functions in nucleosome eviction from DSBs and resection require its ATPase activity, suggesting that Chd1 promotes resection by acting as nucleosome evictor in the opening of chromatin to promote MRX and Exo1 binding/persistence to DSBs. Consistent with a role of chromatin compaction in counteracting MRX and Exo1 accessibility to the DSB ends, assembly of DNA into nucleosomes causes inhibition of both Exo1 resection activity and MRX-dependent activation of Tel1 kinase [Hailemariam *et al.,* 2019; Adkins *et al.,* 2013]. Furthermore, high-throughput single-molecule microscopy has shown that MRN searches for free DNA ends by one-dimensional facilitated diffusion and transiently dissociates from the DNA backbone to bypass a nucleosome [Myler *et al.,* 2017].

The decreased DSB resection in *chd1* mutants impairs DSB repair by SSA, which requires that resection of the DSB ends reaches the complementary DNA sequences. Furthermore, the lack of Chd1 or of its ATPase activity leads to a reduction of NCO products during ectopic recombination. Consistent with previous findings that the lack of Chd1 does not affect formation of ectopic crossover products in mitotically dividing cells [Wild *et al.,* 2019], the generation of CO products is not slightly affected. In any case, the role of Chd1 appears specific for DSB repair by HR, as the lack of Chd1 affects neither DSB repair by NHEJ nor the association of the Ku complex with DSBs.

The function of Chd1 in promoting MRX binding/persistence to DSBs becomes important to support DNA damage resistance when MRX accumulation at DSBs is suboptimal, such as in the presence of the *rad50-VM* mutation. This mutation reduces MRX association at DSBs and the lack of Chd1 reduces further the amount of $MR^{VM}X$ bound at DSBs. As a consequence, *chd1*Δ *rad50-VM* cells are more sensitive to genotoxic agents compared to each single

mutant. Interestingly, while resection very close to the DSB occurs with similar kinetics in *chd1*Δ and *chd1*Δ *rad50-VM* cells, long-range resection is compromised more severely in *chd1*Δ *rad50-VM* cells compared to both *chd1*Δ and *rad50-VM* single mutants. These findings, together with the observation that overexpression of *EXO1*, which is the main nuclease involved in long-range resection, partially suppresses the DNA damage sensitivity of both *chd1*Δ and *chd1*Δ *rad50-VM* cells, suggests a direct role of Chd1 in supporting Exo1 resection activity. In accord with this hypothesis, Chd1 was found to interacts with Exo1 and to enable MutLγ-Exo1-dependent processing of joint molecules into COs during meiosis I [Wild *et al.,* 2019].

While in mammals CHD1 was shown to promote the recruitment of CtIP at DSBs, the association of Sae2, the yeast CtIP counterpart, does not require Chd1 function. However, it should be pointed out that the localization of CtIP to DSBs in both mammals and *S. pombe* requires the MRN complex [You *et al.,* 2009; Limbo *et al.,* 2007; Williams *et al.,* 2009], whereas Sae2 association with DSBs in *S. cerevisiae* occurs independently of MRX [Lisby *et al.,* 2004]. As the role of mammalian CHD1 in promoting MRN association with DSBs has not been investigated yet, one possibility is that the poor CtIP binding to DSBs in CHD1-depleted cells might be due to a diminished MRN association with DSBs.

In conclusion, I propose that Chd1 increases the accessibility of chromatin to facilitate/stabilize the association of MRX and Exo1 with the DSBs, which in turn initiate DSB processing. The *CHD1* gene is frequently mutated in prostate cancer where these mutations are associated with a poor prognosis [Burkhardt *et al.,* 2013; Grasso *et al.,* 2012; Huang *et al.,* 2012; Shenoy *et al.,* 2017]. Our finding that Mre11 dysfunction can be rendered synthetically lethal with *chd1* mutations in the presence of genotoxic agents suggests that MRX inhibitors in

combination with DNA-damaging chemotherapy could be beneficial in patients whose tumors are defective in CHD1 function.

In conclusion, in this thesis, I have demonstrated novel mechanisms involving the DNA damage checkpoint activation and the chromatin remodeling regulate DSB resection. Since these pathways are conserved from *S. cerevisiae* to humans, the mechanistic insights gained by these studies can supply the molecular bases for the development of new strategies aimed at maximizing the odds of synergistic antitumor efficacy, providing the basis to develop new and more appropriate tools to target specific cancers or patients with defects in DNA repair genes.

METHODS

Yeast strains

Saccharomyces cerevisiae is the experimental model used in this study. The strains are derivatives of W303 (*MATa/α ade2-1 can1-100 his3-11,15 leu2-3,112 trp1-1 ura3-1 rad5-535*), JKM139 (*MATa ho hmlΔ::ADE1 hmrΔ::ADE1 ade1-100 leu2-3,112 lys5 trp1::hisG ura3-52 ade3::GAL-HO*), YMV45 (*ho hml::ADE1 mata::hisG hmr::ADE1 leu2::leu2(Asp718-SalI)-URA3-pBR332-MATa ade3::GAL::HO ade1 lys5 ura3-52 trp1::hisG*), tGI354 (*ho hml::ADE1 MATa-inc hmr::ADE1 ade1 leu2-3,112 lys5 trp1::hisG ura3-52 ade3::GAL10::HO arg5,6::MATa::HPH*). Strain genotypes are listed in Table 1. Strain JKM139, used to detect DSB resection, HO checkpoint and to perform ChIP analysis, strain YMV45 for DSB repair by SSA and strain tGI354, used to detect ectopic recombination, was kindly provided by J. Haber (Brandeis University, Waltham, USA). Strain used to monitor Lys+ recombinants was kindly provided by S. Jinks-Robertson (Duke University School of Medicine, Durham, USA). The *ddc1-T602A* and *rad9-STAA* alleles were kindly provided by J. Diffley (The Francis Crick Institute, London UK) and B. Pfander (Max Planck Institute of Biochemistry, Martinsried, Germany). The JKM139 *mre11-H125N exo1Δ sgs1Δ* strain was kindly provided by G. Ira (Baylor College of Medicine, Houston, USA). The pRS316 DDC2-RAD53-3FLAG (DDC2-RAD53) plasmid was kindly provided by D. Stern (University of California, San Francisco).

Gene disruptions and tag fusions were generated by one-step PCR homology cassette amplification and standard yeast transformation method.

Yeast strain	Relevant genotype	Source
JKM139	*MAT*a *hml*Δ::*ADE1, hmr*Δ*::ADE1, ade1-100, lys5, leu2-3,112, trp1::hisG ura3-52, ho, ade3::GAL-HO*	Lee *et al.*, 1998
DMP 7241/35C	JKM139 *MAT*a *exo1*Δ*::LEU2 sgs1*Δ*::NATMX ddc1-T602A::URA3*	This study
DMP 6928/10C	JKM139 *MAT*a *exo1*Δ*::LEU2 sgs1*Δ*::NATMX rad24*Δ*::KANMX*	This study
YLL 1643.1	JKM139 *MAT*a *bar1*Δ*::HPHMX*	Gobbini *et al.*, 2018
DMP 6433/6C	JKM139 *MAT*a *bar1*Δ*::TRP1 YKU70-3HA::URA3*	Gobbini *et al.*, 2018
DMP 7194/2B	JKM139 *MAT*a *bar1*Δ*::TRP1 YKU70-3HA::URA3 chd1*Δ*::HPHMX*	This study
DMP 7251/10A	JKM139 *MAT*a *bar1*Δ*::TRP1 YKU70-3HA::URA3 chd1-E514A::LEU2*	This study
YLL 4201.5	JKM139 *MAT*a *chd1*Δ*::HPHMX*	This study
YLL 4291.4	JKM139 *MAT*a *CHD1-18MYC::URA3*	This study
YLL 4350.1	JKM139 *MAT*a *chd1-E514A::LEU2*	This study
YLL 4351.1	JKM139 *MAT*a *chd1-K407R::LEU2*	This study
DMP 7081/8A	JKM139 *MAT*a *ddc1*Δ*::KANMX*	This study
DMP 7244/4B	JKM139 *MAT*a *ddc1-T602A::URA3 DPB4-3HA::TRP1*	This study
DMP 7245/2A	JKM139 *MAT*a *ddc1*Δ*::KANMX DPB4-3HA::TRP1*	This study
YLL 4276.8	JKM139 *MAT*a *dls1*Δ*::URA3*	This study
DMP 7298/1D	JKM139 *MAT*a *dls1*Δ*::URA3 MRE11-18MYC::TRP1*	This study
YLL 4344.A	JKM139 *MAT*a *dpb3*Δ*::URA3*	This study
DMP 7324/5D	JKM139 *MAT*a *dpb3*Δ*::URA3 dpb4Δ::HPHMX RAD9-3HA::TRP1*	This study
DMP 7280/11D	JKM139 *MAT*a *dpb3*Δ*::URA3 MRE11-18MYC::TRP1*	This study
DMP 7246/4D	JKM139 *MAT*a *dpb3*Δ*::URA3 RAD9-3HA::TRP1*	This study
DMP 7328/10D	JKM139 *MAT*a *dpb4*Δ*::HPH RAD9-3HA::TRP1 hta2*Δ*::NATMX hta1-S129A::URA3*	This study

DMP 7354/3C	JKM139 *MAT*a *dpb4Δ::HPHMX POL2-3HA::URA3*	This study
YLL 4312.3	JKM139 *MAT*a *DPB4-3HA::TRP1*	This study
YLL 4227.23	JKM139 *MAT*a *dpb4-A62S::KANMX*	This study
DMP 7137/11A	JKM139 *MAT*a *dpb4-A62S::KANMX MRE11-18MYC::TRP1*	This study
YLL 4382.14	JKM139 *MAT*a *dpb4-A62S::KANMX POL2-3HA::URA3*	This study
DMP 7071/6D	JKM139 *MAT*a *dpb4-A62S::KANMX RAD9-3HA::TRP1*	This study
DMP 7070/14B	JKM139 *MAT*a *dpb4-A62S::KANMX sae2Δ::HPHMX*	This study
DMP 7069/18A	JKM139 *MAT*a *dpb4-A62S::KANMX tel1Δ::NATMX*	This study
YLL 4311/A	JKM139 *MAT*a *dpb4-A62S-3HA::TRP1*	This study
YLL 4182.1	JKM139 *MAT*a *dpb4Δ::HPHMX*	This study
DMP 7281/1D	JKM139 *MAT*a *dpb4Δ::HPHMX MRE11-18MYC::TRP1*	This study
DMP 7101/1D	JKM139 *MAT*a *dpb4Δ::HPHMX RAD9-3HA::TRP1*	This study
DMP 7285/10B	JKM139 *MAT*a *dpb4Δ::HPHMX rad9Δ::KANMX TRP1::rad9-ST462,474AA-3HA::URA3*	This study
DMP 7081/4B	JKM139 *MAT*a *exo1Δ::LEU2 sgs1Δ::NATMX*	This study
DMP 7081/10A	JKM139 *MAT*a *exo1Δ::LEU2 sgs1Δ::NATMX ddc1Δ::KANMX*	This study
DMP 7243/10C	JKM139 *MAT*a *exo1Δ::LEU2 sgs1Δ::NATMX rad53-K227A::KANMX*	This study
DMP 7242/13C	JKM139 *MAT*a *exo1Δ::LEU2 sgs1Δ::NATMX rad9Δ::KANMX TRP1::rad9-ST462,474AA*	This study
YLL 1959.2	JKM139 *MAT*a *EXO1-18MYC::TRP1*	Manfrini *et al.*, 2015
DMP 7385/4A	JKM139 *MAT*a *EXO1-18MYC::TRP1 chd1Δ::HPHMX*	This study
DMP 7386/10C	JKM139 *MAT*a *EXO1-18MYC::TRP1 chd1-E514A::LEU2*	This study
DMP 7387/6D	JKM139 *MAT*a *EXO1-18MYC::TRP1 chd1-K407R::LEU2*	This study
YLL 4274.9	JKM139 *MAT*a *ISW2-3HA::TRP1*	This study

DMP 7349/3A	JKM139 *MAT*a *ISW2-3HA::TRP1 dpb4Δ::HPHMX*	This study
DMP 7348/5C	JKM139 *MAT*a *ISW2-3HA::TRP1 dpb4-A62S::KANMX*	This study
YLL 4264.1	JKM139 *MAT*a *isw2Δ::HPHMX*	This study
DMP 7323/3B	JKM139 *MAT*a *isw2Δ::HPHMX dpb4Δ::HPHMX MRE11-18MYC::TRP1*	This study
DMP 7195/7D	JKM139 *MAT*a *isw2Δ::HPHMX MRE11-18MYC::TRP1*	This study
DMP 7107/1A	JKM139 *MAT*a *isw2Δ::HPHMX RAD9-3HA::TRP1*	This study
YLL 1854.2	JKM139 *MAT*a *MRE11-18MYC::TRP1*	Clerici *et al.*, 2006
DMP 7373/9B	JKM139 *MAT*a *MRE11-18MYC::TRP1 rad50-V1269M::KANMX chd1Δ::HPHMX*	This study
DMP 7076/1D	JKM139 *MAT*a *MRE11-18MYC::TRP1 chd1Δ::HPHMX*	This study
DMP 7311/8D	JKM139 *MAT*a *MRE11-18MYC::TRP1 chd1-E514A::LEU2*	This study
DMP 7312/4D	JKM139 *MAT*a *MRE11-18MYC::TRP1 chd1-K407R::LEU2*	This study
DMP 6021/4A	JKM139 *MAT*a *MRE11-18MYC::TRP1 rad50-V1269M::KANMX*	Cassani *et al.*, 2016
DMP 7240/4B	JKM139 *MAT*a *mre11-H125N::URA3 exo1Δ::TRP1 sgs1Δ::KANr ddc1Δ::KANMX*	This study
YLL 1769.1	JKM139 *MAT*a *mre11Δ::NATMX*	Gobbini *et al.*, 2015
YLL 4382.57	JKM139 *MAT*a *POL2-3HA::URA3*	This study
YLL 4017.7	JKM139 *MAT*a *rad24Δ::KANMX*	This study
DMP 7271/9C	JKM139 *MAT*a *rad24Δ::KANMX DPB4-3HA::TRP1*	This study
YLL 3501.1	JKM139 *MAT*a RAD50-HA::URA3	This study
DMP 7265/23B	JKM139 *MAT*a RAD50-HA::URA3 *ddc1Δ::KANMX*	This study
DMP 7265/16D	JKM139 *MAT*a RAD50-HA::URA3 *exo1Δ::LEU2 sgs1Δ::NATMX*	This study
DMP 7265/13C	JKM139 *MAT*a RAD50-HA::URA3 *exo1Δ::LEU2 sgs1Δ::NATMX ddc1Δ::KANMX*	This study
DMP 7266/29B	JKM139 *MAT*a RAD50-HA::URA3 *exo1Δ::LEU2 sgs1Δ::NATMX rad24Δ::KANMX*	This study

DMP 7266/25B	JKM139 *MAT*a RAD50-HA::URA3 *rad24Δ::KANMX*	This study
DMP 5819/3D	JKM139 *MAT*a *rad50-V1269M::KANMX*	Cassani *et al.*, 2016
DMP 7094/3B	JKM139 *MAT*a *rad50-V1269M::KANMX chd1Δ::HPHMX*	This study
YLL 3077.12	JKM139 *MAT*a *rad51Δ::HPHMX*	This study
YLL 3421.2	JKM139 *MAT*a *RAD9-3HA::TRP1*	Clerici *et al.*, 2014
DMP 7317/7D	JKM139 *MAT*a *RAD9-3HA::TRP1 bar1Δ::TRP1*	This study
DMP 7317/9D	JKM139 *MAT*a *RAD9-3HA::TRP1 bar1Δ::TRP1 dpb4Δ::HPHMX*	This study
DMP 7317/9A	JKM139 *MAT*a *RAD9-3HA::TRP1 dot1Δ::KANMX bar1Δ::TRP1*	This study
DMP 7317/7A	JKM139 *MAT*a *RAD9-3HA::TRP1 dot1Δ::KANMX bar1Δ::TRP1 dpb4Δ::HPHMX*	This study
YLL 3426.1	JKM139 *MAT*a *RAD9-3HA::TRP1 hta2Δ::NATMX hta1-S129A::URA3*	This study
DMP 5793/6C	JKM139 *MAT*a *rad9Δ::KANMX*	This study
YLL 4176.17	JKM139 *MAT*a *rad9Δ::KANMX TRP1::rad9-ST462,474AA::URA3*	This study
YLL 4345.9	JKM139 *MAT*a *rad9Δ::KANMX TRP1::rad9-ST462,474AA-3HA::URA3*	This study
YLL1523.3	JKM139 *MAT*a *sae2Δ::KANMX*	Gobbini *et al.*, 2015
YLL 3136.13	JKM139 *MAT*a *SAE2-18MYC::TRP1*	This study
DMP 7309/5D	JKM139 *MAT*a *SAE2-18MYC::TRP1 chd1-E514A::LEU2*	This study
DMP 7310/1C	JKM139 *MAT*a *SAE2-18MYC::TRP1 chd1-K407R::LEU2*	This study
YLL 4232.5	JKM139 *MAT*a *SAE2-18MYC::TRP1 chd1Δ::HPHMX*	This study
YLL 1794.3	JKM139 *MAT*a *tel1Δ::NATMX*	Gobbini *et al.*, 2015
yZZ 535	JKM139 *mre11-H125N::URA3 exo1Δ::TRP1 sgs1Δ::KANr*	Zhu *et al.*, 2008
W303	*MAT*a/α *ade2-1 can1-100 his3-11,15 leu2-3,112 trp1-1 ura3-1 rad5-535*	Bonetti *et al.*, 2009
DMP 6742/4D	W303 *MAT*a *exo1Δ::HIS3 sgs1Δ::TRP1 rad9Δ::URA3*	This study

DMP 7292/2A	W303 *MAT*a *chd1*Δ*::HPHMX*	This study
DMP 7145/1D	W303 *MAT*a *chd1*Δ*::HPHMX rad50-V1269M::KANMX*	This study
DMP 7252/3A	W303 *MAT*a *chd1-E514A::LEU2*	This study
DMP 7252/3B	W303 *MAT*a *chd1-E514A::LEU2 rad50-V1269M::KANMX*	This study
DMP 7289/2D	W303 *MAT*a *chd1-K407R::LEU2*	This study
DMP 7289/6B	W303 *MAT*a *chd1-K407R::LEU2 rad50-V1269M::KANMX*	This study
YBP 269	W303 *MAT*a *ddc1-T602A::HIS3MX6*	Pfander & Diffley, 2011
YLL 4277.1	W303 *MAT*a *dls1*Δ*::URA3*	This study
DMP 7152/7B	W303 *MAT*a *dls1*Δ*::URA3 dpb4-A62S::KANMX*	This study
DMP 7143/1D	W303 *MAT*a *dls1*Δ*::URA3 tel1*Δ*::HIS3*	This study
DMP 7153	W303 *MAT*a *dls1*Δ*::URA3 tel1*Δ*::HIS3 dpb4-A62S::KANMX*	This study
DMP 7355/2C	W303 *MAT*a *DLS1-3HA::TRP1 DPB4-18MYC::URA3*	This study
DMP 7356/10B	W303 *MAT*a *DLS1-3HA::TRP1 dpb4-A62S-18MYC::URA3*	This study
YLL 2479.1	W303 *MAT*a *dnl4*Δ*::KANMX*	This study
YLL 3193.1	W303 *MAT*a *dot1*Δ*::NATMX*	This study
MUT 31.9A	W303 *MAT*a *dpb11-L410F*	This study
DMP 4302/3	W303 *MAT*a *dpb3*Δ*::URA3*	This study
DMP 7351/1C	W303 *MAT*a *DPB4-3HA::TRP1 DPB3-18MYC::URA3*	This study
DMP 6389/3C	W303 *MAT*a *dpb4-A62S::KANMX*	This study
DMP 7039/3D	W303 *MAT*a *dpb4-A62S::KANMX sae2*Δ*::HIS3*	This study
DMP 7039/7C	W303 *MAT*a *dpb4-A62S::KANMX sae2*Δ*::HIS3*	This study
DMP 7040/1A	W303 *MAT*a *dpb4-A62S::KANMX tel1*Δ*::HIS3*	This study

DMP 7350/6A	W303 *MAT*a *dpb4-A62S-3HA::TRP1 DPB3-18MYC::URA3*	This study
DMP 7039/5C	W303 *MAT*a *dpb4Δ::HPHMX sae2Δ::HIS3*	This study
DMP 7039/8D	W303 *MAT*a *dpb4Δ::HPHMX sae2Δ::HIS3*	This study
DMP 7040/4C	W303 *MAT*a *dpb4Δ::HPHMX tel1Δ::HIS3*	This study
DMP 6657/8A	W303 *MAT*a *exo1Δ::HIS3 sgs1Δ:::TRP1 mre11-H125N*	This study
DMP 5058/11B	W303 *MAT*a *exo1Δ::HIS3 sgs1Δ::TRP1*	This study
DMP 6757/14C	W303 *MAT*a *exo1Δ::HIS3 sgs1Δ::TRP1 ddc1Δ::KANMX*	This study
DMP 6601/4C	W303 *MAT*a *exo1Δ::HIS3 sgs1Δ::TRP1 ddc1-T602A::HIS3MX6*	This study
MUT 31.9A	W303 *MAT*a *exo1Δ::HIS3 sgs1Δ::TRP1 dpb11-L410F*	This study
DMP 6745/2C	W303 *MAT*a *exo1Δ::HIS3 sgs1Δ::TRP1 rad24Δ::KANMX*	This study
MUT 30.6B	W303 *MAT*a *exo1Δ::HIS3 sgs1Δ::TRP1 rad24-E334**	This study
DMP 6602/12A	W303 *MAT*a *exo1Δ::HIS3 sgs1Δ::TRP1 TRP1::dpb11ΔN*	This study
DMP 7009/18C	W303 *MAT*a *exo1Δ::LEU2 sgs1Δ::TRP1 hta1-S129A::URA3 hta2Δ::KANMX*	This study
DMP 7014/8A	W303 *MAT*a *exo1Δ::LEU2 sgs1Δ::TRP1 sml1Δ::KANMX mec1Δ::HIS3*	This study
DMP 7110/8C	W303 *MAT*a *exo1Δ::LEU2 sgs1Δ::URA3 rad53-K227A::KANMX*	This study
YLL 3718.1	W303 *MAT*a *fun30Δ::TRP1*	This study
YLL 2409	W303 *MAT*a *hta1-S129A::URA3 hta2Δ::KANMX*	This study
YLL 4189.3	W303 *MAT*a *isw2Δ::HIS3*	This study
DMP 7115/2D	W303 *MAT*a *isw2Δ::HIS3 dpb4-A62S::KANMX*	This study
SJR 3956.1	W303 *MATa leu2-3,112 ura3-1 his3-11,15 ade2-1 RAD5 CAN1* (donor + recipient + galactose-inducible I-*Sce*I)	Guo *et al.*, 2017
DMP 6657/14D	W303 *MAT*a *mre11-H125N*	This study
YLL 3932.5	W303 *MAT*a *rad24Δ::KANMX*	This study

MUT 30.6B	W303 *MAT*a *rad24-E334**	This study
DMP 5781/1B	W303 *MAT*a *rad50-V1269M::KANMX*	Cassani *et al.*, 2016
DMP 2760/3B	W303 *MAT*a *rad53-K227A::KANMX*	Longhese *et al.*, 2000
DMP 7225/5B	W303 *MAT*a *rad53-K227A::KANMX dpb4-A62S::KANMX sae2Δ::HIS3*	This study
DMP 7225/9B	W303 *MAT*a *rad53-K227A::KANMX sae2Δ::HIS3*	This study
YBP 301	W303 *MAT*a *rad9::NAT-NT2 TRP1::rad9-ST462,474AA*	Pfander & Diffley, 2011
DMP 7067/2B	W303 *MAT*a *rad9::NAT-NT2 TRP1::rad9-ST462,474AA fun30Δ::TRP1 exo1Δ::HIS3*	This study
DMP 7015/5B	W303 *MAT*a *rad9::NAT-NT2TRP1::rad9-ST462,474AA exo1Δ::HIS3 sgs1Δ::TRP1*	This study
YLL1255.6	W303 *MAT*a *rad9Δ::KANMX*	This study
DMP 2949/1C	W303 *MAT*a *rad9Δ::URA3*	Bonetti *et al.*, 2015
DMP 7197/10A	W303 *MAT*a *rad9Δ::URA3 dpb4-A62S:: KANMX sae2Δ::HIS3*	This study
DMP 7065/11D	W303 *MAT*a *rad9Δ::URA3 dpb4-A62S::KANMX*	This study
DMP 7066/17A	W303 *MAT*a *rad9Δ::URA3 dpb4-A62S::KANMX tel1Δ::HIS3*	This study
DMP 7196/5C	W303 *MAT*a *rad9Δ::URA3 sae2Δ::HIS3*	This study
DMP 7064/10A	W303 *MAT*a *rad9Δ::URA3 tel1Δ::HIS3*	This study
YLL 1069.3	W303 *MAT*a *sae2Δ::KANMX*	Gobbini *et al.*, 2015
YLL 490.4	W303 *MAT*a *sml1Δ::KANMX mec1Δ::HIS3*	This study
DMP 7116/9B	W303 *MAT*a *tel1Δ::HIS3 isw2Δ::HIS3 dpb4-A62S::KANMX*	This study
DMP 3335/2A	W303 *MAT*a *tel1Δ::HIS3*	Gobbini *et al.*, 2015
YLL 4190	W303 *MATα DPB3-18MYC::URA3*	This study
YLL 4191.1	W303 *MATα DPB4-18MYC::URA3*	This study
DMP 6389/2D	W303 *MATα dpb4-A62S::KANMX*	This study

DMP 7040/10C	W303 *MATα dpb4-A62S::KANMX tel1Δ::HIS3*	This study
YLL 3759.1	W303 *MATα dpb4Δ::HPHMX*	This study
DMP 7040/8D	W303 *MATα dpb4Δ::HPHMX tel1Δ::HIS3*	This study
DMP 5055/5C	W303 *MATα exo1Δ::HIS3 sgs1Δ::TRP1*	This study
DMP 7042/1B	W303 *MATα exo1Δ::HIS3 sgs1Δ::TRP1 dot1Δ::NATMX*	This study
DMP 6743/4B	W303 *MATα exo1Δ::HIS3 sgs1Δ::TRP1 fun30Δ::TRP1*	This study
DMP 7226/2C	W303 *MATα rad53-K227A::KANMX dpb4-A62S::KANMX*	This study
DMP 7047/4D	W303 *MATα tel1Δ::HIS3 isw2Δ::HIS3*	This study
YMV45	*ho hml::ADE1 mata::hisG hmr::ADE1 leu2::leu2(Asp718-SalI)-URA3*-pBR332-*MATa ade3::GAL::HO ade1 lys5 ura3-52 trp1::hisG*	Vaze *et al.*, 2002
YLL 4304.3	YMV45 *chd1Δ::TRP1*	This study
YLL 4329.1	YMV45 *chd1-E514A::LEU2*	This study
YLL 4394.1	YMV45 *chd1-K407R::LEU2*	This study
YLL 4405.1	YMV45 *rad50-V1269M::KANMX*	This study
YLL 4406.1	YMV45 *rad50-V1269M::KANMX chd1Δ::TRP1*	This study
YLL 4339.6	YMV45 *rad52Δ::HPHMX*	This study
YLL 4307.3	YMV45 *rad52Δ::HPHMX chd1Δ::TRP1*	This study
YLL 4338.1	YMV45 *rad52Δ::HPHMX chd1-E514A::LEU2*	This study
YLL 4395.1	YMV45 *rad52Δ::HPHMX chd1-K407R::LEU2*	This study
SJR 4269.1	SJR 3956.1 *MAT*a *mlh1Δ::LEU2 sgs1Δ::NAT exo1Δ::loxP-HPH-loxP*	Guo *et al.*, 2017
DMP 7185/14C	SJR 3956.1 *MAT*a *mlh1Δ::LEU2 ddc1Δ::HIS3*	This study
DMP 7183/1B	SJR 3956.1 *MAT*a *mlh1Δ::LEU2 rad24Δ::HIS3*	This study
DMP 7258/23C	SJR 3956.1 *MAT*a *mlh1Δ::LEU2 rad53-K227A::KANMX*	This study

DMP 7270/1C	SJR 3956.1 *MAT*a *mlh1Δ::LEU2 rad53-K227A::KANMX sgs1Δ::NAT exo1Δ::loxP-HPH-loxP*	This study
DMP 7185/8B	SJR 3956.1 *MAT*a *mlh1Δ::LEU2 sgs1Δ::NAT exo1Δ::loxP-HPH-loxP ddc1Δ::HIS3*	This study
DMP 7183/6D	SJR 3956.1 *MAT*a *mlh1Δ::LEU2 sgs1Δ::NAT exo1Δ::loxP-HPH-loxP rad24Δ::HIS3*	This study
DMP 7257/21A	SJR 3956.1 *MAT*a *rad9::NAT-NT2 TRP1::rad9-ST462,474AA mlh1Δ::LEU2*	This study
DMP 7269/4B	SJR 3956.1 *MAT*a *rad9::NAT-NT2 sgs1Δ::URA3 exo1Δ::HIS3 TRP1::radST462,474AA mlh1Δ::LEU2*	This study
tGI354	*ho hmlΔ::ADE1 MATa-inc hmrΔ::ADE1 ade1 leu2-3;112 lys5 trp1::hisG ura3-52 ade3::GAL::HO arg5,6::MATa::HPHMX*	Saponaro *et al.*, 2010
YLL 4306.6	tGI354 *chd1Δ::TRP1*	This study
YLL 4330.1	tGI354 *chd1-E514A::LEU2*	This study
YLL 4403.38	tGI354 *rad50-V1269M::KANMX*	This study
YLL 4404.23	tGI354 *rad50-V1269M::KANMX chd1Δ::TRP1*	This study

Table 1. *Saccharomyces cerevisiae* strains used in this study.

Yeast growth media

YEP (Yeast-Extract Peptone) is the standard rich medium for *S. cerevisiae* and contains 10 g/L yeast extract, 20 g/L peptone and 50 mg/L adenine. YEP must be supplemented with 2% glucose (YEPD), 2% raffinose (YEPR) or 2% raffinose and 3% galactose (YEPRG) as carbon source. YEP-based selective media are obtained including 400 μg/mL G418, 300 μg/mL hygromicin-B (HPH) or 100 μg/ml nourseothricin (NAT). Solid media are obtained including 2% agar. Stock solutions are 50% glucose, 30% raffinose, 30% galactose, 80 mg/mL G418, 50 mg/mL hygromicin-B, 50 mg/mL nourseothricin. YEP and glucose stock solution are autoclave-sterilized and stored at RT. Sugars and antibiotics stock solutions are sterilized by microfiltration and stored at

30°C/37°C and -20°C, respectively. S.C. (Synthetic Complete) is the minimal growth medium for *S. cerevisiae* and contains 1.7 g/L YNB (Yeast Nitrogen Base) without amino acids, 5 g/L ammonium sulphate, 200 μM inositol, 25 mg/L uracil, 25 mg/L adenine, 25 mg/L hystidine, 25 mg/L leucine, 25 mg/L tryptophan. S.C. can be supplemented with drop-out solution (20 mg/L arginine, 60 mg/L isoleucine, 40 mg/L lysine, 10 mg/L methionine, 60 mg/L phenylalanine, 50 mg/L tyrosine), based on yeast strains requirements. One or more amino acid/base can be omitted to have S.C selective media (e.g. S.C.-ura is S.C. lacking uracil). Solid media are obtained by including 2% agar. Stock solutions are 17 g/L YNB + 50 g/L ammonium sulphate (or 10 g/L monosodic glutamic acid), 5 g/L uracil, 5 g/L adenine, 5 g/L hystidine, 5 g/L leucine, 5 g/L tryptophan, 100X drop out solution (2 g/L arginine, 6 g/L isoleucine, 4 g/L lysine, 1 g/L methionine, 6 g/L phenylalanine, 5 g/L tyrosine), 20 mM inositol. All these solutions are sterilized by micro-filtration and stored at 4°C. VB sporulation medium contains 13.6 g/L sodium acetate, 1.9 g/L KCl, 0.35 g/L MgSO4, 1.2 g/L NaCl and pH is adjusted to 7.0. To obtain solid medium include 2% agar. Media are autoclave-sterilized. All experiments in this thesis were performed at 26°C.

Synchronization of yeast cells with nocodazole

Nocodazole allows to synchronize a population of yeast cells in G2 phase of the cell cycle. This drug causes the depolymerization of microtubules, thus activating the mitotic checkpoint which arrests cell cycle at the metaphase to anaphase transition. To synchronize a population of exponentially growing yeast cells in YEPD, 5 μg/mL nocodazole, together with DMSO at a final

concentration of 1% (use a stock solution of nocodazole 0,5 mg/mL in 100% DMSO), are added to cell cultures at the concentration of $8x10^6$ cells/mL. If the percentage of dumbbell cells reaches 95%, cells are considered G2-arrested.

Transformation of *S. cerevisiae* cells

YEPD exponentially growing yeast cells are harvested by centrifugation and washed with 1 mL 1 M lithium acetate (LiAc) pH 7.5. Cells are then resuspended in 1 M LiAc pH 7.5 to obtain a cells/LiAc 1:1 solution. 24 µL cells/LiAc are incubated 1 hour at RT with 90 µL 50% PEG (PolyEthylene Glycol) 4000, 8 µL carrier DNA (salmon sperm DNA) and 4-10 µL PCR DNA of interest (divide these quantities for transformation with plasmids).
After the addition of 12 µL 60% glycerol, cells are incubated at RT for 1 hour, heat-shocked at 42°C for 10-20 minutes and plated on appropriate selective medium.

Search for mutations that sensitize *tel1*Δ or *exo1*Δ *sgs1*Δ cells to CPT

To search for suppressor mutations of the CPT-sensitivity of *exo1*Δ *sgs1*Δ cells, $5x10^6$ *exo1*Δ *sgs1*Δ cells were plated on YEPD in the presence of CPT or phleomycin. Survivors were crossed to wild-type cells to identify by tetrad analysis the suppression events that were due to single-gene mutations. To search for mutations that sensitize *tel1*Δ cells to CPT, *tel1*Δ cells were mutagenized with ethyl methanesulfonate and plated on YEPD plates. Approximately 100.000 survival colonies were replica-plated on YEPD plates

with or without CPT. Clones sensitive to CPT were transformed with a plasmid containing wild-type *TEL1* to identify those that lost the DNA damage hypersensitivity. The corresponding original clones were then crossed with wild-type cells to identify by tetrad analysis the clones in which the increased DNA damage sensitivity was due to the simultaneous presence of *tel1*Δ and a single-gene mutation. Genomic DNA suppressors was analyzed by next-generation Illumina sequencing (IGA technology services) to identify mutations altering open reading frames within the reference *S. cerevisiae* genome.

To confirm that the *rad24-E334** and *dpb11-L410F* alleles were responsible for the suppression of the *exo1*Δ *sgs1*Δ sensitivity, the *URA3* gene was integrated downstream of the *rad24-E334** and *dpb11-L410F* stop codon, and the resulting strain was crossed to wild-type cells to verify by tetrad dissection that the suppression of the *exo1*Δ *sgs1*Δ sensitivity co-segregated with the *URA3* allele. To confirm that the *dpb4-A62S* mutation was responsible for the increased DNA damage sensitivity of *tel1*Δ cells, a *KANMX* gene was integrated downstream of the *dpb4-A62S* stop codon and the resulting strain was crossed to *tel1Δ* cells to verify by tetrad dissection that the increased CPT sensitivity co-segregated with *TEL1* deletion and the *KANMX* allele.

Extraction of yeast genomic DNA (Teeny yeast DNA preps)

About $5x10^8$ yeast cells from overnight exponentially growing cultures (or cultures treated to induce damage) are harvested by centrifugation and washed with 1 mL of a 0.9 M sorbitol, 0.1 M EDTA pH 7.5 solution. Dried pellet can eventually be stored -20°C or it can be resuspended in 400 µL of the previous

solution supplemented with 14mM β-mercaptoethanol. Yeast cells wall is digested by 1-hour incubation at 37°C with 0.4 mg/mL 20T zymolyase. Spheroplasts are harvested by 1-minute centrifugation and resuspended in 400 µL 1X TE (10 mM Tris-HCl pH 7.5, 1 mM EDTA pH 7.5). After addition of 90 µL of a solution containing 278 mM EDTA pH 8.5, 445 mM Tris-base and 2.2% SDS, spheroplasts are incubated 30 minutes at 65°C. Following the addition of 80 µL 5M potassium acetate, samples are kept on ice for 1 hour. Cell residues are eliminated by 30 minutes centrifugation at 4°C. DNA is then precipitated with chilled 100% ethanol, resuspended in 500 µL 1X TE and incubated 1 hour with 25 µL 1 mg/mL RNase to eliminate RNA. DNA is then precipitated with 500 µL isopropanol and resuspended in the appropriate volume of 1X TE.

Polymerase Chain Reaction (PCR)

PCR allows to obtain high copy number of a specific DNA fragment starting from a very low quantity of DNA. The reaction is directed to the DNA fragment of interest, by using a couple of oligonucleotides flanking the specific DNA sequence. These oligonucleotides work as primers for the DNA polymerase. The reaction consists of several polymerization cycles, based on 3 main temperature-dependent steps: denaturation of DNA (which occurs over 90°C), primer annealing to the DNA (it typically takes place at 45-55°C depending on primers features), synthesis of the sequence of interest by a thermophilic DNA polymerase (which usually works at 72°C). Different polymerases with different properties (processivity, fidelity, working temperature) are commercially available and suitable for different purposes.

Taq polymerase is generally used for analytical or mutagenic PCR. High-fidelity polymerases, like Phusion and VENT polymerases, are generally employed when 100% accuracy is required. The typical 50 µL PCR mixture contains 1µL template DNA, 0.5 µM each primer, 200 µM dNTPs, 5 µL 10X Reaction Buffer, 1 mM MgCl2, 1-2 U DNA polymerase and water to 50 µL. The typical cycle-program for a reaction is as follows: step 1, 2 minutes denaturation at 94- 95°C; step 2, 30 seconds denaturation at 94-95°C; step 3, 1 minute annealing at primers Tm (melting temperature); step 4, 1 minute synthesis per kb at 72°C; step 5, return to step 2 and repeat 30 times; step 6, 10 minutes at 72°C. The choice of primers sequences determines the working Tm, which depends on the length (L) and GC% content of the oligonucleotides and can be calculated as follows: Tm = 59.9 + 0.41(GC%) – 675/L.

Agarose gel electrophoresis

Agarose gel electrophoresis is the easiest and most common way to separate and analyze DNA molecules. This technique allows the separation of DNA fragments based on their different molecular weight (or length in kb). The purpose of this technique might be to visualize the DNA, to quantify it or to isolate a particular DNA fragment. The DNA is visualized by the addition in the gel of Ethidium Bromide (EtBr), a fluorescent dye that intercalates between the bases of nucleic acids. Ethidium Bromide absorbs UV light and emits the energy as visible orange light, revealing the DNA molecules to which it is bound. To pour a gel, agarose powder is mixed with 1X TAE (0.04 M Tris-Acetate, 0.001 M EDTA) to the desired concentration, and the solution is heated until it is completely melted. Most gels are between 0.8% and 2%

agarose. A 0.8% gel displays good resolution of large DNA fragments (5-10 Kb), while a 2% gel shows good resolution of small fragments (0.2-1 Kb). Ethidium Bromide is added to the gel at a final concentration of 1 μg/mL to facilitate visualization of the DNA after electrophoresis. After cooling the gel solution to about 60°C, it is poured into a casting tray containing a sample comb and it is allowed to solidify at RT or at 4°C. Then, the gel is placed into an electrophoresis chamber, it is covered with 1X TAE buffer, and the comb is removed. Samples containing DNA mixed with loading buffer are pipetted into the sample wells. The loading buffer contains 0.05% bromophenol blue and 5% glycerol, which give colour and density to the sample. A marker containing DNA fragments of known length and concentration is loaded in parallel to determine the size and the quantity of DNA fragments in the samples. Current is applied and DNA migrates toward the positive electrode. When adequate migration has occurred, DNA fragments are visualized by placing the gel under an UV transilluminator.

Spot assays

Cells grown overnight were diluted to $1x10^7$ cells/ml. 10-fold serial dilutions were spotted on YEPD with or without indicated concentrations of DNA damaging drugs. Plates were incubated for 3 days at 28°C or 30°C.

Viability assay

To determine viability in DSB assays, cells were grown overnight in YEPR and, the day after, dilutions were plated onto YEPRG plates that were incubated

at 30°C for 3 days. The number of colonies was counted and percentage of colony formation on YEPRG plates was determined relative to colony formation on YEPD plates (no HO induction).

Plasmid relegation assay

The centromeric pRS316 plasmid was digested with the BamHI restriction enzyme before being transformed into the cells. Parallel transformation with undigested pRS316 DNA was used to determine the transformation efficiency. Efficiency of re-ligation was determined by counting the number of colonies that were able to grow on medium selective for the plasmid marker and was normalized respect to the transformation efficiency for each sample. The re-ligation efficiency in mutant cells was compared to that of wild-type cells that was set up to 100%.

Recombination assay

To measure recombination frequency, we used a strain carrying the lys2::I-*Sce*I recipient allele at the *LYS2* locus on chromosome II containing an I-*Sce*I cleavage site, the *lys2* donor allele (*lys2Δ3'*) at the *CAN1* locus on chromosome V and a galactose-inducible I-*Sce*I gene inserted at the *HIS3* locus on chromosome XV (*his3D::kanMX-pGAL*-I-*Sce*I) [Guo *et al.,* 2017]. I-*Sce*I expression was induced by adding galactose (1% final) to cells growing exponentially in YEPR. Following galactose addition, cells were plated on YEPD and SC-lys media, incubated at 30°C and repair frequencies were calculated as the ratio of Lys^+ to total colonies.

Data for each strain were based on at least three independent experiments, with 15 independent cultures per experiment.

DSB resection at *MAT* locus (Southern blot method)

YEPR exponentially growing cell cultures of JKM139 derivative strains, carrying the HO cut site at the *MAT* locus, were transferred to YEPRG at time zero. Genomic DNA was extracted at different time points following the induction of the HO endonuclease. The, *Ssp*I-digested genomic DNA was precipitated by adding 0.3 M NaAc pH 5.2, 5 mM EDTA pH 8 and two volumes EtOH 100%. After chilling overnight, samples are centrifuged 30 minutes at 4°C and pellet is resuspended in alkaline gel loading buffer (50 mM NaOH, 1 mM EDTA pH 8, 2.5% Ficoll (type 400) and 0.025% bromophenol blue). Denatured DNA is loaded onto a 0.8% agarose gel, previously equilibrated in alkaline electrophoresis buffer (50 mM NaOH, 1 mM EDTA pH 8), and a glass plate is placed on the gel to prevent the dye from diffusing from the agarose during the run. Denaturing gel is run slowly at low voltages (e.g. 30V overnight). After the DNA has migrated about 14 cm, the gel can be stained with 0.5 μg/mL Ethidium Bromide in 1X TAE buffer for 1 hour and DNA is visualized by placing the gel under an UV transilluminator. Gel is then soaked in 0.25 N HCl for 7 minutes with gentle agitation, rinsed with water for 10 minutes, soaked in 0.5 NaOH, 1.5 M NaCl for 30 minutes and rinsed again with water for 10 minutes. DNA is blotted overnight by capillary transfer onto neutral nylon membrane using 10X SSC. Membrane is then neutralized in 0.5 M Tris-HCl pH 7.5, 1 M NaCl, air dried and UV-crosslinked. Hybridization is

carried out by incubating the membrane for 5 hours at 42°C with pre-hybridization buffer (5X SSPE, 50% formamide, 4X denhardt's solution + BSA, 6% destran sulphate, 100 µg/mL salmon sperm DNA, 200 µg/mL tRNA carrier), followed by overnight incubation at 42°C with the pre-hybridization buffer supplemented with the single-stranded RNA (ssRNA) probe, that anneals with the unresected strand at one side of the HO-induced DSB [Casari *et al.*, 2021]. This probe was obtained by in vitro transcription using Promega Riboprobe System-T7 and plasmid pML514 as a template. Plasmid pML514 was constructed by inserting in the pGEM7Zf *Eco*RI site a 900-bp fragment containing part of the *MAT* locus (coordinates 200870 to 201587 on chromosome III) and labelling it with [α-32P]-UTP. Following hybridization, membrane is washed twice with 5X SSPE (20X SSPE: 3 M NaCl, 200 mM NaH2PO4, 20mM EDTA, pH 7.4) at 42°C for 15 minutes, 30 minutes with 1X SSPE 0.1% SDS at 42°C, 30 minutes with 0.1X SSPE 0.1% SDS at 42°C, twice with 0.2X SSPE 0.1% SDS at 68°C for 15 minutes and 5 minutes with 0.2X SSPE at RT. Finally, membrane is air dried and exposed to an autoradiography film.

Quantitative analysis of DSB resection was performed by calculating the ratio of band intensities for ssDNA and total amount of DSB products. The resection efficiency was normalized with respect to the HO cleavage efficiency for each time point. The amount of ssDNA was normalized to cut efficiency by subtracting the value of the uncut band from the total amount of DSB products for each time point. Densitometric analysis of band intensities was performed using Scion Image Beta 4.0.2 software.

DSB resection at *MAT* locus (qPCR method)

Quantitative PCR (qPCR) analysis of DSB resection at the *MAT* locus in JKM139 derivative strains was carried out as described in Zierhut *et al.*, 2008. Genomic DNA was extracted at different time points following the induction of the HO endonuclease. Different oligonucleotides were designed to detect ssDNA at specific distances from the DSB (0.15kb, 0.65kb, 0.9kb, 1.7kb, 3.5kb, 6.5kb and 8.9 kb). The DNA was digested with both *Ssp*I and *Rsa*I restriction enzymes.

A mock reaction without the restriction enzymes was performed in parallel. qPCR was performed on both digested and mock samples using SsoFast EvaGreen supermix (Biorad) with the Bio-Rad CFX Connect™ Real-Time System apparatus. For each time point, Ct values were normalized to those obtained from the mock sample, and then further normalized to values obtained from an amplicon in KCC4 control gene. Finally, the value obtained was normalized to the HO cut efficiency, also measured by qPCR by using oligonucleotides that anneal on opposite sides with respect to the HO cutting sequence. The percentage of HO cut was calculated by comparing the Ct values before and after the HO induction in the undigested samples.

DSB repair by SSA

DSB repair by SSA in YMV45 strains were detected by Southern blot analysis using an Asp718-*Sal*I fragment containing part of the *LEU2* gene as a probe [Trovesi *et al.*, 2011].

To determine the efficiency of DSB repair by SSA, the normalized intensity of the SSA product band was divided by the total amount of SSA and cut products, and it was normalized to cut efficiency by subtracting the value of the uncut band from the total amount of DSB products for each time point.

DSB repair by ectopic recombination

DSB repair by ectopic recombination was detected by Southern blot method in tGI354 background [Trovesi *et al.,* 2011]. To determine the repair efficiency, the intensity of the uncut band at 2h after HO induction (maximum efficiency of DSB formation) was subtracted to the normalized values of NCO and CO bands at the subsequent time points after galactose addition. The obtained values were divided by the normalized intensity of the uncut *MATa* band at time zero before HO induction (100%).

Western blotting

Protein extracts for western blot analysis were prepared by trichloroacetic acid (TCA) precipitation. Total protein extracts are prepared from 10^8 cells, collected from exponentially growing yeast cultures (or cultures treated to induce damage). Cells are harvested by centrifugation, washed with 1 mL 20% trichloracetic acid (TCA), to prevent proteolysis, and then resuspended in 100 or 200 μL 20% TCA. After the addition of acid-washed glass beads, the samples were vortexed for 10 min. The beads were washed with 200 μL of 5% TCA twice and the extract was collected in a new tube. The crude extract was precipitated by centrifugation at 850 xg for 10 min. TCA was discarded and

samples were resuspended in 70 µL 6X Laemmli buffer (60 mM Tris, pH 6.8, 2% SDS, 10% glycerol, 100mM DTT, 0.2% bromophenol blue) and 30 µL 1M Tris (pH 8.0). Prior to loading, samples were boiled at 95°C for 2 minutes and centrifuged at 850 xg for 10 min.

Supernatant containing the solubilized proteins were separated on 10% polyacrylamide gels. (10% Running gel: 375 mM Tris-HCl pH 8.8, 0,1% SDS, 10% Acrylamide, 0,13% Bisacrylamide, 0,1% APS, 0.001% Temed – Stacking gel: 125 mM Tris-HCl pH 6.8, 0,1% SDS, 5% Acrylamide, 0,14% Bisacrylamide, 0,1% APS, 0.001% Temed). Less or more concentrated gels are used to separate big or small proteins, respectively (e.g. 6% polyacrylamide gels are employed to visualize Pol2, 15% to visualize Dls1). Proteins are separated based on their molecular weight by polyacrylamide gel electrophoresis in the presence of sodium dodecyl sulphate (SDS-PAGE). When adequate migration has occurred, proteins are blotted onto nitrocellulose membrane. Membrane is usually saturated by 1-hour incubation in 1X TBS (150 mM NaCl, 50 mM Tris-HCl pH 8) supplemented with 4% milk and 0.2% triton X-100. Membranes are then incubated for 2 hours with primary antibodies (in 1X TBS + 4% milk + 0.2% triton) and washed three times for 10 minutes with 1X TBS. Subsequently membranes are incubated for 1 hour with secondary antibodies (in 1X TBS + 4% milk + 0,2% triton) and again washed three times with 1X TBS. Detection is performed with ECL (Enhanced ChemiLuminescence - Genespin) and autoradiography films according to the manufacturer.

Rad53 was detected by using anti-Rad53 polyclonal antibodies (ab104232) (1:2000) from Abcam. HA- or Myc-tagged proteins were detected by using anti-HA (12CA5) (1:2000) or anti-Myc (9E10) (1:1000) antibodies,

respectively. Rad51 was detected by using anti-Rad51 antibodies (ab63798) (1:2000) from Abcam.

Coimmunoprecipitation (CoIP)

$2x10^9$ exponentially growing cells are collected by centrifugation, washed with water, and put on ice. Total protein extracts were prepared by breaking cells in 400 µl of buffer containing 50 mM HEPES pH 7.5, 300 mM NaCl, 20% glycerol, 1 mM sodium orthovanadate, 60 mM β- glycerophosphate and protease inhibitor cocktail (Roche Diagnostics). 200 µL glass beads are added and cells are mechanically disrupted by 14 breakage cycles composed by 30 seconds vortexing and 30 seconds interval each. Glass beads are then washed with 200 µL cold breaking buffer and the resulting extracts, once separated from the beads, are centrifuged at 4°C at 14000 rpm for 20 minutes. Clarified and quantified protein extracts were incubated for 2 h at 4°C with 50 µl of Protein G-Dynabeads and 5 µg anti-HA (12CA5) antibodies. 15 µL normalized extracts are kept as "input". The resins were then washed twice with 1 ml of breaking buffer and once with 1 ml PBS. IP samples are finally mixed with 30 µL of Laemmli buffer (15 µL for input samples) and boiled for 3 minutes. Bound proteins were visualized by western blotting with anti-HA (12CA5) (1:2000) or anti-Myc (9E10) (1:1000) antibodies after electrophoresis on a 10% or 15% SDS-polyacrylamide gel.

Chromatin immunoprecipitation (ChIP) and qPCR

YEPR exponentially growing cell cultures (50 mL at concentration of $8x10^6$ cells/mL) of JKM139 derivative strains, carrying the HO cut site at the *MAT* locus, were transferred to YEPRG at time zero. Crosslinking was done with 1% formaldehyde for 5 min (Mre11, Rad50, Rad51), 10 min (Rad9, Sae2) or 15 min (Dpb4, Dpb4-A62S, Pol2, Isw2, Chd1, H3 histone and H2A histone). The reaction was stopped by adding 0.125 M Glycine for 5 min. Treated cells are kept on ice until centrifugation at 3000 rpm for 5 minutes at 4°C.

Cell pellet is washed with 30 mL HBS buffer (50 mM HEPES pH 7.5, 140 mM NaCl) and then with 25 mL ChIP lysis buffer (50 mM HEPES pH 7.5, 140 mM NaCl, 1 mM EDTA pH 8, 1% IGEPAL CA-630, 0.1% Sodium deoxycholate). After centrifugation at 3000 rpm for 5 minutes, the supernatant is carefully and completely removed. Then 0.4 mL of ChIP lysis buffer, supplemented with complete anti-proteolitic tablets (Roche) and 1 mM phenylmethylsulfonyl fluoride (PMSF), is added and samples are resuspended and stored at -80°C. The following day, cells are broken at 4°C with glass beads by mechanical disruption. After breaking cells, the glass beads are eliminated. This passage is followed by centrifugation at 4°C at 14000 rpm for 30 minutes. Pellet is resuspended in 0.5 mL ChIP lysis buffer, supplemented with antiproteolitics and PMSF, and then sonicated (5 cycles of 25 seconds at 40% power output), to share DNA in fragments of 500-1000 bp. After centrifugation at 4°C at 10000 rcf for 5 minutes 460 µL supernatant are retained and further clarified by centrifugation at 4°C at 10000 rcf for 15 minutes. 400 µL of clarified supernatant are immunoprecipitated with Dynabeads coated with specific antibodies, while 5 µL supernatant are kept as “input DNA”.

Immunoprecipitation was performed by incubating samples with Dynabeads Protein G (Thermo Fisher Scientific) for 3 h at 4°C in the presence of 5 μg anti-HA (12CA5) or antiMyc antibodies (9E10). H2A and H3 histones were immunoprecipitated by using 5 μg anti-H2A (39945, Active Motif) and 4 μg anti-H3 (ab1791, Abcam) antibodies, respectively. Rad51 by using 3 μg anti-Rad51 (ab63798, Abcam) After 3 hours incubation with the desired antibodies, dynabeads are washed RT as follow: twice with SDS buffer (50 mM HEPES pH 7.5, 1 mM EDTA pH 8, 140 mM NaCl, 0.025% SDS), once with High-Salt buffer (50 mM HEPES pH 7.5, 1 mM EDTA pH 8, 1 M NaCl), once with T/L buffer (20 mM Tris-HCl pH 7.5, 250 mM LiCl, 1 mM EDTA pH 8, 0.05% sodium deoxycholate, 0.5% IGEPAL CA630), and finally twice with T/E buffer (20 mM Tris-HCl pH 7.5, 0.1 mM EDTA pH 8). All the washes are done by pulling down Dynabeads and then nutating them for 5 minutes with the specific washing buffer. After the last wash, Dynabeads are resuspended in 145 μL 1X TE + 1% SDS, shaked on a vortex for 2 minutes, kept at 65°C for 10 minutes, shaked on vortex again and then pulled down. Then, 120 μL of the supernatant are put at 65°C overnight for reverse cross-linking. Also the previously taken input DNA samples must be put at 65°C overnight after the addition of 115 μL of 1X TE + 1% SDS buffer. The next day DNA is purified by using QIAGEN QIAquick PCR purification kit. 600 μL PB buffer are added to each sample and, after vortexing, the sample is loaded onto spin columns, followed by centrifugation at 5000 rpm for 1 minute. 400 μL PE buffer are added to the columns, followed by centrifugation at 14000 rpm for 1 minute, then 300 μL PE buffer are added to the columns again and, after 5 minutes waiting, columns are centrifuged at 14000 rpm for 2 minutes. Finally, 25 μL EB buffer are added in the columns and, after 1-minute incubation, DNA is eluted

by centrifuging at 14000 rpm for 1 minute. Elution is repeated a second time in the same way, then input DNA is diluted 1:50 in EB buffer.

Quantification of immunoprecipitated DNA was achieved by qPCR on a Bio-Rad CFX Connect™ Real-Time System apparatus or on a Bio-Rad MiniOpticon apparatus and by using Bio-Rad CFX Maestro 1.1 software. Triplicate samples in 20 µl reaction mixture containing 10 ng of template DNA, 300 nM for each primer (located at different distances from the HO-induced DSB and at the *ARO1* locus of chromosome IV), 2× SsoFast™ EvaGreen® supermix (Bio-Rad #1725201) (2X reaction buffer with dNTPs, Sso7d-fusion polymerase, MgCl2, EvaGreen dye and stabilizers) were run in white 96-well PCR plates Multiplate (Bio-Rad #MLL9651) or 48-well PCR plates Multiplate (BioRad #MLL4851). The qPCR program was as follows: step 1, 98°C for 2 min; step 2, 90°C for 5 s; step 3, 60°C for 15 s; step 4, return repeat 40 times from step 2. At the end of the cycling program, a melting program (from 65°C to 95°C 23 with a 0.5°C increment every 5 s) was run to test the specificity of each qPCR.

Data are expressed as fold enrichment at the HO-induced DSB over that at the non-cleaved *ARO1* locus, after normalization of the ChIP signals to the corresponding input for each time point. Fold enrichment was then normalized to the efficiency of DSB induction (cut efficiency). For histone loss, the fold enrichment from each sample after HO induction was divided by the fold enrichment from uninduced cells, and log2 of the resulting values was calculated.

Purification of Dpb3-Dpb4 and Dls1-Dpb4 heterodimers

Design, expression and purification of Dpb4 heterodimers was performed as previously described [Mangiagalli *et al.*, 2021]. Briefly, the genes coding for Dpb4, Dpb4^{A62S}, Dpb3 and Dls1 were optimized for the expression in *E. coli* cells and chemically synthetized (Genscript, Piscataway, NJ, USA). *DPB4* and *DPB4-A62S* genes were cloned in frame with a C-terminal 6xHis-Tag into pET-21a vector (EMD, Millipore, Billerica, MA, USA) between *Nde*I and *Xho*I sites. The *DPB3* and *DLS1* genes were cloned in frame with a C-terminal Strep-Tag into a modified pET-28 vector between *Nco*I and *Xho*I 24 sites. *E. coli* BL21 (DE3) cells were co-transformed with the above plasmids to obtain Dpb3-Dpb4, Dpb3-Dpb4^{A62S}, Dls1-Dpb4, and Dls1-Dpb4^{A62S} heterodimers. Transformed cells were selected on LB agar plates supplemented with ampicillin (100 mg/L) and kanamycin (50 mg/L). Heterodimers were produced in autoinduction ZYM-5052 medium [Studier *et al.*, 2005] supplemented with ampicillin (100 mg/L) and kanamycin (50 mg/L), extracted and purified by immobilized ion metal affinity chromatography (Jena Bioscience, Jena, Germany) followed by Strep purification on Strep-Tactin resin (IBA Lifesciences, Gottingen, Germany). High concentrated fractions were buffer-exchanged with phosphate buffer (10 mM, pH 7) by gel filtration on PD-10 columns (GE Healthcare, Little Chalfont, UK). Protein concentration was determined by the Bradford assay (Bio-Rad, Hercules, USA), using bovine serum albumin as a standard. SDS-PAGE was performed on 14% acrylamide gels and stained with Gel-Code Blue (Pierce, Rockford, USA) after electrophoresis. Broad-range, pre-stained molecular-mass markers (GeneSpin, Milan, Italy) were used as standards.

Circular dichroism spectroscopy

CD spectra of purified proteins were obtained in phosphate buffer at the concentration of 2 μM with a J-815 spectropolarimeter (JASCO, Europe, Lecco, Italy), using a 0.1-cm path length cuvette. Spectra were collected in the 190-260 range with 0.2 nm data pitch and 20 nm/min scanning speed. All spectra were corrected for buffer contribution, averaged from four independent acquisitions, and smoothed by using a third-order least-square polynomial fit. Thermal denaturation ramps were obtained measuring the variation of CD signal at 208 nm when progressively heating the sample from 25 to 90°C. Data were analyzed with OriginPro 2020 (OriginLab Corporation, Northampton, USA). Measurements were performed in triplicate.

Electrophoretic Mobility Shift Assay (EMSA)

EMSA was performed by incubating 1.5 pmol of 61 bp 32P-labeled dsDNA (5'-GACGCTGCCGAATTCTACCAGTGCCTTGCTAGGACATCTTTGCCC ACCTGCAGGTTCACCC-3') [Tsubota *et al.*, 2003] with purified Dpb3-Dpb4 and Dpb3-Dpb4^{A62S} (0, 0.75, 1.5, 3, 7, 13, 20 pmol) or Dls1-Dpb4 and Dls1-Dpb4^{A62S} (0, 20, 40, 80, 100, 120, 160 pmol) in ice for 10 min in binding buffer (20 mm HEPES-NaOH, pH 7.5, 0.5 mM EDTA, 0.05% NP-40, 10% (v/v) glycerol and 60 μg/mL BSA) to a final volume of 50 μl. Reactions were loaded on a nondenaturing 6% acrylamide/bisacrylamide gel and separated by running for 2 h at 150 V at 4°C using a low-ionic strength buffer (6.73 mM Tris-HCl pH 7.5, 3.3 mM NaOAc pH 5 and 1 mM EDTA). Gels were soaked for 15 min in 10% methanol, 10% acetic acid solution, vacuum dried and exposed to an autoradiography film.

3D Modelling

The 3D structure of Dpb3-Dpb4 heterodimer was extracted from PDB 6WJV (http://doi.org/10.2210/pdb6WJV/pdb). The 3D model of Dls1 was predicted by I-TASSER web server [Yang & Zhang, 2015] and superimposed on the 3D structure of Dpb3 in the Dpb4-Dpb3 heterodimer using Pymol 2.4.1 software. The figures were prepared using UCSF Chimera X 0.93 software [Goddard *et al.,* 2018].

Quantification and statistical analysis

Quantification and statistical analysis were performed using Microsoft Excel Professional 365 software or PRISM (GraphPad). Data are expressed as mean values ± standard deviation (s.d). P-values were determined by using unpaired two-tailed t-test. No statistical methods or criteria were used to estimate size or to include or exclude samples.

REFERENCES

Adkins NL, Niu H, Sung P, Peterson CL (2013) Nucleosome dynamics regulates DNA processing. *Nat Struct Mol Biol* **20**, 836-842.

Aksenova A, Volkov K, Maceluch J, Pursell ZF, Rogozin IB, Kunkel TA, Pavlov YI, Johansson E (2010) Mismatch repair-independent increase in spontaneous mutagenesis in yeast lacking non-essential subunits of DNA polymerase ε. *PLoS Genet* **6**, e1001209.

Alatwi HE, Downs JA (2015) Removal of H2A.Z by INO80 promotes homologous recombination. *EMBO Rep* **16**, 986-994.

Aparicio T, Baer R, Gautier J (2014) DNA double-strand break repair pathway choice and cancer. *DNA Repair* **19**, 169-175.

Araki H, Hamatake RK, Morrison A, Johnson AL, Johnston LH, Sugino A (1991) Cloning *DPB3*, the gene encoding the third subunit of DNA polymerase II of *Saccharomyces cerevisiae*. *Nucleic Acids Res* **19**, 4867-4872.

Araki H, Leem SH, Phongdara A, Sugino A (1995) Dpb11, which interacts with DNA polymerase II(epsilon) in *Saccharomyces cerevisiae*, has a dual role in S-phase progression and at a cell cycle checkpoint. *Proc Natl Acad Sci USA* **92**, 11791-11795.

Aylon Y, Kupiec M (2004) DSB repair: the yeast paradigm. *DNA Repair* **3**, 797-815.

Babst M, Wendland B, Estepa EJ, Emr SD (1998) The Vps4p AAA ATPase regulates membrane association of a Vps protein complex required for normal endosome function. *EMBO J* **17**, 2982-2993.

Bakkenist CJ, Kastan MB (2003) DNA damage activates ATM through intermolecular autophosphorylation and dimer dissociation. *Nature* **421**, 499-506.

Bantele SCS, Ferriera P, Gritenaite D, Boos D, Pfander B (2017) Targeting of the Fun30 nucleosome remodeller by the Dpb11 scaffold facilitates cell cycle-regulated DNA end resection. *Elife* **6**, e21687.

Bantele SCS, Lisby M, Pfander B (2019) Quantitative sensing and signalling of single-stranded DNA during the DNA damage response. *Nat Commun* **10**, 944.

Bassing CH, Alt FW (2004) The cellular response to general and programmed DNA double strand breaks. *DNA Repair* **3**, 781-796

Bellelli R, Belan O, Pye VE, Clement C, Maslen SL, Skehel JM, Cherepanov P, Almouzni G, Boulton SJ (2018) POLE3-POLE4 is a histone H3-H4 chaperone that maintains chromatin integrity during DNA replication. *Mol Cell* **72**, 112-126.

Bennett G, Peterson CL (2015) SWI/SNF recruitment to a DNA double-strand break by the NuA4 and Gcn5 histone acetyltransferases. *DNA Repair* **30**, 38-45.

Bernstein KA, Gangloff S, Rothstein R (2010) The RecQ DNA helicases in DNA repair. *Annu Rev Genet* **44**, 393-417.

Bizard AH, Hickson ID (2014) The dissolution of double Holliday Junctions. *Cold Spring Harb Perspect Biol* **6**, a016477.

Boersma V, Moatti N, Segura-Bayona S, Peuscher MH, van der Torre J, Wevers BA, Orthwein A, Durocher D, Jacobs JJL (2015) MAD2L2 controls DNA repair at telomeres and DNA breaks by inhibiting 5' end resection. *Nature* **521**, 537-540.

Bonetti D, Colombo CV, Clerici M, Longhese MP (2018) Processing of DNA ends in the maintenance of genome stability. *Front Genet* **9**, 390.

Bonetti D, Villa M, Gobbini E, Cassani C, Tedeschi G, Longhese MP (2015) Escape of Sgs1 from Rad9 inhibition reduces the requirement for Sae2 and functional MRX in DNA end resection. *EMBO Rep* **16,** 351-361.

Bosotti R, Isacchi A, Sonnhammer EL (2000) FAT, a novel domain in PIK-related kinases. *Trends Biochem Sci* **25**, 225-227.

Burkhardt L, Fuchs S, Krohn A, Masser S, Mader M, Kluth M, Bachmann F, Huland H, Steuber T, Graefen M, Schlomm T, Minner S, Sauter G, Sirma H, Simon R (2013) CHD1 is a 5q21 tumor suppressor required for ERG rearrangement in prostate cancer. *Cancer Res* **73**, 2795-805.

Cannavo E, Cejka P (2014) Sae2 promotes dsDNA endonuclease activity within Mre11-Rad50-Xrs2 to resect DNA breaks. *Nature* **514**, 122-125.

Cannavo E, Cejka P, Kowalczykowski SC (2013) Relationship of DNA degradation by *Saccharomyces cerevisiae* Exonuclease 1 and its stimulation by RPA and Mre11-Rad50-Xrs2 to DNA end resection. *Proc Natl Acad Sci USA* **110**, 1661-1668.

Cannavo E, Reginato G, Cejka P (2019) Stepwise 5' DNA end-specific resection of DNA breaks by the Mre11-Rad50-Xrs2 and Sae2 nuclease ensemble. *Proc Natl Acad Sci USA* **116**, 5505-5513.

Casari E, Gobbini E, Clerici M, Longhese MP (2021) Resection of a DNA double-strand break by alkaline gel electrophoresis and Southern blotting. *Methods Mol Biol* **2153**, 33-45.

Casari E, Rinaldi C, Marsella A, Gnugnoli M, Colombo CV, Bonetti D, Longhese MP (2019) Processing of DNA Double-Strand Breaks by the MRX complex in a chromatin context. *Front Mol Biosci* **6**, 43.

Cassani C, Gobbini E, Wang W, Niu H, Clerici M, Sung P, Longhese MP (2016) Tel1 and Rif2 regulate MRX functions in end-tethering and repair of DNA Double-Strand Breaks. *PLoS Biol* **14**, e1002387.

Cejka P (2015) DNA end resection, nucleases team up with the right partners to initiate homologous recombination. *J Biol Chem* **290**, 22931-22938.

Cejka P, Cannavo E, Polaczek P, Masuda-Sasa T, Pokharel S, Campbell JL, Kowalczykowski SC (2010) DNA end resection by Dna2-Sgs1-RPA and its stimulation by Top3-Rmi1 and Mre11- Rad50-Xrs2. *Nature* **467**, 112-116.

Cejka P, Kowalczykowski SC (2010) The full-length *Saccharomyces cerevisiae* Sgs1 protein is a vigorous DNA helicase that preferentially unwinds Holliday junctions. *J Biol Chem* **285**, 8290-8301.

Chai B, Huang J, Cairns BR, Laurent BC (2005) Distinct roles for the RSC and Swi/Snf ATP-dependent chromatin remodelers in DNA double-strand break repair. *Genes Dev* **19**, 1656-1661.

Chambers AL, Brownlee PM, Durley SC, Beacham T, Kent NA, Downs JA (2012) The two different isoforms of the RSC chromatin remodeling complex play distinct roles in DNA damage responses. *PLoS One* **7**, e32016.

Chambers AL, Downs JA (2012) The RSC and INO80 chromatin-remodeling complexes in DNA double-strand break repair. *Prog Mol Biol Transl Sci* **110**, 229-261.

Chang HHY, Pannunzio NR, Adachi N, Lieber MR (2017) Non-homologous DNA end joining and alternative pathways to double-strand break repair. *Nat Rev Mol Cell Biol* **18**, 495-506.

Chen H, Donnianni RA, Handa N, Deng SK, Oh J, Timashev LA, Kowalczykowski SC, Symington LS (2015) Sae2 promotes DNA damage resistance by removing the Mre11-Rad50-Xrs2 complex from DNA and attenuating Rad53 signaling. *Proc Natl Acad Sci USA* **112**, 1880-1887.

Chen X, Cui D, Papusha A, Zhang X, Chu CD, Tang J, Chen K, Pan X, Ira G (2012) The Fun30 nucleosome remodeller promotes resection of DNA double-strand break ends. *Nature* **489**, 576-580.

Chen X, Niu H, Chung WH, Zhu Z, Papusha A, Shim EY, Lee SE, Sung P, Ira G (2011) Cell cycle regulation of DNA double-strand break end resection by Cdk1-dependent Dna2 phosphorylation. *Nat Struct Mol Biol* **18**, 1015-1019.

Chiruvella KK, Liang Z, Wilson TE (2013) Repair of double-strand breaks by end joining. *Cold Spring Harb Perspect Biol* **5**, a012757.

Chung WH, Zhu Z, Papusha A, Malkova A, Ira G (2010) Defective resection at DNA double-strand breaks leads to de novo telomere formation and enhances gene targeting. *PLoS Genet* **6**, e1000948.

Ciccia A, Elledge SJ (2010) The DNA damage response, making it safe to play with knives. *Mol Cell* **40**, 179-204.

Clapier CR, Cairns BR (2009) The biology of chromatin remodeling complexes. *Annual review of biochemistry* **78**, 273-304.

Clapier CR, Iwasa J, Cairns BR, Peterson CL (2017) Mechanisms of action and regulation of ATP-dependent chromatin-remodelling complexes. *Nature reviews Molecular cell biology* **18**, 407-422.

Clerici M, Mantiero D, Guerini I, Lucchini G, Longhese MP (2008) The Yku70-Yku80 complex contributes to regulate double-strand break processing and checkpoint activation during the cell cycle. *EMBO Rep* **9**, 810-818.

Clerici M, Mantiero D, Lucchini G, Longhese MP (2005) The *Saccharomyces cerevisiae* Sae2 protein promotes resection and bridging of double strand break ends. *J Biol Chem* **280**, 38631-38638.

Clerici M, Mantiero D, Lucchini G, Longhese MP (2006) The *Saccharomyces cerevisiae* Sae2 protein negatively regulates DNA damage checkpoint signalling. *EMBO Rep* **7**, 212-218.

Clerici M, Trovesi C, Galbiati A, Lucchini G, Longhese MP (2014) Mec1/ATR regulates the generation of single-stranded DNA that attenuates Tel1/ATM signaling at DNA ends. *EMBO J* **33**, 198-216.

Corona DF, Eberharter A, Budde A, Deuring R, Ferrari S, Varga-Weisz P, Wilm M, Tamkun J, Becker PB (2000) Two histone fold proteins, CHRAC-14 and CHRAC-16, are developmentally regulated subunits of chromatin accessibility complex (CHRAC). *EMBO J* **19**, 3049-3059.

Corona DF, Längst G, Clapier CR, Bonte EJ, Ferrari S, Tamkun JW, Becker PB (1999) ISWI is an ATP-dependent nucleosome remodeling factor. *Mol Cell* **3**, 239-245.

Costelloe T, Louge R, Tomimatsu N, Mukherjee B, Martini E, Khadaroo B, Dubois K, Wiegant WW, Thierry A, Burma S, van Attikum H, Llorente B (2012) The yeast Fun30 and human SMARCAD1 chromatin remodellers promote DNA end resection. *Nature* **489**, 581-584.

Cussiol JR, Jablonowski CM, Yimit A, Brown GW, Smolka MB (2015) Dampening DNA damage checkpoint signalling via coordinated BRCT domain interactions. *EMBO J* **34**, 1704-1717.

Dalal S, Rosser MF, Cyr DM, Hanson PI (2004) Distinct roles for the AAA ATPases NSF and p97 in the secretory pathway. *Mol Biol Cell* **15**, 637-648.

Daley JM, Kwon Y, Niu H, Sung P (2013) Investigations of homologous recombination pathways and their regulation. *Yale J Biol Med* **86**, 453-461.

Daley JM, Palmbos PL, Wu D, Wilson TE (2005) Nonhomologous End Joining in yeast. *Annu Rev Genet* **39**, 431–451.

Dang W, Bartholomew B (2007) Domain architecture of the catalytic subunit in the ISW2- nucleosome complex. *Molecular and cellular biology* **27**, 8306-8317.

Dang W, Kagalwala MN, Bartholomew B (2007) The Dpb4 subunit of ISW2 is anchored to extranucleosomal DNA. *J Biol Chem* **282**, 19418-19425.

Davis AJ, Chen DJ (2013) DNA double strand break repair via non-homologous end-joining. *Transl Cancer Res* **2**, 130-143.

de Jager M, van Noort J, van Gent DC, Dekker C, Kanaar R, Wyman C (2001) Human Rad50/Mre11 is a flexible complex that can tether DNA ends. *Mol Cell* **8**, 1129-1135.

Delacroix S, Wagner JM, Kobayashi M, Yamamoto K, Karnitz LM (2007) The Rad9-Hus1-Rad1 (9-1-1) clamp activates checkpoint signaling via TopBP1. *Genes Dev* **21**, 1472-1477.

Delamarre A, Barthe A, de la Roche Saint-André C, Luciano P, Forey R, Padioleau I, Skrzypczak M, Ginalski K, Géli V, Pasero P, Lengronne A (2020) MRX increases chromatin accessibility at stalled replication forks to promote nascent DNA resection and cohesin loading. *Mol Cell* **77**, 395-410.

Deng C, Brown JA, You D, Brown JM (2005) Multiple endonucleases function to repair covalent topoisomerase I complexes in *Saccharomyces cerevisiae*. *Genetics* **170**, 591-600.

Deshpande AM, Ivanova IG, Raykov V, Xue Y, Maringele L (2011) Polymerase epsilon is required to maintain replicative senescence. *Mol Cell Biol* **31**, 1637-1645.

Deshpande RA, Williams G.J, Limbo O, Williams RS, Kuhnlein J, Lee JH, Classen S, Guenther G, Russell P, Tainer JA, Paull TT (2014) ATP-driven Rad50 conformations regulate DNA tethering, end resection, and ATM checkpoint signaling. *EMBO J* **33**, 482-500.

Di Virgilio M, Callen E, Yamane A, Zhang W, Jankovic M, Gitlin AD, Feldhahn N, Resch W, Oliveira TY, Chait BT, Nussenzweig A, Casellas R, Robbiani DF, Nussenzweig MC (2013) Rif1 prevents resection of DNA breaks and promotes immunoglobulin class switching. *Science* **339**, 711-15.

Dibitetto D, Ferrari M, Rawal CC, Balint A, Kim T, Zhang Z, Smolka MB, Brown GW, Marini F, Pellicioli A (2016) Slx4 and Rtt107 control checkpoint signalling and DNA resection at double-strand breaks. *Nucleic Acids Res* **44**, 669-682.

Downs JA, Lowndes NF, Jackson SP (2000) A role for *Saccharomyces cerevisiae* histone H2A in DNA repair. *Nature* **408**, 1001-1004.

Dudášová Z, Dudáš A, Chovanec M (2004) Non-homologous end-joining factors of *Saccharomyces cerevisiae*. *FEMS Microbiol Rev* **28**, 581-601.

Dueva R, Iliakis G (2013) Alternative pathways of non-homologous end joining (NHEJ) in genomic instability and cancer. *Translational cancer research* **2**.

Durocher D, Henckel J, Fersht AR, Jackson SP (1999) The FHA domain is a modular phosphopeptide recognition motif. *Mol Cell* **4**, 387-394.

Eapen VV, Sugawara N, Tsabar M, Wu WH, Haber JE (2012) The *Saccharomyces cerevisiae* chromatin remodeler Fun30 regulates DNA end resection and checkpoint deactivation. *Mol Cell Biol* **32**, 4727-4740.

Ellison V, Stillman B (2003) Biochemical characterization of DNA damage checkpoint complexes: clamp loader and clamp complexes with specificity for 5' recessed DNA. *PLoS Biol* **1**, 33.

Farnung L, Ochmann M, Engeholm M, Cramer P (2021) Structural basis of nucleosome transcription mediated by Chd1 and FACT. *Nat Struct Mol Biol* **28**, 382-387.

Farnung L, Vos SM, Wigge C, Cramer P (2017) Nucleosome-Chd1 structure and implications for chromatin remodelling. *Nature* **550**, 539-542.

Feng Q, Wang H, Ng HH, Erdjument-Bromage H, Tempst P, Struhl K, Zhang Y (2002) Methylation of H3-lysine 79 is mediated by a new family of HMTases without a SET domain. *Curr Biol* **12**, 1052-1058.

Ferguson DO, Holloman WK (1996) Recombinational repair of gaps in DNA is asymmetric in *Ustilago maydis* and can be explained by a migrating D-loop model. *Proc Natl Acad Sci USA* **93**, 5419-5424.

Ferrari M, Dibitetto D, De Gregorio G, Eapen VV, Rawal CC, Lazzaro F, Tsabar M, Marini F, Haber JE, Pellicioli A (2015) Functional interplay between the 53BP1-ortholog Rad9 and the Mre11 complex regulates resection, end-tethering and repair of a double-strand break. *PLoS Genet* **11**, e1004928.

Ferrari M, Rawal CC, Lodovichi S, Vietri MY, Pellicioli A (2020) Rad9/53BP1 promotes DNA repair via crossover recombination by limiting the Sgs1 and Mph1 helicases. *Nat Commun* **11**, 3181.

Ferretti LP, Lafranchi L, Sartori AA (2013) Controlling DNA-end resection: a new task for CDKs. *Front Genet* **4**, 99.

Finn K, Lowndes NF, Grenon M (2012) Eukaryotic DNA damage checkpoint activation in response to double-strand breaks. *Cell Mol Life Sci* **69**, 1447-1473.

Fishman-Lobell J, Rudin N, Haber JE (1992) Two alternative pathways of double-strand break repair that are kinetically separable and independently modulated. *Mol Cell Biol* **12**, 1292-1303.

Fitz Gerald JN, Benjamin JM, Kron SJ (2002) Robust G1 checkpoint arrest in budding yeast, dependence on DNA damage signaling and repair. *J Cell Sci* **115**, 1749-1757.

Friedberg EC (2003) DNA damage and repair. *Nature* **421**, 436-440.

Friedberg EC, Walker GC, Siede W, Wood RD (2005) DNA repair and mutagenesis. *American Society for Microbiology Press*.

Gangaraju VK, Prasad P, Srour A, Kagalwala MN, Bartholomew B (2009) Conformational changes associated with template commitment in ATP-dependent chromatin remodeling by ISW2. *Mol Cell* **35**, 58-69.

Garcia V, Phelps SE, Gray S, Neale MJ (2011) Bidirectional resection of DNA double-strand breaks by Mre11 and Exo1. *Nature* **479**, 241-244.

Giannattasio M, Lazzaro F, Plevani P, Muzi-Falconi M (2005) The DNA damage checkpoint response requires histone H2B ubiquitination by Rad6-Bre1 and H3 methylation by Dot1. *J Biol Chem* **280**, 9879-9886.

Gilbert CS, Green CM, Lowndes NF (2001) Budding yeast Rad9 is an ATP-dependent Rad53 activating machine. *Mol Cell* **8**, 129-136.

Gkikopoulos T, Schofield P, Singh V, Pinskaya M, Mellor J, Smolle M, Workman JL, Barton GJ, Owen-Hughes T (2011) A role for Snf2-related nucleosome-spacing enzymes genome-wide nucleosome organization. *Science* **333**, 1758-1760.

Gnesutta N, Nardini M, Mantovani R (2013) The H2A/H2B-like histone-fold domain proteins at the crossroad between chromatin and different DNA metabolisms. *Transcription* **4**, 114-119.

Gobbini E, Cassani C, Vertemara J, Wang W, Mambretti F, Casari E, Sung P, Tisi R, Zampella G, Longhese MP (2018) The MRX complex regulates Exo1 resection activity by altering DNA end structure. *EMBO J* **37**, e98588.

Gobbini E, Cesena D, Galbiati A, Lockhart A, Longhese MP (2013) Interplays between ATM/Tel1 and ATR/Mec1 in sensing and signaling DNA double-strand breaks. *DNA Repair* **12**, 791-799.

Gobbini E, Villa M, Gnugnoli M, Menin L, Clerici M, Longhese MP (2015) Sae2 Function at DNA Double-Strand Breaks is bypassed by dampening Tel1 or Rad53 activity. *PLoS Genet* **11**, e1005685.

Goddard TD, Huang CC, Meng EC, Pettersen EF, Couch GS, Morris JH, Ferrin TE (2018) UCSF ChimeraX: Meeting modern challenges in visualization and analysis. *Protein Sci* **27**, 14-25.

Goswami P, Abid Ali F, Douglas ME, Locke J, Purkiss A, Janska A, Eickhoff P, Early A, Nans A, Cheung AMC, Diffley JFX, Costa A (2018) Structure of DNA-CMG-Pol epsilon elucidates the roles of the non-catalytic polymerase modules in the eukaryotic replisome. *Nat Commun* **9**, 5061.

Granata M, Lazzaro F, Novarina D, Panigada D, Puddu F, Abreu CM, Kumar R, Grenon M, Lowndes NF, Plevani P, Muzi-Falconi M (2010) Dynamics of Rad9 chromatin binding and checkpoint function are mediated by its dimerization and are cell cycle-regulated by CDK1 activity. *PLoS Genet* **6**, e1001047.

Grasso CS, Wu YM, Robinson DR, Cao X, Dhanasekaran SM, Khan AP, Quist MJ, Jing X, Lonigro RJ, Brenner JC, Asangani IA, Ateeq B, Chun SY, Siddiqui J, Sam L, Anstett M, Mehra R, Prensner JR, Palanisamy N, Ryslik GA, Vandin F, Raphael BJ, Kunju LP, Rhodes DR, Pienta KJ, Chinnaiyan AM, Tomlins SA (2012) The mutational landscape of lethal castration-resistant prostate cancer. *Nature* **487**, 239-243.

Gravel S, Chapman JR, Magill C, Jackson SP (2008) DNA helicases Sgs1 and BLM promote DNA double-strand break resection. *Genes Dev* **22**, 2767-2772.

Grenon M, Costelloe T, Jimeno S, O'Shaughnessy A, Fitzgerald J, Zgheib O, Degerth L, Lowndes NF (2007) Docking onto chromatin via the *Saccharomyces cerevisiae* Rad9 Tudor domain. *Yeast* **24**, 105-119.

Guo X, Hum YF, Lehner K, Jinks-Robertson S (2017) Regulation of hetDNA length during mitotic double-strand break repair in yeast. *Mol Cell* **67**, 539-549.

Haber JE (2016) A life investigating pathways that repair broken chromosomes. *Annu Rev Genet* **50**, 1-28.

Hada A, Hota SK, Luo J, Lin YC, Kale S, Shaytan AK, Bhardwaj SK, Persinger J, Ranish J, Panchenko AR, Bartholomew B (2019) Histone octamer structure is altered early in ISW2 ATP-dependent nucleosome remodeling. *Cell Rep* **28**, 282-294.

Hailemariam S, Kumar S, Burgers PM (2019) Activation of $Tel1^{ATM}$ kinase requires Rad50 ATPase and long nucleosome-free DNA but no DNA ends. *J Biol Chem* **294**, 10120-10130.

Hammet A, Magill C, Heierhorst J, Jackson SP (2007) Rad9 BRCT domain interaction with phosphorylated H2AX regulates the G1 checkpoint in budding yeast. *EMBO Rep* **8**, 851-857.

Hanson PI, Whiteheart SW (2005) AAA+ proteins: have engine, will work. *Nat Rev Mol Cell Biol* **6**, 519-529.

Harrison JC, Haber JE (2006) Surviving the breakup, the DNA damage checkpoint. *Annu Rev Genet* **40**, 209-235.

Hartlepp KF, Fernández-Tornero C, Eberharter A, Grüne T, Müller CW, Becker PB (2005) The histone fold subunits of *Drosophila* CHRAC facilitate nucleosome sliding through dynamic DNA interactions. *Mol Cell Biol* **25**, 9886-9896.

Hauer MH, Gasser SM (2017) Chromatin and nucleosome dynamics in DNA damage and repair. *Genes Dev* **31**, 2204-2221.

He H, Li Y, Dong Q, Chang AY, Gao F, Chi Z, Su M, Zhang F, Ban H, Martienssen R, Chen YH, Li F (2017) Coordinated regulation of heterochromatin inheritance by Dpb3-Dpb4 complex. *Proc Natl Acad Sci USA* **114**, 12524-12529.

He J, Shi LZ, Truong LN, Lu CS, Razavian N, Li Y, Negrete A, Shiloach J, Berns MW, Wu X (2012) Rad50 zinc hook is important for the Mre11 complex to bind chromosomal DNA double-stranded breaks and initiate various DNA damage responses. *J Biol Chem* **287**, 31747-56.

Hefferin ML, Tomkinson AE (2005) Mechanism of DNA double-strand break repair by non-homologous end joining. *DNA Repair* **4**, 639–648.

Helena JM, Joubert AM, Grobbelaar S, Nolte EM, Nel M, Pepper MS, Coetzee M, Mercier AE (2018) Deoxyribonucleic acid damage and repair: capitalizing on our understanding of the mechanisms of maintaining genomic integrity for therapeutic purposes. *Int J Mol Sci* **19**, 1148.

Hennig BP, Bendrin K, Zhou Y, Fischer T (2012) Chd1 chromatin remodelers maintain nucleosome organization and repress cryptic transcription. *EMBO Rep* **13**, 997-1003.

Hoeijmakers JH (2009) DNA damage, aging, and cancer. *N Engl J Med* **361**, 1475-1485.

Hohl M, Kwon Y, Galván SM, Xue X, Tous C, Aguilera A, Sung P, Petrini JH (2011) The Rad50 coiled-coil domain is indispensable for Mre11 complex functions. *Nat Struct Mol Biol* **18**, 1124-1131.

Hopfner KP, Putnam CD, Tainer J A (2002) DNA double-strand break repair from head to tail. *Curr Opin Struct Biol* **12**, 115-122.

Huang S, Gulzar ZG, Salari K, Lapointe J, Brooks JD, Pollack JR (2012) Recurrent deletion of CHD1 in prostate cancer with relevance to cell invasiveness. *Oncogene* **31**, 4164-70.

Huertas P (2010) DNA resection in eukaryotes: deciding how to fix the break. *Nat Struct Mol Biol* **17**, 11-16.

Huertas P, Cortés-Ledesma F, Sartori AA, Aguilera A, Jackson SP (2008) CDK targets Sae2 to control DNA-end resection and homologous recombination. *Nature* **455**, 689-692.

Huyen Y, Zgheib O, Ditullio RA Jr, Gorgoulis VG, Zacharatos P, Petty TJ, Sheston EA, Mellert HS, Stavridi ES, Halazonetis TD (2004) Methylated lysine 79 of histone H3 targets 53BP1 to DNA double-strand breaks. *Nature* **432**, 406-411.

Iida T, Araki H (2004) Noncompetitive counteractions of DNA polymerase epsilon and ISW2/yCHRAC for epigenetic inheritance of telomere position effect in *Saccharomyces cerevisiae*. *Mol Cell Biol* **24**, 217-227.

Ivanov EL, Sugawara N, Fishman-Lobell J, Haber JE (1996) Genetic requirements for the single-strand annealing pathway of double-strand break repair in *Saccharomyces cerevisiae*. *Genetics* **142**, 693-704.

Jackson S, Bartek J (2009) The DNA-damage response in human biology and disease. *Nature* **461**, 1071-1078.

Javaheri A, Wysocki R, Jobin-Robitaille O, Altaf M, Côté J, Kron SJ (2006) Yeast G1 DNA damage checkpoint regulation by H2A phosphorylation is independent of chromatin remodeling. *Proc Natl Acad Sci USA* **103**, 13771-13776.

Kari V, Mansour WY, Raul SK, Baumgart SJ, Mund A, Grade M, Sirma H, Simon R, Will H, Dobbelstein M, Dikomey E, Johnsen SA (2016) Loss of CHD1 causes DNA repair defects and enhances prostate cancer therapeutic responsiveness. *EMBO Rep* **17**, 1609-1623.

Keelagher RE, Cotton VE, Goldman AS, Borts RH (2011) Separable roles for Exonuclease I in meiotic DNA double-strand break repair. *DNA Repair* **10**, 126-137.

Kowalczykowski SC (2015) An overview of the molecular mechanisms of recombinational DNA repair. *Cold Spring Harb Perspect Biol* **7**, a016410.

Krejci L, Altmannova V, Spirek M, Zhao X (2012) Homologous recombination and its regulation. *Nucleic Acids Res* **40**, 5795-5818.

Krishnaprasad GN, Anand MT, Lin G, Tekkedil MM, Steinmetz LM, Nishant KT (2014) Variation in crossover frequencies perturb crossover assurance without affecting meiotic chromosome segregation in *Saccharomyces cerevisiae*. *Genetics*, **199**, 399-412.

Kukimoto I, Elderkin S, Grimaldi M, Oelgeschläger T, Varga-Weisz PD (2004) The histone-fold protein complex CHRAC-15/17 enhances nucleosome sliding and assembly mediated by ACF. *Mol Cell* **13**, 265-277.

Lacoste N, Utley RT, Hunter JM, Poirier GG, Côte J (2002) Disruptor of telomeric silencing-1 is a chromatin-specific histone H3 methyltransferase. *J Biol Chem* **277**, 30421-3044.

Lammens K, Bemeleit DJ, Möckel C, Clausing E, Schele A, Hartung S, Schiller CB, Lucas M, Angermüller C, Söding J, Strässer K, Hopfner KP (2011) The Mre11:Rad50 structure shows an ATP-dependent molecular clamp in DNA Double-Strand Break repair. *Cell* **145**, 54-66.

Lan L, Ui A, Nakajima S, Hatakeyama K, Hoshi M, Watanabe R, Janicki SM, Ogiwara H, Kohno T, Kanno S, Yasui A (2010) The ACF1 complex is required for DNA double-strand break repair in human cells. *Mol Cell* **40**, 976-987.

Lazzaro F, Sapountzi V, Granata M, Pellicioli A, Vaze M, Haber JE, Plevani P, Lydall D, Muzi-Falconi M (2008) Histone methyltransferase Dot1 and Rad9 inhibit single-stranded DNA accumulation at DSBs and uncapped telomeres. *EMBO J* **27**, 1502-1512.

Lee JH, Paull TT (2005) ATM activation by DNA double-strand breaks through the Mre11-Rad50-Nbs1 complex. *Science* **308**, 551-554.

Lee MS, Higashide MT, Choi H, Li K, Hong S, Lee K, Shinohara A, Shinohara M, Kim KP. (2021) The synaptonemal complex central region modulates crossover pathways and feedback control of meiotic double-strand break formation. *Nucleic Acids Res* **49,** 7537-7553.

Lee SE, Moore JK, Holmes A, Umezu K, Kolodner RD, Haber JE (1998) *Saccharomyces* Ku70, Mre11/Rad50 and RPA proteins regulate adaptation to G2/M arrest after DNA damage. *Cell* **94**, 399-409.

Lee SJ, Duong JK, Stern DF (2004) A Ddc2-Rad53 fusion protein can bypass the requirements for *RAD9* and *MRC1* in Rad53 activation. *Mol Biol Cell* **15**, 5443-5455.

Lee Y, Park D, Iyer VR (2017) The ATP-dependent chromatin remodeler Chd1 is recruited by transcription elongation factors and maintains H3K4me3/H3K36me3 domains at actively transcribed and spliced genes. *Nucleic Acids Res* **45**, 8646.

Lempiäinen H, Halazonetis TD (2009) Emerging common themes in regulation of PIKKs and PI3Ks. *EMBO J* **28**, 3067-3073.

Li X, Tyler JK (2016) Nucleosome disassembly during human non-homologous end joining followed by concerted HIRA- and CAF-1-dependent reassembly. *Elife* **5**, e15129.

Lieber MR (2010) The mechanism of double-strand DNA break repair by the non-homologous DNA end-joining pathway. *Annu Rev Biochem* **79**, 181-211.

Lieleg C, Ketterer P, Nuebler J, Ludwigsen J, Gerland U, Dietz H, Mueller-Planitz F, Korber P (2015) Nucleosome spacing generated by ISWI and CHD1 remodelers is constant regardless of nucleosome density. *Mol Cell Biol* **35**, 1588-605.

Lilley DMJ (2017) Holliday junction-resolving enzymes-structures and mechanisms. *FEBS Lett* **591**, 1073-1082.

Limbo O, Chahwan C, Yamada Y, de Bruin RA, Wittenberg C, Russell P (2007) Ctp1 is a cell-cycle-regulated protein that functions with Mre11 complex to control double-strand break repair by homologous recombination. *Mol Cell* **28**, 134-146.

Lisby M, Barlow JH, Burgess RC, Rothstein R (2004) Choreography of the DNA damage response, spatiotemporal relationships among checkpoint and repair proteins. *Cell* **118**, 699-713.

Litwin I, Pilarczyk E, Wysocki R (2018) The Emerging Role of Cohesin in the DNA Damage Response. *Genes* **9**, 581.

Liu Y, Cussiol JR, Dibitetto D, Sims JR, Twayana S, Weiss RS, Freire R, Marini F, Pellicioli A, Smolka MB (2017) TOPBP1(Dpb11) plays a conserved role in homologous recombination DNA repair through the coordinated recruitment of 53BP1(Rad9). *J Cell Biol* **216**, 623-639.

Longhese MP, Bonetti D, Guerini I, Manfrini N, Clerici M (2009) DNA double-strand breaks in meiosis: checking their formation, processing and repair. *DNA Repair* **8**, 1127-1138.

Longhese MP, Bonetti D, Manfrini N, Clerici M (2010) Mechanisms and regulation of DNA end resection. *EMBO J* **29**, 2864-74.

Longhese MP, Clerici M, Lucchini G (2003) The S-phase checkpoint and its regulation in *Saccharomyces cerevisiae*. *Mutat Res* **532**, 41-58.

Longhese MP, Paciotti V, Neecke H, Lucchini G (2000) Checkpoint proteins influence telomeric silencing and length maintenance in budding yeast. *Genetics* **155**, 1577-1591.

Lusser A, Urwin DL, Kadonaga JT (2005) Distinct activities of CHD1 and ACF in ATP-dependent chromatin assembly. *Nat Struct Mol Biol* **12**, 160-166.

Madabhushi R, Gao F, Pfenning AR, Pan L, Yamakawa S, Seo J, Rueda R, Phan TX, Yamakawa H, Pao PC, Stott RT, Gjoneska E, Nott A, Cho S, Kellis M, Tsai LH (2015) Activity-Induced DNA Breaks Govern the Expression of Neuronal Early-Response Genes. *Cell* **161**, 1592-605.

Majka J, Binz SK, Wold MS, Burgers PMJ (2006) Replication protein A directs loading of the DNA damage checkpoint clamp to 5'-DNA junctions. *J Biol Chem* **281**, 27855-27861.

Majka J, Burgers PMJ (2003) Yeast Rad17/Mec3/Ddc1: a sliding clamp for the DNA damage checkpoint. *Proc Natl Acad Sci USA* **100**, 2249-2254.

Manfrini N, Guerini I, Citterio A, Lucchini G, Longhese MP (2010) Processing of meiotic DNA double strand breaks requires cyclin-dependent kinase and multiple nucleases. *J Biol Chem* **285**, 11628-11637.

Manfrini N, Trovesi C, Wery M, Martina M, Cesena D, Descrimes M, Morillon A, d'Adda di Fagagna F, Longhese MP (2015) RNA-processing proteins regulate Mec1/ATR activation by promoting generation of RPA-coated ssDNA. *EMBO Rep* **16**, 221-31.

Mangiagalli, M. Barbiroli A, Santambrogio C, Ferrari C, Nardini M, Lotti M, Brocca S (2021) The activity and stability of a cold-active acylaminoacyl peptidase rely on its dimerization by domain swapping. *Int J Biol Macromol* **181**, 263-274.

Mantiero D, Clerici M, Lucchini G, Longhese MP (2007) Dual role for *Saccharomyces cerevisiae* Tel1 in the checkpoint response to double-strand breaks. *EMBO Rep* **8**, 380-387.

Marsella A, Cassani C, Casari E, Tisi R, Longhese MP (2019) Structure-function relationships of the Mre11 protein in the control of DNA end bridging and processing. *Curr Genet* **65**, 11-16.

Martens JA, Winston F (2002) Evidence that Swi/Snf directly represses transcription in *S. cerevisiae*. *Genes Dev* **16**, 2231-2236.

Mathiasen DP, Lisby M (2014) Cell cycle regulation of homologous recombination in *Saccharomyces cerevisiae*. *FEMS Microbiol Rev* **38**, 172-184.

Matveeva EA, He P, Whiteheart SW (1997) N-ethylmaleimide-sensitive fusion protein contains high and low affinity ATP-binding sites that are functionally distinct. *J Biol Chem* **272**, 26413-26418.

McConnell AD, Gelbart ME, Tsukiyama T (2004) Histone fold protein Dls1p is required for Isw2-dependent chromatin remodeling in vivo. *Mol Cell Biol* **24**, 2605-2613.

McKinnon PJ (2012) ATM and the molecular pathogenesis of ataxia telangiectasia. *Annu Rev Pathol* **7**, 303-321.

McVey M, Lee SE (2008). MMEJ repair of double-strand breaks (director's cut): deleted sequences and alternative endings. *Trends Genet* **24**, 529-38.

Mehta A, Haber J (2014) Sources of DNA double-strand breaks and models of recombinational DNA repair. *Cold Spring Harb Perspect Biol* **6**, a016428.

Menin L, Ursich S, Trovesi C, Zellweger R, Lopes M, Longhese MP, Clerici M (2018) Tel1/ATM prevents degradation of replication forks that reverse after topoisomerase poisoning. *EMBO Rep* **19**, e45535.

Mimitou EP, Symington LS (2008) Sae2, Exo1 and Sgs1 collaborate in DNA double-strand break processing. *Nature* **455**, 770-774.

Mimitou EP, Symington LS (2010) Ku prevents Exo1 and Sgs1- dependent resection of DNA ends in the absence of a functional MRX complex or Sae2. *EMBO J* **29**, 3358-3369.

Mimitou EP, Yamada S, Keeney S (2017) A global view of meiotic double-strand break end resection. *Science* **355**, 40-45.

Mizuguchi G, Shen X, Landry J, Wu WH, Sen S, Wu C (2004) ATP-driven exchange of histone H2AZ variant catalyzed by SWR1 chromatin remodeling complex. *Science* **303**, 343-348.

Moore S, Berger ND, Luijsterburg MS, Piett CG, Stanley FKT, Schräder CU, Fang S, Chan JA, Schriemer DC, Nagel ZD, van Attikum H, Goodarzi AA

(2019) The CHD6 chromatin remodeler is an oxidative DNA damage response factor. *Nat Commun* **10**, 241.

Mordes DA, Nam EA, Cortez D (2008) Dpb11 activates the Mec1-Ddc2 complex. *Proc Natl Acad Sci USA* **105**, 18730-18734.

Morillo-Huesca M, Clemente-Ruiz M, Andújar E, Prado F (2010) The SWR1 histone replacement complex causes genetic instability and genome-wide transcription misregulation in the absence of H2A.Z. *PLoS One* **5**, e12143.

Morin I, Ngo H-P, Greenall A, Zubko MK, Morrice N, Lydall D (2008) Checkpoint-dependent phosphorylation of Exo1 modulates the DNA damage response. *EMBO J* **27**, 2400-2410.

Morrison AJ, Highland J, Krogan NJ, Arbel-Eden A, Greenblatt JF, Haber JE, Shen X (2004) INO80 and gamma-H2AX interaction links ATP-dependent chromatin remodeling to DNA damage repair. *Cell* **119**, 767-775.

Moynahan ME, Jasin M (2010) Mitotic homologous recombination maintains genomic stability and suppresses tumorigenesis. *Nat Rev Mol Cell Biol* **11**, 196-207.

Mueller JE, Bryk M (2007) Isw1 acts independently of the Isw1a and Isw1b complexes in regulating transcriptional silencing at the ribosomal DNA locus in *Saccharomyces cerevisiae*. *J Mol Biol* **371**, 1-10.

Muramatsu S, Hirai K, Tak YS, Kamimura Y, Araki H (2010) CDK-dependent complex formation between replication proteins Dpb11, Sld2, Pol epsilon, and GINS in budding yeast. *Genes Dev* **24**, 602-612.

Myler LR, Gallardo IF, Soniat MM, Deshpande RA, Gonzalez XB, Kim Y, Paull TT, Finkelstein IJ (2017) Single-molecule imaging reveals how Mre11-Rad50-Nbs1 initiates DNA break repair. *Mol Cell* **67**, 891-898.

Nakada D, Matsumoto K, Sugimoto K (2003) ATM-related Tel1 associates with double-strand breaks through an Xrs2-dependent mechanism. *Genes Dev* **17**, 1957-1962.

Narlikar GJ, Sundaramoorthy R, Owen-Hughes T (2013) Mechanisms and functions of ATP-dependent chromatin-remodeling enzymes. *Cell* **154**, 490-503.

Nassif N, Penney J, Pal S, Engels WR, Gloor GB (1994) Efficient copying of nonhomologous sequences from ectopic sites via Pelement-induced gap repair. *Mol Cell Biol* **14**, 1613-1625.

Navadgi-Patil VM, Burgers PM (2008) Yeast DNA replication protein Dpb11 activates the Mec1/ATR checkpoint kinase. *J Biol Chem* **283**, 35853-35859.

Navadgi-Patil VM, Burgers PM (2009) The unstructured C-terminal tail of the 9-1-1 clamp subunit Ddc1 activates Mec1/ATR via two distinct mechanisms. *Mol Cell* **36**, 743-753.

Navas TA, Zhou Z, Elledge SJ (1995) DNA polymerase epsilon links the DNA replication machinery to the S phase checkpoint. *Cell* **80**, 29-39.

Negrini S, Gorgoulis V, Halazonetis, T (2010) Genomic instability - an evolving hallmark of cancer. *Nat Rev Mol Cell Biol* **11,** 220-228.

Ngo GHP, Lydall D (2015) The 9-1-1 checkpoint clamp coordinates resection at DNA double strand breaks. *Nucleic Acids Res* **43**, 5017-5032.

Nguyen AT, Zhang Y (2011) The diverse functions of Dot1 and H3K79 methylation. *Genes Dev* **25**, 1345-1358.

Nicolette ML, Lee K, Guo Z, Rani M, Chow JM, Lee SE, Paull TT (2010) Mre11–Rad50–Xrs2 and Sae2 promote 5′ strand resection of DNA double-strand breaks. *Nat Struct Mol Biol* **17**, 1957.

Nimonkar AV, Genschel J, Kinoshita E, Polaczek P, Campbell JL, Wyman C, Modrich P, Kowalczykowski SC (2011) BLM-DNA2- RPA-MRN and EXO1-BLM-RPA-MRN constitute two DNA end resection machineries for human DNA break repair. *Genes Dev* **25**, 350-362.

Nimonkar AV, Ozsoy AZ, Genschel J, Modrich P, Kowalczykowski SC (2008) Human exonuclease 1 and BLM helicase interact to resect DNA and initiate DNA repair. *Proc Natl Acad Sci USA* **105**, 16906-16911.

Niu H, Chung WH, Zhu Z, Kwon Y, Zhao W, Chi P, Prakash R, Seong C, Liu D, Lu L, Ira G, Sung P (2010) Mechanism of the ATP-dependent DNA end-resection machinery from *Saccharomyces cerevisiae*. *Nature* **467**, 108-111.

Nyberg KA, Michelson RJ, Putnam CW, Weinert TA (2002) Toward maintaining the genome, DNA damage and replication checkpoints. *Annu Rev Genet* **36**, 617-656.

O'Driscoll M, Jeggo PA (2006) The role of double-strand break repair - insights from human genetics. *Nat Rev Genet* **7**, 45-54.

O'Driscoll M, Ruiz-Perez VL, Woods CG, Jeggo PA, Goodship JA (2003) A splicing mutation affecting expression of ataxia-telangiectasia and Rad3-related protein (ATR) results in Seckel syndrome. *Nat Genet* **33**, 497-501.

O'Neil NJ, Bailey ML, Hieter P (2017) Synthetic lethality and cancer. *Nat Rev Genet* **18**,613-623.

Oh J, Al-Zain A, Cannavo E, Cejka P, Symington LS (2016) Xrs2 dependent and independent functions of the Mre11-Rad50 complex. *Mol Cell* **64**, 405-415.

Ohya T, Maki S, Kawasaki Y, Sugino A (2000) Structure and function of the fourth subunit (Dpb4p) of DNA polymerase epsilon in *Saccharomyces cerevisiae*. *Nucleic Acids Res* **28**, 3846-3852.

Osley MA, Tsukuda T, Nickoloff JA (2007) ATP-dependent chromatin remodeling factors and DNA damage repair. *Mutat Res* **618**, 65-80.

Palmbos PL, Wu D, Daley JM, Wilson TE (2008) Recruitment of *Saccharomyces cerevisiae* Dnl4-Lif1 complex to a double-strand break requires interactions with Yku80 and the Xrs2 FHA domain. *Genetics* **180**, 1809-1819.

Papamichos-Chronakis M, Watanabe S, Rando OJ, Peterson CL (2011) Global regulation of H2A.Z localization by the INO80 chromatin-remodeling enzyme is essential for genome integrity. *Cell* **144**, 200-213.

Paull TT, Deshpande RA (2014) The Mre11/Rad50/Nbs1 complex: recent insights into catalytic activities and ATP-driven conformational changes. *Exp Cell Res* **329**, 139-147.

Paull TT, Gellert M (1998) The 3’ to 5’ exonuclease activity of Mre11 facilitates repair of DNA double-strand breaks. *Mol Cell* **1**, 969-979.

Pellicioli A, Lee SE, Lucca C, Foiani M, Haber JE (2001) Regulation of *Saccharomyces* Rad53 checkpoint kinase during adaptation from DNA damage-induced G2/M arrest. *Mol Cell* **7**, 293-300.

Peritore M, Reusswig KU, Bantele SCS, Straub T, Pfander B (2021) Strand-specific ChIP-seq at DNA breaks distinguishes ssDNA versus dsDNA binding and refutes single-stranded nucleosomes. *Mol Cell* **81**, 1841-1853.e4.

Perry J, Kleckner N (2003) The ATRs, ATMs, and TORs are giant HEAT repeat proteins. *Cell* **112**, 151-155.

Pfander B, Diffley JF (2011) Dpb11 coordinates Mec1 kinase activation with cell cycle-regulated Rad9 recruitment. *EMBO J* **30**, 4897-4907.

Pointner J, Persson J, Prasad P, Norman-Axelsson U, Strålfors A, Khorosjutina O, Krietenstein N, Svensson JP, Ekwall K, Korber P (2012) CHD1 remodelers regulate nucleosome spacing in vitro and align nucleosomal arrays over gene coding regions in *S. pombe*. *EMBO J* **31**, 4388-403.

Poli J, Gasser SM, Papamichos-Chronakis M (2017) The INO80 remodeller in transcription, replication and repair. *Philos Trans R Soc Lond B Biol Sci* **372**, 20160290.

Poot RA, Dellaire G, Hülsmann BB, Grimaldi MA, Corona DF, Becker PB, Bickmore WA, Varga-Weisz PD (2000) HuCHRAC, a human ISWI chromatin remodelling complex contains hACF1 and two novel histone-fold proteins. *EMBO J* **19**, 3377-3387.

Prakash R, Satory D, Dray E, Papusha A, Scheller J, Kramer W, Krejci L, Klein H, Haber JE, Sung P, Ira G (2009) Yeast Mph1 helicase dissociates Rad51-made D-loops: implications for crossover control in mitotic recombination. *Genes Dev* **23**, 67-79.

Puddu F, Granata M, Di Nola L, Balestrini A, Piergiovanni G, Lazzaro F, Giannattasio M, Plevani P, Muzi-Falconi M (2008) Phosphorylation of the budding yeast 9-1-1 complex is required for Dpb11 function in the full activation of the UV-induced DNA damage checkpoint. *Mol Cell Biol* **28**, 4782-4793.

Puddu F, Oelschlaegel T, Guerini I, Geisler NJ, Niu H, Herzog M, Salguero I, Ochoa-Montaño B, Viré E, Sung P, Adams DJ, Keane TM, Jackson SP (2015) Synthetic viability genomic screening defines Sae2 function in DNA repair. *EMBO J* **34**, 1509-1522.

Puddu F, Piergiovanni G, Plevani P, Muzi-Falconi M (2011) Sensing of replication stress and Mec1 activation act through two independent pathways involving the 9-1-1 complex and DNA polymerase ε. *PLoS Genet* **7**, e1002022.

Radman-Livaja M, Quan TK, Valenzuela L, Armstrong JA, van Welsem T, Kim T, Lee LJ, Buratowski S, van Leeuwen F, Rando OJ, Hartzog GA (2012) A key role for Chd1 in histone H3 dynamics at the 3' ends of long genes in yeast. *PLoS Genet* **8**, e1002811.

Reginato G, Cannavo E, Cejka P (2017) Physiological protein blocks direct the Mre11-Rad50-Xrs2 and Sae2 nuclease complex to initiate DNA end resection. *Genes Dev* **31**, 2325-2330.

Rinaldi C, Pizzul P, Longhese MP, Bonetti D (2021) Sensing R-Loop-Associated DNA Damage to Safeguard Genome Stability. *Front Cell Dev Biol* **8**, 618157.

Roos WP, Thomas AD, Kaina B (2016) DNA damage and the balance between survival and death in cancer biology. *Nat Rev Cancer* **16**, 20–33.

Rother MB, van Attikum H (2017) DNA repair goes hip-hop: SMARCA and CHD chromatin remodellers join the break dance. *Philos Trans R Soc Lond B Biol Sci* **372**, 20160285.

Roy R, Chun J, Powell SN (2012) BRCA1 and BRCA2, different roles in a common pathway of genome protection. *Nat Rev Cancer* **12**, 68-78.

Rüthemann P, Balbo Pogliano C, Codilupi T, Garajovà Z, Naegeli H (2017) Chromatin remodeler CHD1 promotes XPC-to-TFIIH handover of nucleosomal UV lesions in nucleotide excision repair. *EMBO J* **36**, 3372-3386.

San Filippo J, Sung P, Klein H (2008) Mechanism of eukaryotic homologous recombination. *Annu Rev Biochem* **77**, 229-257.

Sánchez-Molina S, Mortusewicz O, Bieber B, Auer S, Eckey M, Leonhardt H, Friedl AA, Becker PB (2011) Role for hACF1 in the G2/M damage checkpoint. *Nucleic Acids Res* **39**, 8445-8456.

Saponaro M, Callahan D, Zheng X, Krejci L, Haber JE, Klein HL, Liberi G (2010) Cdk1 targets Srs2 to complete synthesis-dependent strand annealing and to promote recombinational repair. *PLoS Genet* **6**, e1000858.

Sartori AA, Lukas C, Coates J, Mistrik M, Fu S, Bartek J, Baer R, Lukas J, Jackson SP (2007) Human CtIP promotes DNA end resection. *Nature* **450**, 509-514.

Savitsky K, Sfez S, Tagle DA, Ziv Y, Sartiel A, Collins FS, Shiloh Y, Rotman G (1995) The complete sequence of the coding region of the ATM gene reveals similarity to cell cycle regulators in different species. *Hum Mol Genet* **4**, 2025-2032.

Schwartz MF, Duong JK, Sun Z, Morrow JS, Pradhan D, Stern DF (2002) Rad9 phosphorylation sites couple Rad53 to the *Saccharomyces cerevisiae* DNA damage checkpoint. *Mol Cell* **9**, 1055-1065.

Schwartz MF, Lee SJ, Duong JK, Eminaga S, Stern DF (2003) FHA domain-mediated DNA checkpoint regulation of Rad53. *Cell Cycle* **2**, 384-396.

Sebesta M, Krejci L (2016) Mechanism of Homologous Recombination. *DNA Replication, Recombination, and Repair* 73-109.

Seeber A, Hauer M, Gasser SM (2013) Nucleosome remodelers in double-strand break repair. *Curr Opin Genet Dev* **23**, 174-184.

Seol JH, Shim EY, Lee SE (2018) Microhomology-mediated end joining: good, bad and ugly. *Mutat Res* **809**, 81-87.

Seong C, Sehorn MG, Plate I, Shi I, Song B, Chi P, Mortensen U, Sung P, Krejci L (2008) Molecular anatomy of the recombination mediator function of *Saccharomyces cerevisiae* Rad52. *J Biol Chem* **283**, 12166-12174.

Shenoy TR, Boysen G, Wang MY, Xu QZ, Guo W, Koh FM, Wang C, Zhang LZ, Wang Y, Gil V, Aziz S, Christova R, Rodrigues DN, Crespo M, Rescigno P, Tunariu N, Riisnaes R, Zafeiriou Z, Flohr P, Yuan W, Knight E, Swain A, Ramalho-Santos M, Xu DY, de Bono J, Wu H (2017) CHD1 loss sensitizes prostate cancer to DNA damaging therapy by promoting error-prone double-strand break repair. *Ann Oncol* **28**, 1495-1507.

Shibata A, Moiani D, Arvai AS, Perry J, Harding SM, Genois MM, Maity R, van Rossum-Fikkert S, Kertokalio A, Romoli F, Ismail A, Ismalaj E, Petricci E, Neale MJ, Bristow RG, Masson JY, Wyman C, Jeggo PA, Tainer JA (2014) DNA double-strand break repair pathway choice is directed by distinct MRE11 nuclease activities. *Mol Cell* **53**, 7-18.

Shim EY, Chung WH, Nicolette ML, Zhang Y, Davis M, Zhu Z, Paull TT, Ira G, Lee SE (2010) *Saccharomyces cerevisiae* Mre11/Rad50/Xrs2 and Ku proteins regulate association of Exo1 and Dna2 with DNA breaks. *EMBO J* **29**, 3370-3380.

Shim EY, Hong SJ, Oum JH, Yanez Y, Zhang Y, Lee SE (2007) RSC mobilizes nucleosomes to improve accessibility of repair machinery to the damaged chromatin. *Mol Cell Biol* **27**, 1602-1613.

Shim YS, Choi Y, Kang K, Cho K, Oh S, Lee J, Grewal SI, Lee D (2012) Hrp3 controls nucleosome positioning to suppress non-coding transcription in eu- and heterochromatin. *EMBO J* **31**, 4375-87.

Shroff R, Arbel-Eden A, Pilch D, Ira G, Bonner WM, Petrini JH, Haber JE, Lichten M (2004) Distribution and dynamics of chromatin modification induced by a defined DNA double-strand break. *Curr Biol* **14**, 1703-1711.

Simic R, Lindstrom DL, Tran HG, Roinick KL, Costa PJ, Johnson AD, Hartzog GA, Arndt KM (2003) Chromatin remodeling protein Chd1 interacts with transcription elongation factors and localizes to transcribed genes. *EMBO J* **22**, 1846-1856.

Sinha KK, Gross JD, Narlikar GJ (2017) Distortion of histone octamer core promotes nucleosome mobilization by a chromatin remodeler. *Science* **355**, eaaa3761.

Smeenk G, Wiegant WW, Marteijn JA, Luijsterburg MS, Sroczynski N, Costelloe T, Romeijn RJ, Pastink A, Mailand N, Vermeulen W, van Attikum H (2013) Poly(ADP-ribosyl)ation links the chromatin remodeler SMARCA5/SNF2H to RNF168-dependent DNA damage signaling. *J Cell Sci* **126**, 889-903.

Smolle M, Venkatesh S, Gogol MM, Li H, Zhang Y, Florens L, Washburn MP, Workman JL (2012) Chromatin remodelers Isw1 and Chd1 maintain chromatin structure during transcription by preventing histone exchange. *Nat Struct Mol Biol* **19**, 884-892.

Smolle MM (2018) Chd1 bends over backward to remodel. *Nat Struct Mol Biol* **25**, 2-3.

Strathern JN, Klar AJ, Hicks JB, Abraham JA, Ivy JM, Nasmyth KA, McGill C (1982) Homothallic switching of yeast mating type cassettes is initiated by a double-stranded cut in the *MAT* locus. *Cell* **31**, 183-192.

Strickfaden H, McDonald D, Kruhlak MJ, Haince JF, Th'ng JPH, Rouleau M, Ishibashi T, Corry GN, Ausio J, Underhill DA, Poirier GG, Hendzel MJ (2013) Poly(ADP-ribosyl)ation links the chromatin remodeler SMARCA5/SNF2H to RNF168-dependent DNA damage signaling. *J Cell Sci* **126**, 889-903.

Studier FW (2005) Protein production by auto-induction in high-density shaking cultures. *Protein Expr Purif* **41**, 207-234.

Sturzenegger A, Burdova K, Kanagaraj R, Levikova M, Pinto C, Cejka P, Janscak P (2014) DNA2 cooperates with the WRN and BLM RecQ helicases to mediate long-range DNA end resection in human cells. *J Biol Chem* **289**, 27314-27326.

Sun Z, Hsiao J, Fay DS, Stern DF (1998) Rad53 FHA domain associated with phosphorylated Rad9 in the DNA damage checkpoint. *Science* **281**, 272-274.

Sung P, Krejci L, Van Komen S, Sehorn MG (2003) Rad51 recombinase and recombination mediators. *J Biol Chem* **278**, 42729-42732.

Sweeney FD, Yang F, Chi A, Shabanowitz J, Hunt DF, Durocher D (2005) *Saccharomyces cerevisiae* Rad9 acts as a Mec1 adaptor to allow Rad53 activation. *Curr Biol* **15**, 1364-1375.

Syed A, Tainer JA (2018) The MRE11-RAD50-NBS1 complex conducts the orchestration of damage signaling and outcomes to stress in DNA replication and repair. *Annu Rev Biochem* **87**, 263-294.

Symington LS (2016) Mechanism and regulation of DNA end resection in eukaryotes. *Crit Rev Biochem Mol Biol* **51**, 195-212.

Symington LS, Gautier J (2011) Double-strand break end resection and repair pathway choice. *Annu Rev Genet* **45**, 247-271.

Symington LS, Rothstein R, Lisby M (2014) Mechanisms and regulation of mitotic recombination in *Saccharomyces cerevisiae*. *Genetics* **198**, 795-835.

Tisi R, Vertemara J, Zampella G, Longhese MP (2020) Functional and structural insights into the MRX/MRN complex, a key player in recognition and repair of DNA double-strand breaks. *Comput Struct Biotechnol J* **18**, 1137-1152.

Tkáč J, Xu G, Adhikary H, Young JTF, Gallo D, Escribano-Díaz C, Krietsch J, Orthwein A, Munro M, Sol W, Al-Hakim A, Lin ZY, Jonkers J, Borst P, Brown GW, Gingras AC, Rottenberg S, Masson JY, Durocher D (2016) HELB is a feedback inhibitor of DNA end resection. *Mol Cell* **61**, 405-418.

Toh GW, O'Shaughnessy AM, Jimeno S, Dobbie IM, Grenon M, Maffini S, O'Rorke A, Lowndes NF (2006) Histone H2A phosphorylation and H3 methylation are required for a novel Rad9 DSB repair function following checkpoint activation. *DNA Repair* **5**, 693-703.

Tran PT, Erdeniz N, Dudley S, Liskay RM (2002) Characterization of nuclease-dependent functions of Exo1p in *Saccharomyces cerevisiae*. *DNA Repair* **1**, 895-912.

Trovesi C, Falcettoni M, Lucchini G, Clerici M, Longhese MP (2011) Distinct Cdk1 requirements during single-strand annealing, noncrossover, and crossover recombination. *PLoS Genet* **7**, e1002263.

Trujillo KM, Yuan SS, Lee EY, Sung P (1998) Nuclease activities in a complex of human recombination and DNA repair factors Rad50, Mre11, and p95. *J Biol Chem* **273**, 21447-21450.

Truong LN, Li Y, Shi LZ, Hwang PY, He J, Wang H, Razavian N, Berns MW, Wu X (2013) Microhomology-mediated end joining and homologous recombination share the initial end resection step to repair DNA double-strand breaks in mammalian cells. *Proc Natl Acad Sci USA* **110**, 7720-5.

Tsabar M, Hicks WM, Tsaponina O, Haber JE (2016) Re-establishment of nucleosome occupancy during double-strand break repair in budding yeast. *DNA Repair* **47**, 21-29.

Tsubota T, Maki S, Kubota H, Sugino A, Maki H (2003) Double-stranded DNA binding properties of *Saccharomyces cerevisiae* DNA polymerase epsilon and of the Dpb3p-Dpb4p subassembly. *Genes Cells* **8**, 873-888.

Tsubota T, Tajima R, Ode K, Kubota H, Fukuhara N, Kawabata T, Maki S, Maki H (2006) Double-stranded DNA binding, an unusual property of DNA polymerase epsilon, promotes epigenetic silencing in *Saccharomyces cerevisiae*. *J Biol Chem* **281**, 32898-32908.

Tsukuda T, Fleming AB, Nickoloff JA, Osley MA (2005) Chromatin remodelling at a DNA double-strand break site in *Saccharomyces cerevisiae*. *Nature* **438**, 379-383.

Tsukuda T, Lo YC, Krishna S, Sterk R, Osley MA, Nickoloff JA (2009) INO80-dependent chromatin remodeling regulates early and late stages of mitotic homologous recombination. *DNA Repair* **8**, 360-369.

van Attikum H, Fritsch O, Gasser SM (2007) Distinct roles for SWR1 and INO80 chromatin remodeling complexes at chromosomal double-strand breaks. *EMBO J* **26**, 4113-4125.

van Attikum H, Fritsch O, Hohn B, Gasser SM (2004) Recruitment of the INO80 complex by H2A phosphorylation links ATP-dependent chromatin remodeling with DNA double-strand break repair. *Cell* **119**, 777-788.

van Leeuwen F, Gafken PR, Gottschling DE (2002) Dot1p modulates silencing in yeast by methylation of the nucleosome core. *Cell* **109**, 745-756.

Vaze MB, Pellicioli A, Lee SE, Ira G, Liberi G, Arbel-Eden A, Foiani M, Haber JE (2002) Recovery from checkpoint-mediated arrest after repair of a double-strand break requires Srs2 helicase. *Mol Cell* **10**, 373-385.

Villa M, Cassani C, Gobbini E, Bonetti D, Longhese MP (2016) Coupling end resection with the checkpoint response at DNA double-strand breaks. *Cell Mol Life* **73**, 3655-3663.

Wang H, Elledge SJ (1999) DRC1, DNA replication and checkpoint protein 1, functions with DPB11 to control DNA replication and the S-phase checkpoint in *Saccharomyces cerevisiae*. *Proc Natl Acad Sci* **96**, 3824-3829.

Wang H, Elledge SJ (2002) Genetic and physical interactions between *DPB11* and *DDC1* in the yeast DNA damage response pathway. *Genetics* **160**, 1295-1304.

Wang H, Xu X (2017) Microhomology-mediated end joining: new players join the team. *Cell Biosci* **7**, 6.

Wang W, Daley JM, Kwon Y, Krasner DS, Sung P (2017) Plasticity of the Mre11-Rad50-Xrs2-Sae2 nuclease ensemble in the processing of DNA-bound obstacles. *Genes Dev* **31**, 2331-2336.

Weibezahn J, Schlieker C, Bukau B, Mogk A (2003) Characterization of a trap mutant of the AAA+ chaperone ClpB. *J Biol Chem* **278**, 32608-32617.

Westmoreland JW, Resnick MA (2016) Recombinational repair of radiation-induced double-strand breaks occurs in the absence of extensive resection. *Nucleic Acids Res* **44**, 695-704.

Wiest NE, Houghtaling S, Sanchez JC, Tomkinson AE, Osley MA (2017) The SWI/SNF ATP-dependent nucleosome remodeler promotes resection initiation at a DNA double-strand break in yeast. *Nucleic Acids Res* **45**, 5887-5900.

Wild P, Susperregui A, Piazza I, Dörig C, Oke A, Arter M, Yamaguchi M, Hilditch AT, Vuina K, Chan KC, Gromova T, Haber JE, Fung JC, Picotti P, Matos J (2019) Network rewiring of homologous recombination enzymes during mitotic proliferation and meiosis. *Mol Cell* **75**, 859-874.

Williams GJ, Hammel M, Radhakrishnan SK, Ramsden D, Lees-Miller SP, Tainer JA (2014) Structural insights into NHEJ: Building up an integrated picture of the dynamic DSB repair super complex, one component and interaction at a time. *DNA Repair* **17**, 110-120.

Williams RS, Dodson GE, Limbo O, Yamada Y, Williams JS, Guenther G, Classen S, Glover JN, Iwasaki H, Russell P, Tainer JA (2009) Nbs1 flexibly tethers Ctp1 and Mre11-Rad50 to coordinate DNA double-strand break processing and repair. *Cell* **139**, 87-99.

Wilkinson NA, Mnuskin KS, Ashton NW, Woodgate R (2020) Ubiquitin and Ubiquitin-Like Proteins Are Essential Regulators of DNA Damage Bypass. *Cancers* **12**, 2848.

Wysocki R, Javaheri A, Allard S, Sha F, Coté J, Kron SJ (2005) Role of Dot1-dependent histone H3 methylation in G1 and S phase DNA damage checkpoint functions of Rad9. *Mol Cell Biol* **25**, 8430-8443.

Yang J, Zhang Y (2015) I-TASSER server: new development for protein structure and function predictions. *Nucleic Acids Res* **43**, 174-181.

You Z, Shi LZ, Zhu Q, Wu P, Zhang YW, Basilio A, Tonnu N, Verma IM, Berns MW, Hunter T (2009) CtIP links DNA double-strand break sensing to resection. *Mol Cell* **36**, 954-969.

Yu C, Gan H, Serra-Cardona A, Zhang L, Gan S, Sharma S, Johansson E, Chabes A, Xu RM, Zhang Z (2018) A mechanism for preventing asymmetric histone segregation onto replicating DNA strands. *Science* **361**, 1386-1389.

Yuan Z, Georgescu R, Schauer GD, O'Donnell ME, Li H (2020) Structure of the polymerase epsilon holoenzyme and atomic model of the leading strand replisome. *Nat Commun* **11**, 3156.

Zakharyevich K, Ma Y, Tang S, Hwang PY, Boiteux S, Hunter N (2010) Temporally and biochemically distinct activities of Exo1 during meiosis: double-strand break resection and resolution of double Holliday junctions. *Mol Cell* **40**, 1001-1015.

Zhou BR, Feng H, Ghirlando R, Li S, Schwieters CD, Bai Y (2016) A small number of residues can determine if linker histones are bound on or off dyad in the chromatosome. *J Mol Biol* **428**, 3948-3959.

Zhou CY, Johnson SL, Gamarra NI, Narlikar GJ (2016) Mechanisms of ATP dependent chromatin remodeling motors. *Annu Rev Biophys* **45**, 153-181.

Zhou J, Li J, Serafim RB, Ketchum S, Ferreira CG, Liu JC, Coe KA, Price BD, Yusufzai T (2018) Human CHD1 is required for early DNA-damage signaling and is uniquely regulated by its N terminus. *Nucleic Acids Res* **46**, 3891-3905.

Zhu Z, Chung WH, Shim EY, Lee SE, Ira G (2008) Sgs1 helicase and two nucleases Dna2 and Exo1 resect DNA double-strand break ends. *Cell* **134**, 981-994.

Zierhut C, Diffley JF (2008) Break dosage, cell cycle stage and DNA replication influence DNA double strand break response. *EMBO J* **27**, 1875-1885.

Zimmermann M, Lottersberger F, Buonomo SB, Sfeir A, de Lange T (2013) 53BP1 regulates DSB repair using Rif1 to control 5' end resection. *Science* **339**, 700-704.

Zofall M, Persinger J, Kassabov SR, Bartholomew B (2006) Chromatin remodeling by ISW2 and SWI/SNF requires DNA translocation inside the nucleosome. *Nat Struct Mol Biol* **13**, 339-346.

Zou L, Elledge SJ (2003) Sensing DNA damage through ATRIP recognition of RPA-ssDNA complexes. *Science* **300**, 1542-1548.

APPENDIX

Methods in Molecular Biology

2021; 2153:33-45

doi:10.1007/978-1-0716-0644-5_3

Resection of a DNA Double-Strand Break by Alkaline Gel Electrophoresis and Southern Blotting

Erika Casari[1], Elisa Gobbini[1], Michela Clerici[1], Maria Pia Longhese[1*]

[*] Corresponding Author

[1] Dipartimento di Biotecnologie e Bioscienze, Università degli Studi di Milano-Bicocca, Milano, 20126, Italy

Frontiers in Molecular Biosciences

2019; 6:43

doi:10.3389/fmolb.2019.00043

Processing of DNA Double-Strand Breaks by the MRX Complex in a Chromatin Context

Erika Casari[1§], Carlo Rinaldi[1§], Antonio Marsella[1],

Marco Gnugnoli[1], Chiara Vittoria Colombo[1], Diego Bonetti[1],

Maria Pia Longhese[*]

[§] These authors have contributed equally to this work

[*] Corresponding Author

[1] Dipartimento di Biotecnologie e Bioscienze, Università degli Studi di Milano-Bicocca, Milano, 20126, Italy

Current Genetics

2019 Feb; 65(1):11-16

doi: 10.1007/s00294-018-0861-5

Structure-function relationships of the Mre11 protein in the control of DNA end bridging and processing

Antonio Marsella[1], Corinne Cassani[1], **Erika Casari**[1],

Renata Tisi[1], Maria Pia Longhese[1*]

[*] Corresponding Author

[1] Dipartimento di Biotecnologie e Bioscienze, Università degli Studi di Milano-Bicocca, Milano, 20126, Italy